UNIVERSIDADE DA CORUÑA

Programa de Doctorado en Ciencias de la Salud

DOCTORAL THESIS

Targeting protein degradation as a novel cancer therapeutic strategy: small-molecule inhibitors of the E3 ubiquitin-ligase Hakai

Alba Casas Pais

2021

Director:

Dr. Angélica Figueroa Conde-Valvís

The director of this doctoral thesis, **Dr. Angélica Figueroa Conde-Valvís**, group leader of Epithelial Plasticity and Metastasis Group at the Instituto de Investigación Biomédica de A Coruña (INIBIC),

CERTIFIES THAT

This work, entitled '*Targeting protein degradation as a novel cancer therapeutic strategy: small-molecule inhibitors of the E3 ubiquitin-ligase Hakai*', was carried out by **Alba Casas Pais** under my supervision at the Instituto de Investigación Biomédica de A Coruña (INIBIC), and gathers the conditions of originality and scientific rigour that are required to be publicly defended and which qualify for an international PhD.

And for the record and to all appropriate purposes, I sign this certificate in A Coruña, on April 17, 2021.

FIGUEROA CONDE-VALVIS ANGELICA - 52988974X

Firmado digitalmente por FIGUEROA CONDE-VALVIS ANGELICA - 52988974X
Fecha: 2021.04.17 10:09:28 +02'00'

Signed: Angélica Figueroa Conde-Valvís

(*Director and tutor*)

CASAS PAIS ALBA - 45909584C

Firmado digitalmente por CASAS PAIS ALBA - 45909584C
Fecha: 2021.04.17 09:53:18 +02'00'

Signed: Alba Casas Pais

(*PhD student*)

ZENTRUM FÜR PATHOBIOCHEMIE
UND GENETIK
MEDIZINISCHE UNIVERSITÄT WIEN
Institut für Medizinische Genetik

Part of this research has been carried out during a predoctoral stay in 2019 at the *Institut für Medizinische Genetik*, *Medizinische Universität Wien* (Vienna, Austria), under the supervision of Dr. Helmut Dolznig. This predoctoral stay was funded by the inMOTION programme INDITEX-UDC 2019.

Aos meus pais

AGRADECIMIENTOS

Aunque pueda sonar como la típica frase que se suele decir cuando se cierra una gran etapa como es esta, lo cierto es que nunca pensé que llegaría hasta aquí. Sin embargo, y aunque el camino ha sido largo, me parece que fue ayer cuando me imaginaba el final de mi tesis doctoral como un horizonte muy lejano. Y eso es en gran parte por todas aquellas personas que me han acompañado a lo largo de todo este tiempo, haciendo el camino mucho más sencillo, y a las que quisiera dar las gracias en estas líneas.

En primer lugar, quisiera dar las gracias a mi directora, la Dra. Angélica Figueroa. Gracias por haberme abierto las puertas al mundo de la investigación, por haber apostado y confiado en mí desde que pisé por primera vez el laboratorio, y por tu optimismo inagotable, que ha sido un gran arma para combatir mis momentos de frustración.

Gracias también a los donantes de muestras, ya que sin su generosidad y altruismo una parte de esta tesis doctoral no hubiese sido posible. A Gabriela, por haberme tratado siempre con tanto cariño, por haberse interesado por mi proyecto desde el primer minuto, y por demostrarme que la investigación y la clínica pueden juntarse para remar en la misma dirección. Al Dr. Concha, por su enorme amabilidad, y por haberme ayudado pacientemente siempre que he necesitado su experiencia.

Gracias por supuesto a todos mis compañeros del INIBIC, porque en mayor o menor medida todos habéis contribuido a que esto sea un poquito más fácil. Gracias por vuestros consejos y palabras de ánimo. Porque gestos que puedan parecer pequeños como un 'oye, si lo necesitas puedes revelar en mi turno' se agradecen un montón. Y porque siempre que he necesitado ayuda he tenido a alguien dispuesto a ofrecerla. Gracias Isa y a Sara, por vuestra paciencia, y por ser la voz de la experiencia que nos da las respuestas que nadie más en el labo puede darnos. Gracias a María, por librarme de más de un embrollo administrativo y otros muchos no administrativos.

Quisiera dar las gracias en especial a Olaia, mi 'mamá de laboratorio', quien me ha ayudado a dar los primeros pasos como investigadora. Gracias por haberme enseñado una enorme parte de *lo que sé a día de hoy, por aguantar las tropecientas veces que te he interrumpido con 'Olaia, una duda', por ser mi compañera de batalla con los experimentos imposibles, y en definitiva por haberme ayudado siempre que lo he necesitado. A Andrea, por esas 'ofis' improvisadas que más de una vez nos han servido de terapia antiestrés. Por todos los buenos momentos que hemos compartido tanto dentro como fuera del laboratorio, que han hecho que este viaje sea mucho más ameno. Y, sobre todo, gracias por haberme dado tu lasaña de verduras aquel día en la cafetería, ese momento lo llevo en el corazón, jaja. A Marta, por enseñarnos a todos la innovadora técnica de hacer geles sin pocillos, y por tener siempre una sonrisa y una actitud positiva. Y también por haber rotulado con tanto empeño el 'tubo de agua para equilibrar la centri' que aún guardo de recuerdo. A Maca y Andrea, mis alumnas aventajadas. Por haberme apoyado y aguantado estos últimos meses de cuesta arriba, cuando apenas me he aguantado ni yo.*

Gracias a mis inflamadas, Oly y Jenny. Gracias por haberme hecho siempre un hueco en vuestra poyata, por ser las mejores vecinas de campana de cultivos, por vuestra amabilidad y cariño, y, en definitiva, por ser esa clase de gente de la que vale la pena rodearse. A María, porque desde que nos embarcamos juntas en el máster y después en el doctorado, has pasado de ser mi compañera a ser una gran amiga. Gracias por todas esas tardes de té que han acabado siendo terapia, por aguantarme mirando cómo picas colonias cuando tengo que hacer tiempo en cultivos, y por estar ahí siempre que lo he necesitado. A Sil, nuestra especialista en embaucarte en planes y todo tipo de actividades deportivas. Gracias por hacerme un hueco en tu grupo de Rollers, y sobre todo por tu buen humor y energía positiva. Te debo una tarde en el rocódromo.

I would also like to thank all the people in the Institute of Medical Genetics in Vienna, who welcomed me with open arms. I would like to especially thank Dr. Helmut Dolznig, for warmly welcoming me as a member of the group and for being the coolest scientist I have ever met. Thanks to Simone, for always being so nice to me, for having the best pronunciation of 'lavavajillas manual', for all the bagels we shared, and especially for becoming a friend in such a short time. To Claudia and Anna-Lena, for all the times we have lunch together at 11 a.m. in the morning and dinner at 5 p.m. in the evening (your weird schedules!), and for having visited each and every Christmas market in Vienna with me. To Faith, Carina, Janik, Julia. Thank you all for making me feel at home. You have been part of one of the best experiences of my life, and I will always carry you in my heart. I miss you so much.

A Dani. Por todos esos tejemanejes dignos de premio Nobel con los que podría escribir otra tesis. Por ser un pilar fundamental en el grupo. Porque desde que has cogido mi mano nunca me has soltado. Porque te has sacado un doctorado a mayores en buscarle solución a mis problemas, y porque tu forma de hacerme reír como nadie sabe hacerlo me ha ayudado muchas veces a dejar los agobios a un lado. Porque tu visión de la vida me ha hecho crecer como persona. Por haber *sido mi mayor apoyo. Gracias, porque sin ti nada de esto hubiese sido lo mismo. Gracias por hacerme la vida mucho más bonita.*

Por último, aunque para mí más importante, quisiera dar las gracias a mis padres, ya que sin su apoyo incondicional jamás hubiese llegado hasta este momento. Mamá, Papá, gracias por estar sempre aí, e facerme ser a persoa que son agora. Papá, gracias por apoiarme sempre en todas as miñas decisións, por querer a miña felicidade por riba de todo, e porque a cara de orgullo coa que me miras fai que me motive a seguir mellorando día a día. Mamá, non podo expresar con palabras o agradecida que estou por todo o que fixeches e segues facendo por min, pois calquera cousa que diga sería insuficiente. Aínda así, gracias, porque ninguén coma ti sabe axudarme a levantarme despois de cada pedra que atopo no camiño, por camiñar sempre da man comigo, por transmitirme todos teus os valores, por ser o meu exemplo a seguir, e por ser en definitiva a mellor nai que se pode ter. Aínda que cadaquén di de súa nai que é a mellor, a mellor téñoa eu, de iso non me cabe a menor dúbida.

Gracias a todos, de corazón.

Alba

INDEX

LIST OF ABBREVIATIONS ... VII

FIGURE INDEX ... XIII

TABLE INDEX ... XVII

SUMMARY ... XIX

I. INTRODUCTION ... 1

1. Epidemiology and etiology of cancer ... 3

2. Hallmarks of cancer: physiological alterations of tumour cells ... 4

3. Malignant tumours of epithelial origin: carcinomas ... 7

  3.1. Characteristics of carcinomas ... 7

  3.2. Colorectal cancer ... 9

    3.2.1. Genetic alterations and consensus molecular subtypes (CMS) of colorectal cancer . 10

4. Epithelial-mesenchymal transition (EMT) ... 11

  4.1. Physiological and pathological EMT ... 11

    4.2.1. Molecular regulation of EMT during tumour progression ... 13

  4.3. E-cadherin loss as a hallmark of EMT process ... 14

  4.4. Regulation of EMT by tumour microenvironment ... 16

  4.5. EMT and stemness ... 17

5. The ubiquitination system ... 19

  5.1. Ubiquitin and ubiquitination process ... 19

  5.2. Classification of E3 ubiquitin-ligases ... 20

  5.3. EMT regulation by E3 ubiquitin-ligases ... 22

  5.4. E3 ubiquitin-ligases as anticancer drug targets ... 22

6. E3 ubiquitin-ligase Hakai ... 23

  6.1. Discovery and molecular structure of E3 ubiquitin-ligase Hakai ... 23

  6.2. Physiological and pathological roles of E3 ubiquitin-ligase Hakai ... 25

    6.2.1. Hakai role during embryonic development ... 26

    6.2.2. Hakai role during tumour progression ... 26

  6.3. Hakai involvement in oncogenic signalling pathways ... 29

  6.4. E3 ubiquitin-ligase Hakai as a potential therapeutic target ... 31

7. Drug discovery: small molecule identification ... 32

  7.1. Small-molecule inhibitors for cancer treatment ... 32

  7.2. Small-molecule identification: virtual screening ... 33

II. HIPOTHESIS AND OBJECTIVES ... 35

III. MATHERIALS AND METHODS ... 39

A. MATERIALS AND METHODS RELATED TO OBJECTIVE 1 41
1. Virtual Screening and binding pocket analysis..41
    1.1. Screening of structural analogues of Hakin-1 41
2. Inhibitors, reagents and antibodies...42
3. Cell culture 44
4. Western Blotting 44
    4.1. Protein extraction from cultured cells 44
    4.2. Protein quantification by the bicinchoninic acid (BCA) method 45
    4.3. Sample preparation for Western Blotting 46
    4.4. Sodium dodecyl sulfate–polyacrylamide gel electrophoresis (SDS-PAGE) and protein transfer to PVDF membrane 46
    4.5. Antibody incubation 48
5. Ubiquitination assay..48
6. Immunoprecipitation assays 49
7. Cell cytotoxicity assay (MTT)..50
8. Cell proliferation assay (BrdU)...51
9. Phenotypic characterization...52
10. Gene expression analysis by quantitative polymerase chain reaction (qPCR) 52
    10.1. Purification of total RNA from cultured cells 52
    10.2. cDNA synthesis from isolated RNA 53
    10.3. Real time quantitative Reverse Transcription PCR (RT-qPCR) 53
11. Immunofluorescence assay 54
12. Cell migration assays 55
    12.1. Wound healing assay 55
    12.2. Boyden chamber migration assay...56
13. Cell invasion assay...57
14. Soft agar colony formation assay...57
15. Tumour xenograft model 58
16. Histological techniques 59
    16.1. Sectioning of paraffin-embedded tissue 59
    16.2. Immunohistochemistry assay for Paraffin-Embedded Sections (IHQ-P) 59
    16.3. Hematoxylin and eosin (H&E) staining...60
17. *In vivo* TUNEL assay 61
18. Quantification of lung micrometastasis from *in vivo* mouse model......................................61
    18.1. DNA extraction from FFPE tissue samples 61
    18.2. Micrometastasis detection by quantitative polymerase chain reaction (qPCR) 62

19. Statistical analysis 63

B. MATERIALS AND METHODS RELATED TO OBJECTIVE 2 65

1. Antibodies 65

2. Cell culture 65

3. Establishment of spheroid cultures (3D) from human colorectal cancer cell lines 66

3.1 Multicellular spheroid formation (3D culture) from human colorectal cancer cell lines 66

3.2. Co-culture of colorectal cancer spheroids with cancer-associated fibroblasts (CAFs) 66

3.2.1. Production of silicone casting devices for collagen gels 66

3.2.2. Embedding of colorectal cancer spheroids and CAFs in collagen gels 67

4. Immunofluorescence assay for collagen gels 69

5. Collagen gel spheroid invasion assay 69

5.1. Knockdown of Hakai by siRNA transfection 70

5.2. Spheroid embedding in collagen gels 70

6. Near-Infrared Western Blot detection 71

7. Collagen gel contraction assay 72

8. Culture of colon cancer cell lines in CAF conditioned medium 73

9. Establishment of patient-derived colorectal organoid culture 74

9.1. Preparation of specific mediums for patient-derived colorectal organoid culture 74

9.2. Isolation of patient-derived colorectal cancer stem cells. 76

10. Cancer Stem Cell tumorsphere formation 77

11. Analysis of the expression levels of stem and differentiation markers by qPCR. 78

12. Analysis of mRNA expression of stem markers in FFPE tumour samples from *in vivo* xenograft mouse model 79

IV. RESULTS 81

A. RESULTS RELATED TO OBJECTIVE 1 83

1. Search for potential small-molecule inhibitors of E3 ubiquitin-ligase Hakai by *in silico* screening 83

2. Hakin-1 small-molecule inhibitor reduces Hakai-induced ubiquitination of E-cadherin 84

2.1. Hakin-1 blocks Hakai-E-cadherin interaction 84

2.2. Hakin-1 reduces Hakai-induced ubiquitination 85

2.3. Hakin-1 inhibits Hakai-induced ubiquitination of E-cadherin complex 85

2.4. Hakin-1 treatment inhibits E-cadherin degradation 86

3. Hakin-1 reduces cell viability, proliferation, migration, invasion and oncogenic potential while increases cell differentiation *in vitro*. 87

3.1. Hakin-1 reduces cell viability 87

3.2. Hakin-1 reduces cell proliferation 88

3.3. Hakin-1 increases epithelial cell differentiation 90

        - 3.3.1. Hakin-1 reverts mesenchymal phenotype in colorectal cancer cell lines 90
        - 3.3.2. Hakin-1 modulates the protein expression levels of EMT markers 91
        - 3.3.3. Hakin-1 increases E-cadherin expression at cell-cell contacts 94
    - 3.4. Hakin-1 reduces cell invasion 95
    - 3.5. Hakin-1 reduces cell migration 96
    - 3.6. Hakin-1 reduces oncogenic potential 96
- 4. Hakin-1 shows an additive but not a synergistic effect in combination with 5-FU 97
    - 4.1. Hakin-1 shows an additive cytotoxic effect in combination with 5-fluorouracil 98
    - 4.2. Hakin-1 shows an additive antiproliferative effect in combination with 5-fluorouracil ... 99
    - 4.3. Hakin-1 does not show a synergistic effect on cell migration in combination with 5-fluorouracil 99
- 5. Analysis of novel Hakin-1 analogues *in vitro* 100
    - 5.1. Effect of Hakin-1 analogues on cell viability 101
    - 5.2. Effect of Hakin-1 analogues in Hakai-induced ubiquitination 102
    - 5.3. Effect of Hakin-1 analogues on epithelial phenotype 103
    - 5.4. Effect of Hakin-1 analogues on E-cadherin subcellular localization 104
- 6. Effect of Hakin-1 on tumour progression and carcinogenesis *in vivo* 106
    - 6.1. Hakin-1 decreases tumour size and induces cell differentiation *in vivo* 106
    - 6.2. Hakin-1 reduces on cell proliferation and angiogenesis, while no effect was detected on apoptosis 108
    - 6.3. Hakin-1 regulates the expression of EMT-related markers 110
    - 6.4. Hakin-1 inhibits lung micrometastases *in vivo*. 111
    - 6.5. Hakin-1 treatment does not cause cytotoxicity in liver and kidney 112

B. RESULTS RELATED TO OBJECTIVE 2 115

- 1. Study of Hakai role in tumour progression in a co-culture model of colon cancer tumour spheroids and cancer-associated fibroblasts (CAFs) 115
    - 1.1. Establishment of co-culture model of multicellular tumour spheroids and CAFs 115
    - 1.2. Analysis of Hakai and E-cadherin subcellular localization in co-cultures of multicellular tumour spheroids and CAFs 116
    - 1.3. Effect of Hakai silencing on the development of invasive structures in colorectal cancer spheroids embedded into a collagen matrix 119
    - 1.4. Effect of Hakai transient knockdown in contractility of cancer-associated fibroblasts .. 120
    - 1.5. Study of Hakai involvement in the interaction between CAFs and carcinoma cells during tumour progression 121
- 2. Analysis of the potential role of Hakai in the acquisition of stem properties 122
    - 2.1. Establishment of patient-derived colorectal organoid culture 122
    - 2.2 Hakai expression is remarkably increased in tumorsphere cultures 124

2.3. Hakin-1 reduces the expression of stem markers and increases the expression of differentiation markers *in vitro* 125

2.4. Hakin-1 reduces the expression of NANOG, SOX2 and c-MYC stem markers *in vivo* 127

V. DISCUSSION 129

VI. CONCLUSIONS 143

VII. REFERENCES 147

VIII. APPENDIXES 167

APPENDIX A 169

APPENDIX B 185

APPENDIX C 209

LIST OF ABBREVIATIONS

5-FU	5-fluorouracil
ABC	ATP-binding cassette
ANPEP	Alanyl aminopeptidase
ATCC	American Type Culture Collection
ATP	Adenosine triphosphate
BCA	Bicinchoninic Acid
BSA	Bovine serum albumin
bHLH	Basic helix-loop-helix
BMPs	Bone morphogenic proteins
BrdU	Bromodeoxyuridine (5-bromo-2'-deoxyuridine)
BSA	Bovine serum albumin
Bcl-2	B-cell lymphoma-2
°C	Degree Celsius
Ca^{+2}	Calcium
CAFs	Cancer-associated fibroblasts
CBL	Casitas B-lineage lymphoma
CDH1	Cadherin 1, E-cadherin
cDNA	Complementary deoxyribonucleic acid
CDX2	Caudal type homeobox 2
CMS	Consensus molecular subtype
CO_2	Carbon dioxide
CRC	Colorectal cancer
CRLs	Cullin-RING ubiquitin-ligases
CSCs	Cancer stem cells
DAB	3,3'- Diaminobenzidine
DAPI	4′,6-diamidino-2-phenylindole
DEPC	Diethyl pyrocarbonate
DNA	Deoxyribonucleic acid
DMEM	Dulbecco's Modified Eagle's Medium
DMSO	Dimethyl sulfoxide

DUBs	Deubiquitinating enzymes
ECM	Extracellular matrix
EGFR	Epidermal growth-factor receptor
EGFR-TKIs	Tyrosine kinase inhibitors of the epidermal growth factor receptor
EGM	Endothelial Cell Growth Medium
EMP	Epithelial-mesenchymal plasticity
EMT	Epithelial-mesenchymal transition
EMT-TFs	Epithelial-mesenchymal transition inducing transcription factors
ERα	Estrogen receptor alpha
FBS	Fetal bovine serum
FDA	U.S. Food and Drug Administration
FFPE	Formalin-fixed paraffin-embedded
g	Gravitational force equivalent (g-force)
GAPDH	Glyceraldehyde 3-phosphate dehydrogenase
GSK-3β	Glycogen synthase kinase-3β
Hakai-MDCK	Hakai-overexpressing MDCK cells
Hakin-1	Hakai inhibitor 1
HCC	Hepatocellular carcinoma
HDI	Human Development Index
H&E	Hematoxylin and eosin
HECT	Homologous to E6-associated protein carboxyl terminus
hESCs	Human embryonic stem cells
HIF-1α	Hypoxia inducible factor-1α
HISC	Human Intestinal Stem Cell medium
HPRT	Hypoxanthine guanine phosphoribosyl transferase
HTS	High throughput screening
HRP	Horseradish peroxidase
HYB	Hakai-pY-binding
IC_{50}	Half maximal inhibitory concentration
IHC-P	Immunohistochemistry for paraffin embedded samples
KLF4	Kruppel-like factor 4
JAMs	Junction adhesion molecules

KU	Kunitz unit
LGR5	Leucine-rich repeat-containing G-protein coupled receptor 5
LOH	Loss of heterozygosity
m^6A	N^6-Methyladenosine
mA	Milliampere
MDCK	Madin Darby Canine Kidney
mESC	Mouse embryonic stem cell
MET	Mesenchymal-epithelial transition
mg/kg	Milligrams per kilogram
miRNA	Micro ribonucleic acid
ml	Millilitre
mM	Millimolar
MMPs	Matrix metalloproteinases
mRNA	Messenger RNA
MSI	Microsatellite instability
MTT	3-(4,5-dimethylthiazol-2-yl)-2,5-diphenyltetrazolium bromide
MYC	MYC proto-oncogene, bHLH transcription factor
NaCl	Sodium chloride
NANOG	Nanog homeobox
NEM	N-ethylmaleimide
ng	Nanogram
nm	Nanometre
nM	Nanomolar
No	Number
NSCLC	Non-small-cell lung carcinoma
NTC	Non-targeting negative control
nmol	Nanomole
PBS	Phosphate-buffered saline
PBST	Phosphate-buffered saline, 0.1% Triton X-100
PCR	Polymerase Chain Reaction
PIK3CA	Phosphatidylinositol-4,5-bisphosphate 3-kinase catalytic subunit alpha
pmol	Picomole

PMSF	Phenylmethylsulfonyl fluoride
PPIs	Protein-protein interactions
PROTACs	Proteolysis-targeting chimeras
PSF	Polypyrimidine tract-binding protein-associated splicing factor
pTyr	Tyrosine-phosphorylated, phosphotyrosine
PVDF	Polyvinylidene difluoride
PKD1	Protein kinase D1
qPCR	Quantitative polymerase chain reaction
RB	Retinoblastoma protein
RBPs	Ribonucleic acid binding proteins
RBR	RING-between-RING
RING	Really interesting new gene
RNA	Ribonucleic acid
RPL13	Ribosomal protein L13
RPLP0	Ribosomal protein lateral stalk subunit P0
rpm	Revolutions per minute
RPMI	Roswell Park Memorial Institute
RPS5	Ribosomal protein S5
RT	Room temperature
RT-qPCR	Quantitative Reverse Transcription Polymerase Chain Reaction
RT-PCR	Reverse Transcription Polymerase Chain Reaction
SD	Standard deviation
SDS	Sodium dodecyl sulfate
SDS-PAGE	Sodium dodecyl sulfate-polyacrylamide gel electrophoresis
SEM	Standard error of the mean
siRNA	Small interfering ribonucleic acid
Slug	Snail family transcriptional repressor 2
Snai1	Snail family transcriptional repressor 1
SOX2	SRY-box transcription factor 2
Src	Proto-oncogene tyrosine-protein kinase Src
TBST	Tris buffered saline-Tween 20
TBST	Tris buffered saline, 0.1% Triton X-100

TGF-β	Transforming growth factor-β
TME	Tumour microenvironment
TNF	Tumour necrosis factor
TPD	Targeted protein degradation
Tris-HCl	Tris-hydrochloride
TUNEL	Terminal deoxynucleotidyl transferase dUTP nick end labelling
Twist1	Twist basic helix-loop-helix transcription factor 1
Twist2	Twist basic helix-loop-helix transcription factor 2
V	Volt
VEGF	Vascular endothelial growth factor
VS	Virtual screening
ZEB1	Zinc finger E-box-binding homebox 1
ZEB2	Zinc finger E-box-binding homebox 2
ZO-1	Zonula occludens protein 1
µg	Microgram
µl	Microlitre
µm	Micrometre
µM	Micromolar

FIGURE INDEX

Figure 1. Estimated number of new cases of cancer and number of cancer-related deaths in 2020, in both sexes 3

Figure 2. Hallmarks of cancer. Schematic representation of the biological capabilities acquired during malignant transformation of tumour cells....................5

Figure 3. Schematic representation of epithelial cell-cell junctions (tight junctions, adherens junctions and desmosomes) and cell-matrix junctions (hemidesmosomes) 8

Figure 4. Major events that take place during tumour progression and metastasis....................9

Figure 5. Schematic representation of genetic changes that are associated with the adenoma-carcinoma sequence in colorectal cancer 10

Figure 6. Schematic representation of consensus molecular subtypes (CMS) of colorectal cancer.. 11

Figure 7. Molecular and phenotypic changes that epithelial cells undergo during EMT process 13

Figure 8. Structural organization of E-cadherin protein at adherens junctions....................15

Figure 9. Activation of EMT process by stromal cell-secreted factors....................17

Figure 10. The ubiquitin conjugation system....................20

Figure 11. Catalytic mechanisms of RING, HECT and RBR E3 ubiquitin-ligases....................21

Figure 12. Hakai-mediated disruption of adherens junctions....................24

Figure 13. Comparison of the structure of pTyr binding domain between Hakai and Cbl E3 ligases....................25

Figure 14. Schematic representation of Hakai upstream signaling pathways....................30

Figure 15. *In silico* screening of small-molecule inhibitors of the E3 ubiquitin-ligase Hakai 83

Figure 16. Effect of Hakin-1 on Hakai-E-cadherin interaction....................84

Figure 17. Hakin-1 effect on Hakai-dependent ubiquitination 85

Figure 18. Effect of Hakin-1 treatment on Hakai-mediated ubiquitination of E-cadherin complex 86

Figure 19. Effect of Hakin-1 on E-cadherin degradation..87

Figure 20. Hakin-1 treatment reduces cell viability of epithelial tumour cell lines......................88

Figure 21. Antiproliferative effect of Hakin-1 in tumour epithelial cells..................................89

Figure 22. Effect of Hakin-1 in different human cancer cells..90

Figure 23. Hakin-1 effect on epithelial phenotype in cancer cell lines......................................91

Figure 24. Effect of Hakin-1 on epithelial differentiation in HT29 cells....................................92

Figure 25. Effect of Hakin-1 on epithelial differentiation in LoVo cells....................................92

Figure 26. Effect of Hakin-1 on E-cadherin and Hakai mRNA expression levels......................93

Figure 27. Hakin-1 effect on E-cadherin expression at cell-cell contacts..................................94

Figure 28. Hakin-1 reduces cell invasion in epithelial tumour cells..95

Figure 29. Hakin-1 reduces cell migration in HT29 tumour cells..96

Figure 30. Effect of Hakin-1 treatment in the acquisition of anchorage independent cell growth in epithelial cells..97

Figure 31. Additive effect of Hakin-1 and 5-fluorouracil (5-FU) on cell viability.....................98

Figure 32. Hakin-1 shows an additive antiproliferative effect in combination with 5-fluorouracil (5-FU)..99

Figure 33. Effect of Hakin-1 on cell migration in combination with 5-fluorouracil................100

Figure 34. Effect of Hakin-1 analogues on cell viability...101

Figure 35. Effect of Hakin-1 analogues on Hakai-mediated ubiquitination..............................102

Figure 36. Effect of Hakin-A7 on Hakai-mediated ubiquitination..103

Figure 37. Effect of Hakin-1 analogues on epithelial phenotype...104

Figure 38. Effect of analogue compounds of Family A on E-cadherin expression at cell-cell contacts 105

Figure 39. Effect of analogue compounds of Family B on E-cadherin expression at cell-cell contacts..105

Figure 40. Hakin-1 effect on tumour growth and phenotype in immunodeficient mice (BALB/c, nu/nu)...107

Figure 41. Hakin-1 effect on cell proliferation *in vivo*..108

Figure 42. Hakin-1 does not affect cell apoptosis in tumour xenograft mouse model..............109

Figure 43. Effect of Hakin-1 on angiogenesis...110

Figure 44. Effect of Hakin-1 on expression levels of EMT markers and Hakai substrate Cortactin *in vivo*..111

Figure 45. Effect of Hakin-1 on Hakai expression levels in xenografted tumours *in vivo*........111

Figure 46. Effect of Hakin-1 on macro- and micrometastasis formation.................................112

Figure 47. Intact cell morphology and tissue structure of liver and kidney in xenograft mouse model upon treatment with Hakin-1...113

Figure 48. Establishment of colorectal cancer spheroids..115

Figure 49. Co-culture of colorectal cancer spheroids and cancer-associated fibroblasts (CAFs)... 116

Figure 50. Hakai and E-cadherin subcellular localization in co-cultures of colorectal cancer spheroids and cancer-associated fibroblasts (CAFs)..117

Figure 51. Hakai and E-cadherin subcellular localization in co-cultures of colorectal cancer spheroids and cancer-associated fibroblasts (CAFs)..118

Figure 52. Effect of Hakai transient knockdown in the development of invasive structures.......120

Figure 53. Effect of Hakai transient knockdown in contraction capacity of cancer-associated fibroblasts..121

Figure 54. Hakai expression levels in colorectal cancer cell lines under treatment with CAF conditioned medium...122

Figure 55. Establishment of patient-derived colorectal organoid culture................................124

Figure 56. Analysis of the potential role of Hakai in the acquisition of stem properties............125

Figure 57. Effect of Hakin-1 on the acquisition of stem properties *in vitro*..............................126

Figure 58. Effect of Hakin-1 on the expression levels of stem markers *in vivo*..........................127

TABLE INDEX

Table 1. Hakai inhibitor compound 1 (Hakin-1) used for *in vitro* and *in vivo* assays, and analogue compounds used for *in vitro* assays..42

Table 2. Primary and secondary antibodies used for Western Blot, Immunoprecipitation, Immunofluorescence, and Immunohistochemistry for paraffin embedded samples (IHC-P) 43

Table 3. Composition of the 1% Triton X-100 lysis buffer used for protein extraction................45

Table 4. Composition of 10% acrylamide gels used for SDS-PAGE..47

Table 5. Forward and reverse sequences of primers used for RT-qPCR......................................54

Table 6. Primary and secondary antibodies used for Western Blot and immunofluorescence assays..65

Table 7. Composition of collagen gel solution...68

Table 8. Composition of acrylamide gels used for SDS-PAGE in Near-Infrared detection Western Blot..72

Table 9. Composition of collagen gel solution for CAF contraction assays.................................73

Table 10. Composition of disinfection medium used for organoid culture.................................75

Table 11. Composition of human intestinal stem cell medium (HISC) used for organoid culture 75

Table 12. Composition of stem cell medium used for tumorsphere culture................................78

Table 13. Forward and reverse sequences of primers used for RT-qPCR..................................79

SUMMARY

RESUMEN

El carcinoma es el tipo más frecuente de cáncer, y surge de la transformación maligna de las células epiteliales. Durante las etapas tempranas de la progresión tumoral, tiene lugar un proceso conocido como transición epitelio-mesénquima (TEM). La TEM se caracteriza por una expresión disminuida de la E-cadherina, un supresor tumoral responsable de los contactos célula-célula en el epitelio. La E3 ubiquitina-ligasa Hakai fue el primer regulador postraduccional descrito de la E-cadherina, y su importancia durante la progresión tumoral ha sido ampliamente descrita. En los últimos años, las enzimas E3 ubiquitina-ligasas han cobrado importancia como dianas terapéuticas, ya que su inhibición específica evitaría efectos secundarios más amplios en comparación con otros miembros de la vía ubiquitina-proteasoma. Además, la TEM se ha asociado con otros aspectos de la progresión tumoral, tales como el desarrollo de resistencia a fármacos o la adquisición de propiedades de célula madre tumoral (CSC). Los objetivos del presente proyecto fueron la identificación y validación de un inhibidor de pequeña molécula de la E3 ubiquitina-ligasa Hakai, y el estudio del papel de Hakai en la adquisición de propiedades de CSC y otros aspectos de la progresión tumoral. Los resultados obtenidos mostraron que el inhibidor de Hakai (Hakin-1) no solo reduce la ubiquitinización de E-cadherina mediada por Hakai, sino que además muestra un importante efecto antitumoral tanto *in vitro* como *in vivo*, siendo por tanto un prometedor agente terapéutico para el tratamiento del cáncer mediante la inhibición de la TEM. Por otro lado, Hakai podría estar implicado en el desarrollo de CSCs, lo que abre una nueva vía de estudio para superar la resistencia a fármacos.

RESUMO

O carcinoma é o tipo máis frecuente de cancro, e xorde da transformación maligna das células epiteliais. Durante as primeiras etapas da progresión tumoral, ocorre un proceso coñecido como transición epitelio-mesénquima (TEM). A TEM caracterízase por unha expresión diminuída da E-cadherina, un supresor tumoral responsable das unións célula-célula no epitelio. A E3 ubiquitina-ligasa Hakai foi o primeiro regulador postraducional descrito da E-cadherina, e a súa importancia durante a progresión tumoral está amplamente descrita. Nos últimos anos, as enzimas E3 ubiquitina-ligasas gañaron importancia como dianas terapéuticas, xa que a súa inhibición específica podería evitar efectos secundarios máis amplos en comparación con outros membros da vía ubiquitina-proteasoma. Ademais, a TEM está asociada con outros aspectos da progresión tumoral, como por exemplo o desenvolvemento de resistencia a fármacos ou a adquisición de propiedades de célula nai tumoral (CSC). Os obxectivos do presente traballo foron a identificación e validación dun inhibidor de pequena molécula da E3 ubiquitina-ligasa Hakai, e o estudo do papel de Hakai na adquisición de características de CSC e outros aspectos da progresión tumoral. Os resultados obtidos amosaron que o inhibidor de Hakai (Hakin-1) non só reduce a ubiquitinización de E-cadherina mediada por Hakai, senón que ademais amosa un importante efecto antitumoral tanto *in vitro* como *in vivo*, sendo polo tanto un prometedor axente terapéutico para o tratamento do cancro mediante a inhibición da TEM. Por outra banda, Hakai podería estar implicado no desenvolvemento de CSCs, o que abre unha nova vía de estudo para superar a resistencia a fármacos.

ABSTRACT

Carcinoma is the most common type of cancer, and arises from the malignant transformation of epithelial cells. At the early stages of carcinoma progression, a process known as epithelial-mesenchymal transition (EMT) takes place. EMT is characterized by the downregulation of E-cadherin, a tumour suppressor responsible for cell adhesion in the epithelium. The E3 ubiquitin-ligase Hakai was the first reported posttranslational regulator of the E-cadherin stability, and its importance during tumour progression and disease has been widely demonstrated. E3 ubiquitin-ligase enzymes have recently emerged as promising therapeutic targets, as their specific inhibition would avoid wider side effects compared to other members of the ubiquitin pathway. EMT has also been associated with other aspects of tumour progression, such as the acquisition of therapeutic resistance or the development of cancer stem cells (CSCs). The aims of this project were the identification and validation of a small-molecule inhibitor for the E3 ubiquitin-ligase Hakai, and the study of the involvement of Hakai in the acquisition CSC properties and other aspects of tumour progression. Results showed that Hakai inhibitor (Hakin-1) reduced Hakai-dependent ubiquitination of E-cadherin, showing an important antitumor effect both *in vitro* and *in vivo*, therefore being a promising therapeutic agent for cancer treatment through the inhibition of EMT. On the other hand, Hakai may play a role in the development of CSCs, opening a new research field to overcome therapeutic resistance.

I. INTRODUCTION

1. Epidemiology and etiology of cancer

Cancer represents a high prevalence disease and the second leading cause of death worldwide, behind cardiovascular disease. According to the last data published by the World Health Organization, cancer burden has increased to 19.3 million new cases and 10 million cancer deaths in 2020, which is due to several factors, such as ageing and population growth. Around 22.6% of men and 18.6% of women develop cancer in their lifetime, and 12.6% of men and 8.9% of women die from this disease. Moreover, the number of new cancer cases is expected to increase from 19.3 million in 2020 to 30.2 million in 2040.

Taking into consideration the data provided by GLOBOCAN database in 2020, breast cancer (11.7%), lung cancer (11.4%) and colorectal cancer (CRC) (10%) represent the three types of cancer with the highest incidence worldwide, considering both men and women (**Figure 1A**). Regarding the mortality rate, lung cancer is responsible for the largest number of deaths (18%), followed by colorectal cancer (9.4%) and liver cancer (8.3%). Breast cancer ranks in fifth position (6.9%) despite its high incidence, as it is usually associated with a favourable outcome (**Figure 1B**).

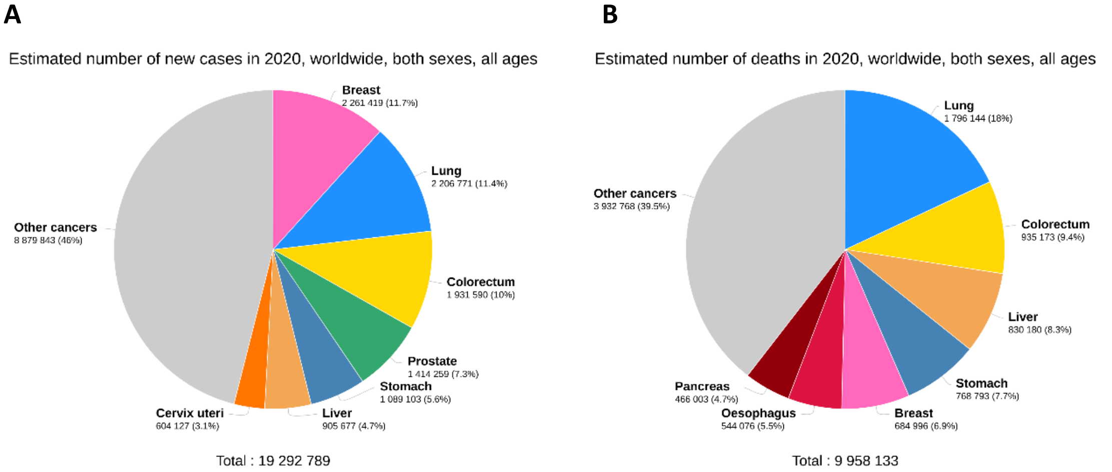

Figure 1. Estimated number of new cases of cancer and number of cancer-related deaths in 2020, in both sexes. (**A**) Pie-chart of estimated number of new cases of different cancers. (**B**) Pie-chart of estimated number of deaths related to different cancer types. Images obtained from GLOBOCAN 2020 database (International Agency for Research on Cancer).

In terms of cancer incidence depending on gender, breast cancer is the most frequently diagnosed cancer in women (24.5%), followed by colorectal cancer (9.4%) and lung cancer (8.4%). Breast cancer is also the leading cause of cancer-related death in women (15.5%), followed by lung cancer (13.7%) and colorectal cancer (9.5%). On the other hand, lung cancer is the one with the highest incidence in men (14.3%), being prostate (14.1%) and colorectum (10.6%) the second and third most common type of cancer in this gender, respectively. Regarding the number of deaths, lung cancer is also the leading cause of cancer death in men (21.5%), followed by liver cancer (10.4%) and colorectal cancer (9.3%).

Concerning the geographical distribution of cancer incidence, in a great number of cancers, incidence rates in countries with an elevated Human Development Index (HDI) are higher (around 2-3 times as much) than in those countries with a lower HDI. Nevertheless, the differences in mortality rates between countries with high and low HDI are smaller. This is because the incidence of cancers related with a poor survival is higher in countries with lower HDI and the access to early diagnosis and effective treatment in such countries is more complicated. Lung cancer ranks first in incidence in both countries with high and low HDI in males, followed by prostate cancer. In females, breast cancer is located in first place in both developed and developing countries. In this case, colorectal cancer ranks in second place in developed countries, while cervical cancer is the one that is in second position in countries with lower HDI. In the case of Spain, colorectal cancer is the most prevalent cancer (14.3%), followed by prostate cancer (12.3%) and breast cancer (12.1%) [1].

Cancer is a heterogeneous disease that arises from the transformation of normal cells into tumour cells. This malignant transformation is the result of a multistep process in which the interaction between genetic factors and the exposition to external agents takes place. While only 5-10% of cancers can be attributed to genetic causes, most cases (90-95%) are driven by environmental factors [2,3]. About one in three cancer-related deaths are due to widely described behavioural and dietary risks, such as high body mass index, lack of physical activity, unhealthy eating habits, and tobacco and alcohol use [4–6]. Moreover, cancer development is also determined by the exposition to external agents such as ultraviolet and ionizing radiation, chemical carcinogens (asbestos, arsenic, or aflatoxins) and certain chronic infections (Helicobacter pylori, Human papillomavirus (HPV), Hepatitis B and C virus, or Epstein-Barr virus). Therefore, cancer burden can be reduced not only by an early detection and treatment, but also by avoiding the above-mentioned risk factors [7].

2. Hallmarks of cancer: physiological alterations of tumour cells

Tumour progression is a multistep and complex process that involves multiple genetic alteration, causing changes at a molecular and a cellular level, thus resulting in a progressive transformation of normal cells into malignant ones. Six characteristic biological capabilities that cells acquire during carcinogenesis, known as hallmarks of cancer, been described. These acquired characteristics include: 1) sustaining proliferative signalling, 2) insensitivity to growth suppressors, 3) evasion of cell death (apoptosis), 4) acquisition of unlimited replicative potential, 5) ability to induce angiogenesis, and 6) ability to invade new tissues and metastasize [8] (**Figure**

2). In the last years, two additional hallmarks have been described: 7) reprogram of energy metabolism and 8) evasion of immune system [9].

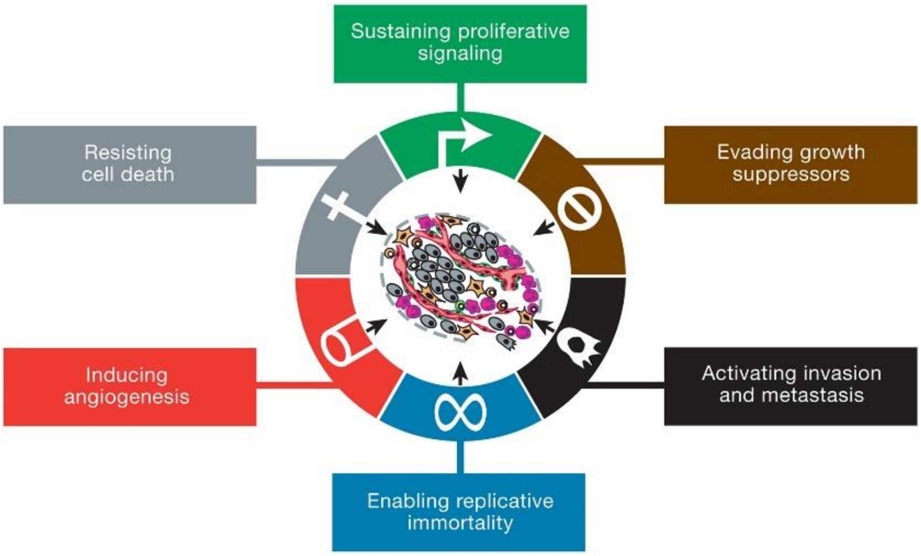
Sustaining proliferative signaling
Resisting cell death
Evading growth suppressors
Inducing angiogenesis
Activating invasion and metastasis
Enabling replicative immortality

Figure 2. Hallmarks of cancer. Schematic representation of the biological capabilities acquired during malignant transformation of tumour cells. Image obtained from Hanahan and Weinberg, 2011.

- *Sustained cell growth signalling:* One of the fundamental features of cancer cells is their ability to proliferate over time [10]. Normal tissues control the production and release of signals that promote cell growth and division, thus ensuring the maintenance of cell number and tissue homeostasis. However, in tumour cells, specific characteristics are acquired that cause these signals to be deregulated and the proliferative controls necessary for tissue homeostasis to be evaded. These include the generation of their own growth factor ligands, the increased levels of receptor proteins displayed at the cell surface or the signal stimulation of normal cells within the tumour stroma, which in turn produce growth factors that stimulate back the tumour cells [9].

- *Avoidance of growth-inhibiting signals:* In addition to the above-mentioned ability of cancer cells to induce and sustain cell proliferation, they also must avoid programs that negatively regulate this process, which are mostly dependent on tumour suppressor genes. Retinoblastoma protein (RB) and p53 proteins represent the two prototype and best characterized tumour suppressors. On the one hand, RB protein inhibits cell proliferation at the G1/S transition level, through the transcriptional repression of E2F transcription factor. Growth factor signals stimulate the inactivation of RB protein by the activation of Cyclin D and Cyclin-dependent kinases that phosphorylate RB, thus causing the dissociation of E2F from RB and the subsequent activation of the cell cycle [11]. On the other hand, p53 acts as one of the most important barriers against malignant transformation through the regulation of cell cycle arrest, senescence, and apoptosis. While RB protein transduces signals that originate mainly outside the cell, p53 links many stress response pathways such as hypoxia, DNA damage and oxidative stress, acting as a transcriptional regulator [12,13]. Besides growth suppressors, there is another way of growth inhibition that is mediated by cell-cell contacts, also known as contact inhibition. This process has been widely observed *in vitro* for normal cells, which form monolayers and inhibit growth once they have reached a full confluence. However, this contact inhibition is abolished in cancer cells [9].

- *Cell death resistance*: Another barrier that tumour cells escape during cancer development is cell death by apoptosis. This process is triggered by physiological stress that occurs during tumour progression, such as DNA damage caused by excessive proliferation, or as a result of anticancer therapy. Apoptosis can be induced through the activation of both intrinsic and extrinsic pathways, which converge in the activation of proteolytic enzymes such caspases, a family of cysteine proteases that act as death effector molecules. In the intrinsic ('mitochondrial') pathway, caspase activation involves the permeabilization of B-cell lymphoma-2 (Bcl-2) proteins from the mitochondrial outer membrane [14]. On the other hand, in the extrinsic ('receptor') pathway, activation of caspases is initiated through the activation of death receptors such as tumour necrosis factor (TNF) receptor family [15,16].

- *Unlimited replicative potential*: unlike most normal cells, which are only able to replicate a limited number of times, cancer cells are able to pass through an unlimited number of successive division cycles. The limited replicative potential is maintained by two fundamental barriers: senescence and cell death (apoptosis). Once cells have divided a certain number of times, they enter the senescence state, and those who are able to overcome this first barrier then enter the apoptosis process. The overcoming of this second barrier causes the acquisition of unlimited replicative potential, in a process that has been termed as immortalization [9]. The mechanism of acquisition of replicative senescence remained unknown until the discovery of telomere erosion and telomerase. Telomeres are composed of repetitive DNA sequences that protect the ends of chromosomes from degradation and recombination. They shorten progressively in each cell division, as DNA polymerases need RNA-based priming in the lagging DNA strand and they work unidirectionally. Therefore, the length of telomeric DNA has been proposed as a 'molecular clock' that dictates the number of divisions a cell can undergo before reaching replicative senescence. Telomerase is the responsible enzyme for adding telomeric DNA repeats to the telomere, and it is almost absent in normal cells. However, it is increased in cancer cells and other spontaneously immortalized cells. The increase of telomeric DNA by telomerase counters the progressive shortening that telomeres suffer under normal conditions, thus conferring an endless replicative potential [17,18].

- *Angiogenesis induction:* As well as normal tissues, tumours need to be provided with nutrients and oxygen and at the same time they need to remove metabolic wastes and carbon dioxide. To address these requirements, a tumour-associated vasculature is generated through angiogenesis.

In normal conditions, this process takes place during embryogenesis and after that it remains quiescent, except in some physiological processes such as wound healing and female reproductive cycling, in which it is activated in a transient way. Conversely, during tumour progression, angiogenesis is almost constantly activated, thus causing normally quiescent vasculature to develop new vessels that enhance tumour growth [9,19].

- *Invasive and metastatic capacity*: A number of cells that are present in the primary tumour are able to invade adjacent tissues, intravasate both in blood and lymph vessels (which allows their passive transport to distant organs), extravasate into the parenchyma of distant tissues and give rise to metastasis in secondary organs that are located far away from the primary tumour. This multistep process of invasion and metastasis is also known as invasion-metastasis cascade [20]. Metastatic cancer cells usually develop alterations in their shape as well as in the adhesion to other cells and the extracellular matrix (ECM), as a result of a process named epithelial-mesenchymal transition (EMT) [21], which will be explained in detail in the following sections.

3. Malignant tumours of epithelial origin: carcinomas

3.1. Characteristics of carcinomas

Carcinomas arise as a result of the transformation of epithelial cells and nowadays represent around 90 per cent of all human cancers, since epithelial tissues are the most abundant throughout the body. The epithelium covers all the exposed parts of the body, including the external skin, the inner lining of the digestive tract, and the lining of the cavities of every organ.

Epithelial cells exhibit an apicobasal polarization and are characterized by a localized distribution of adhesion molecules (such as cadherins and integrins), by the polarized organization of the cytoskeleton, and by the presence of a basement membrane. They are connected to each other through cell-cell junctions, which are essential for the maintenance of tissue homeostasis, forming a layer of cells that serves as a barrier between the internal and external environments [22,23]. There are four different types of cell-cell junctions: 1) tight junctions, mainly composed of occludin, claudines and junction adhesion molecules (JAMs) and responsible for the regulation of the diffusion of ions and solutes in the paracellular space and the maintenance of the cell polarity by the regulation of the segregation of proteins and lipids from the membrane; 2) adherens junctions, where cadherins represent the main type of transmembrane proteins and that are responsible for the maintenance of cell-cell adhesion through the regulation of the actin cytoskeleton and the activation of signalling pathways; 3) gap junctions, aggregates of intercellular channels composed of connexin hexamers that allow the direct cell-cell transfer of small molecules and ions; and 4) desmosomes, which are composed of two subtypes of transmembrane cadherins (desmocollin and desmoglein) as well as adaptor proteins (plakoglobin, plakophillin, and desmoplakin), responsible for the binding to cytokeratin intermediate filaments [24–26] (**Figure 3**).

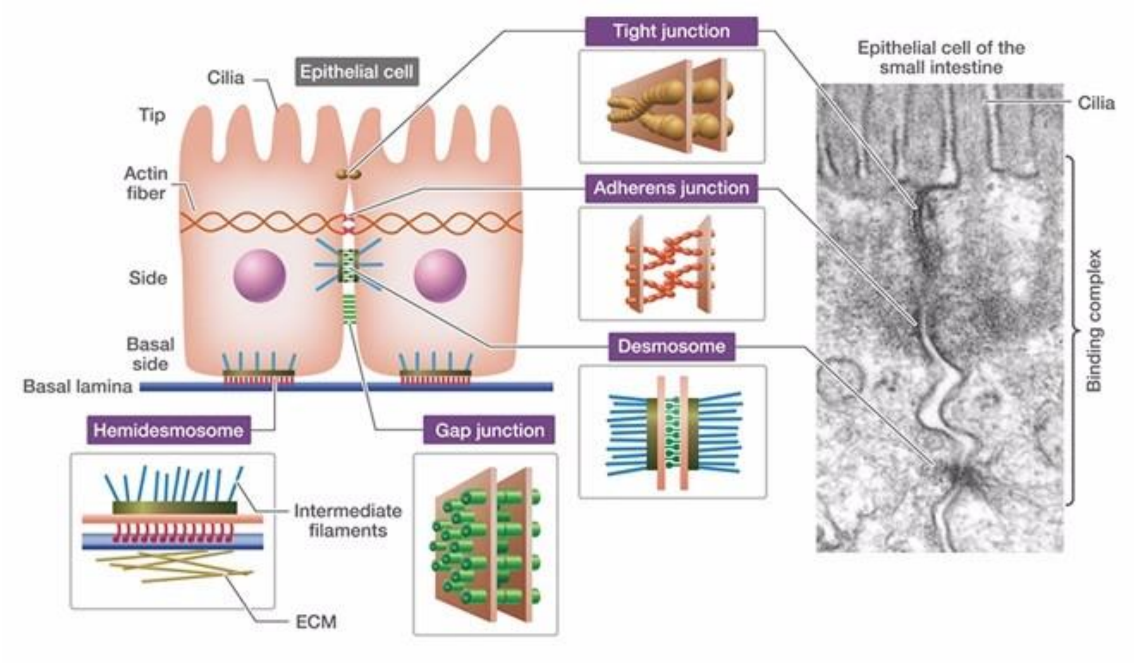
Tight junction
Epithelial cell of the small intestine
Cilia
Epithelial cell
Cilia
Tip
Actin fiber
Adherens junction
Side
Binding complex
Basal side
Desmosome
Basal lamina
Hemidesmosome
Gap junction
Intermediate filaments
ECM

Figure 3: Schematic representation of epithelial cell-cell junctions (tight junctions, adherens junctions and desmosomes) and cell-matrix junctions (hemidesmosomes). Source: Creative Proteomics. https://www.creative-proteomics.com/cell/images/1-Cell-Adhesion-Assay.JPG

In addition to being connected to each other through cell-cell junctions, epithelial cells are also linked to an extracellular matrix (ECM) that is essential for their differentiation and polarization. This attachment of epithelial cells to the ECM takes place through cell-matrix junctions, including focal adhesions and hemidesmosomes [27]. Intercellular junctions are involved in many cellular processes ranging from cytoskeletal dynamics to proliferation, transcription, and differentiation, being regulated not only during embryonic development but also during tumour progression. Epithelial cells display certain motility and are able to separate from neighbouring cells. However, they always remain within the epithelial layer and do not detach from it under normal conditions [22,23].

During carcinoma development, epithelial cells acquire motile characteristics as a result of the loss of apicobasal polarization, the disruption of cell-cell and cell-matrix junctions and the reorganization of the actin cytoskeleton. These changes in cell polarity and cell-cell contacts are due to epithelial-mesenchymal transition (EMT) process, which is widely accepted to be a key event during carcinogenesis [28]. Another important event during the development of carcinomas is the remodelling of the extracellular matrix, which is required for cancer cells to invade stromal tissue and become a malignant tumour. The matrix metalloproteinases (MMPs) represent the most important family associated with matrix remodelling during carcinogenesis [29]. These proteases cleave ECM proteins and are not only responsible for ECM degradation and invasion but also for cell growth, inflammation or angiogenesis [30,31]. MMP expression is induced at the beginning of the metastatic process, and it is maintained until the settlement of a metastatic niche in a distant organ [32].

Carcinomas usually develop in the basal layer of the epithelium, giving rise to a premalignant lesion known as adenoma, which is limited to the epithelial cell layer. Epigenetic and genetic changes lead to the malignant transformation of cells and the development of a carcinoma *in situ*, which is still bounded by the basement membrane. Further alterations may trigger the acquisition of invasive properties and the subsequent disruption of the basal membrane, as a result of the EMT process. As previously mentioned, cells are then able to intravasate into lymph or blood vessels and extravasate into secondary sites, where they remain individually as a micrometastasis or form a macrometastasis through mesenchymal-epithelial transition (MET) [33] (**Figure 4**).

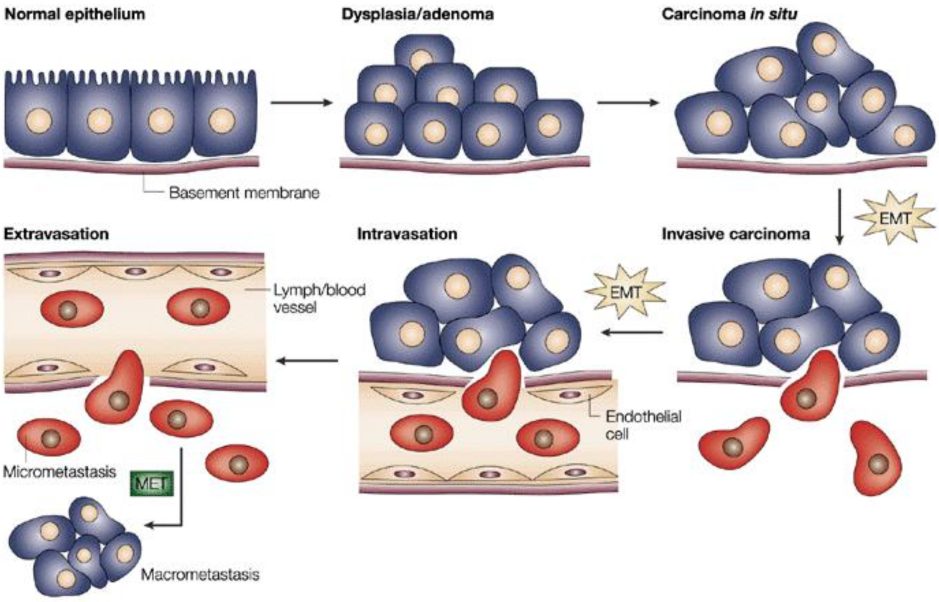

Figure 4. Major events that take place during tumour progression and metastasis. Cellular transformation due to genetic alterations may result in dysplasia (adenoma), which eventually may give rise to a carcinoma *in situ*. Further alterations can induce local invasion and intravasation, after tumour cells have undergone EMT, which confers an invasive phenotype to cancer cells as a result of the loss of cell-cell adhesions, ECM degradation and increased motility. Cancer cells are then extravasated into secondary sites, giving rise to micrometastasis that may lead to macrometastasis by means of mesenchymal-epithelial transition (MET). Image obtained from Thiery, 2002.

3.2. Colorectal cancer

Colorectal cancer (CRC) represents a major health issue worldwide, as it is the third most common type of cancer and the second most common cause of cancer-related deaths [1]. Almost all colorectal cancers are adenocarcinomas, which arise from the intestinal epithelium. Colorectal cancer is a heterogeneous disease, as it shows differences in clinical presentation, prognosis and molecular characteristics. Surgical resection is the first choice for colorectal cancer treatment. However, for those patients with unresectable lesions few therapeutic options are available [34]. Such therapeutic options include chemotherapy and radiotherapy, and are intended to reduce tumour size as well as prevent further tumour growth and dissemination.

Current chemotherapy is based on the use of both individual drugs (mainly fluoropyrimidines such as 5-fluorouracil) and combined therapy, being FOLFOX (5-fluorouracil + oxaliplatin), FOXFIRI (5-fluorouracil + irinotecan), CAPOX (capecitabine + 5-fluorouracil) and CAPIRI (capecitabine + irinotecan) the most used combined regimens in first-line treatment [35]. Another therapeutic approach that has recently emerged is targeted therapy, which added in combination with the above-mentioned chemotherapeutic agents has increased the overall survival of CRC patients [36,37]. However, targeted agents such as epidermal growth-factor receptor (EGFR) inhibitors or vascular endothelial growth factor (VEGF) inhibitors, are few in number and only suitable for patients with certain mutational profiles [38].

3.2.1. Genetic alterations and consensus molecular subtypes (CMS) of colorectal cancer

As previously mentioned, CRC is very heterogenous at the molecular level, which makes it very difficult to determine prognostic and diagnostic markers. Moreover, CRC heterogeneity is responsible for large variations between individual treatment responses, especially for targeted therapies. CRC was one of the first solid tumours to be characterized at the molecular level [36]. The canonical model of CRC consists in a stepwise accumulation of genetic and epigenetic events that lead to adenoma and subsequently to carcinoma development. These genetic alterations include the loss of function of tumour suppressor genes such as adenomatous polyposis coli (APC), TP53 and SMAD4 and the activation of oncogenes such as KRAS or PIK3CA [39,40] (**Figure 5**).

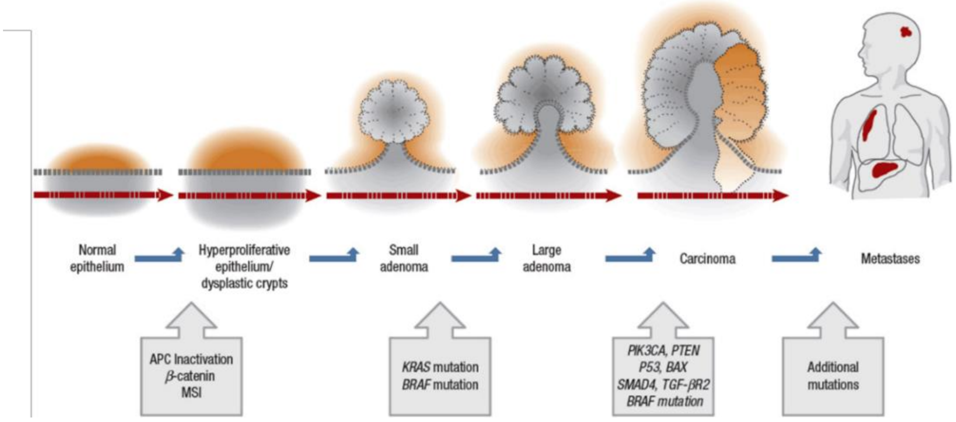

Figure 5. Schematic representation of genetic changes that are associated with the adenoma-carcinoma sequence in colorectal cancer. The main driver mutations of the transitions between each tumour stage are shown. Image modified from: Basicmedical Key. https://basicmedicalkey.com/colorectal-cancer-2/

The molecular classification of colorectal cancer has changed in the last years. Traditionally, it was based on microsatellite instability (MSI) and chromosomal instability, with both prognostic and predictive value. For example, MSI^+ tumours are associated with a good patient outcome in early stages. However, in the metastatic scenario, an MSI^+ phenotype is an indicator of poor prognosis [41]. Nowadays, a more detailed classification of colorectal cancer, based on intrinsic gene expression profiles, has been proposed. This classification considers four biologically distinct consensus molecular subtypes (CMS): CMS1 (MSI Immune), hypermutated, microsatellite unstable, and with strong immune activation; CMS2 (Canonical), epithelial, with chromosomal instability and significant activation of WNT and MYC signalling; CMS3 (Metabolic), epithelial, with evident metabolic dysregulation; and CMS4 (Mesenchymal), showing a pronounced activation of transforming growth factor β (TGF-β), overexpression of EMT genes, stromal invasion and angiogenesis (**Figure 5**). Therefore, a better understanding of drug response in each CMS group may be a great step forward in precision medicine [42,43].

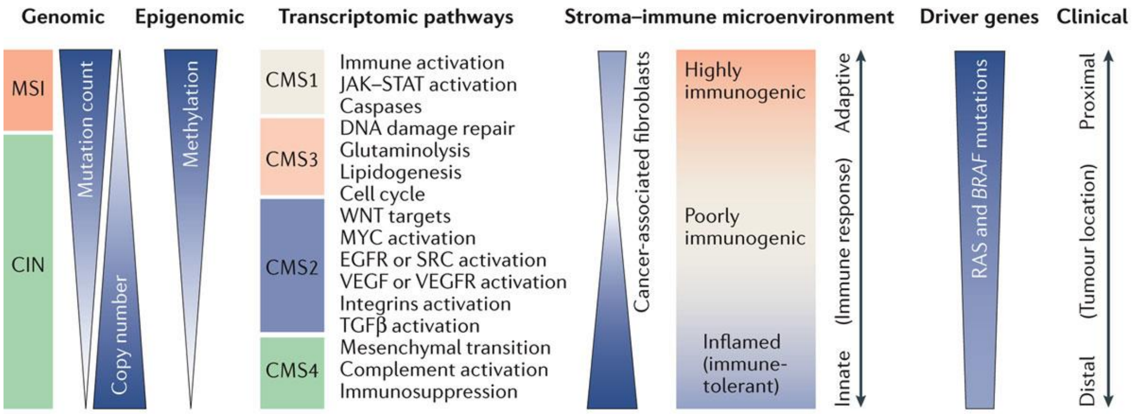
Genomic
Epigenomic
Transcriptomic pathways
Stroma–immune microenvironment
Driver genes
Clinical
MSI
CIN
Mutation count
Copy number
Methylation
CMS1
CMS3
CMS2
CMS4
Immune activation
JAK–STAT activation
Caspases
DNA damage repair
Glutaminolysis
Lipidogenesis
Cell cycle
WNT targets
MYC activation
EGFR or SRC activation
VEGF or VEGFR activation
Integrins activation
TGFβ activation
Mesenchymal transition
Complement activation
Immunosuppression
Cancer-associated fibroblasts
Highly immunogenic
Poorly immunogenic
Inflamed (immune-tolerant)
Adaptive
(Immune response)
Innate
RAS and BRAF mutations
Proximal
(Tumour location)
Distal

Figure 6. Schematic representation of consensus molecular subtypes (CMS) of colorectal cancer. Representative transcriptomic pathways of each CMS subtype are detailed, as well as their genomic and epigenomic characteristics, driver mutations (KRAS and BRAF), immunogenic degree of tumour microenvironment and tumour location. Image obtained from Dienstmann *et al.*, 2017.

4. Epithelial-mesenchymal transition (EMT)

4.1. Physiological and pathological EMT

Epithelial and mesenchymal cell types were first described at the end of the 19th century, according to cell shape and organization observed during embryonic development. The inter-conversion between epithelial and mesenchymal cells was initially described by Frank Lillie in 1908 [33]. However, it was not until the late 1980s that Elisabeth Hay and Garry Greenburg described EMT as a distinct cell process [44]. EMT process has been gaining importance since then, as its involvement in a number of physiological and pathological processes such as embryonic development, tissue repair, wound healing, stem cell behaviour, tissue/organ fibrosis and tumour progression has been described [45].

EMT is a highly conserved cellular program in which epithelial cells lose their apicobasal polarization and cell-cell junctions, giving rise to mesenchymal cells with enhanced migratory and invasive capabilities [46]. The transition of epithelial to mesenchymal cells is not an irreversible process, as cells also undergo a mesenchymal-epithelial (MET) process both during embryonic development and disease [47]. Moreover, cells may lose their epithelial phenotype just partially, by losing some of their epithelial traits or showing a combination of epithelial and mesenchymal features. This is considered as a partial EMT, which has been observed in development, wound healing, fibrosis and cancer progression. These cells that undergo a partial EMT have been referred to as 'metastable', and display a high level of plasticity between epithelial and mesenchymal phenotypes [48]. Therefore, despite EMT has traditionally been considered as a binary switch, nowadays is considered as a stepwise process with different intermediate states [49]. This ability of cells to reversibly change their phenotype and adopt intermediate epithelial and mesenchymal features has been recently termed as epithelial-mesenchymal plasticity (EMP) [50].

EMT process has traditionally been classified into three different subtypes, according to the biological setting in which it takes place: 1) Type I EMT, which takes place during implantation, embryogenesis and organ development; 2) Type II EMT, occurring during wound healing, tissue regeneration and organ fibrosis; and 3) Type III EMT, which takes place during malignant transformation of cancer cells [51].

4.2. EMT and carcinogenesis

During the course of tumour progression, EMT process facilitates the acquisition of mesenchymal traits that are associated with a high degree of malignancy. This Type III EMT could be considered as an aberrant version of the EMT that takes place during normal embryonic development. As previously mentioned, upon EMT activation, epithelial cells lose apicobasal polarization and cell-cell junctions and acquire a spindle-shaped mesenchymal morphology [51].

A critical step during EMT process is the loss of the epithelial marker E-cadherin, which is present at adherens junctions. However, this process is also characterized by the disruption of tight junctions, desmosomes and gap junctions. The disruption of tight junctions is accompanied by the downregulation of claudin and occludin as well as the relocation of zonula occludens protein 1 (ZO-1), while the destabilization of desmosomes is caused by the downregulation of plakophilin and desmoplakin [52]. On the other hand, the acquisition of the mesenchymal phenotype is accompanied by the increased expression of mesenchymal markers, such as N-cadherin, Vimentin and Fibronectin [53] (**Figure 7**). Another key event during EMT is the nuclear accumulation of β-catenin, since its interaction with E-cadherin at the cell membrane is lost [54].

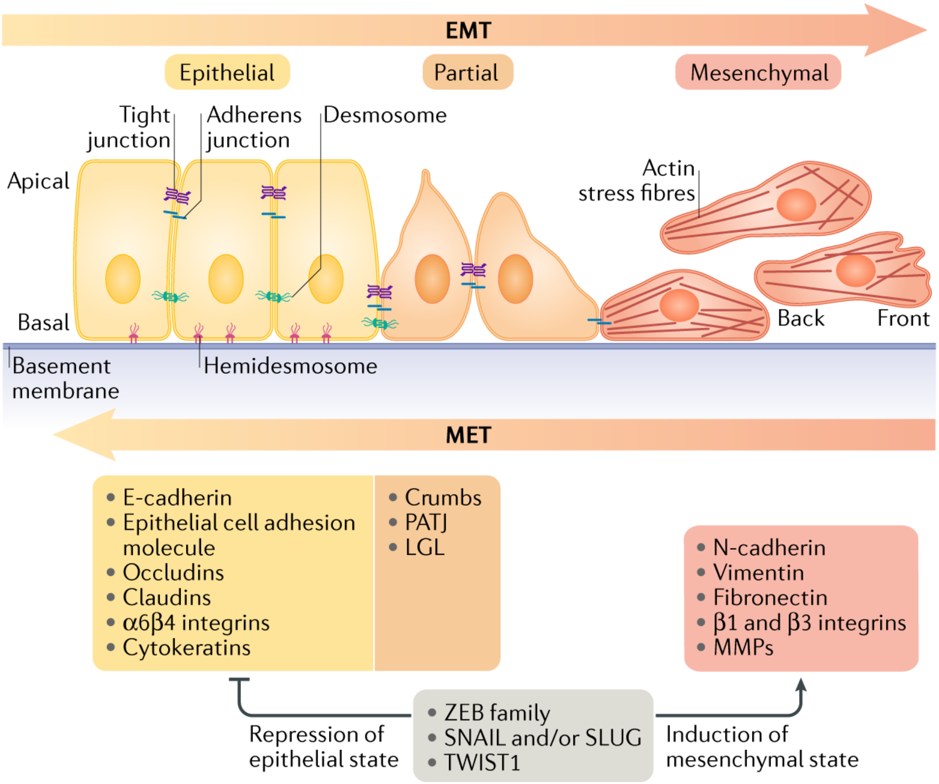
EMT
Epithelial
Partial
Mesenchymal
Tight junction
Adherens junction
Desmosome
Apical
Basal
Actin stress fibres
Back
Front
Basement membrane
Hemidesmosome
MET
• E-cadherin
• Epithelial cell adhesion molecule
• Occludins
• Claudins
• α6β4 integrins
• Cytokeratins
• Crumbs
• PATJ
• LGL
• N-cadherin
• Vimentin
• Fibronectin
• β1 and β3 integrins
• MMPs
Repression of epithelial state
• ZEB family
• SNAIL and/or SLUG
• TWIST1
Induction of mesenchymal state

Figure 7. Molecular and phenotypic changes that epithelial cells undergo during EMT process. Epithelial cells show apicobasal polarity and are joined together by tight junctions, adherens junctions and desmosomes, and they are linked to the basement membrane by hemidesmosomes. EMT activation causes repression of epithelial genes and induces the expression of mesenchymal ones. These changes in gene expression lead to the loss of apicobasal polarization and cell-cell junctions, as well as the reorganization of actin cytoskeleton, thus causing the acquisition of mesenchymal features. Image obtained from Dongre & Weinberg, 2019.

4.2.1. Molecular regulation of EMT during tumour progression

The loss of the epithelial phenotype as well as the subsequent acquisition of mesenchymal features that occurs during EMT process, is tightly controlled at a transcriptional, posttranscriptional and posttranslational level. EMT is transcriptionally regulated by EMT transcription factors (EMT-TFs), which include the zinc-finger E-box-binding homeobox factors Zeb1 and Zeb2, Snail (also called Snai1), Snail2 (also known as Slug) and the basic helix-loop-helix (bHLH) factors Twist1 and Twist2. These EMT-TFs, which are widely considered as master regulators of epithelial and mesenchymal genes, mediate the transcriptional repression of E-cadherin as well as other junctional proteins such as claudins, occludins, cytokeratins or plakophilin [55]. The expression of EMT-TFs can be induced by different signalling pathways, such as Notch, Wnt and transforming growth factor-β (TGF-β) pathways, being the latter the one with the central role during cancer progression. TGF-β signalling pathway is activated by many different ligands, including three distinct TGF-β isoforms, two activins and several bone morphogenic proteins (BMPs). TGF-β binds to TGF-β receptor type 1 or type 2 (TGFβR1 or TGFβR1, respectively) and induces the phosphorylation of SMAD2 and SMAD3, which form a complex with SMAD4. Once formed, the trimeric complex migrates to the nucleus where it functions as a transcription factor, leading to the activation of mesenchymal genes (such as Vimentin and Fibronectin) and EMT-TFs (Snail, Slug, Zeb1 and Twist). These EMT-TF can subsequently increase the expression of TGF-β ligands, thus creating a positive feedback loop that maintains EMT program once activated. Besides promoting EMT through SMAD proteins, TGF-β can induce EMT by the activation of ERK, p38 MAPK, PI3K-AKT and Rho-like GTPases pathways [56,57].

In addition to the direct effect of EMT-TFs on gene expression, EMT process is also regulated by changes at the posttranscriptional level. These posttranscriptional changes include alternative splicing, miRNA-mediated degradation of gene transcripts and the interaction with RNA binding proteins (RBPs). Alternative splicing generates different protein isoforms with different functions in mesenchymal cells in comparison to epithelial ones. This EMT regulation by isoform changes as a result of alternative splicing is well illustrated by CD44 or p120-catenin [58]. On the other hand, microRNAs have recently emerged as key players in the regulation of EMT process. MicroRNAs are small (around 20-22 nucleotides in length) non-coding RNAs that exert a posttranscriptional control on gene expression by binding to specific sequences of mRNA. This pairing causes the degradation of target mRNA, and/or the repression of its subsequent translation [59,60]. The negative regulation of Zeb transcription factors by microRNAs of the miR-200 family and miR-205 was one of the first reported cases of the miRNA regulation of EMT process [61–63]. Regarding to RBPs, they are responsible for controlling different posttranscriptional steps, such as splicing (ESRP1, Zeppo1, SF2/ASF) or polyadenylation (ESRP), and also the mRNA turnover (TTP, HuR) and translation (hnRNPE1) [64].

Finally, posttranslational modifications such as hydroxylation, phosphorylation, ubiquitination, SUMOylation and glycosylation have been also described to regulate EMT process [65–68]. Particularly, Snail is regulated either by phosphorylation or glycosylation. Phosphorylation of Snail, which is mediated both by protein kinase D1 (PKD1) and glycogen synthase kinase-3β (GSK-3β), leads to its ubiquitination and degradation by the proteasome system. Conversely, O-GlcNAcylation results in the inhibition of Snail phosphorylation by GSK-3β, thus resulting in the stabilization of Snail protein [69].

4.3. E-cadherin loss as a hallmark of EMT process

As previously mentioned, the disruption of cell-cell adhesions (tight junctions, adherens junctions, desmosomes and gap junctions) is a characteristic hallmark of the EMT process [23]. Even though all different junctions are functionally relevant, a key role for adherens junctions has been demonstrated, as they are crucial for the regulation of the dynamics of the epithelium and also for the transmission of information from extracellular stimuli to the interior of cells. Adherens junctions are cadherin-dependent adhesive structures which are linked to the actin cytoskeleton [22]. Cadherins belong to a large family of transmembrane or membrane-associated glycoproteins, which regulate adherens junctions in a Ca^{+2} dependent manner. Cadherin family can be subdivided into five different subfamilies: 1) Type I classical cadherins; 2) Type II classical cadherins; 3) Desmosomal cadherins (desmocollins and desmogleins); 4) Proto-cadherins; and 5) Cadherin-related molecules [70]. The type I and type II classical cadherins were initially named according to the tissue in which they were initially found, for instance, E-cadherin (epithelial, CDH1), N-cadherin (neural, CDH2), VE-cadherin (vascular endothelial, CDH5) or K-cadherin (kidney, CDH6) [71].

E-cadherin represents the prototype member of classical cadherins due to its early identification and comprehensive characterization [72]. It is comprised of an extracellular domain and a cytoplasmic domain. The extracellular domain is divided into five repetitive subdomains, also known as cadherin repeats, and binds to Ca^{+2} forming homophilic interactions with the E-cadherin extracellular domains of neighbouring cells. On the other hand, the cytoplasmic domain binds to p120, α, and β-catenin, allowing the stable anchoring to the actin cytoskeleton [73] (**Figure 8**). E-cadherin behaves as a tumour suppressor gene, playing an important role in cell polarity, differentiation, migration and stem cell properties [74]. Its downregulation or completely loss during tumour progression, as well as the mechanisms involved, have been well documented. These include mutation, epigenetic silencing, transcriptional silencing, endocytosis and proteolytic processing.

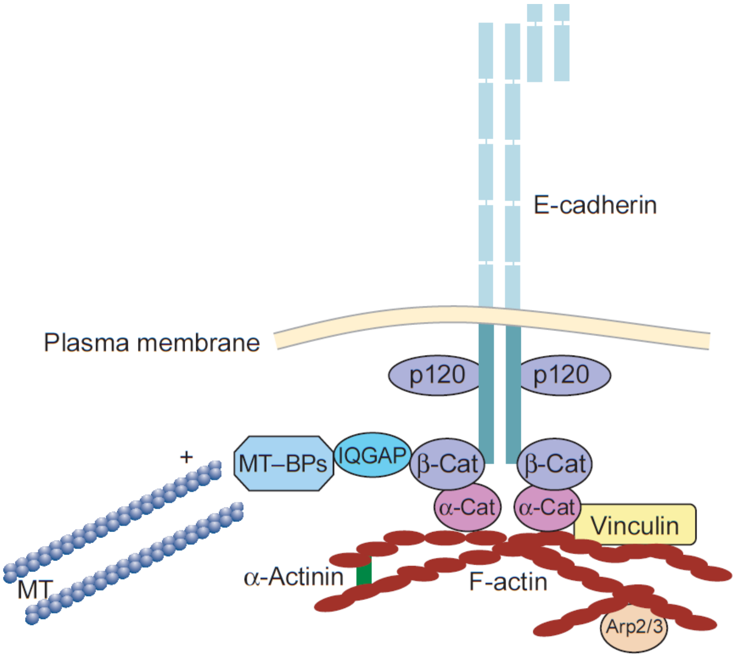

Figure 8. Structural organization of E-cadherin protein at adherens junctions. E-cadherin binds by its extracellular domain (composed of five repetitive subdomains or cadherin repeats) to the extracellular

domains of E-cadherin molecules in neighbouring cells, and by its cytoplasmic domain to α, β, and p120-catenins and therefore to the actin cytoskeleton. Image obtained and modified from D'Souza-Schorey, 2005.

An important number of evidence of E-cadherin role during tumour progression came from studies of loss of heterozygosity (LOH) of chromosome 16q21-22, where the E-cadherin encoding gene (CDH1) is found. This LOH has been demonstrated in gastric, prostate, hepatocellular, oesophageal and breast carcinomas, being specially frequent in the latter one [75]. Regarding to inactivating mutations, they are distributed along the whole coding region, being particularly frequent in breast and diffuse gastric cancer. Moreover, germline and somatic mutations in the E-cadherin gene have been also described for diffuse gastric cancer and breast cancer [76,77]. Regarding to epigenetic silencing, hypermethylation of the CpG island in the promoter region of the E-cadherin gene has been reported in many carcinoma types, and correlates with a decreased expression of E-cadherin protein [78–81]. On the other hand, E-cadherin repressors (Snail, Slug, Twist, Zeb1, Zeb2) have been also associated with tumour progression in different cancer types. They repress E-cadherin expression by binding to E-box sequences that are present in the proximal region of CDH1 promoter [82–85].

Finally, E-cadherin may undergo posttranslational regulation through glycosylation, proteolysis, phosphorylation or ubiquitination. O-glycosylation inhibits E-cadherin transport to the cell membrane, while proteolysis and phosphorylation cause E-cadherin disruption at the plasma membrane [86]. E-cadherin proteolytic cleavage at the cell surface is carried out by matrix metalloproteinases (MMPs), which cleave E-cadherin ectodomain near the plasma membrane [87]. On the other hand, activation of proto-oncogenes such as c-Met, proto-oncogene tyrosine-protein kinase Src (Src) and EGFR leads to the increased phosphorylation of cytoplasmic domain of E-cadherin and thus to its subsequent internalization and ubiquitin-dependent degradation [70]. In 2002, Yasuyuki Fujita and collaborators identified Hakai as the E3 ubiquitin-ligase responsible for the ubiquitination of Src-phosphorylated E-cadherin, and therefore for its internalization and further degradation [88].

4.4. Regulation of EMT by tumour microenvironment

Tumour progression is also regulated by the interaction of cancer cells with tumour microenvironment (TME). Besides tumour cells, TME comprises stromal cells (cancer-associated fibroblasts and immune cells such as T cells, B cells or tumour-associated macrophages), cytokines, chemokines and growth factors secreted by stromal cells, as well as non-cellular components that constitute the extracellular matrix (ECM). These factors secreted by stromal cells may induce EMT in carcinoma cells in a paracrine way, thus promoting tumour progression and metastasis [56,89] (**Figure 9**). Cancer-associated fibroblasts (CAFs) represent a major component of the TME, playing a key role in ECM remodelling and invasion during carcinogenesis. The involvement of CAFs in tumour progression was early demonstrated in prostate cancer, where CAFs were reported to increase tumorigenesis [90]. In addition to its involvement in ECM synthesis and remodelling, CAFs induce EMT in carcinoma cells in a paracrine way, by secreting cytokines (IL-6) and growth factors (VEGF, TGF-β, HGF) [91]. For example, in breast cancer, it has been reported that CAFs induce EMT through paracrine TGF-β1, thus promoting an aggressive phenotype of cancer cells [92]. In non-small-cell lung carcinoma (NSCLC), CAFs induced EMT via IL-6 signalling [93].

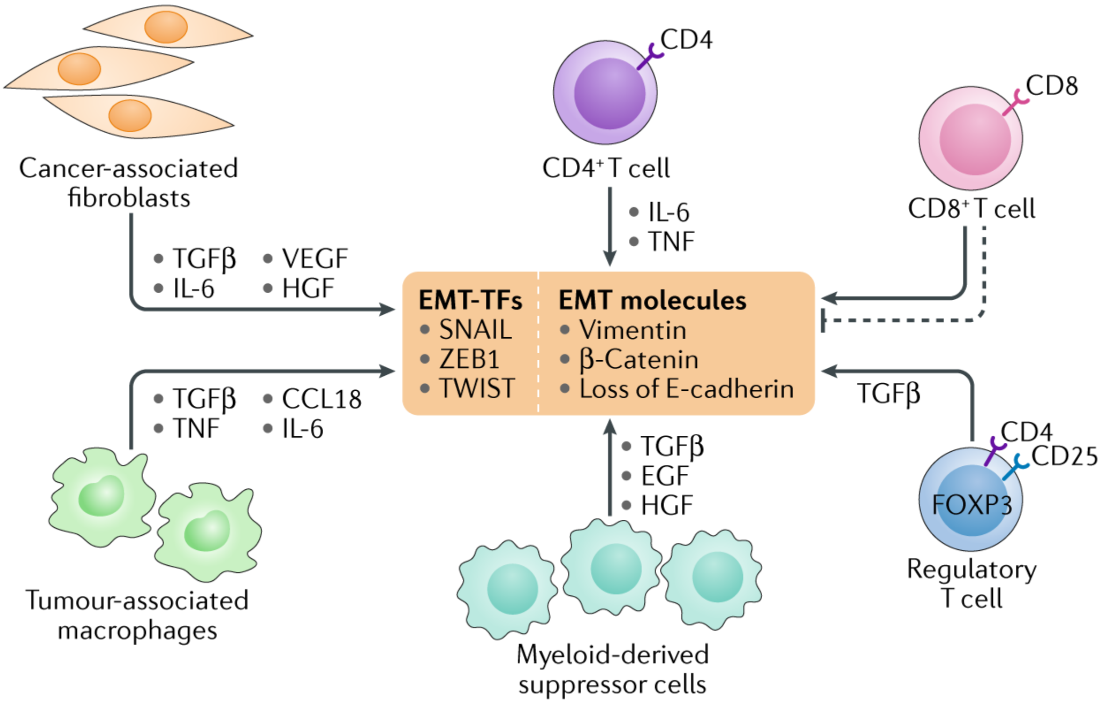
Cancer-associated fibroblasts
• TGFβ • IL-6
• VEGF • HGF
CD4
CD4⁺T cell
• IL-6 • TNF
CD8
CD8⁺T cell
EMT-TFs
• SNAIL
• ZEB1
• TWIST
EMT molecules
• Vimentin
• β-Catenin
• Loss of E-cadherin
• TGFβ • TNF
• CCL18 • IL-6
TGFβ
CD4
CD25
FOXP3
Regulatory T cell
• TGFβ • EGF • HGF
Tumour-associated macrophages
Myeloid-derived suppressor cells

Figure 9. Activation of EMT process by stromal cell-secreted factors. EMT process may be induced in a paracrine way by cytokines, chemokines, and growth factors that are secreted by cancer-associated fibroblasts and immune cells such as CD8$^+$ cytotoxic T cells, CD4$^+$ helper T cells, regulatory T cells, tumour-associated macrophages and myeloid –derived suppressor cells. Image obtained from Dongre & Weinberg, 2019.

4.5. EMT and stemness

EMT programme has traditionally been considered as the main mechanism responsible for the invasion of tumour cells into the surrounding stroma and subsequent intravasation, bloodstream transportation and extravasation in distant organs where they further develop micro or macrometastasis [33]. Nevertheless, following the initial observations that linked EMT process and the development of breast cancer stem cells (CSCs), the entrance in CSC state has been also added to the group of biological processes that are regulated by EMT [94,95]. CSCs represent a minor subpopulation of cells within a tumour which are able to seed new tumours. Nowadays, anticancer therapies target only the bulk population of non-CSCs, and in consequence the CSC pool may promote tumour expansion and drug resistance, leading to a lethal outcome of the disease [96,97]. Many lines of evidence have reported that the expression of EMT-TFs (such as Snail, Slug, Zeb1/2 or Twist) confers CSC properties [98–102]. Moreover, the relationship between EMT and CSC has also been demonstrated through the study of TGF-β and Wnt signalling pathways. The activation of EMT process induces autocrine TGF-β and Wnt-mediated signalling loops that drive the acquisition of a stem phenotype [103].

The fast development of new therapeutic approaches for cancer treatment, such as targeted therapy, has substantially improved the clinical outcome of cancer patients. However, drug resistance and the subsequent tumour relapse is still a major problem. For a long time, drug resistance was considered to be primarily caused by genetic alterations, such as mutations in the drug target that affected drug binding. Nevertheless, cancer stem cells (CSCs) are nowadays considered as the primary cause of drug resistance and tumour relapse, due to their increased self-renewal potential and enhanced drug efflux properties [104]. Besides the acquisition of stem properties, the development of drug resistance has also been attributed to the increased expression of antiapoptotic proteins and the overexpression of ATP-binding cassette (ABC) transporter genes [103]. The ABC superfamily comprises a series of transmembrane protein transporters which are responsible for drug efflux. Among them, ABCB1 (ABC subfamily B, member 1), ABCC1 (ABC subfamily C, member 1) and ABCG2 (ABC subfamily G, member 2) represent the main drivers of drug resistance, as they regulate drug absorption, distribution and elimination, as well as membrane permeability [105]. It has been observed that EMT-TFs Twist, Snail and Foxc2 increased the expression of ABC transporter genes in breast cancer cells [106]. Another example of EMT-mediated regulation of ABC transporter expression during the acquisition of drug resistance is that the expression of cisplatin transporter ATP7B as well as EMT process were inhibited by microRNAs miR-15a and miR-16 in ovarian cancer cells [107]. On the other hand, growing evidence suggests that EMT-TFs confer resistance to tyrosine kinase inhibitors targeting the epidermal growth factor receptor (EGFR-TKIs), which represent a common therapeutic approach in NSCLC treatment. Particularly, Slug was reported to induce therapeutic resistance by preventing gefitinib-induced apoptosis in lung adenocarcinoma cell lines [108]. Moreover, Snail and Slug were also reported to induce drug resistance through the inhibition of p53-mediated apoptosis and the induction of a stem phenotype in ovarian cancer cells [109].

Therefore, due to the fact that EMT process increases not only cell motility and invasion but also the acquisition of stem properties and drug efflux mechanisms, EMT and stemness could work together during the acquisition of therapeutic resistance [110]. The development of EMT inhibitors that work together with current chemotherapy or targeted therapy drugs represents a promising therapeutic approach which could significantly improve the clinical outcome of cancer patients [111,112].

5. The ubiquitination system

5.1. Ubiquitin and ubiquitination process

Ubiquitination is the second most common posttranslational modification, behind phosphorylation, and plays a crucial role in controlling protein degradation, interactions or activity, thus maintaining cell homeostasis. It consists of the covalent conjugation of ubiquitin, a highly conserved 76-amino acid (8.5 kDa) protein, to a substrate protein in an ATP-dependent manner. Based on how ubiquitin protein is linked to the protein substrate, ubiquitination can be classified in three main types: 1) monoubiquitination, when a single ubiquitin moiety is linked to a specific lysine residue of the target protein; 2) polyubiquitination, when two or more ubiquitin molecules bind to the same lysine residue of the substrate protein; and 3) branched ubiquitination, when the polyubiquitin chain contains a variety of linkages instead of a single linkage. Ubiquitination is a reversible process, as the function of E3 ubiquitin-ligases can be reverted by removing the ubiquitin molecules from the protein substrate. This process is carried out by deubiquitinating enzymes (DUBs) [113]. Ubiquitination leads to targeted protein degradation by the proteasome, lysosomes or autophagy, but also regulates transcription, DNA repair or protein localization [114].

Ubiquitin protein, named after its wide distribution among eukaryotes, was firstly identified in 1975 by Gideon Goldstein and colleagues and further characterized over the following decades [115]. Later on, between 1970 and 1990, Aaron Ciechanover, Avram Hershko and Irwin Rose identified the ubiquitin-dependent degradation system, achievement for which they were awarded with the Nobel Prize in Chemistry in 2004. The ubiquitin-dependent degradation system consists on the sequential action of three different enzymes: E1 ubiquitin-activating enzyme, E2 ubiquitin-conjugating enzyme and E3 ubiquitin-ligase [116]. This leads to the conjugation of ubiquitin to substrate proteins and mostly to its subsequent degradation. E1is responsible for the ATP-dependent activation of ubiquitin and the subsequent formation of a thioester bond between the active-site Cys residue of the E1 and the C-terminal residue of ubiquitin. Activated ubiquitin is then transferred to a thiol site of E2 enzyme and finally to an amino group in the substrate protein through de action of the E3 ubiquitin-ligase [117] (**Figure 10**). E3 ligases recruit and bind to specific substrates, therefore, they are responsible for the substrate specificity of ubiquitin-mediated protein degradation [118].

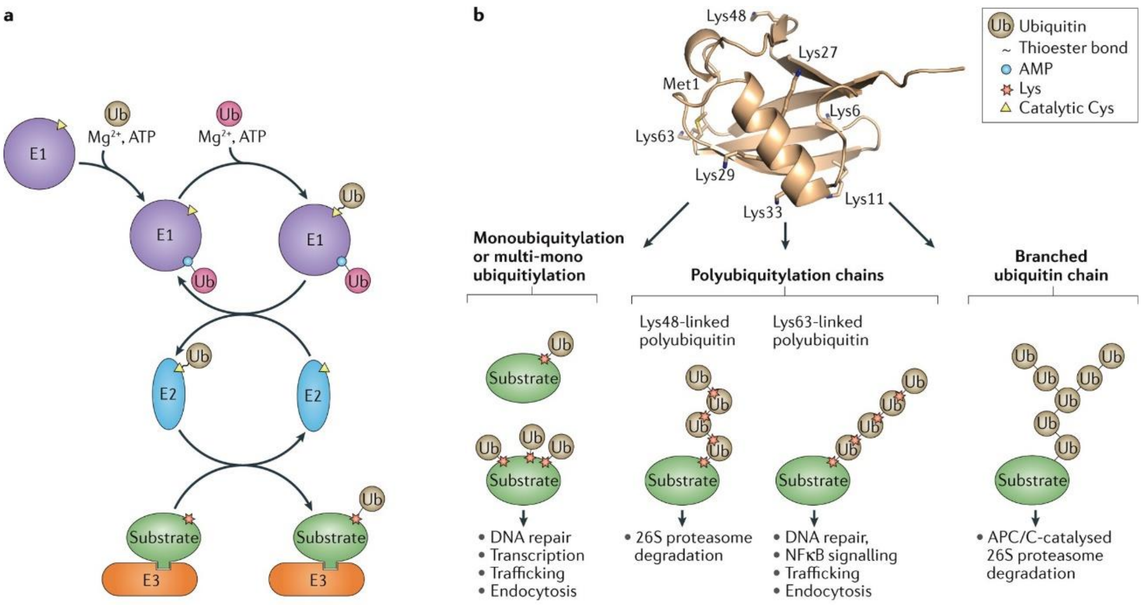
a
E1
Ub
Mg²⁺, ATP
Ub
Mg²⁺, ATP
E1
Ub
E1
Ub
Ub
Ub
E2
E2
Substrate
E3
Ub
Substrate
E3
b
Lys48
Lys27
Met1
Lys6
Lys63
Lys29
Lys33
Lys11
Ub Ubiquitin
~ Thioester bond
○ AMP
✱ Lys
△ Catalytic Cys
Monoubiquitylation or multi-mono ubiquitiylation
Polyubiquitylation chains
Branched ubiquitin chain
Lys48-linked polyubiquitin
Lys63-linked polyubiquitin
Substrate
Ub
Substrate
• DNA repair
• Transcription
• Trafficking
• Endocytosis
• 26S proteasome degradation
• DNA repair,
• NFκB signalling
• Trafficking
• Endocytosis
• APC/C-catalysed 26S proteasome degradation

Figure 10. The ubiquitin conjugation system. (**A**) Ubiquitination process. The sequential action of E1 activating enzyme, E2 conjugating enzyme and E3 ubiquitin-ligase leads to the ubiquitination of substrate proteins. (**B**) Main types of ubiquitination linkages and their molecular implications. A single molecule of ubiquitin can be attached to a substrate protein at a single (monoubiquitination) or multiple (multi-monoubiquitination) lysine sites. Multiple ubiquitin molecules can also be linked to a single lysine residue forming a polyubiquitin chain, which can be linear or branched. The different ubiquitination patterns affect the cellular fate of ubiquitinated proteins. Image obtained from Buetow & Huang, 2016.

5.2. Classification of E3 ubiquitin-ligases

E3 ubiquitin-ligases constitute a big and heterogeneous group of enzymes, as they are the ones that confer substrate specificity to the ubiquitination system. The human genome encodes more than six hundred E3 ligases, while only two E1 enzymes and approximately thirty-eight E2s have been identified in humans. To date, E3 ubiquitin-ligases have been classified into three different classes, according to their specific domains and the mechanism they use to transfer ubiquitin to the target protein: 1) RING (really interesting new gene); 2) HECT (homologous to E6-associated protein carboxyl terminus); and 3) RBR (RING-between-RING) [114].

RING-type E3 ligases, encoded by 270 genes approximately, represent the largest family of E3 ligases and are characterized by its RING or U-box folding catalytic domain. The RING domain allows the direct transference of ubiquitin molecules form E2 conjugating enzyme to the target protein. It contains two Zinc ions coordinated by cysteine residues and histidine residues arranged in a cross-braced configuration that facilitates E2 binding. RING E3s have a varied architecture, and can be found as monomers (i.e. CBL, CNOT4 and RNF38), homodimers (i.e. cIAP2, TRAF6 or RNF4), heterodimers (i.e. BRCA1/BARD1, RNF2/BMI1 and MDM2/MDMX) or multi-subunit complexes (i.e. Cullin-RING ubiquitin-ligases, CRLs). CRL complexes contain a RING E3 (mainly RBX1 or RBX2), a cullin protein (CUL1, 2, 3, 4A/4B, 5 or 7) and a protein substrate receptor. On the other hand, U-box proteins are also considered as RING E3s, since they use the same mechanism to transfer the ubiquitin molecules to the protein substrate and their specific domains is similar to the RING domain although it lacks Zinc ions [119,120]. Among all RING-type E3 ligases, there are a certain number that require substrate phosphorylation at a tyrosine residue (pTyr) for their recognition. They can be classified in three different families, according their recognition domains: (i) SOCS-CL5-RING complex, that combines a typical SH2 recognition domain with a ubiquitin transfer domain (RING), (ii) Cbl family members, and (iii) Hakai, which contains an unusual pTyr-B domain, known as HYB (Hakai-pY-binding) [121].

HECT-type E3 ligases are encoded by 28 genes in humans and they comprise an N-terminal substrate-binding domain and a C-terminal HECT domain. They differ from RING E3s in the ubiquitin transfer to the protein substrate. While RING E3s directly transfer the ubiquitin molecules from E2 to the target protein, HECT E3s ubiquitinate substrates in a two-step reaction. First, ubiquitin is transferred from the active site cysteine of E2 to a cysteine of the HECT domain, forming a thioester bond. Then, ubiquitin is transferred from the HECT domain to a lysine residue of the protein substrate [122]. HECT E3 ligases can be classified into three different subfamilies based on the architecture of the N-terminal domain: NEDD4 family, HERC family and HECT with other protein-protein interaction domains. The NEDD4 family is the largest and best characterized family, and consists of nine members: Nedd4, Nedd4-2/Nedd4l, Itch, Smurf1, Smurf2, Wwp1, Wwp2, Nedl1 and Nedl2 [123].

RBR-type E3 ligases are encoded by more than 12 genes in humans, and share both features of RING and HECT E3 ligases. The RING-between-RING domain is composed of two RING domains (RING1 and RING2) which are separated by an in-between RING (IBR) domain. RING1 binds to E2 conjugating enzyme and shows the same features of RING-type E3s. However, RING2 domain behaves as an HECT domain, since it first forms a thioester bond intermediate with the ubiquitin recruited by RING1 and then transfers the ubiquitin to the substrate protein [113,119].

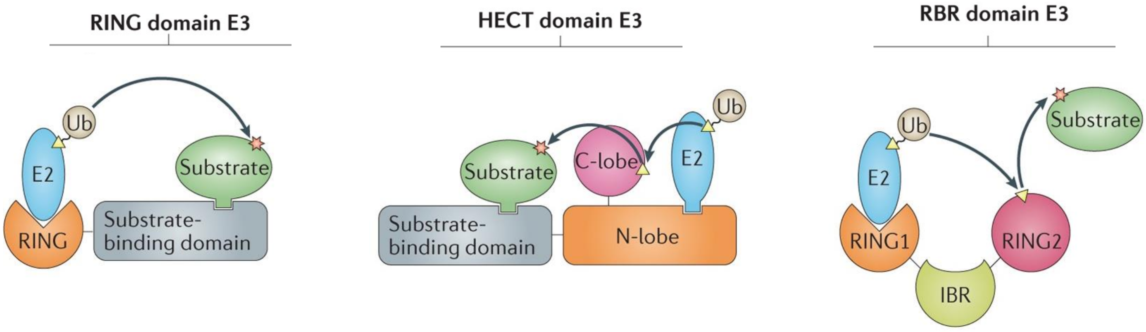

Figure 11. Catalytic mechanisms of RING, HECT and RBR E3 ubiquitin-ligases. RING-type E3 ligases catalyse the direct transfer of ubiquitin molecules from the E2-conjugating enzyme to the substrate protein. Conversely, HECT-type and RBR-type E3 ligases ubiquitinate substrates in a two-step reaction, in which ubiquitin is first transferred from E2-conjugating enzyme to an active site cysteine in the E3 ubiquitin-

ligase and then from the E3 ligase to the protein substrate. Image obtained and modified from Buetow & Huang, 2016.

5.3. EMT regulation by E3 ubiquitin-ligases

Many E3 ubiquitin-ligases have been reported to be important during EMT process and epithelial plasticity, through the regulation of EMT-related proteins [124]. Within the HECT-domain E3 ubiquitin-ligases, Smurf2, a member of the NEDD4 family, has been reported to inhibit TGF-β-induced EMT in epithelial cells [66]. Moreover, members of other HECT-type E3 ligases family have been also reported to regulate EMT. For example, it was observed that HectD1 regulates the stability of Snail, thus affecting EMT process [125].

Among RING-type E3 ligases, F-box proteins have been widely associated with EMT process, as they are responsible for the ubiquitination and subsequent degradation of EMT-TFs. For example, Fbxw1 induces the ubiquitination of Snail1, Snail2 in a GSK-3β-dependent manner. On the other hand, Fbxl14 mediates the degradation of Snail1, Slug, Twist1 and Zeb2, and it is considered to have a specific role in EMT process, as Zeb and Twist proteins are not structurally related with Snail1 [126].

Another example of EMT-related RING E3 ligases is the Casitas B-lineage lymphoma (CBL) family, which ubiquitinate substrate proteins in a tyrosine phosphorylation-dependent manner. For example, it was demonstrated that Cbl-b overexpression prevented EMT process through the ubiquitination and subsequent degradation of EGFR, thus inhibiting the EGFR-ERK/Akt-miR-200c-ZEB1 axis [127]. On the other hand, the E3 ubiquitin-ligase Hakai (also named Cbl-like-1 as it is not a typical Cbl protein due to its different domains and mechanism of action) has been described as the first posttranslational regulator of E-cadherin at cell-cell contacts. Hakai binds to the cytoplasmic domain of tyrosine-phosphorylated E-cadherin, inducing its ubiquitination, endocytosis and further degradation [88]. As previously mentioned, E-cadherin loss is a hallmark of EMT process, and for this reason Hakai is considered a promising therapeutic target for cancer treatment [28].

5.4. E3 ubiquitin-ligases as anticancer drug targets

As stated above, ubiquitination plays a central role by regulating not only protein degradation, interactions or activity, but also DNA integrity, gene expression or metabolism. Therefore, ubiquitination is crucial for a number of biological processes and its deregulation is often associated with many diseases, especially cancer. Mounting evidence suggests that tumour progression is frequently associated with abnormal expression, mutations or disfunction of E3 ubiquitin-ligases, which may have an oncogenic (i.e. MDM2, which ubiquitinates p53) or tumour suppressor (i.e. BRCA1) activity [128].

Given that ubiquitination process is often dysregulated in cancer, a large number of small molecule inhibitors that target E1, E2 and E3 enzymes, as well as the DUBs and the proteasome, have been developed. To date, only proteasome inhibitors (i.e. bortezomib, carfilzomib or ixazomib) have been approved by the U.S. Food and Drug Administration (FDA) and successfully used for cancer treatment. Nevertheless, these drugs have only proved efficacy in the treatment of haematological malignancies, while their clinical activity in solid tumours has usually been limited [129–134]. Nowadays, the interest in E3 ubiquitin-ligases as therapeutic targets is constantly increasing due to their substrate specificity, as their inhibition causes fewer side effects than E1, E2 enzymes, DUBs or the proteasome inhibition [113,135]. The most studied E3 ligase is MDM2, which ubiquitinates p53 causing its downregulation and thus inhibiting cell death. Nutlin-3a, the first inhibitor molecule described for MDM2, inhibits its interaction with p53 causing cell death both *in vitro* and *in vivo*. RG7112, a derivative of Nutlin-3a, has shown an increased antitumor activity *in vitro*, however, clinical trials have not been that successful. Therefore, ongoing efforts are still made to develop inhibitors against the E3 ligases, as it is important to deeply understand their regulation, both in cancer and normal cells [136].

6. E3 ubiquitin-ligase Hakai

6.1. Discovery and molecular structure of E3 ubiquitin-ligase Hakai

As previously mentioned, E3 ubiquitin-ligase Hakai (also named Cbl-like-1 or Cbll1) was identified in 2002 by Yasuyuki Fujita and collaborators as the first posttranslational regulator of E-cadherin stability. Based on previous results, in which they demonstrated that Src-mediated tyrosine phosphorylation of E-cadherin induced the disruption of cell-cell contacts [137], they aimed to determine the mechanism responsible for its degradation. To do so, they analysed proteins that interact with tyrosine-phosphorylated E-cadherin, by using a modified yeast two-hybrid system. They identified an E3 ubiquitin-ligase, Hakai, which means ‘destruction’ in Japanese [88].

The cytoplasmic region of E-cadherin comprises two different domains, CH2 (cadherin homology 2) and (CH3 cadherin homology 3). CH2 domain contains three tyrosine residues that are closely spaced (in mouse: 755,756 and 757). 755 and 756 residues are E-cadherin specific, while 757 residue is present in other cadherins, such as N-cadherin and OB-cadherin. The mutation (Tyr-Phe) of the specific residues abolishes the interaction between Hakai and E-cadherin, while it is not affected when the third residue is mutated. Therefore, Hakai interacts with E-cadherin through Y755 and Y756 (Y753 and Y754 in humans) specific residues. Moreover, Fujita and collaborators also observed that Hakai did not interact with other cadherins (N and OB-cadherin) or the cytoplasmic domain of tyrosine kinase receptors, further supporting the specific interaction between Hakai and tyrosine-phosphorylated E-cadherin. Finally, they also observed that Hakai overexpression induces E-cadherin ubiquitination, endocytosis and further degradation [88,138]. Once internalized, E-cadherin is targeted for lysosomal degradation, through the action of Rab5 and Rab7 GTPases, thus maintaining the mesenchymal phenotype as E-cadherin is not recycled back to the cell membrane through Rab11-containing recycling endosomes [139,140] (**Figure 12**). It is important to mention that, despite additional Hakai-interacting proteins have been reported in recent years [141,142], to date E-cadherin is the only Hakai-regulated protein that is directly related with EMT process.

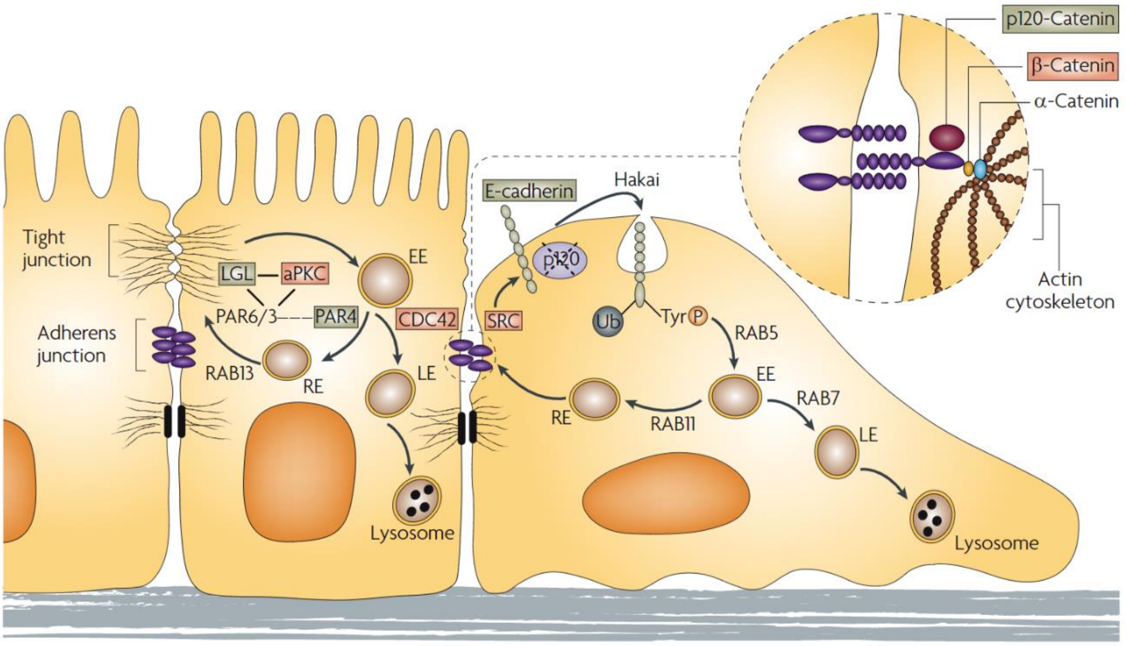

Figure 12. Hakai-mediated disruption of adherens junctions. Src activation induces the phosphorylation and inactivation of p120-catenin, responsible for the inhibition of E-cadherin endocytosis, as well as the phosphorylation of the cytoplasmic domain of E-cadherin in tyrosine residues. Tyrosine-phosphorylated E-cadherin is then recognized and subsequently ubiquitinated by E3 ubiquitin-ligase Hakai. This causes E-cadherin endocytosis into early and late endosomes (EE and LE, respectively) through the action of Rab5 and Rab7 GTPases, and finally its degradation into lysosomes. E-cadherin recycling through Rab11-containing recycling endosomes (RE) is also diminished, thus maintaining the mesenchymal phenotype. Image obtained from Mosesson *et al.*, 2008.

As mentioned above, E3 ubiquitin-ligases are classified into three different classes (RING, HECT and RBR E3 ligases) according to their specific domains and the mechanism they use to transfer ubiquitin to the target protein [114]. The E3 ubiquitin-ligase Hakai was firstly identified a RING-type E3 ligase that resembled the Cbl family, as it also possesses an N-terminal classic RING domain, a short phosphotyrosine (pTyr) recognition sequence and a proline-rich domain in the C-terminal region. However, Hakai is not a typical c-Cbl protein, as the linear order of the domains is different (RING finger-pTyr-Proline rich for Hakai and pTyr binding-RING finger-Proline rich for c-Cbl) (**Figure 13**) and they have no sequence similarities outside these domains [88]. Moreover, the binding mechanism to tyrosine-phosphorylated substrates is different between Hakai and c-Cbl. Hakai forms an atypical pTyr-binding domain, a homodimer consisting of two monomers that are arranged in an anti-parallel configuration. Each monomer is composed by an N-terminal RING domain and a C-terminal pTyr-binding domain that incorporates a zinc coordination motif, both important for dimerization. Hakai dimerization, through the binding of pTyr residues of the Hakai monomers in a zinc-coordinated manner, allows the formation of a phosphotyrosine-binding pocket that recognizes specific tyrosine-phosphorylated substrates (E-cadherin, Cortactin and DOK1). This unusual binding domain formed as a result of the dimerization process is known as HYB (Hakai-pY-binding) domain and comprises amino acids 106–206 [143] (**Figure 13**). Unlike other pTyr binding domains, which function as monomers, the dimeric architecture of the HYB domain is critical for the interaction with tyrosine-phosphorylated targets [144].

To date, besides Hakai, the HYB domain has only been found in ZNF645, an E3 ubiquitin-ligase that is exclusively expressed in normal human testicular tissue [145]. However, it demonstrates different target specificities as although it is able to interact with E-cadherin, it does not interact with another Hakai substrates such as Cortactin. Therefore, due to these unique structural features that make it different from other pTyr binding domains, the HYB domain was proposed as a promising therapeutic target for cancer treatment [143,144,146].

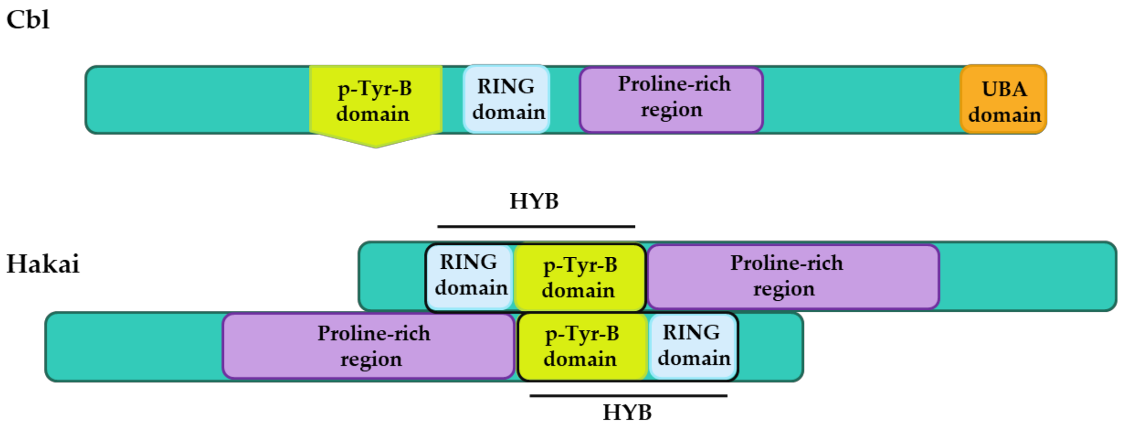

Figure 13. Comparison of the structure of pTyr binding domain between Hakai and Cbl E3 ligases. Schematic representation of the domains of a RING-type E3 ligase from the Cbl family (upper panel) and the homodimeric structure of the HYB domain of Hakai protein described by Mukherjee and collaborators in 2012 (bottom panel). Image obtained from Rodríguez *et al.*, 2020.

6.2. Physiological and pathological roles of E3 ubiquitin-ligase Hakai

Since Fujita and collaborators observed that Hakai expression induced E-cadherin endocytosis in epithelial cells, thus disrupting cell-cell contacts and affecting cell motility, they suggested a possible role for Hakai in the regulation of EMT process, either in embryonic development or tumour progression [88].

6.2.1. Hakai role during embryonic development

The first insight into the role of Hakai in embryonic development resulted from studies carried out in *Drosophila melanogaster*. By using the *Drosophila* homologue of Hakai, the authors observed that the cytoplasmic domain of E-cadherin was completely dispensable for the interaction between Hakai and E-cadherin. This was contrary to the observations that Fujita and collaborators already made in mammals, suggesting an indirect association between these proteins in *Drosophila,* that may involve another component linking the extracellular domain of E-cadherin with cytoplasmic Hakai. Interestingly, the authors observed that Hakai overexpression did not affect E-cadherin levels at the cell surface, which apparently indicates that Hakai is not playing a key role in E-cadherin downregulation in *Drosophila*. By using a Hakai null allele (*hakai*^{1}) they also observed that Hakai activity is crucial for early embryonic development, as the lack of Hakai during embryogenesis causes embryonic lethality. Hakai absence in larval stage or adult flies did not significantly affect epithelial integrity, further supporting the major role of Hakai during early embryogenesis in *Drosophila* [147]. On the other hand, Hakai-mediated ubiquitination of E-cadherin was also reported to play a major role during mesoderm morphogenesis in human embryonic stem cells (hESCs), as the destabilization of adherens junctions releases p120-catenin and induces the nuclear translocation of β-catenin, thus leading to mesoderm differentiation through β-catenin transcriptional activity [148].

The involvement of Hakai in embryonic development has also been observed in studies conducted in *Arabidopsis thaliana*. Based in previous studies that demonstrate Hakai interaction with m^{6}A complex members (i.e. WTAP, Virilizer) in animals [149], the authors wanted to study Hakai potential role in m^{6}A methylation. They demonstrate that the interaction of Hakai with different members of m^{6}A writing complex takes place also in plants, and they also demonstrate that Hakai plays a key role in mRNA m^{6}A methylation, which is necessary for plant developmental decisions during pattern formation [150]. The involvement of Hakai in mRNA m^{6}A methylation was further confirmed in HeLa cells [151]. In mice, Hakai was reported to form a complex with WTAP, Virilizer and Zc3h13 to promote m^{6}A methylation of nuclear RNA and to regulate mouse embryonic stem cell (mESC) self-renewal [152].

6.2.2. Hakai role during tumour progression

As previously mentioned, Hakai was described to be responsible for the ubiquitination of E-cadherin complex, thus inducing its endocytosis and further lysosomal degradation [88]. However, a number of evidence demonstrates that Hakai is not only involved in the downregulation of E-cadherin at cell-cell contacts but also in many aspects of tumour progression, such as cell proliferation, invasion and metastasis [146].

The role of Hakai in cell proliferation was firstly described by Angélica Figueroa and collaborators in 2009. The authors demonstrated that Hakai regulated cell proliferation in an E-cadherin-independent manner, by using newly established Madin-Darby Canine Kidney (MDCK) cells that stably overexpress Hakai protein. They observed that Hakai overexpressing cells had an increased proliferation in comparison with parental MDCK cells, showing that Hakai induces the transition from G0/G1 to S phase. Moreover, Hakai knockdown reduced cell proliferation in MCF-7 and HEK293 epithelial cells, as well as the expression levels of cyclin D1. They also confirmed the role of Hakai during EMT, as Hakai overexpressing cells showed a more fibroblastic morphology (with decreased cell-cell contacts, increased protrusion formation and downregulation of E-cadherin) compared to non-transformed MDCK cells, which show an epithelial phenotype [153]. Moreover, it was also reported that mir-203 negatively regulates Hakai expression by binding to the 3'UTR of Hakai mRNA, thus reducing cell proliferation [154].

Due to this new functional role of Hakai in proliferation, which was independent from E-cadherin, the authors aimed to identify new downstream effectors of Hakai. They described polypyrimidine tract-binding protein-associated splicing factor (PSF) as a novel Hakai-interacting protein. PSF colocalized Hakai in the nucleus, however, PSF is not a substrate for Hakai as there is no evidence that Hakai induces PSF ubiquitination. Instead, Hakai interacts with PSF and promotes PSF RNA-binding ability. Since several PSF-associated transcripts are related with cell cycle arrest, proliferation or apoptosis, Hakai may also regulate tumorigenesis by interacting with PSF in the nucleus and promoting the expression of cancer-related genes [64,155]. In line with the possible role of Hakai in the nucleus during tumour progression, later evidence suggests that Hakai acts as a corepressor of estrogen receptor alpha (ERα) in breast cancer cells. ERα is a ligand-activated transcription factor responsible for cell proliferation which is overexpressed in most of breast cancer cells. Conversely to results previously obtained in MDCK cells, Hakai prevents ERα-mediated proliferation of breast cancer cells by directly binding to ERα and inhibiting its transactivation. Therefore, Hakai may function as a positive or negative regulator of cell proliferation depending on cellular context [156].

Moreover, Hakai was also reported to play a key role in cell-substratum adhesion and cell invasion, as Hakai overexpressing MDCK cells showed a reduced substratum adhesion and an increased invasive capability in comparison with non-transformed MDCK cells [157]. Moreover, Hakai-overexpressing cells show anchorage-independent growth potential while parental MDCK are not able to grow in soft agar, thus suggesting that Hakai also exhibits an oncogenic potential [153]. The involvement of Hakai in tumour progression has been confirmed not only *in vitro* but also *in vivo*, by using a xenograft immunodeficient mouse model. Hakai overexpressing and non-transformed MDCK cells were injected into the flank of athymic mice, and tumour formation was analysed. Hakai overexpressing cells were able to form tumours in all injection sites, which were palpable 18 days post-injection. Conversely, none of the mice injected non-transformed MDCK cells developed tumours. In addition, the histological analysis of tumour sections revealed that Hakai overexpression enhanced the oncogenic potential and proliferation, as well as blood vessel infiltration. Although histological analysis did not show the presence of macrometastasis in the lung, kidney and liver, the qPCR analysis of the presence of Hakai-MDCK DNA showed micrometastasis formation in the lung [158].

6.2.2.1 Role of Hakai in different carcinoma types

Hakai role during tumour progression was also confirmed by analysing human samples of healthy colon epithelium and colon adenocarcinoma. Hakai expression was significantly increased in colon and gastric adenocarcinoma cells, both in nucleus and cytoplasm, in comparison with healthy colon tissue [153]. Importantly, recent studies demonstrate that Hakai expression, when compared to healthy tissue, is gradually increased in adenoma and in different TNM stages (stage I to stage IV) of colon adenocarcinoma. Therefore, Hakai was proposed as a novel biomarker for colon cancer progression [158]. In addition, it was also demonstrated that Slit-Robo signalling induced Hakai-mediated downregulation of E-cadherin in colorectal cancer, being associated with an increased metastatic potential and poor outcome of patients [159].

Hakai expression was analysed in other types of cancer besides colorectal carcinoma, for instance, it was recently reported to be overexpressed in NSCLC tissues in comparison with adjacent normal lung tissues. Hakai upregulation was associated with an increased tumour size and an enhanced proliferation, migration and invasive capacity, being proposed as biomarker for the development and progression of NSCLC [160,161]. In addition, it has been demonstrated that overexpression of miR-212-3p reduces cell proliferation, invasion and migration in NSCLC cells through its action on Hakai [162]. On the other hand, miR-545-3p has also been described to exhibit an antitumor potential in NSCLC cells trough Hakai inhibition [163]. Importantly, Hakai was also reported to be involved in the acquisition of gefitinib resistance, as its overexpression was observed both in gefitinib-resistant HCC827 cells and tumour samples of patients with acquired gefitinib resistance [164]. Moreover, it was also demonstrated that Hakai knockdown resulted in an enhanced chemosensitivity of NSCLC to cisplatin treatment [161]. Therefore, Hakai was proposed as a promising therapeutic target for NSCLC treatment [161,164].

Hakai was also described to act as an oncoprotein in hepatocellular carcinoma (HCC), by inducing Ajuba degradation through neddylation. Despite its oncogenic role in several carcinoma types, Ajuba acts as a tumour suppressor in HCC cells, and its downregulation triggers E-cadherin loss, nuclear translocation of β-catenin and Cyclin D1 upregulation, therefore promoting tumour progression both *in vitro* and *in vivo*. Hakai interacts with Ajuba through its HYB domain, inducing its neddylation and subsequent degradation [165]. In addition, Hakai-mediated E-cadherin ubiquitination, internalization and lysosomal degradation has been reported to be involved in hepatocyte polarity loss and tumour progression in HCC [166].

6.3. Hakai involvement in oncogenic signalling pathways

Src-mediated E-cadherin downregulation during EMT was firstly described by Palacios *et al.* in 2005. The authors demonstrated that, upon Src activation, E-cadherin is degraded in the lysosome through the action of several Rab GTPases [139]. However, upstream regulation of E-cadherin degradation was not described until 2008, when Shen *et al.* proposed that Ca^{+2} depletion-mediated activation of Cdc42 Rab GTPase enhances EGFR signalling through Src activation. This results in the phosphorylation of E-cadherin in tyrosine residues and its subsequent ubiquitination by Hakai, leading to lysosomal degradation of E-cadherin protein and the disruption of cell-cell adhesions [167]. Later on, it was demonstrated that the adaptor protein Rack1, initially described as a substrate and inhibitor of Src kinase, stabilizes cell-cell adhesions through the inhibition of E-cadherin phosphorylation. Therefore, upon Ca^{+2} depletion and subsequent restoration, Rack1 inhibits Hakai-mediated ubiquitination and lysosomal degradation of E-cadherin by acting on Src. Moreover, Rack1 was also described to maintain cell-cell adhesions by inhibiting HGF-mediated E-cadherin endocytosis [168] (**Figure 14A**).

As previously mentioned, TGF-β represents another signalling pathway that plays an important role during EMT process [57]. In 2006, Janda *et al.* demonstrated that MAPK and TGF-β signalling pathways cooperate to regulate E-cadherin expression at the beginning of EMT. Interestingly, they demonstrate that the posttranslational regulation of E-cadherin via lysosomes is an early event during EMT, as it precedes its transcriptional repression, conversely to most genes that are regulated by TGF-β and Raf crosstalk. This occurs as a result of the increased endocytosis and lysosomal degradation induced by the synergistic activation of both pathways. Moreover, the authors demonstrated that Raf/MAPK and TGF-β cooperation drives Hakai-mediated E-cadherin ubiquitination. On the one hand, TGF-β acts at a transcriptional level to induce Hakai expression, while Raf/MAPK pathway induces tyrosine phosphorylation of E-cadherin, as it triggers the expression of many tyrosine kinases that may directly phosphorylate E-cadherin, such as Src [169] (**Figure 14B**).

Hakai has also been described to be involved in Slit-Robo signalling pathway in colorectal carcinoma, as mentioned above. Slit represents a family of secreted extracellular matrix proteins which bind to Roundabout (Robo) family of transmembrane receptors to regulate a number of cellular processes that involve cell migration. Particularly, Slit2 has been described to regulate cell migration during malignant transformation. Based on this background, the authors demonstrated that the interaction between Robo1 receptor and Slit2 protein induces epithelial-mesenchymal transition through the recruitment of Hakai, which thereafter ubiquitinates E-cadherin an induces its lysosomal degradation [159] (**Figure 14C**).

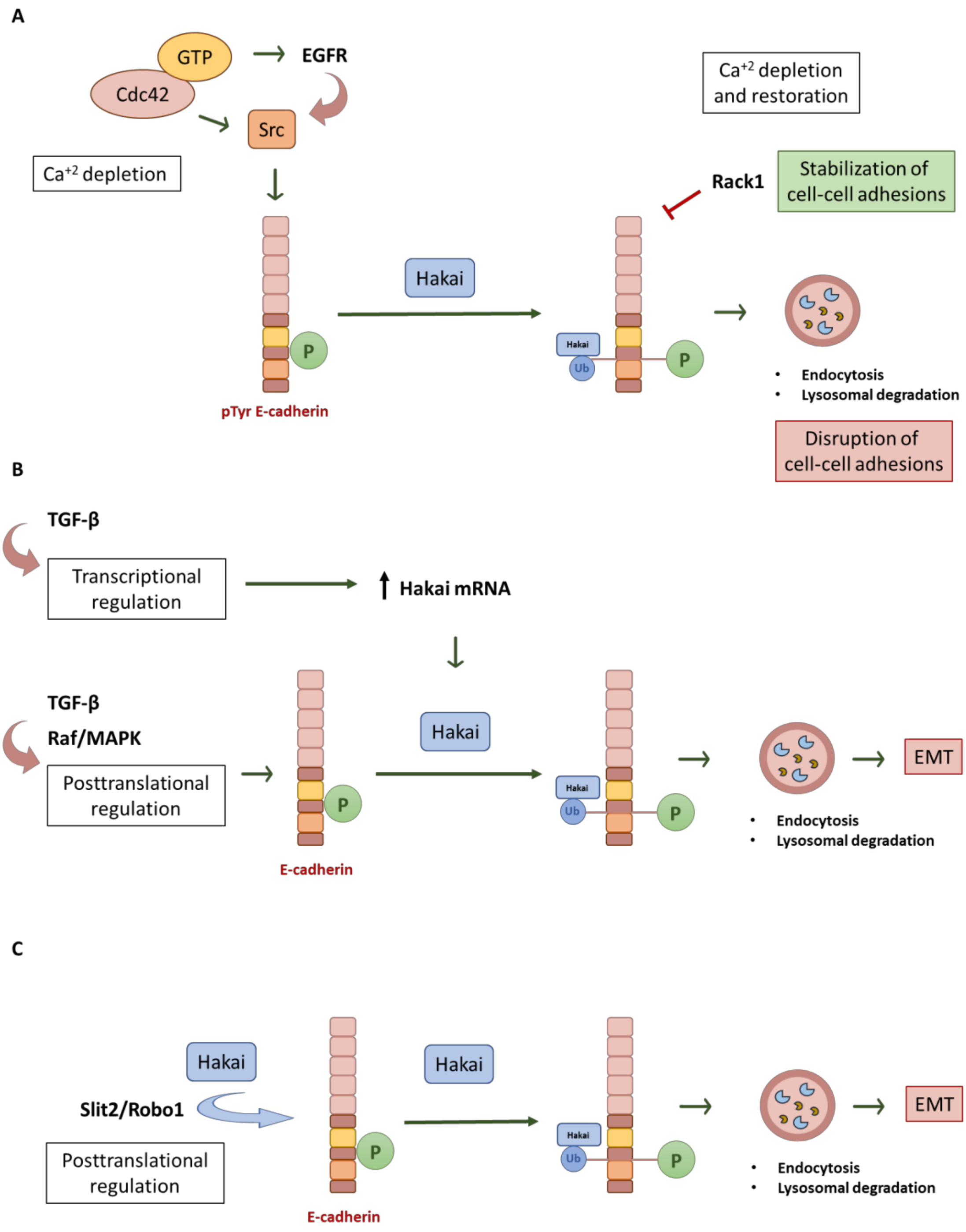
A
GTP
EGFR
Cdc42
Src
Ca+2 depletion
Ca+2 depletion and restoration
Rack1
Stabilization of cell-cell adhesions
Hakai
P
pTyr E-cadherin
Hakai
Ub
P
Endocytosis
Lysosomal degradation
Disruption of cell-cell adhesions
B
TGF-β
Transcriptional regulation
Hakai mRNA
TGF-β
Raf/MAPK
Posttranslational regulation
Hakai
P
E-cadherin
Hakai
Ub
P
EMT
Endocytosis
Lysosomal degradation
C
Hakai
Slit2/Robo1
Posttranslational regulation
Hakai
P
E-cadherin
Hakai
Ub
P
EMT
Endocytosis
Lysosomal degradation

Figure 14. Schematic representation of Hakai upstream signaling pathways. (**A**) Ca^{+2} depletion activates Rab GTPase Cdc42, which thereafter induces Src activation through EGFR signaling, triggering Hakai-mediated ubiquitination and lysosomal degradation of E-cadherin and causing the disruption of cell-cell contacts. Upon Ca^{+2} depletion and subsequent restoration, Rack1 inhibits Src-mediated phosphorylation of

E-cadherin, thus stabilizing cell-cell contacts. (**B**) Crosstalk between TGF-β and Raf/MAPK signaling pathways that regulate E-cadherin expression at the onset of EMT. (**C**) Slit-Robo interaction induces Hakai recruitment and malignant transformation during colorectal carcinoma, through Hakai-mediated ubiquitination and further degradation of E-cadherin. Image modified from Aparicio *et al*., 2012.

6.4. E3 ubiquitin-ligase Hakai as a potential therapeutic target

As mentioned above, ubiquitination process is usually dysregulated during tumour progression, and therapeutic strategies targeting E1, E2 and E3 enzymes as well as the deubiquitinating enzymes (DUBs) and the proteasome, have been developed in recent years. However, to date, among all drugs targeting members of the ubiquitin pathway, only three proteasome inhibitors have been approved by the FDA. The first inhibitor of 26S proteasome, bortezomib, was approved in 2003, and its introduction into clinical practice represented an improvement in complete remission, overall survival and progression-free rates in patients with multiple myeloma. Later on, carfilzomib and ixazomib were approved by FDA, in 2012 and 2015 respectively [129–132]. However, despite these drugs have been successful in treating haematological malignancies, they have shown a limited effect in the treatment of solid tumours [133,134]. Despite the successful inhibition of the proteasome in cancer treatment, the inhibition of proteasome-related DUBs (i.e. PSMD14, USP14 or UCHL5) may be a better therapeutic strategy than the inhibition of the proteasome itself, as they represent more specific anticancer targets [170]. For the same reason, E3 ubiquitin-ligases have been proposed as better therapeutic targets nowadays, as their inhibition would avoid broader side effects due to their substrate specificity [113,135].

Considering the previously described implication of E3 ubiquitin-ligase Hakai in many aspects of tumour progression, especially its major role in E-cadherin downregulation during EMT, it began to be considered as a promising therapeutic target for cancer treatment [146,153,157]. Furthermore, its increased expression in colorectal and lung carcinoma samples, compared to healthy tissues, has only reinforced its great potential as a drug target [158,160]. However, it is important to take into account the role of Hakai not only in pathological but also in physiological conditions, as its loss affects cell survival [147,158]. Therefore, the complete inhibition of Hakai may not necessarily be the best therapeutic strategy.

Another important feature that makes Hakai a good therapeutic target is the HYB (Hakai-pY-binding) domain. As described above, the dimeric architecture of the HYB domain makes it structurally different from other pTyr binding domains. Besides Hakai, the HYB domain has only been found in testis-specific ZNF645 E3 ligase, although they do not share the same target specificities [143–145]. Therefore, the development of a targeted therapy against Hakai HYB domain would allow the inhibition of the interaction between Hakai and E-cadherin, thus inhibiting Hakai ubiquitin-ligase activity without affecting its expression levels. This may prevent

E-cadherin downregulation and EMT triggering, having a major impact on the development of early-stage carcinomas, thus inhibiting tumour progression.

7. Drug discovery: small molecule identification

7.1. Small-molecule inhibitors for cancer treatment

Current therapeutic approaches for cancer treatment are focused on the identification and targeting of molecular drivers of cancer, usually showing fewer side effects than traditional chemotherapy. Two main strategies are commonly used in targeted cancer therapy: 1) biological agents such as antibodies, which show high selectivity but are usually limited to the cell surface; and 2) small molecules, which differ in selectivity but can potentially bind to a broader range of intracellular and extracellular targets. So far, the FDA has approved 43 small-molecule inhibitors with anti-oncogenic activity, most of them designed against intracellular kinases. Nevertheless, a large number of targets are currently being investigated, among which are those involved in protein-protein interactions, tumour metabolism, and immune response [171].

It is well established that protein-protein interactions (PPIs) play a major role in the regulation of many biological processes, such as cell division, apoptosis or cell cycle arrest. Alterations in the balance of PPIs are usually involved in the development of many diseases, including cancer. Nowadays, the interest in targeting PPIs for cancer treatment, both with antibodies or small molecules is constantly increasing [172]. PPIs have traditionally been considered as ‘undruggable’ targets, since they have large, flat and featureless interfaces, which make them more difficult to target than receptors or enzymes with well-defined catalytic sites. However, due to the extensive evidence from molecular, cellular and *in vivo* studies that support the great potential of PPIs as therapeutic targets, important efforts are currently being made to develop small-molecule inhibitors that can modulate their activity [172–174]. These small molecules are designed to bind a ‘hot spot’ in the target protein, thus disrupting key binding interactions. They are usually designed to block the interaction between a globular protein and a single peptide chain on the partner interacting protein, by binding into pockets in the surface of the globular protein [175–177]. In the last years, several PPI inhibitors have been developed for cancer treatment, for example those targeting p53-MDM2 interactions (i.e. Nutlin-3) or antiapoptotic BCL-2 proteins [178,179].

A promising therapeutic strategy in drug discovery is targeted protein degradation (TPD), which has recently emerged as an alternative to traditional pharmacologic approaches. It is based on the development of small molecules that induce the degradation of a target protein by modulating the activity of E3 ubiquitin-ligases. There are two main types of small molecules that induce protein degradation, also known as ‘degraders’: 1) hetero-bifunctional degraders or ‘proteolysis-targeting chimeras’ (PROTACs), and 2) non-chimeric compounds, which are known as molecular glues. Both PROTACs and molecular glues act by inducing the association between an E3 ubiquitin-ligase and a protein target [180,181]. Among the six hundred E3 ubiquitin-ligases, only some of them have been used in PROTAC-mediated targeted protein degradation. An example is MDM2, which has been used to develop a PROTAC (named A1874) against bromodomain-containing protein (BRD4), widely associated with cancer development. A1874 PROTAC significantly induced MDM2-mediated degradation of BRD4 in colorectal cancer and melanoma cells [182].

7.2. Small-molecule identification: virtual screening

Over the last decades, the identification of new small molecules that can potentially influence the activity of a protein target has been carried out by high throughput screening (HTS). It represents a well-established strategic approach which aims to identify ‘hit’ compounds (drug candidates) against a target of interest by analysing and assaying a great number of molecules. Nowadays, it is used not only by industry but also in the academic field [183]. However, despite its great importance in classical drug discovery, HTS has certain limitations in identifying hits that target PPIs, such as low hit rates, weakly potent hits or the challenge of excluding false positives [175]. Moreover, HTS may be expensive and time consuming, which has led to the development of a cheaper and effective computational approach, known as virtual screening [184].

Virtual screening (VS; also known as *in silico* screening) consists of the identification of the early ‘hits’ among a computer-based collection of compounds. Unlike HTS, which represents an experimental approach, VS is a theoretical one. It can be used alone, as an independent method to identify hit candidates, or as a complementary tool to HTS. VS consists of the virtual docking of a large number of compounds into the binding pocket of a protein target and the subsequent assessment of the tightness of the fit. The virtual compound library can be obtained from different sources, such as public (i.e. PubChem, ChEMBL or ChemSpider) and commercial (ChemBridge, ChemDiv or Life Chemicals) supplier databases [185]. Among the compounds that bind most strongly to the target protein, some of them are selected for further hit identification. Therefore, VS allows to analyse a huge number of compounds and also differentiate between active and inactive ones, thus reducing the number of molecules that need to be tested in order to identify hit candidates. For this reason, VS has become an essential tool in drug discovery over the last years [186].

II. HIPOTHESIS AND OBJECTIVES

As previously mentioned, E3 ubiquitin-ligase Hakai plays a major role during EMT and tumour progression, by downregulating E-cadherin at cell-cell contacts. Hakai recognizes tyrosine-phosphorylated E-cadherin through a novel pTyr-binding domain, known as HYB (Hakai-pY-binding) domain, which is formed as a result of a dimerization process. On the other hand, there is increasing evidence that links the EMT process with the acquisition of therapeutic resistance and the development of CSCs. Considering this information as well as the aforementioned background, the general hypothesis of this project was as follows:

- The specific inhibition of E3 ubiquitin-ligase Hakai with small molecules represents a good therapeutic approach for cancer treatment. Moreover, Hakai might be involved other aspects of tumour progression besides EMT, such as the acquisition of CSC properties.

In order to confirm this hypothesis, the following objectives were established:

OBJECTIVE 1

1. Develop a small-molecule inhibitor specifically targeting Hakai HYB domain, and analyse its antitumour effect both *in vitro* and *in vivo*.

1.1. Search for potential small-molecule inhibitors of E3 ubiquitin-ligase Hakai by virtual screening and select hit candidates.
1.2. Study the effect of the selected small-molecule inhibitor on Hakai-mediated E-cadherin ubiquitination and Hakai-E-cadherin interaction, by biochemical assays.
1.3. Analyse the antitumor effect of the selected compound *in vitro*, by using colorectal cancer cell lines and a Hakai-overexpression model.
1.4. Analyse the antitumor effect of the selected compound *in vivo*, by using a xenograft model in BALB/c immunodeficient mice.

OBJECTIVE 2

2. Study the involvement of E3 ubiquitin-ligase Hakai in other aspects of carcinogenesis, with the main focus in the acquisition CSC properties.

2.1. Deepen the study of the role of Hakai in tumour progression, by using co-cultures colorectal cancer cell lines and CAFs in a collagen matrix or '*in vitro* carcinoma assay'.
2.2. Establish stem cell-derived organoid cultures by using samples of colorectal cancer patients, to further analyse the involvement of Hakai in stemness as well as other aspects of carcinogenesis.
2.3. Analyse the potential role of Hakai in the acquisition of stem properties and the potential ability of Hakai inhibitor compound to regulate stemness *in vitro*, by using tumorsphere cultures or colorectal cancer cells.

III. MATHERIALS AND METHODS

A. MATERIALS AND METHODS RELATED TO OBJECTIVE 1

1. Virtual Screening and binding pocket analysis

In silico studies were carried out in collaboration with Dr. Federico Gago (Department of Biomedical Sciences, School of Medicine and Health Sciences, University of Alcalá) and Dr. Álvaro Cortés (Computational Chemistry-UK, RD Platform Technology & Science, GSK Medicines Research Centre, Hertfordshire, UK). The X-ray crystal structure of the phosphotyrosine-binding domain of Hakai (PDB 3VK6) [143] was downloaded from the Protein Data Bank, and Hakai dimer was modelled using the proper symmetry operations. Amino acid protonation was carried out using the pdb2pqr server at a pH of 7.2. 3D models for the ligands were built using the Virtual Screening and Data Management Integrated Platform (VSDMIP), as previously described [187,188]. Briefly, the initial 3D coordinates for each ligand were generated with CORINA. Thereafter, ALFA [189] was used to generate a large variety of conformers for each of which MOPAC-calculated atomic partial charges were assigned by employing the AM1 semiempirical model and the ESP method. All ligand models were stored in the VSDMIP database to be used in the different virtual screening campaigns.

Ligands in the eMolecules catalogue [https://www.emolecules.com/info/products-screening-compounds.html] were downloaded and processed as described above. Only molecules presenting a carboxylic acid moiety and/or a phosphate group capable of mimicking a phosphotyrosine residue were considered. Next, CRDOCK [190] was used to lodge the selected molecules inside the binding pocket of Hakai by using the CRScore scoring function and the BFGS energy minimizer. The ligands were then ranked according to the predicted score and the top 350 molecules were re-evaluated by using an in-house implementation of the HYDE scoring function [191]. Finally, the best 20 molecules were visually inspected to select a final set of 10 molecules for subsequent experimental validation. Finally, one compound, named Hakin-1 (Hakai inhibitor 1), was selected to perform further *in vitro* and *in vivo* studies.

To better analyse the results of the virtual screening campaign, in-house cGRILL software [191] was used. Affinity maps were produced within the binding pocket of Hakai phosphotyrosine-binding domain based on the van der Waals, Coulombic and hydrogen bonding interactions of hypothetical atomic probes. The negatively charged acceptor probe (=O) was used to map possible locations for the molecular recognition of the phosphotyrosine residue to help filtering the docking solutions during the visual inspection of the poses.

1.1. Screening of structural analogues of Hakin-1

The screening of structural analogues of Hakin-1 was carried out under the advice of the medical chemist Dr. Guido Kurz (Oncostellae biopharmaceutical company). Structural analogues are compounds that display a similar structure to another compound, but they differ from it in one or more atoms, functional groups or substructures. Even though analogous compounds are chemically very similar to each other, they may exhibit very different physical, chemical, biochemical, or pharmacological properties. Eight analogous compounds were selected and purchased from Vitas-M Lab. They were classified in four different families according to their chemical modifications, referred to as Family A (Hakin A-7, Hakin A-8, Hakin A-9), Family B (Hakin A-23 and Hakin A-25), Family C (Hakin A-10 and Hakin A-16) and Family D (Hakin A-6.1) for confidentiality reasons.

2. Inhibitors, reagents and antibodies

All inhibitor compounds were resuspended in DMSO (Sigma-Aldrich) to a 100 mM stock concentration, both for *in vitro* and *in vivo* assays. The highest concentration of DMSO was used as the vehicle control for the experiments. After resuspension in DMSO, all inhibitor compounds were aliquoted and stored at -20°C, protected from light. Hakin-1, as well as its analogue compounds, are detailed in **Table 1.**

Table 1. Hakai inhibitor compound 1 (Hakin-1) used for *in vitro* and *in vivo* assays, and analogue compounds used for *in vitro* assays.

Compound	Chemical name	MW	Provider/ Catalogue No
Hakin-1	4-(5-{[2-(4-nitrophenyl)-2-oxoethyl]thio}-1H-tetrazol-1-yl)benzoic acid	385.5	Chembridge / 6640684
Hakin A-7	Not shown for confidentiality reasons	358.35	Vitas-M Lab / ---
Hakin A-8	Not shown for confidentiality reasons	374.81	Vitas-M Lab / ---
Hakin A-9	Not shown for confidentiality reasons	419.26	Vitas-M Lab / ---
Hakin A-6.1	Not shown for confidentiality reasons	355.38	Vitas-M Lab / ---
Hakin A-10	Not shown for confidentiality reasons	347.4	Vitas-M Lab / ---
Hakin A-16	Not shown for confidentiality reasons	349.37	Vitas-M Lab / ---
Hakin A-23	Not shown for confidentiality reasons	380.84	Vitas-M Lab / ---
Hakin A-25	Not shown for confidentiality reasons	380.38	Vitas-M Lab / ---

5-fluorouracil (5-FU) was purchased from Sigma-Aldrich and resuspended in DMSO to a final stock concentration of 10 mg/ml. Once resuspended, 5-FU was subsequently aliquoted and stored at 4°C, protected from light.

Primary and secondary antibodies used for the experiments related to this objective, as well as their dilution, reference and the assay they were used for, are detailed in the following table.

Table 2. Primary and secondary antibodies used for Western Blot, Immunoprecipitation, Immunofluorescence, and Immunohistochemistry for paraffin embedded samples (IHC-P) assays.

Primary antibodies	**Dilution**	**Performed assay**	**Provider/ Catalogue No**
CD31	1:100	IHC-P	Abcam ab28364
Cortactin	1:1000	Western Blot	Millipore 05-180
	1:100	IHC-P	Millipore 05-180
E-Cadherin	1:1000	Western Blot	BD Biosciences 610182
	2 ug	Immunoprecipitation	BD Biosciences 610182
	1:200	Immunofluorescence	BD Biosciences 610182
	1:400	IHC-P	Cell Signalling Technology 243E10
FLAG® clone M2	1:4000	Western Blot	Sigma-Aldrich F3165
GAPDH	1:10000	Western Blot	Invitrogen 39-8600
HA (12CA5)	1:1000	Western Blot	Sigma-Aldrich, 11583816001
Hakai	1:1000	Western Blot	Invitrogen 36-2800
	1:250	IHC-P	Invitrogen 36-2800
Ki67	1:150	IHC-P	Dako M7240
N-Cadherin	1:1000	Western Blot	Abcam ab18203
	1:100	IHC-P	Abcam ab18203
Vimentin	1:1000	Western Blot	Cell Signalling Technology D21H3

Secondary antibodies	**Dilution**	**Performed assay**	**Reference**
Mouse IgG HRP Linked	1:10000	Western Blot	GE healthcare NA934
Rabbit IgG HRP Linked	1:10000	Western Blot	GE healthcare NA931
Mouse IgG Alexa Fluor 488	1:200	Immunofluorescence	Life Technologies A28175

3. Cell culture

MDCK epithelial cell line was obtained from American Type Culture Collection (ATCC® CCL-34™). MDCK cell lines that stably express Hakai protein (Hakai-MDCK) were kindly provided by Dr. Yasuyuki Fujita (MRC Laboratory of Molecular Cell Biology, UCL). Different Hakai-MDCK clones were obtained from two independent transfections, all of them with comparable phenotypes [153]. Hakai-MDCK clone 4 and clone 11 were used for this project. MDCK cell line was cultured in Dulbecco's Modified Eagle Medium (DMEM) (Thermo Fisher Scientific), and Hakai-MDCK cell lines were cultured in DMEM supplemented with 800 µg/ml G418 (Sigma-Aldrich), to maintain gene overexpression. HEK293 (ATCC® CRL-1573™) and HEK293T (ATCC® CRL-11268™) were obtained from ATCC and cultured in DMEM. Human liver cancer HepG2 (ATCC® HB-8065™), breast cancer MCF7 (ATCC® HTB-22™), and renal cancer ACHN (ATCC® CRL-1611™) cell lines were also cultured in DMEM. Human prostate cancer PC-3 (ATCC® CRL-1435™) cells were cultured in Ham´s F-12 medium (Thermo Fisher Scientific). Urinary bladder cancer 5637 (ATCC® HTB-9™) cell line was cultured in Roswell Park Memorial Institute (RPMI) 1640 medium (Thermo Fisher Scientific).

Human colon adenocarcinoma HT29 cell line was purchased from Sigma-Aldrich and cultured in McCoy's 5A Medium (Thermo Fisher Scientific). Human colorectal adenocarcinoma HCT116 cell line was kindly provided by Dr. Amancio Carnero (Instituto de Biomedicina de Sevilla, IBIS) and was also cultured in McCoy's 5A Medium. Human colon adenocarcinoma LoVo cell line was obtained from ATCC (ATCC® CCL-229™) and cultured in Ham´s F-12 medium.

All culture media were supplemented with 1% penicillin-streptomycin (5000 U/ml, Gibco) and 10% of Fetal Bovine Serum (FBS, Gibco). All cell lines were cultured at 37ºC in a humidified incubator with 5% CO_2 and used only for 1-3 months after being defrosted. Cells were monthly tested for mycoplasma contamination.

4. Western Blotting

4.1. Protein extraction from cultured cells

To perform protein extraction from cultured cells, confluent cultures were used. First, the medium in culture dishes with cells was discarded, and cells were washed using phosphate-buffered saline (PBS). After that, cells were scrapped in 1 ml of PBS, using a plastic cell scraper, and were collected in 1.5 ml Eppendorf tubes. Then, the cellular suspension was centrifuged at 5000 revolutions per minute (rpm) for 5 minutes at room temperature (RT).

After centrifugation, supernatant was discarded and cell pellet was lysed for 20 minutes at 4°C by using 1% Triton X-100 lysis buffer (**Table 3**) supplemented with 10 µg/ml aprotinin

(Sigma-Aldrich), 10 µg/ml leupeptin (Sigma-Aldrich) and 1 mM phenylmethylsulfonyl fluoride (PMSF) (Sigma-Aldrich). PMSF, leupeptin and aprotinin allow to preserve cellular proteins from protease digestion, as they act as protease inhibitors. For immunoprecipitation and ubiquitination experiments, 10 mM N-ethylmaleimide (Sigma-Aldrich) was also added. N-ethylmaleimide (NEM) is a cysteine protease inhibitor, which is commonly used as an inhibitor of deubiquitinating enzymes to preserve the native cell ubiquitination.

Table 3. Composition of the 1% Triton X-100 lysis buffer used for protein extraction.

Reagent	Stock concentration	Volume/50ml	Final concentration
Tris-HCl pH 7.5 (Sigma-Aldrich)	1 M	1 ml	20 mM
NaCl (Sigma-Aldrich)	5 M	1.5 ml	150 mM
Triton X-100 (Sigma-Aldrich)	100%	0.5 ml	1%
Distilled H_2O	---	Up to 50 ml	---

Following the incubation with lysis buffer, protein lysates were centrifuged at 12500 rpm for 10 minutes at 4ºC, and supernatant was collected in ice-cold 1.5 ml Eppendorf tubes. Finally, protein lysates were quantified or stored at -20ºC for subsequent quantification and sample preparation.

4.2. Protein quantification by the bicinchoninic acid (BCA) method

Quantitative determination of total protein was carried out by using *Pierce™ BCA Protein Assay Kit* (Thermo Fisher), a colorimetric assay that is based on bicinchoninic acid (BCA). This test allows to determine the total protein concentration in the sample by comparing it with a protein standard of bovine serum albumin (BSA).

The BCA Protein Assay combines to steps: the reduction of Cu^{2+} to Cu^{1+} by peptide bonds in protein and the colorimetric detection of reduced Cu^{1+} by BCA. Therefore, the first step is the chelation of copper with protein in an alkaline environment to form a light blue complex. This reaction is known as biuret reaction. The second step involves the colour development reaction, in which BCA reacts with the reduced cuprous cation that was formed in the previous step. This generates a purple-coloured reaction product as a result of the chelation of two molecules of BCA with one Cu^{1+}, which exhibits strong absorbance at 562 nm.

Hence, quantification protocol was carried out by following the indications of the commercial kit, for 96-well plate procedure, using a calibration curve of 0, 2, 4, 8, 12, 16 µg BSA, at a stock concentration of 2 µg/ml.

After that, 200 µl of working solution (A:B) were added in each well and the plate was incubated at 37ºC for 30 minutes. Working solution was prepared by mixing 50 parts of BCA Reagent A with 1 part of BCA Reagent B (50:1, Reagent A:B). Once the incubation finished, absorbance was measured at 570 nm using a Nanoquant Infinite M200 plate reader (Tecan Trading AG). Finally, a standard curve was prepared by plotting the 570 nm measurement for each BSA standard (y-axis) vs its concentration in µg/ml (x-axis). The standard curve was used to determine the protein concentration (µg/µl) of each unknown sample.

4.3. Sample preparation for Western Blotting

Once the protein concentration in each sample was determined, protein samples were prepared for loading into acrylamide gels. For sample preparation, 20 µg of each protein sample were mixed with 5X Laemmli buffer (10% SDS, 200 mM Tris-HCl pH 6.8, 50% glycerol, 0.1% bromophenol blue and 10% β-mercaptoethanol) to a final concentration of 1X. Each sample was filled up with distilled water to the final volume needed. Then, samples were heated for 5 minutes at 95ºC for protein denaturation, causing the disruption of secondary and tertiary structures and converting proteins to a linear form, further enabling antibody access to the protein epitope. β-mercaptoethanol also contributes to the denaturation process, by removing tertiary and quaternary structures through the reduction of intramolecular and intermolecular disulfide bonds between thiol groups of cysteine residues. Finally, samples were loaded into acrylamide gels or were stored at -20ºC to perform electrophoresis in a different day.

4.4. Sodium dodecyl sulfate–polyacrylamide gel electrophoresis (SDS-PAGE) and protein transfer to PVDF membrane

Sodium dodecyl sulfate–polyacrylamide gel electrophoresis (SDS-PAGE) was carried out for protein separation, which further allows the study of protein expression levels. In this analytical method, proteins become negatively charged as a consequence of their attachment to SDS anions. Moreover, SDS anions also cause protein denaturation by disrupting non-covalent bonds in the proteins. The negative charge acquired by polypeptide chains, as a result of their interaction with SDS, is proportional to their length. This allows protein separation according to the molecular weight, as the differences between the mobility of proteins in the gel can be attributed only to their size (instead of both their size and charge). Protein separation based only on the polypeptide chain size simplifies the analysis of protein molecules.

SDS-PAGE combines the above-mentioned addition of negative charges to the proteins with a discontinuous buffer system and two different gel layers (also known as stacking gel and resolving gel). In discontinuous buffers systems, the composition of the gel buffer and the running buffer is different, that means the primary anion in the gel is also different from the primary anion in the running buffer. The most widely used SDS-PAGE system is the Laemmli (Tris-glycine) system, in which the stacking gel is buffered at pH 6.8 by Tris-HCl and the resolving gel is buffered to pH 8.8 by Tris-HCl. The different pH of stacking and resolving gels affects the electric charge of glycine ions, that are present in the electrophoresis buffer. Thus, in the stacking gel, the chloride ions act as the leading ions, migrating through the gel more quickly than the protein sample. In the other hand, the glycine ions in the electrophoresis buffer migrate more slowly, acting as trailing ions, as pH 6.8 is near to glycine's isoelectric point. This leads to the protein migration in a sharp band between these two ions. Finally, when proteins enter in the resolving gel, glycine is ionized due to the increase in pH value and migrates faster than in the stacking gel, allowing protein separation based on molecular size.

Western Blot assays were made using 1.5 mm-thick 10% acrylamide gels (mini gel format). Stacking and resolving gel composition for the above-mentioned percentage of acrylamide, are shown in **Table 4.**

Table 4. Composition of 10% acrylamide gels used for SDS-PAGE

Reagent	Stacking gel	Resolving gel
Distilled water (dH_2O)	1.6 ml	3 ml
0.5 M Tris-HCl (pH 6.8) (Sigma-Aldrich)	625 µl	---
1.5 M Tris-HCl (pH 8.8) (Sigma-Aldrich)	---	2.5 ml
50% Glycerol (Sigma-Aldrich)	---	2 ml
40% Acrylamide/Bis-acrylamide (Bio-Rad)	250 µl	2.5 ml
10% SDS (Sigma-Aldrich)	25 µl	100 µl
Tetramethylethylenediamine (TEMED) (NZYTech)	3.75 µl	15 µl
10% Ammonium persulfate (APS) (Sigma-Aldrich)	25 µl	50 µl

Electrophoresis step was done by using the electrophoresis chamber *Mini-PROTEAN® Tetra Vertical Electrophoresis Cell* (Bio-Rad), electrophoresis buffer (25 mM Trizma® base, 192 mM glycine, 0.1% SDS), and the following running conditions: 80V for 10 minutes, and 180 V for 1 hour and 30 minutes at room temperature. Protein molecular weight was determined by using *NZYColour Protein Marker I* (NzyTech).

To carry out blotting step, polyvinylidene difluoride (PVDF) membranes were used (*Immun-Blot PVDF Membrane*, Bio-Rad). Before transfer stack assembly, PVDF membranes were activated in methanol for 15 seconds and incubated thereafter in distilled water for 5 minutes. Blotting step was done according to manufacturer's indications, by using the *Mini Trans-Blot® cell* (Bio-Rad). This system is prepared to perform a wet transfer, in which the gel is placed into a "transfer sandwich" (filter paper-gel-membrane-filter paper) and the tank is filled with transfer buffer (25 mM Trizma® base, 192 mM glycine). Transfer was carried out at 200 mA for 1 hour, placing the tank into an ice box as a cooling system to dissipate the heat produced due to the high current applied.

4.5. Antibody incubation

Once the blotting step finished, membranes were incubated for 1 hour at room temperature using blocking buffer: 5% skim milk powder (Sigma-Aldrich) in TBST (Tris buffered saline-Tween 20: 20mM Tris, 150mM NaCl, 0.1% Tween 20, Sigma-Aldrich). After the incubation with the blocking buffer, incubation with primary antibody against the target protein was carried out overnight at 4°C. Primary antibodies were diluted in blocking buffer, according to the manufacturer's recommended ratio.

After the incubation with the primary antibody, the membrane was rinsed in TBST, in three washes of 10 minutes each. Then, the membrane was incubated with the secondary antibody, also diluted in blocking buffer. The incubation with the secondary antibody solution was carried out for 1 hour at room temperature, and after that the membrane was washed three more times in TBST. Primary antibodies used, as well as the dilutions thereof, are detailed in **Table 2**.

Secondary antibodies are conjugated to HRP (horseradish peroxidase) enzyme, which allows protein detection by chemiluminescence when a chemiluminescent substrate (an organic dye such as luminol) is applied to the blot. Secondary antibodies used, as well as the dilutions thereof, are detailed in **Table 2.** Horseradish peroxidase catalyses the oxidation of luminol to 3-aminophthalate, and in normal conditions the light emitted is usually of low intensity and does not last long enough to make an accurate detection and analysis. To address this issue, most commercially available chemiluminescent substrates are supplied with an enhancer that increases the intensity of the light emitted in the chemiluminescent reaction more than a thousand fold. This phenomenon is known as enhanced chemiluminescence (ECL). Therefore, protein detection was performed by using the *Immobilon® Crescendo Western HRP substrate* detection reagent (Millipore) and the Amersham Imager 600 imaging system (GE Healthcare). After chemiluminescent detection, protein expression levels were quantified by using ImageJ software (National Institutes of Health) or also the quantification software that is included in the Amersham imaging system.

5. Ubiquitination assay

To study Hakai inhibitors' effect over total ubiquitination, HEK293T cells were seeded in 6-well plates, at a cell density of 7.5 x 10^5 cells per well. Cells were transfected 24 hours after seeding, by using pSG-v-Src (0.25 µg), pcDNA-FLAG-Hakai (0.75 µg) and pBSSR-HA-Ubiquitin (0.50 µg) plasmids, and Lipofectamine™ 2000 reagent (Invitrogen). Control plasmid pcDNA3.1 was used to equalize plasmid concentration in the different conditions. Lipofectamine reagent is based on lipid subunits that can form liposomes and complex with negatively charged nucleic acid molecules, allowing them to go through the cell membrane. Complexes were prepared using a DNA (µg) to Lipofectamine 2000 (µl) ratio of 1:2. To increase transfection efficiency, *Opti-MEM™ Reduced Serum Media* (Thermo Fisher) was used.

Transfection complexes were prepared by diluting plasmids and Lipofectamine in *Opti-MEM™* medium in separated Eppendorf tubes, incubating thereafter 5 minutes at room temperature. Then, the diluted lipofectamine and plasmid were combined, mixing gently and incubating for 20 minutes at room temperature to allow the formation of Lipofectamine-DNA complexes. During the incubation time, culture medium was removed from HEK293T cells, washing them with saline and adding 1.25 ml of *Opti-MEM*™ medium in each well. Finally, 250 µl of transfection mix were added to each well, and plates were subsequently incubated at 37°C for six hours.

Once the incubation was finished, Lipofectamine-DNA complexes were discarded by removing *Opti-MEM*™ medium. Finally, cells were washed again with saline and DMEM medium containing the appropriate inhibitor concentrations was added to each well. DMSO was used as a vehicle control, to avoid its effect from being falsely attributed to the drug. Inhibitor's effect over total ubiquitination was evaluated by Western Blot assay 48 hours after transfection, as previously described in section 4. Primary and secondary antibodies used for ubiquitination assays, as well as their dilutions, are detailed in **Table 2.**

6. Immunoprecipitation assays

Inhibitors' effect over E-cadherin ubiquitination was studied by immunoprecipitation assays. In such experiments, HEK293 cells were seeded in 10 cm dishes, at a cell density of 3 million cells per plate. The day after seeding, cells were transfected with the following plasmids: pSG-v-Src (3 µg), pcDNA-FLAG-Hakai (4 µg), pcDNA-Myc-E-cadherin (3 µg) and pBSSR-HA-Ubiquitin (2 µg), by using Lipofectamine™ 2000 transfection reagent (Invitrogen). pcDNA3.1 plasmid was used as a control to equalize the maximum plasmid concentration. Transfection protocol, as well as inhibitor treatment, was carried out as previously described.

Immunoprecipitation assay was carried out the day after transfection. In order to do so, cells were lysed for 30 minutes at 4°C, by using 1% Triton X-100 lysis buffer (**Table 3**), supplemented with protease and deubiquitinase inhibitors as previously described (section 4.1.), as well as 2.5 mM sodium orthovanadate. Sodium orthovanadate is an inhibitor of phosphotyrosine phosphatases which is used to preserve the protein tyrosine-phosphorylation state. This allows to maintain E-cadherin phosphorylation in tyrosine residues by Src kinase, and therefore the study of E-cadherin ubiquitination and Hakai-E-cadherin interaction. Once incubation was finished, cell lysates were centrifuged at 14000 rpm for 10 minutes at 4°C, and supernatant was subsequently collected in a clean, ice-cold, 1.5 ml tube. At the same time, 60 µl of agarose beads (protein G PLUS, Santa Cruz Biotechnology) were incubated with 2 µg of anti-E-cadherin antibody (BD Transduction Laboratories) for 30 minutes at 4°C and under gentle rotation. 2 µg of normal mouse IgG (Santa Cruz Biotechnology) were used as a negative control. After incubation step, beads were washed with 1 ml of lysis buffer and subsequently centrifuged at 3000 rpm for 2 minutes at 4°C.

Antibody-conjugated beads were thereafter incubated with 900 µl of protein lysates, for 2 hours at 4°C and under gentle rotation. The remaining 100 µl were kept on ice in a separated 1.5 ml tube, as a protein input control. After incubation, beads were washed twice with 1ml of lysis buffer and centrifuged at 3000 rpm for 2 minutes at 4°C in each washing step.

Finally, Laemmli buffer (described in section 4.3) was added to each tube (both with beads and with protein lysates), and samples were heated for 5 minutes at 95ºC for protein denaturation and protein-antibody elution from the beads. Samples were then loaded into acrylamide gels or were stored at -20ºC to perform Western Blot assay the following day. Antibodies used for immunoprecipitation assay are shown in **Table 2.**

7. Cell cytotoxicity assay (MTT)

To determine cell viability, cells were seeded in a 96-well plate, at a density of 1 x 10^4 cells per well in 100 µl of appropriate culture medium. 24 hours after seeding, cells were treated for 72 hours with different inhibitor concentrations, refreshing treatment at 48 hours. Cytotoxicity assay was carried out after 72 hours of treatment, by using 3-(4,5-dimethylthiazol-2-yl)-2,5-diphenyltetrazolium bromide (MTT) colorimetric assay (Sigma-Aldrich).

MTT assay allows to determine cell viability in an indirect way, by outlining cell metabolic activity. MTT is a water-soluble tetrazolium salt that in viable cells with an active metabolism is reduced to formazan, which is purple coloured and water insoluble. The reduction of tetrazolium salt MTT into formazan crystals is carried out by mitochondrial dehydrogenases (in particular, succinate dehydrogenase), and it is thus positively correlated with metabolically active cells.

MTT solution was added to the cells 72 hours after treatment, at a final concentration of 0.5 mg/ml, and cells were then incubated at 37°C for 3 hours. Once incubation finished, culture medium was removed very carefully, and formazan crystals were subsequently dissolved by adding 100 µl of dimethyl sulfoxide (DMSO). After solubilization step, plates were incubated for 15 minutes at room temperature, under agitation, and absorbance was measured at 570 nm, using 630 nm as a wavelength reference value. Absorbance was measured by using Infinite® 200

NanoQuant plate reader (Tecan). Finally, half maximal inhibitory concentration (IC_{50}) was calculated by using GraphPad Prism software. This value represents the concentration of compound where percent inhibition is equal to 50, that is, the dose of the inhibitor required to achieve 50% viability of cancer cells.

8. Cell proliferation assay (BrdU)

Quantification of cell proliferation was carried out by using *Cell Proliferation ELISA BrdU (colorimetric)* commercial kit (Roche), which is based on the measurement of 5-bromo-2'-deoxyuridine (BrdU) incorporation during DNA synthesis. BrdU is a synthetic nucleoside that can be incorporated as a thymidine analogue during DNA synthesis. Once incorporated by proliferating cells, BrdU is then detected by using a specific antibody.

To perform BrdU cell proliferation assay, cells were seeded in 96-well plates, at a cell density of 1 x 10^4 cells per well. The following day, cells were treated with the appropriate inhibitor concentrations, and BrdU assay was carried out 48 hours after treatment. To do so, cells were first labelled with 10 µM BrdU under sterile conditions and incubated thereafter at 37°C for 2 hours. Once incubation finished, BrdU labelling solution was removed from the cells and plate was air-dried at room temperature to completely dry the cells. After this step, dry cells were stored for up to one week at 4°C in case in case the immunoassay was performed at a different day.

To continue with BrdU immunodetection, 200 µl of *FixDenat solution (bottle 2)* were added to each well, incubating then the cells for 30 minutes at room temperature. This allows cell fixation and DNA denaturation in the same step. The denaturation of the DNA increases the accessibility of the incorporated BrdU, thus improving subsequent antibody detection. After denaturation step, *FixDenat solution* was removed and 100 µl of anti-BrdU-POD (anti-BrdU antibody conjugated with a peroxidase) working solution were then added to each well, incubating cells for 90 min at room temperature. POD conjugated anti-BrdU antibody binds to the BrdU incorporated in newly synthesized cellular DNA. Anti-BrdU-POD working solution was previously prepared by diluting *Anti-BrdU-POD stock solution (bottle 3)* 1:100 with *Antibody solution dilution (bottle 4)*. Following 90 minutes of incubation with the antibody, cells were washed three times with 100 µl of *Washing buffer solution (bottle 5)* per well, previously diluted 1:10 in distilled water.

After washing step, 100 µl of *Substrate solution (bottle 6)* were added to each well, and plates were incubated at room temperature and in the dark, until colour development was intense enough for photometric detection (around 5-10 minutes). Substrate solution is based on 3,3',5,5'-Tetramethylbenzidine (TMB), a chromogenic substrate which is sensitive to light and whose oxidation by peroxidase enzyme causes the solution to take on a blue colour.

Colour change was subsequently measured by using Infinite® 200 NanoQuant plate reader (Tecan) at the wavelength of 370 nm, using 492 nm as a reference value. The developed colour and thereby the absorbance values directly correlate to the amount of DNA synthesis and hereby to the number of proliferating cells in the respective microcultures. Finally, graphical representation of the results, as well as statistical analysis thereof, was carried out with GraphPad Prism software.

9. Phenotypic characterization

To study the effect of Hakai inhibitors on epithelial differentiation, cells were seeded in 6-well plates, at a cell density of 3.75×10^5 cells per well. The following day, cells were treated with the appropriate inhibitor concentrations (50 µM and 100 µM), diluted in culture medium, using DMSO as vehicle control. Cells were thereafter incubated at 37°C under 5% CO_2 for 48 hours, and epithelial differentiation was evaluated by phase-contrast microscopy. Images were taken by using an Eclipse-Ti microscope (Nikon) and a 20x objective.

10. Gene expression analysis by quantitative polymerase chain reaction (qPCR)

10.1. Purification of total RNA from cultured cells

RNA extraction from cultured cells was carried out by using *TriPure Isolation reagent* (Roche), a monophasic solution of phenol and guanidine isothiocyanate that is designed to isolate separated fractions of RNA, DNA, and proteins from the same sample.

In order to isolate RNA, 1 ml of *TriPure* reagent was added over cell pellet (collected from a 10 cm culture dish) and cells were lysed by vigorous vortexing until homogeneous suspension was obtained. Each homogenized sample was thereafter incubated for 15 minutes at room temperature to ensure the complete dissociation of nucleoprotein complexes. After that, 200 µl of chloroform (Sigma-Aldrich) were added to each sample, and then tubes were shaken vigorously for 15 seconds and centrifuged at 12500 rpm for 15 minutes at 4°C. As a result of the centrifugation step, samples are separated into three different phases. RNA is isolated from the colourless upper aqueous phase, while DNA and proteins are isolated from the interphase and lower red organic phase, respectively.

Therefore, the colourless aqueous phase containing the RNA was transferred to a new 1.5 ml Eppendorf tube, and RNA was precipitated by adding 500 µl of isopropanol (Sigma-Aldrich). After that, the tube was capped and inverted several times to mix the aqueous phase with isopropanol thoroughly, and the sample was incubated for 10 minutes at room temperature to allow RNA precipitation. Samples were then centrifuged at 12500 rpm for 15 minutes at 4°C and supernatant was discarded, and precipitated RNA was washed by adding 1 ml of 70% ethanol and vortexing. After washing step, samples were centrifuged again and supernatant was discarded, removing the excess of ethanol from the RNA pellet by air-drying the sample. Finally, precipitated RNA was resuspended in 20 µl nuclease-free distilled water (Ambion®). RNA concentration and quality were determined by using NanoDrop ND-1000 spectrophotometer (Thermo Fisher).

10.2. cDNA synthesis from isolated RNA

After RNA purification step, reverse transcription polymerase chain reaction (RT-PCR) was carried out to synthesize first-strand cDNA. This allows further quantification of gene expression by real time quantitative Reverse Transcription PCR (RT-qPCR).

Reverse transcription of RNA into DNA was carried out by using *NZY First-Strand cDNA Synthesis Kit* (NZYTech). 500 ng of RNA were used as starting material, which were added to a reaction mix containing 10 µl of *NZYRT 2X Master Mix* (consisting of dNTPs, $MgCl_2$, optimized RT buffer and a combination of random hexamers and oligo$(dT)_{18}$ primers) and 5 µl of *NZYRT Enzyme Mix* (consisting of a reverse transcriptase and a ribonuclease inhibitor, in order to protect RNA against degradation). Reaction mix was filled up to 20 µl with DEPC-treated water.

Once prepared, reaction mix was mixed gently and incubated at 25°C for 10 minutes, to promote RNA denaturation. After that, samples were incubated at 50°C (optimal temperature of reverse transcriptase) for 30 minutes, to promote cDNA synthesis. Reverse transcription reaction was inactivated by heating at 85°C for 5 minutes, chilling on ice immediately after. Finally, 1 µl of *NZY RNase H* was added to each sample, incubating at 37°C for 20 minutes. RNase H specifically degrades RNA template in cDNA-RNA hybrids after first-strand cDNA synthesis. This procedure increases the sensitivity of subsequent RT-qPCR reaction, as PCR primers will bind more easily to the cDNA. Finally, synthesised cDNA was stored at -20°C until RT-qPCR was performed.

10.3. Real time quantitative Reverse Transcription PCR (RT-qPCR)

Quantification of gene expression was accomplished by real time quantitative Reverse Transcription PCR (RT-qPCR), using *LightCycler® 480 SYBR Green I Master* (Roche). The *LightCycler® 480 SYBR Green I Master* is a one-component hot start reaction mix for PCR using the LightCycler® 480 Instrument. The reaction mix contains *FastStart Taq DNA Polymerase*, DNA double-strand-specific *SYBR Green I* dye and dNTPs. PCR was carried out in 96-well plates (*LightCycler® 480 Multiwell Plate 96*, Roche), using 1 µl of cDNA, 0.7 µl of primer F/R, and 5 µl of *SYBR Green I Master 2x* per sample, filling up to 10 µl of final volume with water. Primers used for RT-qPCR are detailed in **Table 5.** Samples were loaded in triplicates and the following PCR program was used: 95°C for 10 minutes (DNA polymerase activation), 40 cycles of amplification [95°C for 10 seconds (denaturation), 60°C for 5 seconds (annealing), 72°C for 10 seconds (extension)], 1 cycle of melting [95°C for 5 seconds, 65°C for 1 minute], and a cooling final step of 40°C for 10 seconds.

Table 5. Forward and reverse sequences of primers used for RT-qPCR

Gene ID	Species	Forward sequence (5'-3')	Reverse sequence (5'-3')
CBLL1	Human	CGCAGACGAATTCCTATAAAGC	CCTTCTTCATCACCAGGTGG
CDH1	Human	AGTGTCCCCCGGTATCTTCC	CAGCCGCTTTCAGATTTTCAT
RPL13	Human	CAAGCGGATGAACACCAAC	TGTGGGGCAGCATACCTC

SYBR Green is a fluorescent dye which can intercalate in double-stranded DNA, in particular at the minor groove. Upon intercalation with double-stranded DNA, *SYBR Green* fluorescence increases up to 1000 times. This allows measurement of the amount of PCR product, since the number of *SYBR Green* molecules incorporated into DNA increases as the amount of DNA product increases. Therefore, the increase in fluorescence is proportional to the amount of product accumulated, which makes *SYBR Green*-based PCR a good approach for relative DNA quantification.

In relative qPCR, the number of DNA copies at the beginning of the process is given as the number of PCR cycles (threshold cycle, or C_t) necessary to achieve a significant increase in fluorescence signal. The value of the threshold cycle (C_t) is inversely proportional to the initial number of template DNA molecules. Therefore, to determine the expression levels of target genes, relative quantification based on $2^{-\Delta\Delta Ct}$ method was carried out. In this quantification method, the expression levels of the genes of interest are relativized to the expression levels of a reference gene, also known as *housekeeping*.

11. Immunofluorescence assay

To perform immunofluorescence assays, cells were seeded in 8-well chambers (*Millicell EZ SLIDE 8-well glass,* Millipore) at a cell density of 12.5 x 10^4 cells per well. 24 hours after seeding, cells were treated with appropriate inhibitor concentrations. Finally, immunofluorescence assay was carried out 48 hours post-treatment.

For immunofluorescence assay, culture medium was removed, and cells were washed once with PBS. Cells were thereupon fixed with 4% paraformaldehyde (PFA) solution in PBS for 15 minutes at room temperature. Once fixation finished, cells were washed three times with PBS and permeabilized for 15 minutes with PBS containing 0.25% Triton X-100. To block unspecific binding of the antibodies, cells were incubated with culture medium supplemented with 10% FBS for at least one hour at room temperature. After that, incubation with primary antibodies diluted in blocking solution was carried out for 2 hours at room temperature. Once incubation with primary antibodies finished, cells were washed three times with PBS and subsequently incubated with secondary antibodies, also diluted in blocking solution, for 1 hour at room temperature. Incubation with secondary antibodies was carried out in the dark, as prolonged exposure to light would compromise the antibody activity due to photo-bleaching of the fluorophores. Primary and secondary antibodies used for immunofluorescence assays are detailed in **Table 2.**

Once incubation with secondary antibodies finished, cells were washed 3 times with PBS and then incubated with Hoechst 33342 (Life Technologies), previously diluted 1:5000 in PBS, for 5 minutes at room temperature and in the dark. Hoechst incubation allows further staining of cell nucleus, by binding to the minor groove of double-stranded DNA. Finally, cells were washed once with PBS and once with distilled water, and silicone chamber was removed. Mounting for microscopy was carried out by using *ProLong Gold antifade reagent* (Invitrogen). Samples were analysed under a fluorescence Olympus BX61 microscope, equipped with an Olympus DP70 digital camera, using a 20x objective and taking 5 pictures for each condition. Fluorescence intensity was quantified by using ImageJ software (National Institutes of Health). Graphical representation of results, as well as statistical analysis, was carried out with GraphPad Prism software.

12. Cell migration assays

12.1. Wound healing assay

The wound-healing assay, or scratch assay, is a simple method that allows the study of directional cell migration *in vitro*. It is called scratch assay because is based on creating a scratch, or cell-free area, in a cell monolayer and then allowing cells to migrate to close the gap. During this process, images are taking at regular intervals to monitor wound closure. There are different approaches to create this scratch, in this case, a mechanical approach was performed, by using 2-well culture-Inserts (Ibidi).

To perform this assay, cells were seeded at a cell density of 7 x 10^5 cells in each well of the insert and were allowed to grow for 24 hours. The day after seeding, cells were treated with 10 µg/ml of mitomycin C (Sigma-Aldrich) for two hours. Mitomycin C treatment is used to stop cell proliferation, as it causes the cross-linking of double-stranded DNA, which results in inhibition of DNA synthesis. This allows to exclusively measure cell migration capacity, as wound is only closed by the migrating cells and not by the proliferating ones. After 2 hours, mitomycin C treatment and 2-well culture inserts were removed.

Once the inserts were removed and wounds were created, cells were treated with the indicated concentrations of inhibitor, in combination or not with 5- fluorouracil (5-FU) (Sigma-

Aldrich), and were allowed to migrate for 72 hours. 5-FU and specific inhibitor treatments were refreshed after 48 hours. Cell migration was monitored by taking pictures at 0, 24, 48 and 72 hours with an Eclipse-Ti microscope (Nikon), using a 4x objective. The migration rate of the cells was quantified with ImageJ software (National Institutes of Health), by using the MRI Wound Healing Tool and analysing three pictures of each condition.

12.2. Boyden chamber migration assay

Cell migration studies were also carried out by using Boyden chamber assay, which is the most widely accepted cell migration technique. This system uses a hollow plastic chamber, which is sealed at one end with a porous membrane (with a pore size of 5-8 μm for cancer cells). At the same time, this plastic chamber is suspended over a larger well containing medium with higher concentration of serum, that acts as a chemoattractant. Cells are then placed inside the and allowed to migrate through the pores, to the other side of the membrane. Finally, migratory cells that were able to pass through the pores are then stained and counted.

Migration assay was carried out by using *QCM™ cell migration kit* (Millipore). First, cells were seeded in 6-well plates, at a cell density of 7.5 x 10^5 cells per well, and treated with appropriate concentrations of Hakin-1, diluted in appropriate culture medium. 24 hours after seeding, culture medium was removed, and FBS starvation was performed by treating cells with Hakin-1 diluted in culture medium not supplemented with FBS. Starvation was carried out for another 24 hours.

The following day, cells were splitted and subsequently seeded in the cell migration chamber, at a cell density of 3 x 10^5 cells per chamber, and in culture medium not supplemented with FBS. Chambers were suspended over a larger well with culture medium containing 30% of FBS, therefore creating an FBS gradient. FBS acts as a chemoattractant that induces cell migration through the membrane. After 16 hours, culture medium was removed (both from inside and outside the chamber), and cells that were not able to migrate (in the upper side of the membrane) were also removed by using a cotton swab. Then, cells that migrated through the membrane, located at the bottom side of the chamber, were stained with Crystal Violet (Merck) for 20 minutes at room temperature. Once incubation with crystal violet finished, chambers were washed with PBS and subsequently allowed to air-dry for 30 minutes at room temperature. Finally, the membrane was cut out, placed on a slide and mounted with a coverslip by using *Glycergel Mounting Medium* (Dako).

Cells that migrated were analysed with an Olympus BX61 microscope, counting the number of cells per 20x field and taking pictures of five fields in each sample. Experiments were performed in triplicates for each condition and the assays were repeated at least three times. Results are expressed as mean ± SD.

13. Cell invasion assay

For invasion assays, a *CytoselectTM 24-Well Cell Invasion Kit* (Cell Biolabs, Inc.) was used. This kit is also based in the Boyden chamber assay, but in this case the upper surface of the membrane is coated with a uniform layer of dried bovine type I collagen matrix. This collagen matrix allows to discriminate between invasive and non-invasive cells, as invasiveness requires proteolysis of the extracellular matrix. Therefore, only invasive cells are able to degrade the collagen matrix layer and pass through the membrane, which allows its subsequent staining and quantification.

First, cells were seeded in 6-well plates, at a cell density of 7.5 x 10^5 cells per well and treated for 24 hours with appropriate concentrations of Hakin-1, previously diluted in normal culture medium. 24 hours after seeding, culture medium was removed, and FBS starvation was performed by treating cells with Hakin-1 diluted in culture medium supplemented only with 1% FBS. Starvation was carried out for another 24 hours.

The next day, cells were splitted and thereafter seeded in the invasion chamber, at a cell density of 3 x 10^5 cells per chamber, in culture medium supplemented with 2% of FBS. Culture medium containing 30% FBS was used for the lower well. 16 hours after seeding, culture medium and non-invasive cells on the top of the membrane were removed. Finally, invasive cells were stained with crystal violet (Merk) and subsequently quantified as previously described.

14. Soft agar colony formation assay

Soft agar colony formation assay is based on the ability of transformed cells to grow independently of an anchorage surface, and it is considered one of the most important tests to study malignant transformation of cells. To carry out this assay, cells were seeded in 12-well plates, previously coated with a layer of 0.75% soft agar (BD Biosciences) in 10% FBS culture medium. This coating solution was prepared by diluting a stock solution of 1.5% agar 1:1 with 20% FBS culture medium. 1.5% agar solution (diluted in culture medium without FBS) was previously heated over 40°C to melt it and allow its dilution in 20% FBS culture medium. Once prepared, the coating solution was added to each well, and plates were kept at room temperature for 2 hours, until agar solidified again.

After that, cells were seeded in triplicates at a cell density of 5 x 10^3 cells per well in a 0.4% solution of soft agar, which was prepared as previously described. The use of two different agar layers prevents cells from adhering to the culture plate and allows transformed cells to form visible colonies. After seeding, each well was allowed to solidify and subsequently covered with 150 µl of culture medium in presence or absence of the appropriate inhibitor concentrations. Treatment was refreshed every 3 days and colony number was quantified after 21 days. Cells that were able to form colonies in this anchorage-independent manner were considered as transformed and carcinogenic.

Finally, quantification was performed by taking pictures of five randomly selected fields of each condition, using a Nikon Eclipse-TI microscope (4x objective). Once pictures were taken, colony number in each field was determined. Experiments were conducted with three triplicates and were repeated three times. Data are represented as mean ± SD.

15. Tumour xenograft model

To study Hakin-1 effect on tumour progression and carcinogenesis *in vivo*, an animal model using athymic mice (BALB/c, nu/nu) was carried out. Xenograft experiments were performed at the Experimental Surgery Unit – Technological Training Center from INIBIC, in compliance with the European Community Law (86/609/EEC) and the Spanish law (R.D. 53/2013). The project experiment (ethic code: 2017/R12) was approved by the Ethics Committee for Animal Experimentation of Xerencia de Xestión Integrada da Coruña (XXIAC).

BALB/c mice lack a thymus and they are immunodeficient, as they are unable to produce T cells. For this reason, all experimental procedure was carried out under sterile conditions. For xenograft model, female mice with an average weight of 19-24 g and six weeks old were used and randomly distributed in four groups. They were kept in a 12/12 hours light/dark cycle with water and food available ad libitum, at an ambient temperature of 22°C and a relative humidity of 70-80%.

One million of MDCK cells, resuspended in DMEM without serum and antibiotic, were subcutaneously inoculated in both flanks in two groups of 3 animals. The same number of Hakai-MDCK cells was injected in two groups of 4 animals. Twenty days after inoculation tumours in Hakai-MDCK were palpable. Then, half of the animals were treated with Hakin-1 (5 mg/kg) and the other half with the same concentration of DMSO every 3 days. Tumour outgrowth was monitored twice a week taking measurements of tumour length (L) and width (W) with an electronic calypter (ATM Enterprises). Tumour volume, expressed as cubic centimetres (cm^3), was calculated as $(\pi LW^2)/6$.

Forty days after inoculation, animals were sacrificed by cervical dislocation. Immediately after animal sacrifice, tumours, lungs, kidneys and livers were collected and fixed in 4% PFA and embedded in paraffin blocks for subsequent histology and/or immunohistochemistry analyses.

16. Histological techniques

16.1. Sectioning of paraffin-embedded tissue

Histological techniques were carried out by using 4 µm-thick sections of paraffin-embedded sample blocks, previously made on a Leica RM2155 microtome (Leica Biosystems). Once sections were made, they were placed on *SuperFrost Plus™* adhesion slides (Thermo Fisher Scientific) and stored at 37°C for a week. This allows the complete adhesion of the sections to the slides. After that, slides were kept at room temperature until histological assay was performed. The night before use, samples were incubated again at 37°C.

16.2. Immunohistochemistry assay for Paraffin-Embedded Sections (IHQ-P)

To perform immunohistochemistry assay, paraffin-embedded tissue samples were used. Before proceeding with the staining protocol, the slides must be deparaffinized and rehydrated, as incomplete removal of paraffin may cause poor staining of the section. Therefore, slides were first deparaffinated at 60°C for 1 hour and subsequently rehydrated, by washing the samples according to the following sequence: xylene, for 2 changes of 10 minutes each, and then EtOH 100%, EtOH 96%, EtOH 70% and distilled water for 10 minutes each. Slides were kept in the distilled water until performing antigen retrieval.

After rehydration step, antigen retrieval was performed. This step is necessary to expose antigenic sites and subsequently allow antibodies to bind, as antibody binding sites are previously masked because of previous formalin fixation. Heat-induced antibody retrieval was carried out by using a 2100 Retriever, immersing the samples in sodium citrate 10 mM (pH 6) or Tris/EDTA (pH 9), according to the antigen of interest, and heating at 100°C for 15 minutes.

Once antigen retrieval finished, samples were cooled and washed two times with distilled water. After that, sections were washed with PBST (PBS, 0.1% Tween 20) for 10 minutes and endogenous peroxidase inhibition was carried out, by immersing the samples in *Dako REAL Peroxidase Blocking Solution* for 10 minutes. Then, samples were washed again with PBST for 10 minutes and subsequently incubated with blocking solution (PBS, 0.2% BSA, 0.1% Tx-100) for 1 hour, to avoid unspecific binding of primary antibody. After that, samples were incubated with primary antibodies at 4°C overnight, placing the slides in a humidified chamber to avoid tissue drying, as it will lead to non-specific binding and ultimately high background staining.

The following day, primary antibody was rinsed by washing the samples three times with PBST, for 10 minutes each. Then, samples were incubated with HRP-linked secondary antibody (Dako) for 1 hour at room temperature. Antibodies used for IHC-P assay are shown in **Table 2.** Once incubation was finished, samples were washed again three times with PBST and then incubated with DAB (3,3'- Diaminobenzidine) chromogenic substrate (Dako), previously diluted

1:50, for 5 minutes at room temperature. In the presence of HRP enzyme, DAB produces a brown precipitate that allows protein detection. DAB staining was stopped by washing slides with distilled water, by means of 3 washes of 5 minutes each.

After that, samples were counterstained with Gill III Hematoxylin solution (Merk), for 30 seconds at room temperature. Hematoxylin staining was stopped by immersing slides in tab water, until hematoxylin excess was rinsed, and placing them in distilled water for 5 minutes. Then, dehydration was carried out by placing samples in and out in 70% EtOH, 96% EtOH and 100% EtOH, 15 times each, and incubating them in xylol for 5 minutes. Finally, samples were mounted with a coverslip by using *DePeX* mounting medium (VWR). Pictures were taken with an Olympus BX61 microscope, equipped with an Olympus DP70 digital camera. Quantification of images was performed with ImageJ software (National Institutes of Health), by analysing 5 photographs of each sample, and the represented results are shown as mean ± SEM.

16.3. Hematoxylin and eosin (H&E) staining

Hematoxylin and eosin (H&E) staining is one of the most commonly used histological stains. It is based on a basophilic and acidophilic staining, which contains an acidic dye (eosin) and a basic dye (hematoxylin). The acidic dye, eosin, stains basic (or acidophilic) structures in red or pink colour. These basic structures include proteins and other components in the cytoplasm. On the other hand, hematoxylin reacts with acidic (or basophilic) structures, such as nucleic acids, staining them bluish violet. Therefore, hematoxylin and eosin staining allows to study cellular and tissue samples in detail, as it stains a broad range of cytoplasmic, nuclear, and extracellular matrix structures.

To carry out H&E staining, samples were first deparaffinated and rehydrated as previously described. Sample hydration allows aqueous reagents to penetrate the cells and tissue elements. After rehydration step, samples were stained for 5 minutes with Harris hematoxylin (Panreac), which consists of oxidized hematoxylin (hematein) and a mordant (aluminium ammonium sulphate, or alum) that increases the positive ionic charge of the hematein. Hematein initially stains acidic structures a red-purple colour. Immediately after haematoxylin staining, samples were rinsed with tap water to change the haematoxylin colour from red (soluble) to blue (insoluble). This is also known as bluing step. Then, samples were counterstained with eosin (Merk) for 5 minutes and subsequently dehydrated as previously described. Finally, *DePeX* polystyrene mounting medium (VWR) was added to each sample, and coverslips were placed over the slides. Pictures were taken with an Olympus BX61 microscope, equipped with an Olympus DP70 digital camera. Mitosis number was determined in ten fields of high magnification (40x objective) per sample. Liver, lung, and kidney images were taken with a 10x objective.

17. *In vivo* TUNEL assay

Tissue sections from tumours were deparaffinised and rehydrated as previously described in section 16.2. After rehydration step, slides were treated with Target Retrieval Solution, Citrate pH 6.1 (Agilent) in microwave at 350 W for 5 min and subsequently rinsed twice with PBS.

Then, a TUNEL (Terminal deoxynucleotidyl transferase dUTP nick end labelling) assay was carried out in tissue sections, using an *in situ Cell Death Detection Kit, Fluorescein* (Roche). This technique allows to detect and quantify apoptotic cell death at single cell level, both in cells and tissues. It is based on the cleavage of genomic DNA that takes place during apoptosis, which produces DNA fragments and single strand breaks in DNA. DNA fragmentation can be detected by labelling free 3'-OH termini of DNA strand breaks with modified nucleotides. Labelling of DNA strand breaks is carried out by Terminal deoxynucleotidyl transferase (TdT), which catalyses polymerization of fluorescein-labelled nucleotides to free 3'-OH DNA ends in a template-independent manner. Fluorescein labels incorporated in fragmented DNA are finally detected and quantified by fluorescence microscopy.

To carry out TUNEL assay, TUNEL reaction mixture was firstly prepared, by diluting the *Enzyme solution* (vial 1 from the kit) 1:10 in *Label solution* (vial 2 from the kit). After that, the area around the tissue was carefully dried, and 50 µl of TUNEL reaction mixture were added to each sample. Slides were thereafter incubated in a humidified atmosphere for 60 minutes, at 37°C and in the dark. Once incubation was finished, samples were washed 3 times with PBS, and nuclei were counterstained with Hoechst 33342 (Life Technologies) for 5 min in darkness. Finally, samples were analysed under an epifluorescence Olympus BX61 microscope with a 20x objective, taking 5 representative pictures of each section. Quantification of positive cells was carried out with ImageJ software, and results are represented as mean ± SEM.

18. Quantification of lung micrometastasis from *in vivo* mouse model

18.1. DNA extraction from FFPE tissue samples

To study Hakin-1 effect on lung micrometastasis formation, DNA was extracted from sections of paraffin-embedded lung blocks. First, 10-15 sections of each sample (4 µm thick) were placed in 1.5 ml Eppendorf tubes, and deparaffinization was carried out using mineral oil as a deparaffinizing agent. Therefore, 600 µl of mineral oil (Sigma-Aldrich) were added to each sample, subsequently incubating them at 95°C for 2 minutes. This allows paraffin to dissolve. After that, samples were centrifuged at 12000 rpm for 3 minutes at room temperature and supernatant (containing oil and paraffin) was carefully removed. Then, this step was repeated, by adding 350 µl of mineral oil to the sample. Incubation and centrifugation were carried out the same as previous step, and supernatant was removed.

From this step on, DNA extraction was continued with *QIAamp DNA Mini Kit* (Qiagen). Therefore, 180 µl of *ATL lysis buffer* were added to the tissue pellet, and samples were homogenized by vortexing. Then, samples were centrifuged again at 12000 rpm for 3 minutes at room temperature, and 3 different phases became visible. The upper (oil) and middle (paraffin) phases were carefully discarded, and 25 µl of proteinase K were added to the lower phase, mixing well by vortexing. Samples were then incubated at 56°C overnight and under agitation, until the whole tissue was completely lysed.

The following day, 500 µl of *lysis buffer AL* were added to each sample, mixing by pulse-vortexing for 15 seconds, and incubating at 70°C for 10 minutes. After incubation, tubes were briefly centrifuged to remove drops from inside the lid. Then, 500 µl EtOH 100% were added to the sample, mixing again by pulse-vortexing for 15 seconds. After mixing, tubes were shortly centrifuged, and the mixture was carefully loaded into the *QIAamp Mini spin* column, placed over a collection tube. Once loaded, columns were centrifuged at 8000 rpm for 1 minute at room temperature, and the collection tube containing the filtrate was discarded. This step was repeated until the whole homogenate passed through the column. Then, columns were placed into a clean collection tube and 500 µl of *washing buffer AW1* were added to them, subsequently centrifuging at 12000 rpm for 1 minute at room temperature. This step was repeated for *washing buffer AW2* but centrifuging 3 minutes instead of 1. After this second washing step, empty columns were centrifuged at 12000 rpm for 1 minute to completely remove *washing buffer AW2*.

Finally, DNA elution was performed by placing the *QIAamp Mini spin* column into a clean 1.5 ml Eppendorf tube and adding 150 µl distilled water. Samples were incubated for 5 minutes at room temperature, to allow complete filter wetting, and then centrifuged at 12000 rpm for 1 min at room temperature. This step was repeated by loading the filtrate into the column again, to increase the extracted amount of DNA. DNA quantification was carried out by using NanoDrop ND-1000 spectrophotometer (Thermo Fisher).

18.2. Micrometastasis detection by quantitative polymerase chain reaction (qPCR)

Micrometastasis detection was carried out by real time quantitative PCR (qPCR), using *LightCycler® 480 SYBR Green I Master* (Roche) and the LightCycler® 480 Instrument. Reaction mixes were prepared as previously described and qPCR was carried out under the following conditions: 95°C for 10 minutes (DNA polymerase activation), 40 cycles of amplification [95°C for 10 seconds (denaturation), 60°C for 5 seconds (annealing), 72°C for 10 seconds (extension)], 1 cycle of melting [95°C for 5 seconds, 65°C for 1 minute], and a cooling final step of 40°C for 10 seconds. Relative DNA levels were calculated by $2^{-\Delta\Delta Ct}$ method. Primers for HA epitope and Hakai present in ectopic HA-tagged Hakai expressed in Hakai-MDCK cells (5´-TCTGGGACGTCGTATGGGTA-3´; 5´-TTCTTCATCACCTTGCGGG-3´) were used for micrometastasis detection. Primers for mouse apolipoprotein B (apob) (5′-CGTGGGCTCCAGCATTCTA-3′; 5′- TCACCAGTCATTTCTGCCTTTG-3′) were used as endogenous control. MDCK cell line was used as negative control, as it does not contain HA-tagged Hakai.

19. Statistical analysis

Shapiro-Wilk and D’Agostino-Pearson omnibus normality tests were used to check if the values come from a Gaussian distribution. Statistical significance of data was determined with unpaired *t* test or Mann-Whitney test for two groups or ANOVA or Kruskal-Wallis tests for more than three groups, depending on whether or not the sample had previously passed the normality test. Significance among the experimental groups indicated in the figures is shown as * $p < 0.05$, **$p < 0.01$ and ***$p < 0.001$. Results obtained are expressed as mean ± SD or mean ± SEM as indicated. Graphic representations as well as statistical analyses were carried out with GraphPad Prism (Version 6, GraphPad Software).

B. MATERIALS AND METHODS RELATED TO OBJECTIVE 2

All techniques within this objective that are related with multicellular tumour spheroid culture and co-culture with fibroblasts, were learned and mostly carried out during the predoctoral stay at the Institute of Medical Genetics (Medical University of Vienna), under the supervision of Dr. Helmut Dolznig.

1. Antibodies

Primary and secondary antibodies used for this section, as well as their dilution, reference and the assay they were used for, are detailed in the following table.

Table 6. Primary and secondary antibodies used for Western Blot and immunofluorescence assays

Primary antibodies	**Dilution**	**Performed assay**	**Reference**
E-cadherin [HECD-1]	1:150	Immunofluorescence	Abcam ab1416
Vinculin	1:1000	Western Blot	Cell Signalling Technology E1E9V
Hakai	1:1000 1:100	Western Blot Immunofluorescence	Invitrogen 36-2800 Invitrogen 36-2800
Secondary antibodies	**Dilution**	**Performed assay**	**Reference**
Rabbit IgG Alexa Fluor 488	1:500	Immunofluorescence	Life Technologies A11034
Mouse IgG Alexa Fluor 594	1:500	Immunofluorescence	Life Technologies A11032
IRDye® 800CW Rabbit IgG	1:20000	Western Blot	LI-COR Biosciences 926-32211

2. Cell culture

Human colon cancer cell lines LS174T [American Type Culture Collection (ATCC®)#CL-188™], SW620 (ATCC®#CCL-227™), HCT116 (ATCC®#CCL-247™), and DLD-1 (ATCC®#CCL-221™) were obtained from the ATCC and used from early passages. All of them were grown in Dulbecco's Modified Eagle's Medium (DMEM) (Thermo Fisher Scientific), supplemented with 10% FBS (Thermo Fisher Scientific), 1% penicillin-streptomycin (Gibco, Thermo Fisher Scientific) and 1% L-glutamine 200mM (Thermo Fisher Scientific). Cancer-associated fibroblasts (CAFs) were isolated from fresh samples of colon adenocarcinomas received at the Institute of Pathology at the Medical University of Vienna, in accordance with the institutional ethical guidelines. Once isolated, CAFs were grown in Endothelial Cell Growth Medium MV 2 (PromoCell) supplemented with 0.05 ml/ml FBS, 5 ng/ml Epidermal Growth

Factor (EGF), 10 ng/ml Basic Fibroblast Growth Factor (bFGF), 20 ng/ml Insulin-like Growth Factor (IGF-1), 0.5 ng/ml Vascular Endothelial Growth Factor 165 (VEGF), 1 µg/ml ascorbic acid, 22.5 µg/ml heparin, and 0.2 µg/ml hydrocortisone. Both CAFs and colon cancer cell lines were cultured at 37°C under 5% CO_2 and 95% humidity BBD 6220 CO_2 Incubator (Thermo Fisher Scientific).

3. Establishment of spheroid cultures (3D) from human colorectal cancer cell lines

3.1 Multicellular spheroid formation (3D culture) from human colorectal cancer cell lines

Spheroid formation was induced by seeding HCT116, DLD1, SW620 and LS174T in 96-well plates (SPL Life Sciences, round bottom, untreated), at a cell density of 2000 cells per well. Spheroids were seeded in 100 µl DMEM (supplemented with 10% FBS, 1% L-glutamine, and 1% penicillin-streptomycin) containing 0.3% methylcellulose (20% of 1.5% methylcellulose solution in DMEM, see below for methylcellulose preparation). After seeding, plates were centrifuged at 300 g for 10 minutes at room temperature and incubated at 37°C for 2 days, until compact spheroids were formed (one spheroid per well). Once spheroids were generated, they were collected for further assays.

Methylcellulose is a water-soluble, non-ionic polymer with hydrophilic glucosidic bonds, derived from the polysaccharide cellulose. It is necessary for spheroid culture as it promotes anchorage-independent spheroid generation and prevents the formation of cell monolayers in a highly reproducible manner. To prepare 1.5% methylcellulose solution in DMEM, 15 g of methylcellulose powder (Sigma-Aldrich, viscosity: 4.000 centipoises) were weighed and placed into a glass bottle containing a magnetic stir bar. After that, methylcellulose was autoclaved for 20 minutes at 121°C, as it needs to be used under sterile conditions. Once autoclaved, methylcellulose was dissolved in 500 ml DMEM (not supplemented) preheated at 60°C, under sterile conditions. Immediately after, methylcellulose solution was mixed for 20 minutes at 60°C, using a magnetic stirrer. Then, 500 ml DMEM containing 2% L-glutamine were added to create a final 1000 ml solution, which was mixed overnight at 4°C with a magnetic stirrer. The following day, methylcellulose solution was aliquoted in 50 ml tubes (Falcon) and centrifuged at 5000 g for 2 hours at room temperature. Finally, supernatant was transferred into fresh 50 ml tubes and pellet was discarded. Tubes were long-term stored at -20°C and stored at 4°C while they were used in cell culture.

3.2. Co-culture of colorectal cancer spheroids with cancer-associated fibroblasts (CAFs)

3.2.1. Production of silicone casting devices for collagen gels

Co-culture of colorectal cancer spheroids with cancer-associated fibroblasts (CAFs) was carried out by embedding spheroids and CAFs in collagen gels. The purpose of collagen embedding is to mimic extracellular matrix (ECM) properties *in vitro*. ECM is composed of a 3D network of fiber-forming proteins, such as collagen, elastin, fibronectin, and glycosaminoglycans. It provides a physical scaffold for cells and it plays a crucial role in many cellular processes, such as cell growth, migration, differentiation, survival, homeostasis, and morphogenesis. To carry out collagen gel culture, gel casting devices were firstly produced by cutting out 2 × 2 cm squares of a silicone foil (Gel dryer sealing gasket, 1 mm thickness, BioRad). After that, holes of 1.4 cm in diameter were made with a puncher into each square. Nylon filters of 1 cm diameter were then prepared by cutting out a hole in the nylon mesh inserts of Medicon syringe filters (100 µm, Becton Dickinson). The silicone casting devices and the nylon meshes were autoclaved, as they need to be used under sterile conditions.

3.2.2. Embedding of colorectal cancer spheroids and CAFs in collagen gels

To carry out colorectal cancer spheroids and CAFs co-culture, silicone casting devices were first placed over the inside surface of lids of 6 cm cell culture dishes, where they firmly attached. Sterile forceps were used to maintain sterile conditions. They were placed over the lid because they do not attach well to the bottom of the dish, as it is treated for cell culture. Once gel casting devices were attached, dishes were placed into the incubator, as they should be warm to help collagen polymerization. They were maintained at 37°C while collagen gel was prepared.

Once gel casting devices were prepared, spheroids were harvested from 96-well plates. 48 spheroids were used for each collagen gel, so they were collected independently in different tubes. Once harvested, spheroids were placed into a 15 ml tube (Sarstedt AG) and subsequently centrifuged at 1500 rpm for 5 minutes. Supernatant was then discarded, and spheroids were resuspended in PBS and transferred to a 1.5 ml Eppendorf tube. After that, they were centrifuged again, at 1500 rpm for 5 minutes, and supernatant was carefully discarded. Finally, spheroid-containing 1.5 Eppendorf tubes (one for each collagen gel) were placed on ice until further use.

Cancer-associated fibroblasts (CAFs), growing in 10 cm dishes, were splitted with TrypLE Select (10X) reagent (Thermo Fisher). Dissociation was inactivated with EGM (Promocell), CAFs were centrifuged at 1500 rpm for 5 minutes, and supernatant was discarded. Cells were subsequently resuspended in EGM and counted with a hemocytometer (Bright-Line Hemocytometer, Hausser Scientific Company). Finally, 3 x 10^5 CAFs were pipetted over the previously prepared spheroid pellets, and tubes containing both spheroids and CAFs were centrifuged at 1500 rpm for 5 minutes. The entire supernatant was carefully removed, and the cell-spheroid pellets were kept on ice while collagen gel was prepared.

For the collagen gel preparation, all steps were performed on ice. A 300 µl collagen solution was prepared for each silicon device. Preparation was carried out into a round-bottom polystyrene tube (Falcon®), previously cooled on ice, by adding the components as indicated in

Table 7. Once components were added, the tube was recapped and collagen solution was mixed thoroughly, centrifuging immediately after to remove air bubbles. Mixing and centrifugation should be carried out shortly, as the tube should be placed on ice as fast as possible to avoid collagen polymerization. Then, collagen pH is neutralized by adding a few drops (about 23 µl in total) of NaOH 1M. As methylcellulose is diluted in DMEM, phenol red acts as an indicator of the pH of collagen solution. After first mix, collagen solution becomes yellow, which indicates that pH is too acid. NaOH 1M is added gradually (i.e. first 10 µl, then 5 µl, then 2 µl, etc.), mixing each time and evaluating the colour change. Once collagen solution reaches a reddish salmon colour, polystyrene tube is briefly centrifuged again, to remove bubbles generated by mixing during neutralization process, and immediately placed on ice.

Table 7. Composition of collagen gel solution

Reagent	Stock concentration	Volume/gel	Final concentration
Collagen I, rat tail (Thermo Fisher)	3 mg/ml	200 µl	2 mg/ml
PBS (Lonza Group AG)	10X	30 µl	1X
Methylcellulose solution	1.5%	70 µl	0.35%

Dishes containing the casting devices were taken out from the incubator and placed into the hood over a piece of polystyrene, to keep them warm. After that, 300 µl of the collagen solution were transferred into each 1.5 ml Eppendorf tube containing the spheroid-cell pellets. Pellets were gently resuspended, to avoid bubble formation, and subsequently transferred into the casting devices. Then, a nylon mesh was added to the casting device and submerged into the collagen solution containing the cells before placing de dishes into the incubator. The ring-shaped nylon mesh facilitates further microscopic analyses by phase contrast and fluorescence microscopy. When tumour spheroids and fibroblasts are cultured without the supporting nylon mesh, collagen gel cylinders shrink due to the contractile forces of the fibroblasts. However, when a nylon mesh is added to the collagen solution before its polymerization, the contracting forces of the fibroblasts and gel shrinking are abolished [192].

Once collagen cell suspension was added to the silicone devices, dishes were incubated for 30 minutes at 37°C to allow polymerization of the collagen solution. During the incubation time, dishes were turned over every 2 minutes until the gels became opaque due to polymerization. This step avoids spheroid sinking at the bottom of the gel, which would make tumour cells travel from the spheroids through the way of least resistance, forming a monolayer that would interfere with further assays. Once gels polymerized, plates were left into the incubator without turning them around until incubation time was finished.

After polymerization of the collagen solution for 30 minutes at 37°C, the silicone foil was removed, and collagen gel cylinders were transferred into 24-well plates containing 1 ml of DMEM supplemented with 10% FBS. Collagen gel cultures were maintained at 37°C and 5% CO_2 for 2-3 days until phase contrast or fluorescence microscopy evaluation was performed.

4. Immunofluorescence assay for collagen gels

Immunofluorescence staining of collagen gels was carried out after 3 days of collagen gel co-culture of HCT116, DLD1, SW620 and LS174T tumour cells with CAFs. First, gels were washed with PBS once and fixed with *Roti®-Histofix* 4% phosphate-buffered formaldehyde solution (Roth) for 40 minutes at room temperature. After fixation step, *Histofix* was removed and gels were washed 2 times with PBS. At this point, gels can be stored at 4°C in case immunofluorescence assay is performed on a different day.

Gels were washed 3 times with TBST (tris buffered saline, 0.1% Triton X-100), for 15 minutes each, and then 3 times with PBST (phosphate-buffered saline, 0.1% Triton X-100), for 15 minutes each, under agitation. Blocking was carried out by incubating gels with blocking solution (PBST/1% BSA) for 3 hours at room temperature and under agitation. After blocking step, gels were incubated with 250 µl of primary antibodies diluted in blocking solution, for 24 hours at 4°C and under agitation. The following day, gels were washed 3 times with PBST for 20 minutes each, and subsequently incubated with blocking solution for 30 minutes. After that, gels were incubated with 250 µl of secondary antibodies diluted in blocking solution for 24 hours at 4°C, under agitation and in the darkness, to avoid fluorophore photobleaching. Primary and secondary antibodies used for collagen gel immunofluorescence, as well as the dilutions thereof, are detailed in **Table 6**.

Gels were washed again 3 times with PBST and incubated with DAPI diluted in PBST (1 µg/ml) for 2 hours, at room temperature, under agitation and in the darkness. Finally, the gels were washed another 3 times with PBST and placed on glass slides. Coverslips were placed over the slides without any mounting medium, just using a few drops of PBS, and samples were analysed under a Zeiss LSM5-Exciter confocal microscope. After the analysis under the confocal microscope, gels were carefully taken out from glass slides, placed back into the plate, and stored at 4°C in the darkness.

5. Collagen gel spheroid invasion assay

Collagen gel spheroid invasion assay was carried out to test Hakai involvement in the acquisition of invasive properties in a 3D model, which is a better physiological approach. To do so, spheroid invasion assay was carried out in HCT116 cells after a transient knockdown of Hakai.

5.1. Knockdown of Hakai by siRNA transfection

To perform Hakai expression knockdown, cells were seeded in 6-well plates at a cell density of 3.75×10^5 cells per well, in a final volume of 2 ml DMEM supplemented with 10% FBS and without antibiotics. Cells were grown overnight to 30% confluence. The following day, transfection was carried out by using *Lipofectamine RNAiMAX* transfection reagent (Thermo Fisher) and a Hakai small interfering RNA (ON TARGETplus siRNA, Dharmacon), with the following sequence: 5′-CUCGAUCGGUCAGUCAGGAAA-3′. RNA interference (RNAi) is a biological process in which double-stranded RNA molecules inhibit gene expression by neutralizing targeted mRNA molecules. RNA interference involves processing and cleavage of longer double-stranded RNA into siRNAs by Dicer enzyme, which is an RNase III-like enzyme. After double-stranded RNA cleavage, siRNAs bind to RISC (RNA induced silencing complex), a multiprotein complex were siRNA strands are separated to form single stranded siRNA. The strand with the more stable 5′-end is integrated into the active RISC complex and acts as a template that allows RISC to recognize complementary messenger RNA (mRNA) transcript. Once recognized, target mRNA is cleaved by argonaute proteins from the complex. Therefore, mRNA is degraded after transcription, thus preventing its translation.

To carry out siRNA transfection assay, 5 nmol siRNA were resuspended in 250 µl of *1X siRNA Buffer* (Dharmacon), resulting in a 20 µM stock. 5 µl (100 pmol) of 20 µM siRNA stock were then diluted in 250 µl *Opti-MEM™ Reduced Serum Media* (Gibco, Thermo Fisher Scientific). *Opti-MEM™* medium was previously prewarmed at 37°C. siRNA mix was resuspended by gently tapping the tube. For the control condition, non-targeting negative control (ON-TARGETplus Control pool, Non-Targeting pool, NTC, Dharmacon) was used. On the other hand, 5 µl Lipofectamine *RNAiMAX* were diluted in 250 µl *Opti-MEM™*, subsequently mixing by inverting the tube around 2-3 times. Once prepared, siRNA and lipofectamine dilutions were incubated for 5 minutes at room temperature and then mixed by pipetting 250 µl of lipofectamine dilution over siRNA dilution. 500 µl lipofectamine-siRNA final solution was incubated for 20 minutes at room temperature. During incubation step, 6-well plates were taken out from the incubator and 500 µl of culture medium were removed from each well, as the final volume after transfection must be 2 ml. Finally, 500 µl of the formed siRNA-lipid complexes were carefully added per well, resulting in a final concentration of 50 nM siRNA. Transfected cells were incubated at 37 °C and 5% CO_2.

5.2. Spheroid embedding in collagen gels

The day after transfection, spheroids were grown from HCT116 transfected cells (both NTC and siRNA). 72 hours after transfection (48h after spheroid seeding) spheroids were embedded into collagen gels, as described in section 3.2.2. However, in this case spheroids were cultured alone (without CAFs), so the nylon mesh was not added to the gel. Another difference with the previous described protocol is that gels were placed into a well containing CAF conditioned medium diluted 1:1 with DMEM 10% FCS, instead of DMEM alone. Neither the DMEM nor the CAF conditioned medium are supplemented with antibiotics, as transient knockdown of Hakai should be maintained. CAF conditioned medium is used for invasion assays as fibroblasts are required to induce invasive spreading of HCT116 cells. Invasive spreading is observed as the formation of extensive structures, which are characterized by a multicellular astral outgrowth into the collagen gels [192]. CAF conditioned medium was harvested from a 2-3 culture of CAFs, using a single-use sterile syringe and filtered by means of a 0.2 μm-pore size syringe filter. Parallel to invasion assay, HCT116 were seeded in 6-well plates, transfected, and incubated for 72 hours at 37 °C and 5% CO_2, to further check Hakai knockdown by Western Blot. This analysis was also performed for HCT116 spheroids grown from transfected cells.

Invasive structure formation was evaluated by phase contrast microscopy, by taking pictures at 0, 24, 48 and 72 hours (cellSens software, Olympus). Invasive area quantification was carried out at 72 hours by using ImageJ software. The invasive area was obtained by subtracting the spheroid area from the outgrowth area, and the percentage of the spheroid that represents the invasion area was calculated for each condition. The represented results are shown as mean ± SD.

6. Near-Infrared Western Blot detection

Western Blot analyses within this chapter were carried out similarly as previously described. However, there are some differences that are summed up in this section. First, protein extraction was carried out by using RIPA buffer (50 mM Tris base pH 7.6,150 mM Sodium chloride, 1% Triton X-100, 0.1% Sodium dodecyl sulfate, 0.5% Sodium deoxycolate) supplemented with 1% PMSF (Sigma-Aldrich) and 2% protease inhibitor mix (200 µg/ml Leupeptin, 200 µg/ml Aprotinin, 30 µg/ml, Benzamidine hydrochloride, 1.000 µg/ml Trypsin inhibitor).

Measurement of protein concentration was carried out by using Bradford Protein Assay, which is based on the absorbance shift that is observed in an acidic solution of *Coomassie Brilliant Blue G-250* dye. The dye exists in three forms: cationic (red), neutral (green), and anionic (blue). Under acidic conditions, the dye is predominantly red. However, protein binding results in a colour change from red to blue, as it stabilizes the blue form of the Coomassie dye. Thus, the amount of protein-Coomassie dye complexes that are present in the sample can be detected at 595 nm, as protein binding increases absorbance from 465 to 595 nm. This allows an accurate quantification of the protein content of the sample. Bradford 1X dye reagent was prepared by diluting 1 part of *Protein Assay Dye Reagent Concentrate* (Bio-Rad) with 4 parts of distilled water, and subsequently filtering. After that, 1 ml of Bradford 1X was pipetted into a polystyrene cuvette, and 1 μl of the protein sample (or 1 μl of RIPA buffer as a blank) was subsequently added.

After incubating the samples for 5 minutes at room temperature, the absorbance was determined at 595 nm with a Biophotometer (BioPhotometer 6131, Eppendorf AG). Western Blot assays were performed using 1.0 mm-thick 10% acrylamide gels (mini gel format). Stacking and resolving gel composition for the above-mentioned percentage of acrylamide, are shown in **Table 8**.

Table 8. Composition of acrylamide gels used for SDS-PAGE in Near-Infrared detection Western Blot

Reagent	**Stacking gel**	**Resolving gel**
30% Acrylamide/Bis-acrylamide (Sigma-Aldrich)	0.5 ml	4 ml
Buffer B, pH 8.8 (1.5 M Tris base, 0.4% SDS)	---	3 ml
Buffer C, pH 6.8 (0.5 M Tris base, 0.4% SDS)	0.75 ml	---
Distilled water (dH_2O)	1.75 ml	5 ml
10% Ammonium persulfate (APS)	30 µl	120 µl
Tetramethylethylenediamine (TEMED) (Merk)	2.5 µl	10 µl

Electrophoresis was carried out as previously described, using a *Tetra Vertical Electrophoresis Cell* (Bio-Rad). After gel electrophoresis, the proteins were transferred onto a nitrocellulose membrane (LI-COR Biosciences), by using the *Mini Trans-Blot® cell* (Bio-Rad) and the previously mentioned blotting conditions. Nitrocellulose membrane was previously hydrated in transfer buffer. Once the blotting step finished, membranes were air dried between Whatman papers (GE Healthcare) for 10 minutes and incubated in *Odyssey blocking buffer* (TBS, LI-COR Biosciences) for 1 hour at room temperature on an orbital shaker.

Then, incubation with primary antibody against the target protein was carried out by placing the blots into a 50 ml tube containing the primary antibody dilution. Primary antibodies were diluted in *Odyssey blocking buffer* containing 0.2% Tween 20 and tubes were shaken overnight at 4°C on a RM10W-80V roller mixer (Zipperer GmbH). After the incubation with the primary antibody, the membrane was rinsed in TBST, in three washes of 10 minutes each. Then, the membrane was incubated with the fluorescence-labelled secondary antibody, also diluted in *Odyssey blocking buffer* (TBS) containing 0.2% Tween 20, for 1 hour at room temperature and in the dark. Primary and secondary antibodies used are detailed in **Table 6.** Once incubation with secondary antibody finished, the membrane was washed three more times in TBST in the dark, and images were acquired by the Odyssey® CLx scanner (LI-COR Biosciences).

7. Collagen gel contraction assay

Collagen gel contraction assay was carried out to test Hakai involvement in contractile forces of the fibroblasts. To carry out this experiment, CAFs were seeded in 6-well plates, at a cell density of 1 x 10^5 CAFs per well, in a final volume of 2 ml EGM. Cells were incubated overnight at 37°C and 5% CO_2. The following day, Hakai knockdown was carried out as previously described, transfecting the cells with 50 nM siRNA or NTC, as appropriate. Following knockdown transfection, CAFs were splitted with TrypLE Select (10X) reagent and counted with a hemocytometer. 1.5 x 10^5 of Hakai siRNA or NTC CAFs were then transferred into 1.5 ml Eppendorf tubes and centrifuged at 300 g for 3 minutes at room temperature. Once centrifugation finished, supernatant was removed and tubes containing the cell pellet were placed on ice for further use. Collagen suspension was prepared as previously explained (section 3.2.2.), but in this case DMEM 5% FBS was used instead of 1.5% methylcellulose solution (**Table 9**).

Table 9. Composition of collagen gel solution for CAF contraction assays

Reagent	Stock concentration	Volume/gel	Final concentration
Collagen I, rat tail (Thermo Fisher)	3 mg/ml	200 µl	2 mg/ml
PBS (Lonza Group AG)	10X	30 µl	1X
DMEM 5% FBS	---	70 µl	---

Thereafter, CAFs were resuspended in 300 µl cold collagen suspension and immediately transferred into a silicone ring, previously attached to the bottom of a 6-well plate and prewarmed at 37°C. Resuspension was carried out thoroughly, by pipetting up and down around 40 times, as CAFs must be well distributed in the gel. Three different collagen gels were made as replicates of each condition (NTC or siRNA). In this case, nylon meshes were not used, as CAFs must be allowed to cause gel shrinking, which enables to evaluate their contractile capacity. Collagen suspension containing CAFs was then incubated at 37°C and 5% CO_2 for 20 minutes. For contraction assays, plates were not turned around, as there are no spheroids that may sink. That is also the reason that silicone rings were placed on the bottom of the plate, as they did not need to be firmly attached.

After collagen polymerization, 3 ml EGM supplemented with 0.5% methylcellulose were added to each well, and silicone rings were carefully removed by using sterile forceps. Methylcellulose avoids gel attachment to the bottom of the plate, which would interfere with CAF-mediated gel shrinking. Also, plate was shaken every hour to keep collagen gels detached from the bottom. Gel sizes were measured at 0, 6, 24 and 72 hours with ImageJ software (National Institutes of Health), using the straight-line tool to scale the diameter of each gel.

8. Culture of colon cancer cell lines in CAF conditioned medium

To further investigate the effect of CAFs-mediated signalling on Hakai expression levels in tumour cells, HCT116, DLD1, SW620 and LS174T tumour cells were cultured in CAF conditioned medium. First, cells were seeded in 6-well plates, at a cell density of 3.75 x 10^5 cells per well in HCT116 and SW620, 2 x 10^5 in DLD1 and 5 x 10^5 in LS174T. The day after seeding, cells were starved in DMEM supplemented with 0.5% FCS and 1% L-glutamine for 24 hours. Cell starvation 24 hours before treatment is a common step in cell-based assays that is used to synchronize all the cells to the same cell cycle phase. By this way, the impact of the cell cycle over treatment response is removed. After starvation step, cells were cultured in CAF conditioned medium for 24 and 48 hours. Control cells were cultured in endothelial cell growth medium (EGM*),* as it is the culture medium used for CAFs. Finally, Hakai expression levels were analysed by Western Blot, as previously described.

9. Establishment of patient-derived colorectal organoid culture

Colorectal cancer organoids were stablished from human biopsies of colorectal cancer patients. Human biopsies were obtained from Gastrointestinal Surgery at Complexo Hospitalario Universitario de A Coruña (CHUAC) under collaboration with Dr. Gabriela Romay (General Surgery Specialist) and Dr. Ángel Concha (Head of the Pathological Anatomy Service, Complexo Hospitalario Universitario de A Coruña, CHUAC). Human colorectal samples were collected by Pathological Anatomy department of Complejo Hospitalario Universitario de A Coruña (CHUAC) under informed consent from the patients. Research Ethics Committee from A Coruña-Ferrol approved their use for investigation according to the standard ethical procedures described in the "Ley Orgánica de Investigación Biomédica" of 14 July 2007 of the Spanish regulation (ethical protocol code: 2017/570). In addition, the following clinical variables were included for each sample: TNM, tumour size, tumour burden, tumour location, histological type, degree of differentiation, intestinal obstruction, perivascular and perineural invasion, affected ganglia, metastasis, Carcinoembryonic antigen (CEA) and mutations.

Tumour biopsies were evaluated and prepared by a specialist of the Pathological Anatomy Service under sterile conditions, by using punch forceps. Samples were then placed onto a sterile gauze pad, previously moistened with sterile PBS. Sterile gauze containing tumour samples was thereafter placed into a urine container, which in turn was placed on ice until further processing at the laboratory. Samples were hereinafter processed as explained in section 9.2., using the culture mediums detailed in section 9.1.

9.1. Preparation of specific mediums for patient-derived colorectal organoid culture

To carry out patient-derived colorectal organoid culture, specific mediums should be prepared before sample processing. All the mediums needed for organoid culture are detailed below.

- Disinfection medium: Disinfection medium is needed to completely disinfect tumour samples, to avoid further contamination of the organoid culture. The composition of the disinfection medium, for a final volume of 500 ml, is shown in **Table 10.** Reagents were used as received from commercial suppliers, except for nystatin, which was acquired as a powder and diluted in DMSO to a stock concentration of 5 mg/ml.

Table 10. Composition of disinfection medium used for organoid culture.

Reagent	Stock concentration	Volume/500ml	Final concentration
DMEM/F-12 (Thermo Fisher)	---	462 ml	---
Penicillin-Streptomycin (Gibco)	10.000 U/ml	12.5 ml	250 ml
Nystatin (Sigma-Aldrich)	5 mg/ml	500 µl	5 µg/ml
Kanamycin Sulphate (Gibco)	10 mg/ml	5 ml	100 µg/ml
Gentamicin (Gibco)	50 mg/ml	500 µl	50 g/ml
Amphotericin B (Gibco)	250 µg/ml	20 l	10 g/ml

- Human Intestinal Stem Cell medium (HISC): HISC is the complete growth medium that is used for establishment, expansion and long-term maintenance of intestinal patient-derived organoid cultures. The composition of the HISC medium, for a final volume of 160 ml, is detailed in the following table.

Table 11. Composition of human intestinal stem cell medium (HISC) used for organoid culture

Reagent	Stock concentration	160 ml	Final concentration
B27 supplement (Gibco)	50X (Commercial)	3.2 ml	1X
N2 supplement (Gibco)	100X (Commercial)	1.6 ml	1X
N-Acetylcysteine (Sigma-Aldrich)	600 mM (in dH$_2$0)	360 µl	1.25 mM
Nicotinamide (Sigma-Aldrich)	820 mM (in dH$_2$0)	2 ml	10 mM
human EGF (Sigma-Aldrich)	500 µg/ml (in 10 mM acetic acid)	17.6 µl	50 ng/ml
Prostaglandine E2(Sigma-Aldrich)	1 mg/ml (in EtOH 100%)	12.4 µl	10 nm
[Leu15]-Gastrin I (Sigma-Aldrich)	100 µM (in PBS/0.1% BSA)	17.6 µl	10 nm
A83-01 (Tocris Bioscience)	500 µM (in DMSO)	160 µl	500 nM
SB202190 (Sigma-Aldrich)	30.1 mM (in DMSO)	16 µl	3 µM
Primocin (Invivogen)	50 mg/ml (Commercial)	400 µl	100 µg/ml
Basal culture medium *	---	71.2 ml	---
pre-HISC medium **	---	81 ml	---

**Basal culture medium:* Basal culture medium for organoid culture was prepared by supplementing DMEM/F-12 medium (Thermo Fisher) with 1% penicillin-streptomycin (5,000 U/mL) (Gibco) and 1% *GlutaMAX*™ supplement (Gibco).

***Pre-HISC (Human Intestinal Stem Cell) medium:* pre-HISC medium is based on Wnt3a, RSPO1 and Noggin factors, that are necessary for intestinal epithelial cell culture. Wnts and R-spondins (such as Wnt3a and RSPO1) induce self-renewal of stem cells as they enhance Wnt/β-catenin signalling pathway. On the other hand, Noggin, is an antagonist of bone morphogenetic protein (BMP) that is involved in tissue development and enables the maintenance and passage of small intestinal organoids *in vitro*. Although Wnt3a, RSPO1 and Noggin are commercially available, they are expensive to use, so conditioned mediums are used instead [193].

Pre-HISC medium was prepared by mixing 23ml Wnt conditioned medium, 11.5 ml RSPO1 conditioned medium, and 6 ml Noggin conditioned medium, resulting in a final volume of 40.5 ml. Conditioned medium was obtained, as previously described (section 5.2.), from L1Wnt3A, HEK293T RSPO1mCherry and HEK293T NogginmCherry cell lines, kindly provided by Dr. Héctor G. Palmer (Vall d'Hebron Institute of Oncology, VHIO).

Wnt conditioned medium was obtained from L1Wnt3A cell line. RSPO1 conditioned medium was obtained from HEK293T RSPO1mCherry cell line. Nogging conditioned medium was obtained from HEK293T NogginmCherry cell line. All cell lines were cultured in DMEM supplemented with 10% FBS and 1% penicillin-streptomycin, at 37°C under 5% CO_2 and 95% humidity. To maintain gene expression, culture medium was supplemented with 400 µg/ml G418 (Sigma-Aldrich) for L1wnt3A, and 200 µg/ml Hygromycin B (Sigma-Aldrich) for HEK293T RSPO1mCherry and HEK293T NogginmCherry cells. One week before conditioned medium preparation, G418 and Hygromycin B were removed from the culture medium. Otherwise, conditioned medium will contain such antibiotics and thus they would be transferred to the organoids.

9.2. Isolation of patient-derived colorectal cancer stem cells.

To carry out stem cell isolation, tumour samples were first placed in a 50 ml tube and washed with cold PBS for 10-15 minutes at 4°C and under rotation (SB3, Cole-Palmer Stuart). This step was repeated twice, changing the PBS in each washing step. PBS was discarded carefully by using a sterile disposable Pasteur pipette. After that, tumour samples were incubated overnight with 30 ml of disinfection medium (**Table 10**), at 4°C and under rotation.

After disinfection of tumour samples overnight, isolation of patient-derived colorectal cancer stem cells was carried out. Biopsies were taken out from the 50 ml tube containing the disinfection medium and placed over a sterile Petri dish, by using sterile disposable forceps. After that, fat and other residual elements were removed from the sample, by using a sterile disposable scalpel. Once isolated, the epithelial tissue was transferred to a clean petri dish together with 1 ml Human Intestinal Stem Cell medium (HISC), to prevent tissue from drying. The composition of the HISC medium, for a final volume of 160 ml, is detailed in **Table 11**.

To create a single cell suspension, samples were thoroughly crushed with the scalpel, until small sections were obtained. 1 ml HISC medium containing tissue sections was thereafter collected in a 15 ml tube, which was filled up to 5 ml with more HISC medium. Then, 50 µl DNAse I (Sigma-Aldrich) and 50 µl of collagenase (Sigma-Aldrich) were added, and samples were incubated for 1 hour at 37°C and 5% CO_2. Collagenase was prepared at a stock concentration of 150 mg/ml in Tris 50 mM/$ClCa_2$ 0.36 mM, and used at a final concentration of 1.5 mg/ml. Meanwhile, DNase I was prepared at a stock concentration of 8 KU/ml in NaCl 150 mM and used at a final concentration of 0.08 KU/ml. Collagenase is able to digest the peptide bonds that are present in collagen, one of the major components of the extracellular matrix. Extracellular matrix degradation by collagenase enables to release cells into suspension. On the other hand, DNase I is an endonuclease that acts on phosphodiester bonds adjacent to pyrimidine nucleotides, cleaving the DNA. DNase I prevents cell aggregation by degrading free DNA, which is released as a consequence of cell lysis during the enzymatic digestion. DNase I suspension is prepared in Tris /$ClCa_2$ because calcium chloride acts as an activator of this enzyme. During tissue digestion with DNase and collagenase, samples were thoroughly resuspended every 15 minutes by using a sterile Pasteur pipette. In the first two turns of pipetting, pipette tip was cut out, to avoid pipette obstruction with tissue fragments.

After tissue digestion, 5 ml of HISC medium were added to the 15 ml tube, and samples were subsequently filtered by using a sterile 100 µm cell strainer (BD Falcon™). Filtrates containing isolated primary cells were thereafter centrifuged, at 1500 rpm for 10 minutes. Then, supernatant was discarded, and cell pellet was resuspended in 3 ml *1X Red Blood Cell (RBC) Lysis Buffer* (Invitrogen) and incubated for 10 minutes at room temperature. *RBC Lysis Buffer* is used for erythrocyte lysis, as it contains ammonium chloride, which allows to lyse red cells without having a strong impact on lymphocytes. Afterwards, 3 ml HISC medium were added to the lysate, and samples were centrifuged at 1500 rpm for 10 minutes. Cell pellet was resuspended in approximately 5-10 ml (depending on the initial sample amount) and cells were counted by using a Neubauer hemocytometer (MarienFeld), without taking lymphocytes into account.

Finally, isolated tumour cells were seeded in low-attachment 24-well plates (Costar® 24-well Clear Flat Bottom Ultra-Low Attachment Multiple Well Plates, Corning), at a cell density of 1.5 x 10^4 cells per well. Organoid formation was monitored by contrast microscopy. Pictures were taken with an Eclipse-Ti microscope (Nikon), using a 20x objective.

10. Cancer Stem Cell tumorsphere formation

To get a first insight into the role of Hakai in the acquisition of stem properties, tumorsphere cultures were established. Tumorspheres are spherical and solid formations that result from the proliferation of cancer stem cells. When cells are seeded in non-adherent plates in a serum-free medium supplemented with growth factors, only stem cells are able to survive and proliferate, thus forming a tumorsphere [194,195].

To carry out cancer stem cell 3D culture (tumorspheres), HCT116 cells were used. Cells were seeded in 24-well ultra-low attachment plates (Costar®), at a cell density of 2 x 10^4 cells per well in stem cell medium (**Table 12**), and subsequently incubated at 37°C and 5% CO_2 for 7 days. In parallel 2D cultures were carried out in adherent plates as a monolayer control. Tumorsphere formation was monitored by phase-contrast microscopy, using an Eclipse-Ti microscope (Nikon). After incubation time, both tumorspheres and 2D cultures were harvested for subsequent analyses.

Table 12. Composition of stem cell medium used for tumorsphere culture

Reagent	Stock concentration	25 ml	Final concentration
B27 supplement (Gibco)	50X (Commercial)	500 µl	1X
GlutaMAX™ supplement (Gibco)	100X (Commercial)	250 µl	1X
human EGF (Sigma-Aldrich)	500 µg/ml (in 10 mM acetic acid)	1 µl	20 ng/ml
human bFGF(Sigma-Aldrich)	100 µg/ml (in 20 mM Tris, pH 7.0)	2.5 µl	10 ng/ml
DMEM/F-12 (Thermo Fisher)	---	24.3 ml	---

11. Analysis of the expression levels of stem and differentiation markers by qPCR.

With the aim to analyse the expression levels of Hakai, as well as stem and differentiation markers in tumorspheres compared to monolayer cultures, stem cell 3D cultures of HCT116 cells were carried out as described in section 10. One week after seeding, mRNA levels of Hakai as wells as pluripotency and differentiation genes in monolayers and tumorspheres were analysed by qPCR as previously described (section 10 from materials and methods related to objective 1), by using the primers listed in **Table 13.**

Table 13. Forward and reverse sequences of primers used for RT-qPCR

Gene ID	Species	Forward sequence (5'-3')	Reverse sequence (5'-3')
ANPEP	Human	CGTCCTACCTCCACACCTTTT	GTCCAGCGGTTCATGATGTC
CBLL1	Human	CGCAGACGAATTCCTATAAAGC	CCTTCTTCATCACCAGGTGG
CDH1	Human	AGTGTCCCCCGGTATCTTCC	CAGCCGCTTTCAGATTTTCAT
CDX2	Human	GCAAGGTTTACACTGCGGAA	TGGAGTCCAATAACCACCCC
HPRT	Human	TGACCTTGATTTATTTTGCATACC	CGAGCAAGACGTTCAGTCCT
KLF4	Human	ACTCGCCTTGCTGATTGTCT	GGCCGAGATCCTTCTTCTTT
cMYC	Dog	CAGAAGAGGCGAACACACAA	GGCCTTTTCATTGTTTCCA
LGR5	Human	AGCAAACCTACGTCTGGACA	ACAGAGGAAAGATGGCAGCT
NANOG	Dog	AAGAGGTGGCAGAAAAGCAA	GGAGGTTTCCAGAAGGGTTC
NANOG	Human	CAGTCTGGACACTGGCTGAA	CTCGCTATTAGGCTCCAAC
RPLP0	Human	TGGTCATCCAGCAGGTGTTCGA	ACAGACACTGGCAACATTGCGG
RPS5	Dog	CAAGCTCTTTGGGAAATGGA	TCATGAGCTTCTTGCCATTG
SOX2	Dog	AACCCCAAGATGCACAACTC	TCTCGTCTCCGACAAAAGT
SOX2	Human	AACCCCAAGATGCACAACTC	GCTTAGCCTCGTCGATGAAC

12. Analysis of mRNA expression of stem markers in FFPE tumour samples from *in vivo* xenograft mouse model

Purification of total RNA from formalin-fixed paraffin-embedded (FFPE) tissue sections was carried out with RNeasy® FFPE Kit (Qiagen), using 10 sections of 4 μm thick per sample, placed in 1.5 ml Eppendorf tubes.

Prior to nucleic acid purification, paraffin must be removed to enable exposure of the sample to proteinase K. Different deparaffinization methods can be used, in this case, deparaffinization was accomplished by using xylene. 1 ml of xylene was added to each sample, vortexing vigorously for 10 seconds and centrifuging afterwards at full speed for 2 minutes. Next, supernatant was removed carefully by pipetting without disturbing the pellet, and 1 ml of absolute ethanol (Sigma-Aldrich) was subsequently added to extract residual xylene from the sample. Samples were centrifuged again at full speed for 2 minutes, ethanol was carefully removed, and tubes were incubated at room temperature with the lid open, until all residual ethanol had evaporated.

Once ethanol completely evaporated, 240 μl of *Buffer PKD* (digestion buffer) were added to the pellet, homogenizing it by vortex immediately after. Then, 10 μl of proteinase K were added to each sample, incubating them at 56 °C for 15 minutes, to increase its activity and promote protein digestion. After 56 °C incubation, samples were incubated at 80 °C for 15 minutes, to reverse formaldehyde modification of nucleic acids, which takes place as a result of paraffin embedding. Therefore, 80 °C incubation is critical for obtaining high quality RNA and optimal performance in downstream applications, such as RT-qPCR.

After deparaffinization step, 10 µl of DNase I stock solution and 16 µl of *DNase I booster buffer* were added to the sample, mixing by gently inverting the tube, as DNase is especially sensitive to physical denaturation. Then, samples were incubated at room temperature for 15 minutes, and 320 µl of *Buffer RBC (Red Blood Cell lysis buffer)* were subsequently added to adjust binding conditions, mixing the lysate thoroughly. After that, 720 µl of absolute ethanol were added to the tube, mixing well by pipetting several times.

Next, 700 µl of the sample were transferred to a *RNeasy MinElute spin column*, previously placed in a 2 ml collection tube. Tubes were thereafter centrifuged at 10000 rpm for 15 seconds, and flow-through was discarded. This step was repeated until the entire sample passed through the column. After that, 500 µl of *Buffer RPE* (washing buffer) were added to the column and samples were centrifuged at 10000 rpm for 15 seconds, and flow-through was discarded. This washing step was carried out once again, but in this case, centrifugation was carried out for 2 minutes. Flow-through was discarded, and columns were centrifuged once more, with the lid open and at full speed. This allows to completely dry the spin column membrane, which is a necessary step to avoid residual ethanol interference with downstream reactions. Once ethanol was totally removed, columns were placed in new 1.5 ml collection tubes and 20 µl of nuclease-free distilled water (Ambion®) were added to each one. Finally, columns were centrifuged at full speed for 1 minute to elute RNA. RNA concentration and quality were determined by using NanoDrop ND-1000 spectrophotometer (Thermo Fisher).

Once RNA isolation from FFPE tumour samples was finished, cDNA synthesis from isolated RNA and real time quantitative reverse transcription PCR (RT-qPCR) were carried out as described in sections 10.2. and 10.3. from materials and methods related to objective 1, respectively.

IV. RESULTS

A. RESULTS RELATED TO OBJECTIVE 1

1. Search for potential small-molecule inhibitors of E3 ubiquitin-ligase Hakai by *in silico* screening

E3 ubiquitin-ligase Hakai has been proposed as a specific target for directed therapies in cancer, due to its phosphotyrosine-binding (HYB) domain, where E-cadherin specifically binds. This HYB domain is formed after Hakai dimerization, and it is structurally different from other phosphotyrosine-binding domains, which makes it a potential drug target for cancer treatment [143,146]. Therefore, a virtual screening workflow was designed in order to identify candidate molecules that were able to inhibit Hakai, in collaboration with Dr. Federico Gago (Department of Biomedical Sciences, School of Medicine and Health Sciences, University of Alcalá) and Dr. Álvaro Cortés (Computational Chemistry-UK, RD Platform Technology & Science, GSK Medicines Research Centre, Hertfordshire, UK). In this method, drug screening is carried out by using computer-generated models to identify, from a large database of compounds, small molecules that are most likely to bind to a specific target [196], in this case, the HYB domain of the E3 ubiquitin-ligase Hakai. Virtual screening was based on the structural information available and the nature of the pTyr-binding pocket, which was explored with the aid of affinity probes [143]. Molecules considered were those that display a negatively charged carboxylate or phosphate group, which would be complementary to the highly positive molecular electrostatic potential of the binding pocket. The selected molecules were docked into the Hakai dimer to evaluate all possible binding poses. After that, they were ranked using the HYDE post-processing scoring function to estimate the interaction energy of the hypothetical Hakai-inhibitor complexes. The first 20 top-ranking molecules were visually inspected, and some of them were selected for subsequent experimental validation. After an initial experimental validation of the selected molecules, one compound, named Hakin-1 (Hakai inhibitor 1), was selected to perform further *in vitro* and *in vivo* studies. These preliminary results were considered to further determine the most appropriate concentration of Hakin-1 for the following experiments. Hakin-1 molecular structure, as well as its predicted binding pose within Hakai dimers, are shown in **Figure 15.**

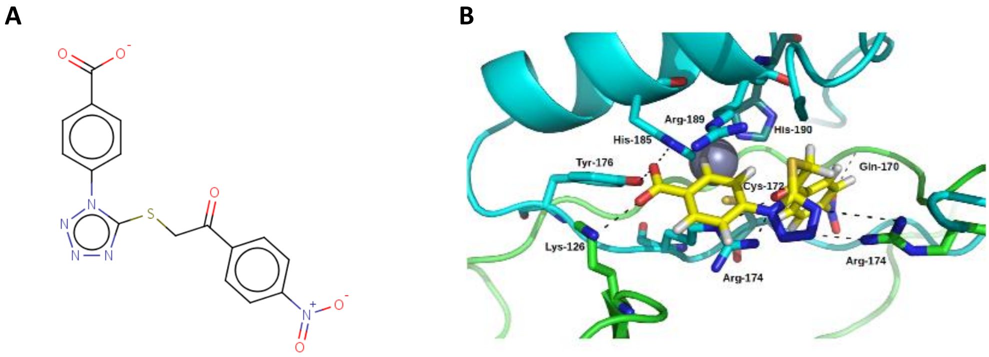

Figure 15. *In silico* screening of small-molecule inhibitors of the E3 ubiquitin-ligase Hakai. (**A**) Chemical structure of Hakin-1 inhibitor compound (4-(5-{[2-(4-nitrophenyl)-2-oxoethyl]thio}-1H-tetrazol-1-

yl)benzoic acid). (**B**) Predicted binding pose for Hakin-1 molecule (represented in yellow) docked within Hakai dimers (represented in blue and green), as determined by the CRDOCK docking program.

2. Hakin-1 small-molecule inhibitor reduces Hakai-induced ubiquitination of E-cadherin

2.1. Hakin-1 blocks Hakai-E-cadherin interaction

To first check whether Hakin-1 had an effect on the interaction between Hakai and E-cadherin, a co-immunoprecipitation experiment was carried out. To do so, HEK293 cells were transiently transfected with 4 µg GFP-Hakai, 3 µg Myc-E-cadherin and 3 µg v-Src. Once cells were transfected, they were subsequently treated with 200 µM Hakin-1 or DMSO, as appropriate. 24 hours after transfection, E-cadherin immunoprecipitation was carried out, and Hakai co-immunoprecipitation was analysed by Western Blot.

As expected, the results show a co-immunoprecipitation when both Hakai and E-cadherin are transiently transfected (**Figure 16**, right panel). Since E-cadherin is located at cell-cell contacts and Hakai is present in the nucleus, endogenous co-immunoprecipitation of these two proteins is very difficult to achieve. Moreover, their interaction takes place only for a short time, as E-cadherin is degraded in a lysosome-dependent manner once it is ubiquitin-labelled by Hakai [88,139]. This also becomes a disadvantage when it comes to detect the interaction between these two proteins. Taking this into account, it is understandable that co-immunoprecipitation was only detected when transfecting both Hakai and E-cadherin. Remarkably, at the same transfecting conditions, co-immunoprecipitation disappeared when cells were treated with 200 µM Hakin-1 (**Figure 16**, left panel). Moreover, treatment with Hakin-1 did not affect Hakai protein levels (**Figure 16**, right panel). These data suggest that Hakin-1 is able to block the interaction between Hakai and E-cadherin, without affecting Hakai expression levels.

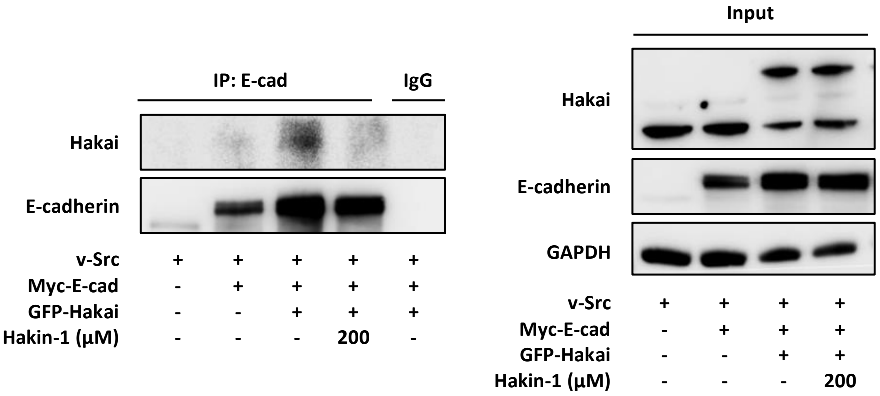

Figure 16. Effect of Hakin-1 on Hakai-E-cadherin interaction. 4 µg GFP-Hakai, 3 µg Myc-E-cadherin and 3 µg v-Src were transiently transfected into HEK293 cells, using pcDNA3.1 to equalize plasmid concentration in the different conditions. Transfected cells were treated with Hakin-1 (200 µM) or DMSO as a vehicle. Immunoprecipitation (IP) was performed with 2 µg of the anti-E-cadherin antibody. Western Blotting was carried out as described in Materials and Methods, using the indicated antibodies.

2.2. Hakin-1 reduces Hakai-induced ubiquitination

To test Hakin-1 effect on Hakai induced ubiquitination, HEK293T cells were transiently transfected with FLAG-Hakai, HA-Ubiquitin and v-Src, in order to induce Hakai ubiquitination pathway. Cells were also treated with two different concentrations of Hakin-1 (100 µM and 200 µM), and DMSO was used as a vehicle control. Inhibitor's effect over total ubiquitination was evaluated by Western Blot assay 48 hours after transfection, using N-ethylmaleimide to prepare protein lysates, in order to preserve the native cell ubiquitination. Western Blot assay showed that Hakin-1 strongly reduced the ubiquitination mediated by Hakai, without affecting Hakai protein levels (**Figure 17A**). Moreover, when Hakai was not overexpressed, and HEK293T cells were only transfected with HA-Ubiquitin and v-Src, Hakin-1 did not affect the ubiquitination smear (**Figure 17B**). This result suggests that Hakin-1 reduced Hakai-mediated overall ubiquitination, as this reduction is only detected when Hakai is overexpressed.

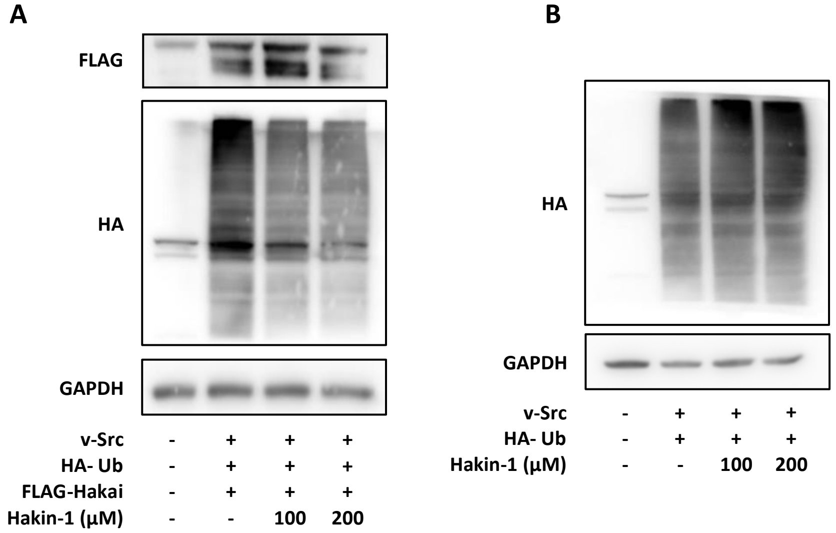

Figure 17. Hakin-1 effect on Hakai-dependent ubiquitination. (**A**) Ubiquitination assay in HEK293T cells transfected with 0.75 µg FLAG-Hakai, 0.25 µg v-Src and 0.5 µg HA-Ubiquitin, in the presence of DMSO or Hakin-1 inhibitor compound (100 µM and 200 µM). Control plasmid pcDNA3.1 was used to equalize plasmid concentration in the different conditions. (**B**) Ubiquitination assay in HEK293T cells transfected with 0.25 µg v-Src and 0.5 µg HA-Ubiquitin, in presence of DMSO or Hakin-1, using pcDNA3.1 plasmid as a control. Western Blotting was carried out as previously described using the indicated antibodies.

2.3. Hakin-1 inhibits Hakai-induced ubiquitination of E-cadherin complex

An immunoprecipitation experiment was carried out to determine if Hakin-1 could specifically inhibit Hakai-mediated ubiquitination of E-cadherin complex. To do so, HEK293 cells were transiently transfected with 3 µg v-Src, 4 µg FLAG-Hakai, 3 µg Myc-E-cadherin and 2 µg HA-Ubiquitin, and thereafter treated with Hakin-1 (100 µM and 200 µM) or DMSO as a vehicle control. E-cadherin immunoprecipitation was carried out 24 hours after transfection, and its ubiquitination smear was subsequently analysed by Western Blot. Results show that, as expected, E-cadherin ubiquitination smear increased when Hakai was overexpressed (**Figure 18A**), as Src transfection induced tyrosine phosphorylation of the E-cadherin complex and thus its ubiquitination by Hakai. Furthermore, the increased E-cadherin ubiquitination smear was reduced when HEK293 cells were treated with Hakin-1, in a dose-dependent manner (**Figure 18A**). Importantly, ubiquitination smear is reduced without affecting Hakai protein levels (**Figure 18B**). This result suggests that Hakin-1 is able to specifically inhibit Hakai-mediated ubiquitination of E-cadherin, by acting through Hakai activity and not by reducing it expression levels.

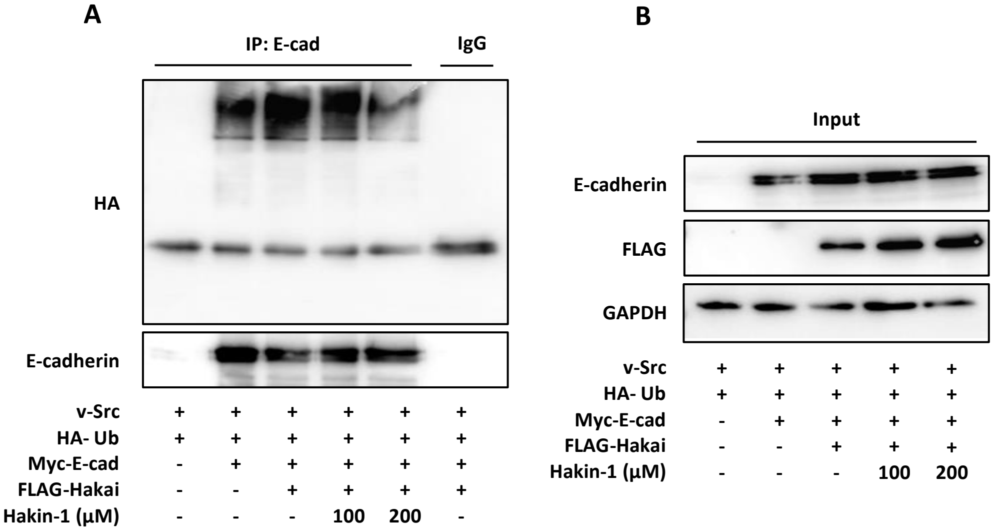

Figure 18. Effect of Hakin-1 treatment on Hakai-mediated ubiquitination of E-cadherin complex. Immunoprecipitation experiment (**A**) and protein input corresponding to total lysates (**B**) are shown. 4 µg FLAG-Hakai, 3 µg Myc-E-cadherin, 3 µg v-Src and 2 µg HA-Ubiquitin were transiently transfected into HEK293 cells, using pcDNA3.1 to equalize plasmid concentration in the different conditions. Transfected cells were treated with Hakin-1 (100 µM and 200 µM) or DMSO as a vehicle. Immunoprecipitation (IP) was performed with 2 µg of the anti-E-cadherin antibody. Western Blotting was carried out as previously described using the indicated antibodies.

2.4. Hakin-1 treatment inhibits E-cadherin degradation

Since Hakin-1 showed an important effect on Hakai-dependent ubiquitination of E-cadherin in the biochemical assays, the effect of Hakai inhibition in E-cadherin protein degradation was also studied. In this case, colorectal cancer HCT116 cells were used, since they provide a greater transfection efficiency compared to other colorectal cancer cell lines, thus allowing a better analysis of the results. This allows to study Hakin-1 effect on E-cadherin degradation in a colorectal cancer model. To perform such analysis, 0.75 µg FLAG-Hakai and 0.25 µg v-Src were transiently transfected into HCT116 cells, which were treated with 50 µM and 100 µM Hakin-1. DMSO was used as a vehicle control. Src kinase was transfected because it promotes Hakai overexpression, and this is a necessary step to have a significantly increased expression of Hakai protein in HCT116 cells.

As expected, Hakai overexpression reduced E-cadherin protein expression levels. Moreover, treatment with Hakin-1 restored E-cadherin expression levels in Hakai-overexpressing cells, in a dose-dependent manner (**Figure 19A**). Quantification of the protein bands was carried out to better visualize Hakin-1 effect, determining relative protein amount in each condition by using GAPDH as a loading control (**Figure 19B**). The effect on E-cadherin degradation is only slightly detected because Western Blot shows total protein, and it is expected to be much more evident at cell-cell contacts. This result indicates that Hakin-1 inhibits Hakai-induced E-cadherin degradation.

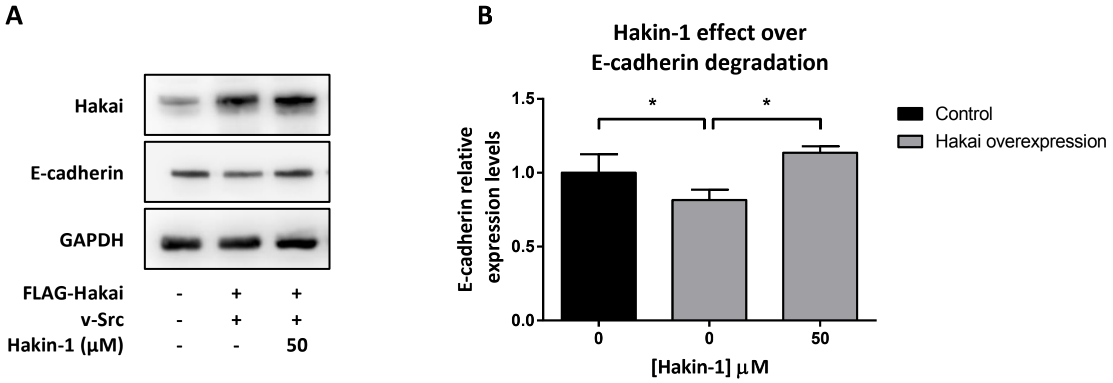

Figure 19. Effect of Hakin-1 on E-cadherin degradation. (**A**) Western Blot analysis of E-cadherin degradation. 0.75 µg FLAG-Hakai and 0.25 µg v-Src were transiently transfected into HCT116 cells, using pcDNA3.1 to equalize plasmid maximum concentration. Transfected cells were treated with Hakin-1 (50 µM and 100 µM) or DMSO as a vehicle. Western Blotting was carried out using the indicated antibodies. (**B**) Quantification of the protein bands was performed with ImageJ software. Relative protein amount in each condition was determined by using GAPDH as a loading control. Results are represented as mean ± SD of three independent experiments (*$p < 0.05$).

Altogether, these results suggest that Hakin-1 inhibits the interaction between Hakai and E-cadherin. Moreover, it reduces both Hakai-mediated ubiquitination of E-cadherin and Hakai-mediated overall ubiquitination, in a dose-dependent manner. Finally, Hakin-1 treatment also inhibits Hakai-induced E-cadherin degradation.

3. Hakin-1 reduces cell viability, proliferation, migration, invasion and oncogenic potential while increases cell differentiation *in vitro*.

3.1. Hakin-1 reduces cell viability

Next, the effect of Hakin-1 on cancer cell viability was studied, by means of MTT assay. Cells were treated with increasing concentrations (ranking from 0 to 400 µM) of Hakin-1 for 72 hours, refreshing treatment at 48 hours. First, cell viability was evaluated in a Hakai overexpression model, using MDCK normal cells and MDCK cells that stably express Hakai protein (Hakai-

MDCK). Two different clones of Hakai-overexpressing cells (clone 4 and clone 11) were used. It has been previously shown that Hakai overexpression in immortalized epithelial MDCK cells induced a fibroblastic-like phenotype accompanied by the loss of E-cadherin protein, as well as cell-cell contacts and apicobasal polarity [141,153,155,157,158].

Hakin-1 treatment had a stronger effect on Hakai-MDCK clones, as they showed lower IC_{50} values (176.3 µM for clone 4 and 165.4 µM for clone 11) than control MDCK non-transformed cells, whose IC_{50} value was 256.6 µM (**Figure 20A**). These results suggest that Hakin-1 might be particularly more effective in cancer cells that show an increased expression of Hakai protein. On the other hand, cell viability under Hakin-1 treatment was also evaluated in colorectal cancer cell lines. Three different cell lines were used: HT29, LoVo and HCT116. A dose-dependent effect of Hakin-1on the viability of these cells was also observed (**Figure 20B**). HCT116 cells seemed to be the most sensitive to treatment since they showed a lower IC_{50} value (245 µM) than HT29 and LoVo cells (289.2 and 303.7 µM respectively).

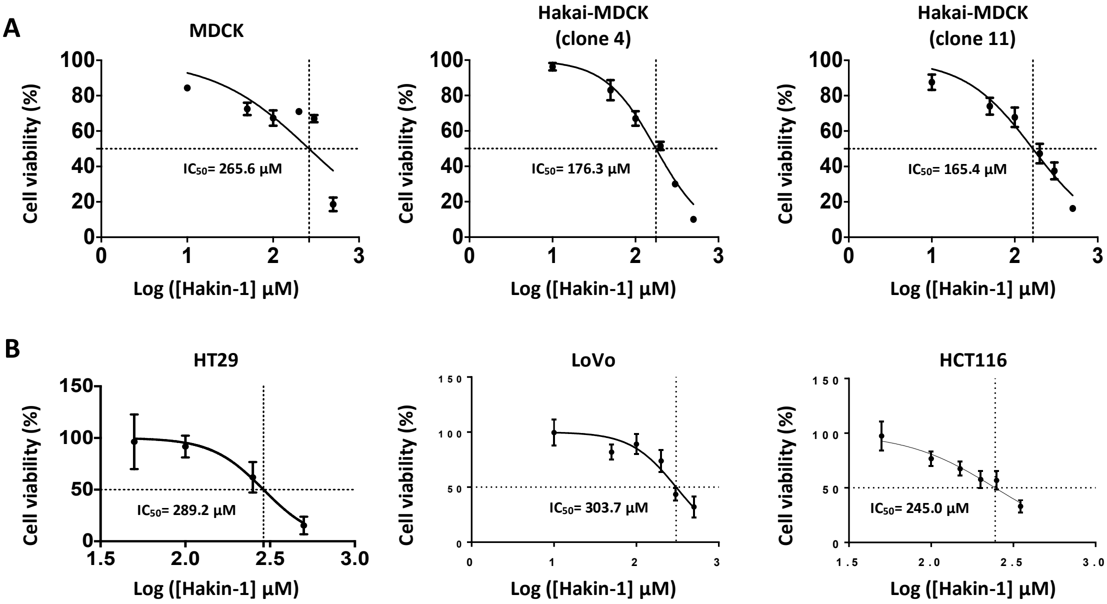

Figure 20. Hakin-1 treatment reduces cell viability of epithelial tumour cell lines. (**A**) MDCK and Hakai-MDCK (clone 4 and clone 11) cells were treated for 72 hours with an increasing range of concentrations of Hakin-1, refreshing treatment at 48 hours. Cell viability was measured by means of the MTT assay. This assay was performed in 6 replicates and results are represented as mean ± SD of three independent experiments. (**B**) Hakin-1 effect on cell viability was also measured, as indicated in (A), for HT29, LoVo and HCT116 tumour cell lines. Half maximal inhibitory concentration (IC_{50}) was calculated by using GraphPad Prism software.

3.2. Hakin-1 reduces cell proliferation

Based on previous results showing that Hakai increases cell proliferation [153–155,158,161,165], Hakin-1 antiproliferative effect was analysed through BrdU assay, treating cells with increasing concentrations (ranking from 0 to 200 μM) of Hakin-1 for 48 hours. First, cell proliferation was evaluated in the Hakai overexpression model (MDCK versus Hakai-MDCK). Hakai-MDCK cells showed an increased proliferation in comparison with normal MDCK cells (**Figure 21A**), thus confirming that Hakai overexpression in MDCK cells strongly increased cell proliferation, as previously demonstrated [153,158]. Remarkably, Hakin-1 was able to significantly reduce proliferation in Hakai-MCDK cells, down to the basal levels of proliferation of non-transformed MDCK cells, even at the lowest dose of 50 μM (**Figure 21A**). Furthermore, no effect on proliferation in MDCK cells was observed after treatment with Hakin-1. This suggests that Hakin-1 is able to abolish the increase in cell proliferation that takes place as a result of Hakai overexpression. This result also suggests that it may function as an anti-proliferative agent when Hakai is highly expressed in epithelial cells. Hakin-1 also showed an antiproliferative effect in HT29, LoVo and HCT116 colorectal cancer cell lines. HCT116 proved to be the most sensitive to treatment since a strong reduction of the proliferation is already observed at 100 μM concentration (**Figure 21B**). This result correlates with those previously obtained in the MTT assay, where Hakin-1 seemed to have a stronger cytotoxic effect on HCT116 cells.

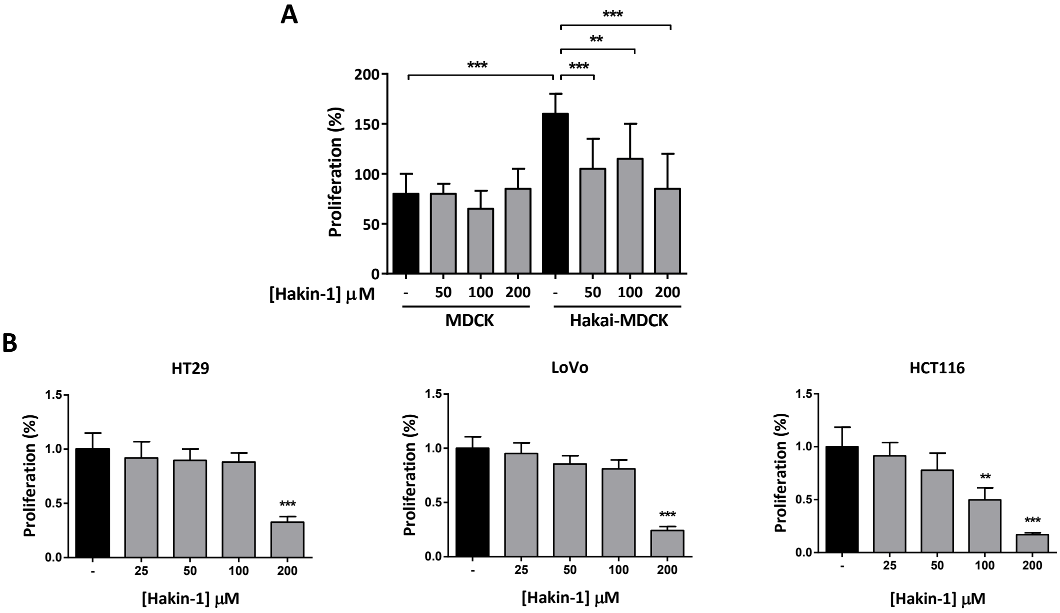

Figure 21. Antiproliferative effect of Hakin-1 in tumour epithelial cells. (**A**) MDCK and Hakai-MDCK cells were treated with increasing concentrations of Hakin-1 for 48h and proliferation was measured by performing a BrdU assay as indicated in Material and Methods. (**B**) HT29, LoVo and HCT116 cells were treated with Hakin-1 for 48 h and proliferation was measured as indicated in (A). Results are expressed as mean ± SD of eight replicates (*p < 0.05; ** p < 0.01; *** p < 0.001). Statistical significance of data was determined with one-way ANOVA statistical test.

In order to make a preliminary examination of the effect of Hakin-1 in other carcinomas, BrdU assays were carried out in a number of human cancer cell lines (Breast cancer MCF7 cells, prostate cancer PC-3 cells, ovary cancer SK-OV3 cells, liver cancer HepG2 cells, bladder cancer

5637 cells and renal cancer ACHN cells). Interestingly, Hakin-1 was able to reduce cell proliferation in MCF7, PC-3, ACHN, HepG2 and 5637 cell lines, while it showed no significant effect in SK-OV3 ovary cells (**Figure 22**). This preliminary result suggests that Hakin-1 could be also effective in other types of carcinomas besides colon cancer.

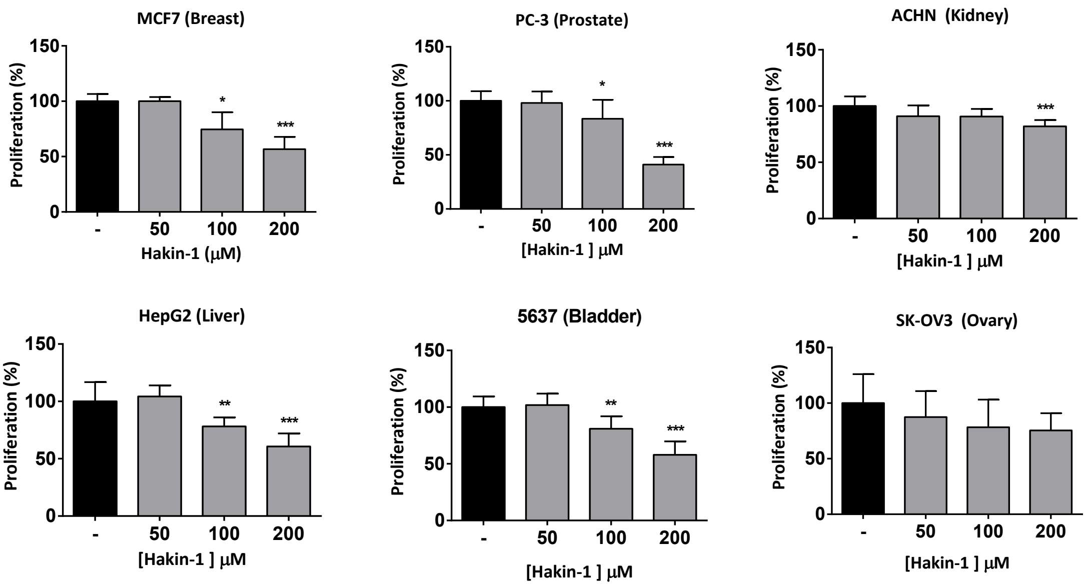

Figure 22. Effect of Hakin-1 in different human cancer cells. Breast cancer MCF7 cells, prostate cancer PC-3 cells, ovary cancer SK-OV3 cells, liver cancer HepG2 cells, bladder cancer 5637 cells and renal cancer ACHN cells, were treated with Hakin-1 for 48 h and proliferation was measured by means of a BrdU assay as indicated in Material and Methods. Results are expressed as mean ± SD of eight replicates (*$p < 0.05$; **$p < 0.01$; ***$p < 0.001$). Statistical significance of data was determined with one-way ANOVA statistical test.

3.3. Hakin-1 increases epithelial cell differentiation

3.3.1. Hakin-1 reverts mesenchymal phenotype in colorectal cancer cell lines

In recent years, it has been demonstrated that EMT is a reversible and transitory process, as once epithelial cells have undergone EMT and have metastasized to distant tissues, they usually revert to the epithelial phenotype, undergoing a mesenchymal-to-epithelial transition (MET) [50,86]. This allows them to settle, proliferate and further develop secondary tumours. The ability of cells to reversibly change their phenotype is known as cellular plasticity, and it is an essential mechanism for metastasis development. Thus, an early prevention of EMT process could be a good therapeutic approach to avoid metastasis formation [48,197,198]. Since Hakai has been described to induce EMT through posttranslational regulation of E-cadherin at cell-cell contacts [88,143], the ability of Hakin-1 to inhibit EMT was also studied.

First, the ability of Hakin-1 to reverse the mesenchymal phenotype was analysed. To do so, MCDK, Hakai-MDCK, and colorectal cancer cell lines (HT29, LoVo and HCT116) were treated with increasing concentrations of Hakin-1 (50 µM and 100 µM), using DMSO as a vehicle control. Phenotypic change was evaluated 48 hours after treatment by contrast microscopy.

Results showed that Hakin-1 treatment effectively induced an epithelial phenotype in Hakai-MDCK cells (**Figure 23A**), which was observed as an increase in cell-cell contacts and a reduction in cytoplasmic protrusions. This effect proved to be more evident in clone 11, even at the lowest dose of 50 µM, as the phenotype acquired after treatment closely resembles the non-transformed MDCK cells phenotype. However, no effect was observed in non-transformed MDCK cells (**Figure 23A**), suggesting once more that Hakin-1 is more effective when Hakai expression is increased. On the other hand, only a slight change in phenotype was observed in HT29, LoVo and HCT116 cells after treatment with Hakin-1 (**Figure 23B**). This phenotypic change was more evident in HT29 cells, as they exhibited a more rounded phenotype after Hakin-1 treatment and formed even more compact colonies.

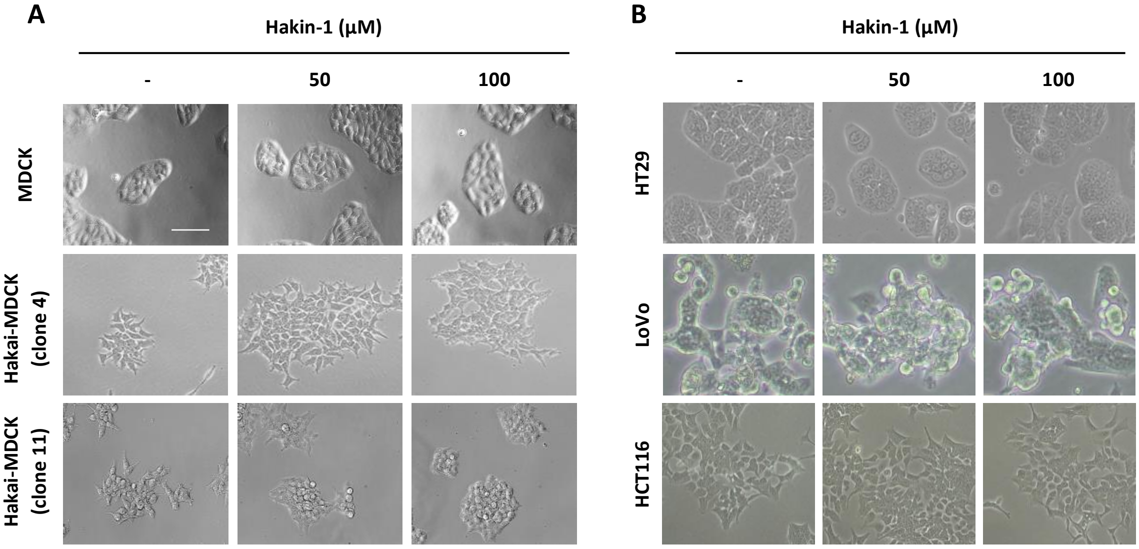

Figure 23. Hakin-1 effect on epithelial phenotype in cancer cell lines. (**A**) Phase-contrast images of MDCK and Hakai-MDCK cells treated for 48 hours with increasing concentrations of Hakin-1 (50 µM and 100 µM) or DMSO as a vehicle control. (**B**) Phase-contrast images of HT29, LoVo and HCT116 cell lines, treated with Hakin-1 as indicated in (A). Images were obtained using an Eclipse-Ti microscope (Nikon) and a 20x objective. Scale bar, 100 µM.

3.3.2. Hakin-1 modulates the protein expression levels of EMT markers

Epithelial-mesenchymal plasticity (EMP) is tightly regulated at the transcriptional, posttranscriptional and posttranslational levels [28,64,199]. Therefore, to further study the possible effect of Hakin-1 on reverting EMT process, the expression levels of EMT makers upon Hakin-1 treatment were analysed. EMT process is characterized by the downregulation of E-cadherin epithelial marker, and an increased expression of mesenchymal markers such as N-cadherin or vimentin [64]. On the other hand, Cortactin has been identified as a new substrate of

E3 ubiquitin-ligase Hakai. As well as E-cadherin, Cortactin is also phosphorylated by Src kinase and thereafter recognized by Hakai [141,143]. For this reason, Hakin-1 effect on Cortactin protein expression levels was also studied.

To study Hakin-1 effect on the protein expression levels of EMT markers, HT29 and LoVo cells were treated with different concentrations of Hakin-1 (50 µM and 100 µM) for 48 hours, using DMSO as a vehicle. Protein expression levels were thereafter analysed by means of Western Blot assay. In HT29 cells, Hakin-1 significantly increased expression levels of both E-cadherin and Cortactin, and this increased expression was observed even at the lowest dose of 50 µM. Moreover, Hakin-1 treatment significantly reduced Vimentin expression at 100 µM concentration (**Figure 24**). This increased expression of Hakai substrates E-cadherin and Cortactin upon Hakin-1 treatment was confirmed in LoVo cells (**Figure 25**).

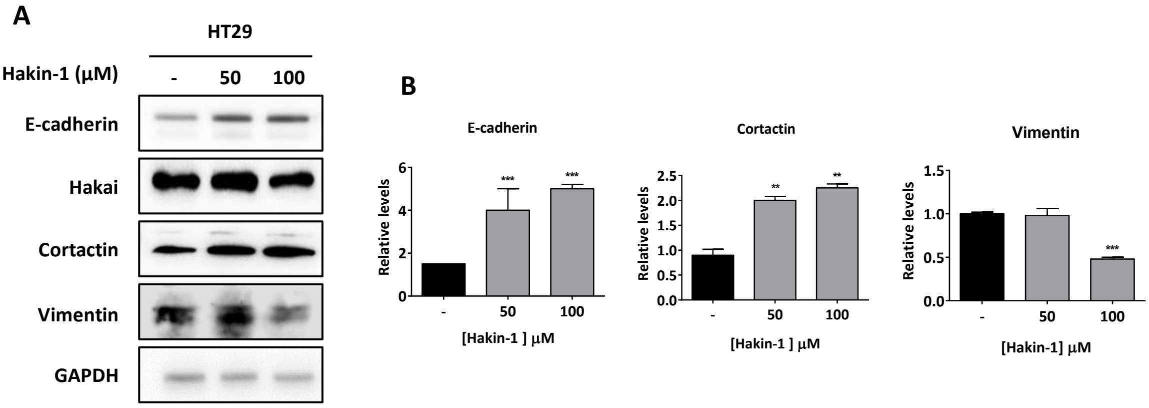

Figure 24. Effect of Hakin-1 on epithelial differentiation in HT29 cells. (**A**) Western Blot analysis of EMT markers and Hakai substrate Cortactin upon Hakin-1 treatment. HT29 cells were treated for 48h with increasing concentrations of Hakin-1 (50 µM and 100 µM) or DMSO as a vehicle control, and Western Blot was carried out using the indicated antibodies. (**B**) Quantification of the images of panel (A) is shown. Relative protein amount in each condition normalized to GAPDH as a loading control. Quantification of the protein bands was performed with ImageJ software. Data are represented as mean ± SD of three independent experiments (*p < 0.05; **p < 0.01; ***p < 0.001).

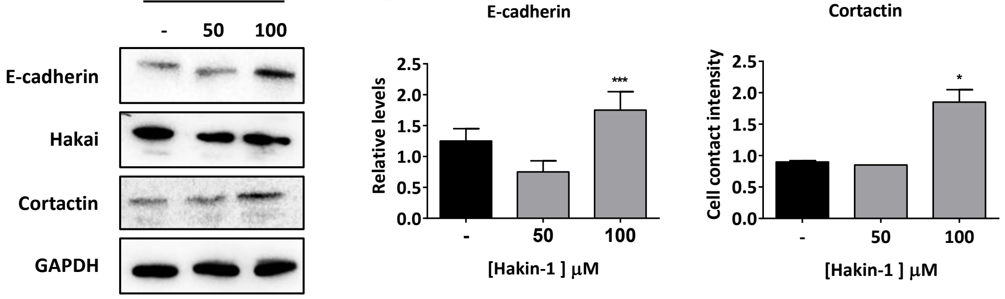

Figure 25. Effect of Hakin-1 on epithelial differentiation in LoVo cells. (**A**) Western Blot analysis of EMT markers and Hakai substrate Cortactin upon Hakin-1 treatment. LoVo cells were treated for 48h with increasing concentrations of Hakin-1 (50 µM and 100 µM) or DMSO as a vehicle control, and Western Blot was carried out using the indicated antibodies. (**B**) Quantification of the images of panel (A) is shown.

Relative protein amount in each condition normalized to GAPDH as a loading control. Quantification of the protein bands was performed with ImageJ software. Data are represented as mean ± SD of three independent experiments (*p < 0.05; **p < 0.01; ***p < 0.001).

As previously mentioned, Hakai acts as a posttranslational regulator of E-cadherin that induces its ubiquitination and subsequent degradation, causing disruption of cell-cell adhesions. This interaction of Hakai with E-cadherin takes place in a tyrosine phosphorylation-dependent manner, that is, after E-cadherin is phosphorylated in tyrosine residues by Src kinase [88]. To further confirm that the effect of Hakin-1 takes place at a posttranslational level, E-cadherin and Hakai mRNA levels were studied. To do so, HT29 and LoVo cells were treated with increasing concentrations of Hakin-1 (50 µM, 80 µM and 100 µM), equalizing the total amount of DMSO for all conditions. 48 hours after treatment, mRNA levels were analysed by RT-qPCR. Results show that Hakin-1 treatment does not affect neither Hakai nor E-cadherin mRNA levels both in HT29 and LoVo cells (**Figure 26**). Therefore, as expected, the effect of Hakai inhibition by Hakin-1 is only observed at a posttranslational level, as E-cadherin protein levels increase (**Figures 24, 25**) while mRNA levels remain constant (**Figure 26**). Moreover, as both Hakai protein and mRNA expression levels were not affected (**Figures 24-26**), this indirectly suggests that Hakin-1 might act on Hakai activity by blocking its HYB interaction domain and in consequence inhibiting E-cadherin ubiquitination and subsequent degradation.

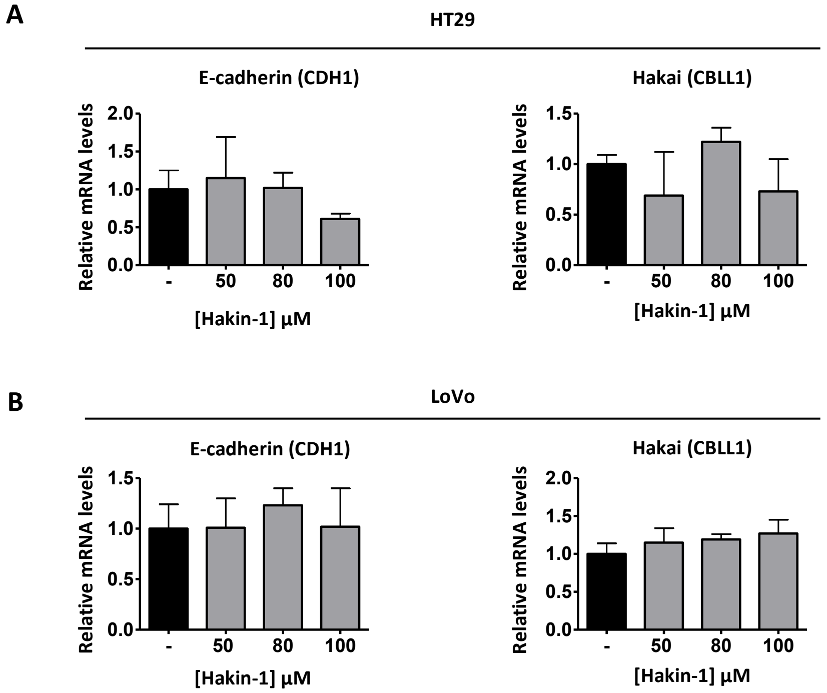

Figure 26. Effect of Hakin-1 on E-cadherin and Hakai mRNA expression levels. RT-qPCR analysis of Hakai and E-cadherin expression after Hakin-1 treatment in HT29 (**A**) and LoVo (**B**) cells. Cells were treated for 48h with increasing concentrations of Hakin-1 (50 µM, 80 µM and 100 µM) or DMSO as a vehicle control, and RT-qPCR was carried out as previously described. RPL13 was used as a reference gene for normalization.

3.3.3. Hakin-1 increases E-cadherin expression at cell-cell contacts

Based on previous results, in which Hakin-1 was observed to increase the expression of the epithelial marker E-cadherin, the effect of Hakin-1 treatment on E-cadherin subcellular localization was studied. Therefore, immunofluorescence assay was carried out to assess if the increase of E-cadherin expression took place at cell-cell contacts. Immunofluorescence analyses were performed in HT29, LoVo and HCT116 cells, after a 48-hour treatment with 50 µM and 100 µM Hakin-1. Results show that Hakin-1 increased E-cadherin expression levels at cell-cell contacts in all tested cells (**Figure 27**). This effect was especially noticeable in HCT116 cells, where E-cadherin is mainly internalized from the cell surface at the control condition. However, after Hakin-1 treatment, E-cadherin expression levels substantially increase at cell-cell contacts. This result suggests that Hakin-1 increases E-cadherin levels at cell-cell contacts, being particularly more effective in HCT116 cells. This increased effectiveness of Hakin-1 in HCT116 correlates with previously observed effect in cell viability and proliferation assays.

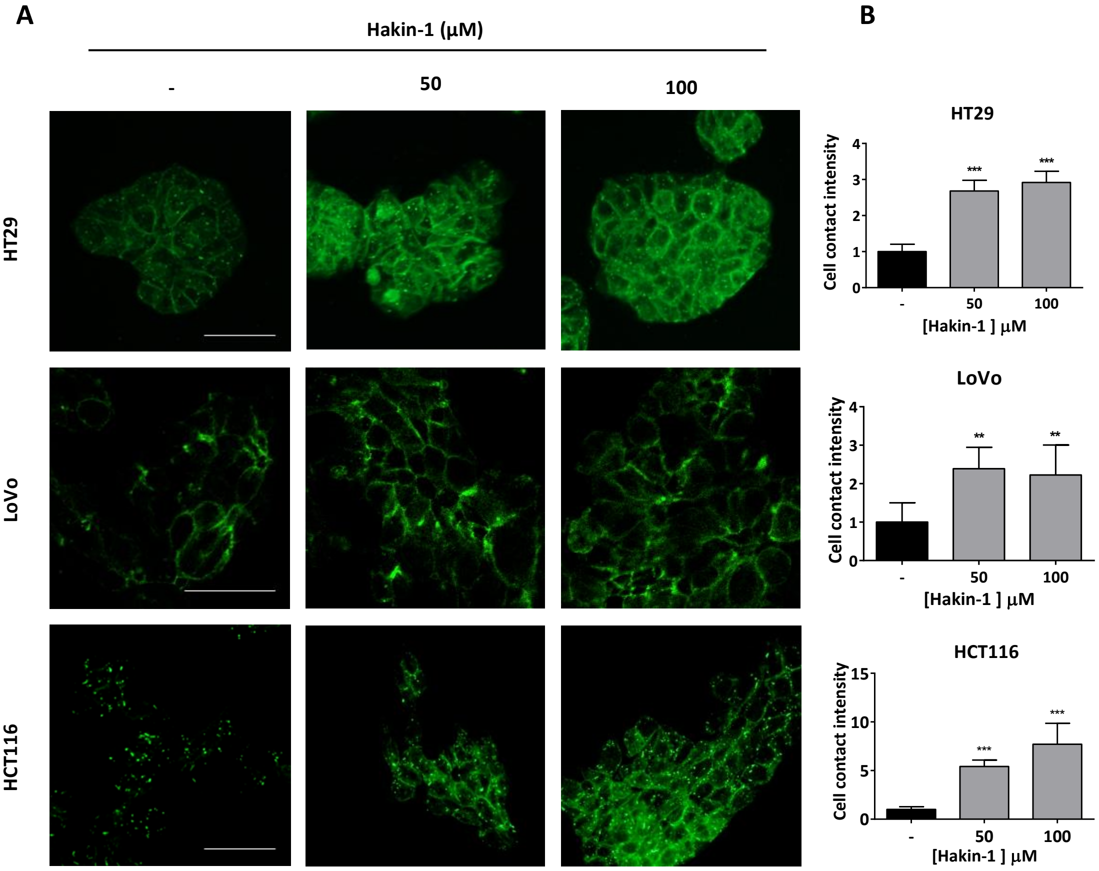

Figure 27. Hakin-1 effect on E-cadherin expression at cell-cell contacts. (**A**) Immunofluorescence analysis of E-cadherin expression in HT29, LoVo and HCT116 cells, after treatment with Hakin-1 for 48 hours. DMSO was used as a vehicle control. Images were obtained with an Olympus BX61 microscope, using a 20x objective in HT29 and HCT116 cells, and a 40x objective in LoVo cells. Scale bar, 50 µm. (**B**) Quantification of E-cadherin staining at cell-cell contacts with ImageJ Software, by using 5 pictures of each condition. Statistical significance was determined with one-way ANOVA statistical test (*$p < 0.05$; **$p < 0.01$; ***$p < 0.001$), using GraphPad Prism software.

3.4. Hakin-1 reduces cell invasion

E-cadherin loss during EMT has also been associated with an increased invasiveness and migration, and therefore with a higher metastatic capacity. As a result of the degradation of the basement membrane, tumour cells invade the adjacent stroma, which further allows the dissemination to distant tissues [21,48,50,56]. Therefore, it was then decided to determine whether Hakin-1 could also inhibit cell invasiveness. Invasion assay was carried out in MDCK, Hakai-MDCK and LoVo cells, after treatment with increasing concentrations of Hakin-1 (50 µM and 100 µM) or DMSO as a vehicle control. Results showed that Hakai-MDCK cells were able to invade extracellular matrix, while non transformed MDCK cells were not (**Figure 28A**). This suggests that Hakai overexpression increases invasive capacity, as previously demonstrated [157,158]. Moreover, number of invasive Hakai-MDCK cells was significantly reduced after Hakin-1 treatment (**Figure 28A**), suggesting that Hakin-1 could affect invasive capacity when Hakai is overexpressed. A strong reduction of invasive capacity upon Hakin-1 treatment was also observed in LoVo cells (**Figure 28B**).

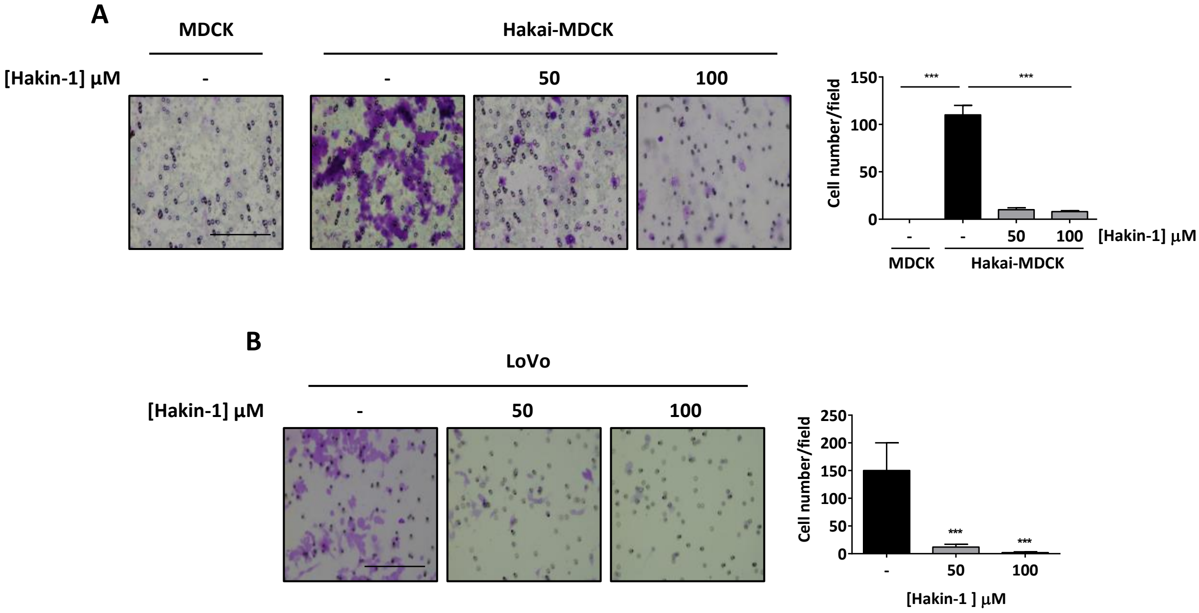

Figure 28. Hakin-1 reduces cell invasion in epithelial tumour cells. (**A**) Invasion assay in MDCK and Hakai-MDCK cells. Cells were treated for 48 hours with Hakin-1 (50 µM and 100 µM) or DMSO as a vehicle control, and invasion assay was carried out as described in Materials and Methods. Images were taken with an Olympus BX61 microscope, using a 10x objective (left panel). Scale bar, 100 µm. Quantification of invasive cells was carried out by counting the number of cells per 10x field, analysing five fields in each sample (right panel). Experiments were performed in triplicates for each condition and the assays were repeated at least three times. Results are expressed as mean ± SD (*$p < 0.05$; **$p < 0.01$; ***$p < 0.001$). (**B**) Invasion assay in LoVo cells, performed and shown as previously indicated.

3.5. Hakin-1 reduces cell migration

Given the previously mentioned association between EMT process and invasive and migration capacities [21,48], the potential ability of Hakin-1 to inhibit cell migration was also analysed. Migration assay was carried out in HT29 tumour cells, as they were not able to invade under the experimental conditions tested for the invasion assay. Cells were treated with increasing concentrations of Hakin-1 (50 µM and 100 µM), and DMSO was used as a vehicle control. 48 hours after treatment, migration assay was performed as described in Materials and Methods. Results showed that Hakin-1 significantly reduced cell migration, even at the lowest dose of 50 µM. This was observed as a lower number of cells that were able to migrate through the membrane (**Figure 29**). This result suggests that Hakin-1 might also be able to inhibit tumour cell migration.

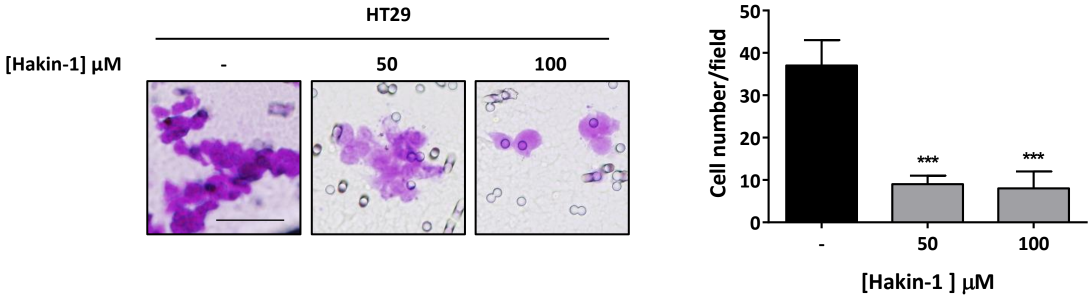

Figure 29. Hakin-1 reduces cell migration in HT29 tumour cells. Migration assay in HT29 cells. Cells were treated for 48 hours with Hakin-1 (50 µM and 100 µM) or DMSO as a vehicle control, and migration assay was carried out as described in Materials and Methods. Images were taken with an Olympus BX61 microscope, using a 20x objective (left panel). Scale bar, 50 µm. Quantification of invasive cells was carried out by counting the number of cells per 20x field, analysing five fields in each sample (right panel). Experiments were performed in triplicates for each condition and the assays were repeated at least three times. Results are expressed as mean ± SD (*$p < 0.05$; **$p < 0.01$; ***$p < 0.001$).

3.6. Hakin-1 reduces oncogenic potential

Malignant transformation of cells can not only be detected by proliferative alterations, such an increased proliferation rate, but also by the loss of contact inhibition and the acquisition of anchorage independent growth potential [200]. The latter refers to the capacity of transformed cells to grow independently of a solid surface. This ability of transformed cells to exhibit anchorage-independent growth is a very important feature of cancer biology, as it has been linked to the aggressiveness of tumour cells, including tumorigenic and metastatic potentials, and it has also been used as a marker of malignant transformation [201]. Moreover, EMT has also been linked to an increased oncogenic potential, as the downregulation of E-cadherin increases anchorage-independent cell growth [202]. To study the possible effect of Hakin-1 on the acquisition of anchorage independent growth potential, a soft agar colony formation assay was carried out. This assay is based on a semi-liquid substrate (soft agar) in which only transformed and carcinogenic cells are able to grow [203]. Colony formation assays were carried out in Hakai-

MDCK and HT29 cells, which were treated every 3 days with 50 µM and 100 µM Hakin-1, using DMSO as a vehicle control. MDCK non-transformed cells were not used for this assay as it was previously reported that they do not have an oncogenic potential *in vitro* neither *in vivo* [153,158]. Results show a significant reduction of colony formation in soft agar in Hakai-MDCK cells after Hakin-1 treatment (**Figure 30A**). This reduction of the oncogenic potential was also observed in HT29 cells, where treatment with Hakin-1 strongly decreased the number of colonies (**Figure 30B**). The same inhibition of colony formation was achieved with both concentrations tested. This result suggests that Hakin-1 might be able to reduce the malignant transformation of epithelial cells.

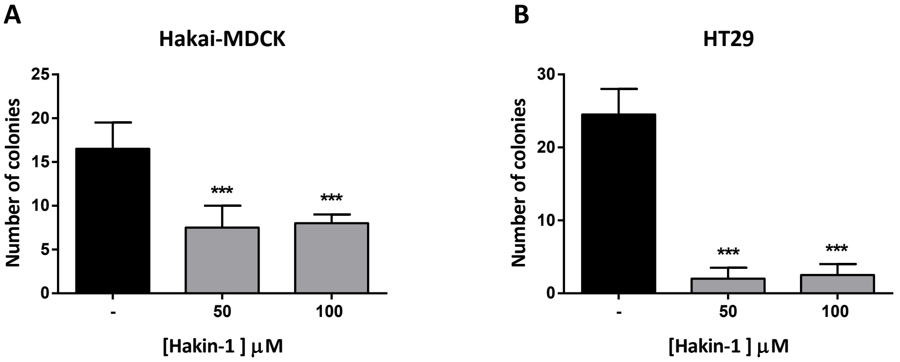

Figure 30. Effect of Hakin-1 treatment in the acquisition of anchorage independent cell growth in epithelial cells. Soft agar colony formation assay in Hakai-MDCK (**A**) and HT29 (**B**) cells. Cells were seeded in a 0.4% solution of soft agar, as described in Materials and Methods, allowing colonies to grow for 21 days (Hakai-MDCK) or 28 days (HT29). Cells were treated with Hakin-1 or DMSO as appropriate, and treatment was refreshed every three days. Quantification of the colonies was performed in triplicates and represented as mean ± SD of three independent experiments (*p < 0.05; **p < 0.01; ***p < 0.001).

Altogether, these results suggest that Hakin-1 is able to reduce epithelial cancer cell viability as well as proliferation. This antiproliferative and cytotoxic effect might be particularly stronger when Hakai is highly expressed, as normal epithelial cells (MDCK) that display lower endogenous levels of Hakai were less affected by Hakin-1 treatment. On the other hand, Hakin-1 might revert EMT process *in vitro*, as cells showed a more epithelial phenotype, as well an increased expression of E-cadherin at cell-cell contacts and a reduced expression of Vimentin mesenchymal marker. Hakin-1 potential ability to revert EMT process *in vitro* was also observed as a reduction of migration and invasive properties of epithelial cancer cells. Finally, Hakin-1 antitumor effect was also observed as a reduction in the oncogenic potential.

4. Hakin-1 shows an additive but not a synergistic effect in combination with 5-FU

The use of 5-fluorouracil (5-FU) as a routine chemotherapeutic agent took place closely after its primary synthesis in 1957, and it has since remained as an essential anti-tumour drug in many treatment routines [204]. 5-FU is an analogue of uracil that acts through the inhibition of thymidylate synthase (TS), which in turn causes the inhibition of DNA synthesis, as deoxythymidine monophosphate (dTMP) is a nucleotide required for DNA replication. 5-FU is intracellularly converted to fluorodeoxyuridine monophosphate (FdUMP), fluorodeoxyuridine triphosphate (FdUTP) and fluorouridine triphosphate (FUTP), active metabolites that prevent the action of TS. Its antitumor effect also relies on the induction of apoptosis, as the starvation of thymidine triphosphate causes the cells to undergo apoptosis [205,206].

5-FU as well as other fluoropyrimidines have been widely used for the treatment of solid cancers, especially breast and colorectal cancer [205]. It has been shown that, despite the objective response rate (ORR) of 5-FU as an individual drug is about 10-15%, it increases to 40-50% when given in combination therapies with leucovorin together with oxaliplatin (FOLFOX) or irinotecan (FOLFIRI) [207,208]. However, despite the increase in the ORR, the disease-free survival of colorectal cancer patients has not effectively been extended, as a relapse normally occurs after treatment. Thus, alternative therapeutic options should be developed to improve the poor outcomes of the existing 5-FU-based therapies for colorectal cancer patients [209]. For this reason, the anti-tumour effect of Hakin-1 was also evaluated in combination with 5-FU.

4.1. Hakin-1 shows an additive cytotoxic effect in combination with 5-fluorouracil

First, the effect of the combined treatment of Hakin-1 and 5-FU on cell viability was analysed. LoVo cells were treated for 72 hours with increasing concentrations of 5-FU (0.005 µg/ml, 0.01 µg/ml, 0.1 µg/ml, 1 µg/ml) and a fixed concentration (100 µM) of Hakin-1. The MTT assay showed that Hakin-1 and 5-FU had an additive rather than a synergistic effect at the lowest concentrations of 5-FU tested (0.005 µg/ml and 0.01 µg/ml) (**Figure 31**). Survival of cells treated with the combination of both drugs was normalized to the viability of cells treated with Hakin-1 alone. Results are represented before normalization (**Figure 31A**), to see the increased effect, and after normalization (**Figure 31B**), to see if it represents an additive or a synergistic effect [206].

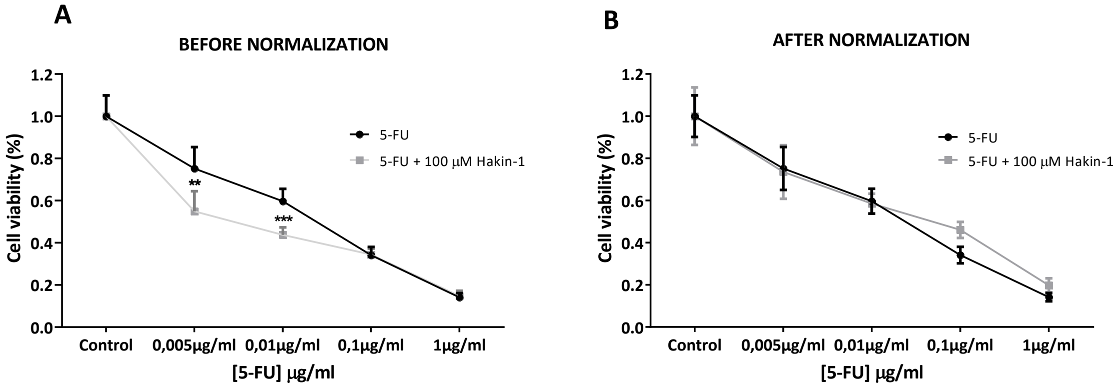

Figure 31. Additive effect of Hakin-1 and 5-fluorouracil (5-FU) on cell viability. LoVo cells were treated for 72 hours with increasing concentrations of 5-FU in combination with a fixed concentration of 100 µM

Hakin-1. Cell viability was determined by means of the MTT assay, as described in Materials and Methods. Results are expressed as mean ± SD of six replicates (*$p < 0.05$; **$p < 0.01$; ***$p < 0.001$). Survival of cells subjected to the combination of both drugs was normalized to the viability of cells treated with 100 μM Hakin-1. Results are represented before (**A**) and after (**B**) normalization of the combination of drugs.

4.2. Hakin-1 shows an additive antiproliferative effect in combination with 5-fluorouracil

Hakin-1 antiproliferative effect in combination with 5-fluorouracil was also studied. To do so, LoVo cells were treated for 72 hours with increasing concentrations of 5-FU (0.005 μg/ml, 0.01 μg/ml, 0.1 μg/ml, 1 μg/ml) and a fixed concentration (100 μM) of Hakin-1, as well as in MTT assay. The BrdU assay showed that Hakin-1 and 5-FU had an additive rather than a synergistic effect on cell proliferation, as observed in cell viability (**Figure 32**). Proliferation of cells treated both with Hakin-1 and 5-FU was normalized to the viability of cells treated with Hakin-1 alone. Results are represented before (**Figure 32A**) and after normalization (**Figure 32B**).

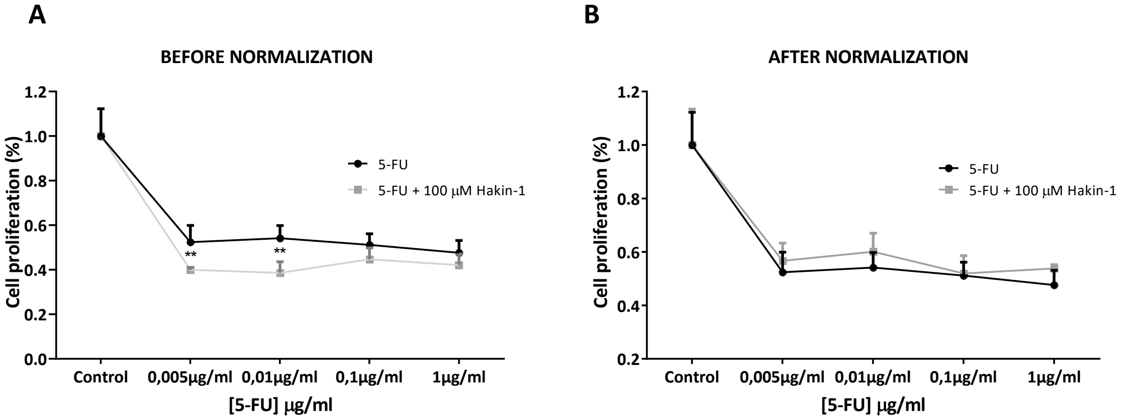

Figure 32. Hakin-1 shows an additive antiproliferative effect in combination with 5-fluorouracil (5-FU). LoVo cells were treated for 48 hours with increasing concentrations of 5-FU in combination with a fixed treatment of 100 μM Hakin-1. Cell proliferation was determined by means of the BrdU assay, as described in Materials and Methods. Results are expressed as mean ± SD of six replicates (*$p < 0.05$; **$p < 0.01$; ***$p < 0.001$). Proliferation of cells subjected to the combination of both drugs was normalized to the viability of cells treated with 100 μM Hakin-1. Results are represented before (**A**) and after (**B**) normalization of the combination of drugs.

4.3. Hakin-1 does not show a synergistic effect on cell migration in combination with 5-fluorouracil

The effect of Hakin-1 on cell migration in combination with 5-FU was also studied. LoVo cells were treated for 72 hours with 200 μM and 0.002 μg/ml 5-FU, both separately and in combination. Wound closure in each condition was analysed at 24, 48 and 72 hours. Treatment with both Hakin-1 and 5-FU reduced cell migration in LoVo cells (**Figure 33**). However, the combination of both treatments did not appear to be more effective than separated treatments, suggesting that Hakin-

1 and 5-FU did not show a synergistic effect on cell migration, as was the case in cell viability and proliferation assays.

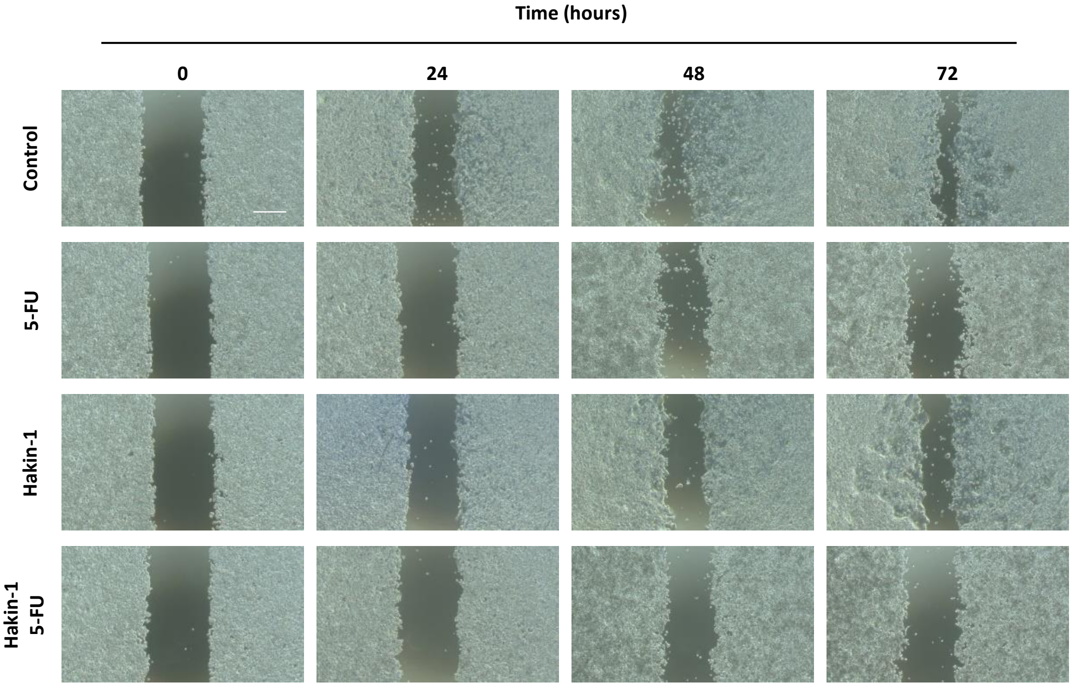

Figure 33. Effect of Hakin-1 on cell migration in combination with 5-fluorouracil. LoVo cells were treated for 72 hours with 200 µM Hakin-1 and 0.002 µg/ml 5-FU as indicated, using DMSO as a vehicle control. Wound healing assay was carried out as described in Materials and Methods. Cell migration was monitored by taking pictures at 0, 24, 48 and 72 hours with an Eclipse-Ti microscope, using a 4x objective. Scale bar, 250 µm.

Taken together, these results indicate that Hakin-1 does not show a synergistic effect in combination with 5-FU when analysing cell viability, proliferation and cell migration, as the overall effect observed with the combined treatment of Hakin-1 and 5-FU is not greater than the sum of the individual effects of each compound.

5. Analysis of novel Hakin-1 analogues *in vitro*

Given the remarkable effect of Hakin-1 on EMT and tumour progression *in vitro*, Hakin-1 analogues were analysed in order to find a compound with greater effectiveness. For this purpose, in collaboration with the expert in medical chemistry Dr. Guido Kurz (Oncostellae biopharmaceutical company), new compounds with the potential to have a similar effect to Hakin-1 were selected according to Markush structure. The selected compounds were classified in four different families based on their chemical modifications, referred to as Family A (Hakin A-7, Hakin A-8, Hakin A-9), Family B (Hakin A-23 and Hakin A-25), Family C (Hakin A-10 and Hakin A-16) and Family D (Hakin A-6.1) for confidentiality reasons. Hakin-1 belongs to Family A; therefore, Hakin A-7, A-8 and A-9 are the closest analogues to Hakin-1 original compound.

5.1. Effect of Hakin-1 analogues on cell viability

To make a first approximation of the potential effect of analogous compounds on Hakai-mediated tumour progression, the effect on cell viability was first analysed by MTT assay. HT29 cells were treated with an increasing range of concentrations of inhibitor compounds for 72 hours, and treatment was refreshed at 48 hours. MTT assay was performed as previously described. Results show that compounds of Family A (Hakin A-7, Hakin A-8, Hakin A-9) significantly reduced cell viability in HT29 cells (**Figure 34A**), being Hakin A-9 and Hakin A-8 the compounds with the lowest IC_{50} value. This IC_{50} value was even lower than that of Hakin-1 original compound. On the other hand, compounds of Family B (Hakin A-23 and Hakin A-25) also reduced cell viability, showing the lowest IC_{50} value for Hakin A-25 (**Figure 34B**). However, compounds of Family C (Hakin A-10 and Hakin A-16) and Family D (Hakin A-6.1) did not show any effect on cell viability in HT29 cells, even at a very high concentration of 500 µM (**Figure 34C, 34D**). For this reason, it was decided to continue with the first two families for further *in vitro* analysis.

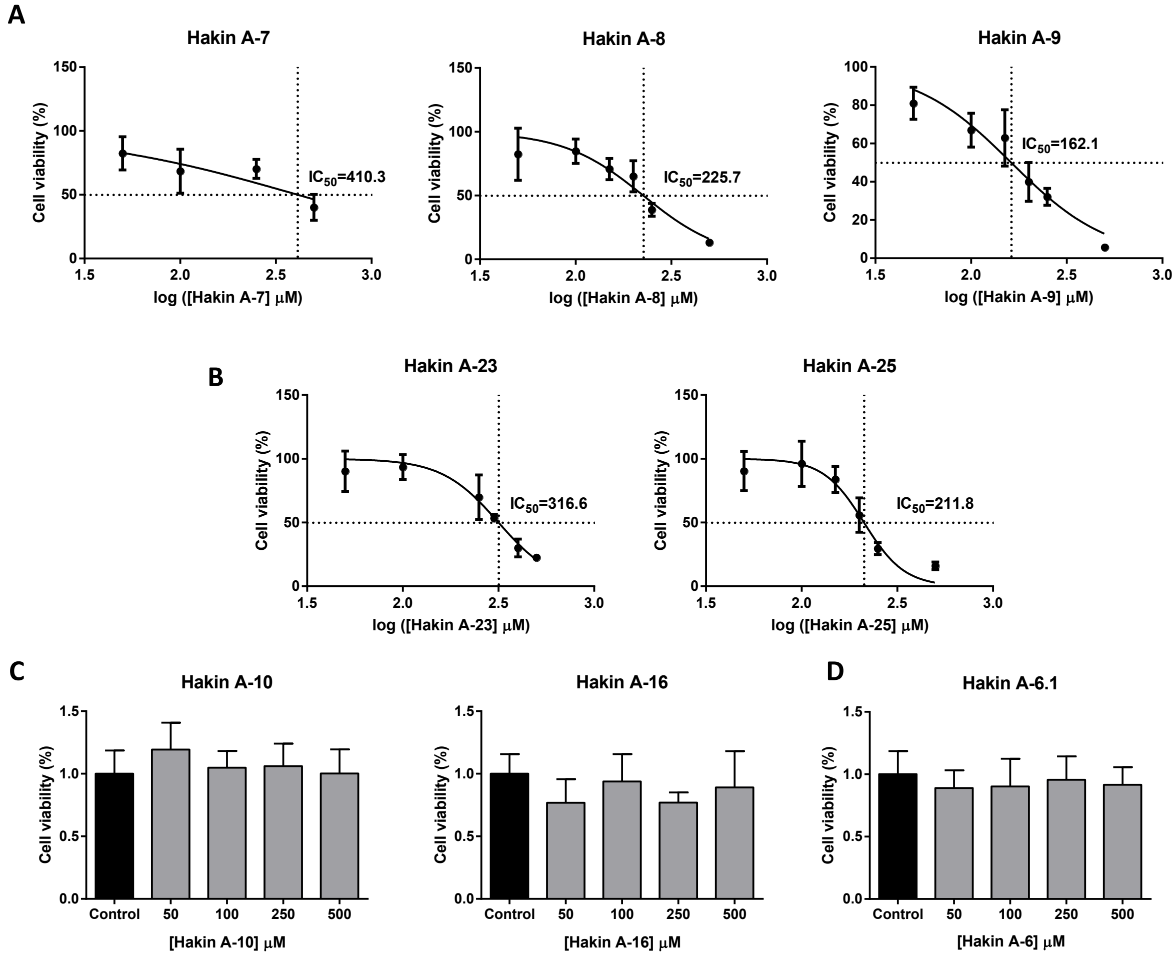

Figure 34. Effect of Hakin-1 analogues on cell viability. HT29 cells were treated for 72 hours with an increasing range of concentrations inhibitor compounds, refreshing treatment at 48 hours. Cell viability was measured by means of MTT assay as previously described. This assay was performed in 6 replicates and results are represented as mean ± SD.

5.2. Effect of Hakin-1 analogues in Hakai-induced ubiquitination

To analyse the effect of Hakin-1 analogues on Hakai induced ubiquitination, HEK293T cells were transiently transfected with FLAG-Hakai, HA-Ubiquitin and v-Src as previously described, in order to induce Hakai ubiquitination pathway. After transfection, cells were treated with two different concentrations of inhibitor compounds, 50 µM and 100 µM. In this case, lower concentrations were used for ubiquitination assays in comparison with Hakin-1, as some of the analogues strongly affected cell viability. DMSO concentration was equalized in all the conditions tested. Inhibitor's effect over total ubiquitination was evaluated by Western Blot assay 48 hours after transfection. Western Blot showed that among all Family A members, only Hakin A-7 was able to reduce the ubiquitination smear (**Figure 35A**). On the other hand, none of the compounds of the Family B (**Figure 35B**) were able to reduce the ubiquitination smear even at the highest tested concentration (100 µM), at which Hakin-1 was able to strongly reduce the ubiquitination smear. The effect of Hakin A-7 on Hakai-mediated ubiquitination was further confirmed in a broader range of concentrations, where it showed a dose-dependent effect (**Figure 36**).

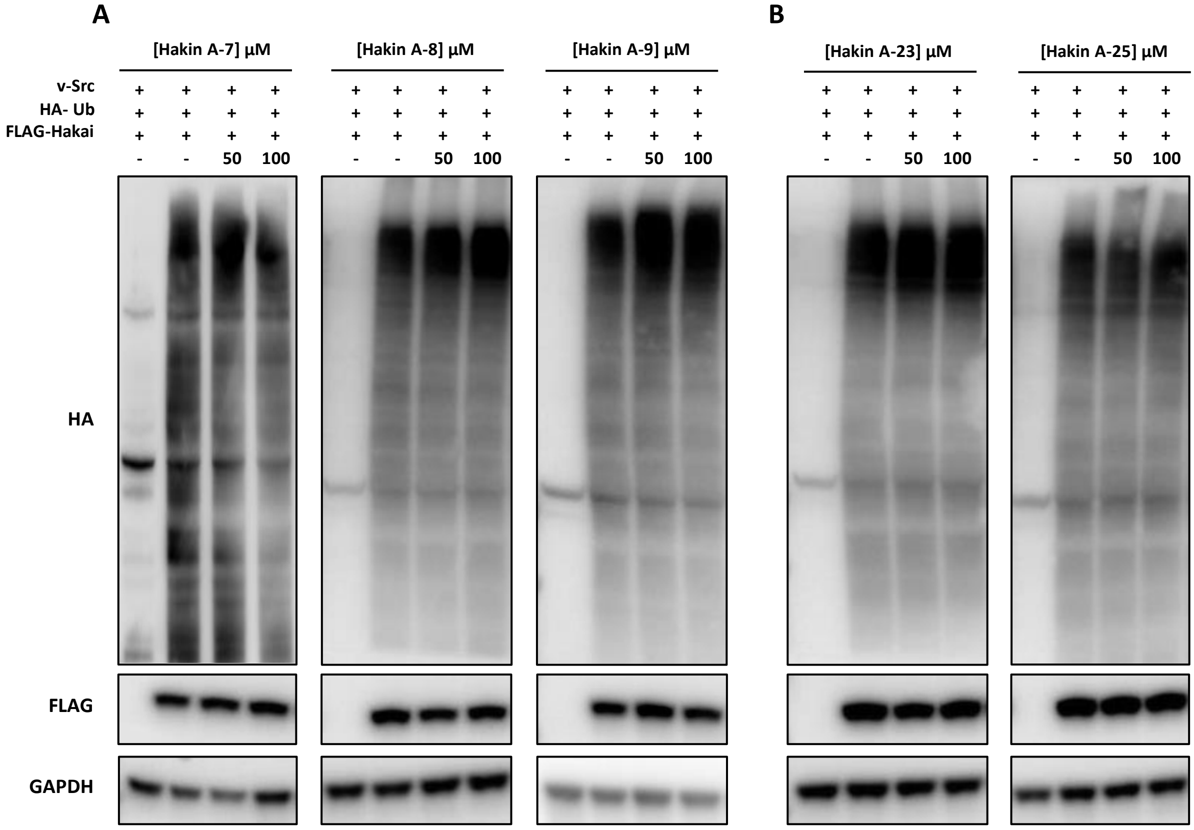

Figure 35. Effect of Hakin-1 analogues on Hakai-mediated ubiquitination. Ubiquitination assay in HEK293T cells transfected with 0.75 µg FLAG-Hakai, 0.25 µg v-Src and 0.5 µg HA-Ubiquitin, and subsequently treated with Hakin-1 analogue compounds, using DMSO as a vehicle. (**A**) Effect of Hakin A-7, Hakin A-8 and Hakin A-9. (**B**) Effect of Hakin A-23 and Hakin A-25. HEK293 cells were treated for 48 hours and Western Blot was carried out using the indicated antibodies.

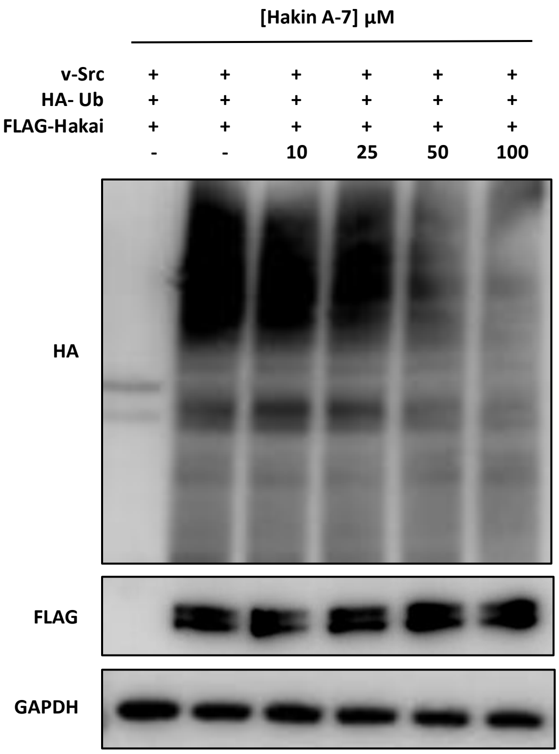

Figure 36. Effect of Hakin-A7 on Hakai-mediated ubiquitination. Ubiquitination assay in HEK293T cells transfected with 0.75 µg FLAG-Hakai, 0.25 µg v-Src and 0.5 µg HA-Ubiquitin, in the presence of DMSO or Hakin-A7. HEK293 cells were treated for 48 hours and Western Blot was carried out using the indicated antibodies.

5.3. Effect of Hakin-1 analogues on epithelial phenotype

The ability of the analogous compounds to reverse mesenchymal phenotype of colorectal cancer cells was also analysed. To do so, LoVo cells were treated with increasing concentrations of Hakin-1 analogues (50 µM and 100 µM), using DMSO as a vehicle control. Phenotypic change was evaluated 48 hours after treatment by contrast microscopy. Regarding to the analogues of Family A, microscopic analysis showed that treatment with Hakin A-7 and Hakin A-9 slightly induced the formation of more compact colonies at the highest concentration of 100 µM, while treatment with Hakin A-8 did not seem to have a detectable impact on epithelial phenotype (**Figure 37A**). In the case of Family B analogues, a tendency to form more compact colonies was observed after treatment with Hakin A-25, even at the lowest dose tested, while no remarkable phenotypic change was observed after treatment with Hakin A-23 (**Figure 37B**). These results suggest that Hakin A-7, Hakin A-9 and Hakin A-25 are able to reverse mesenchymal phenotype.

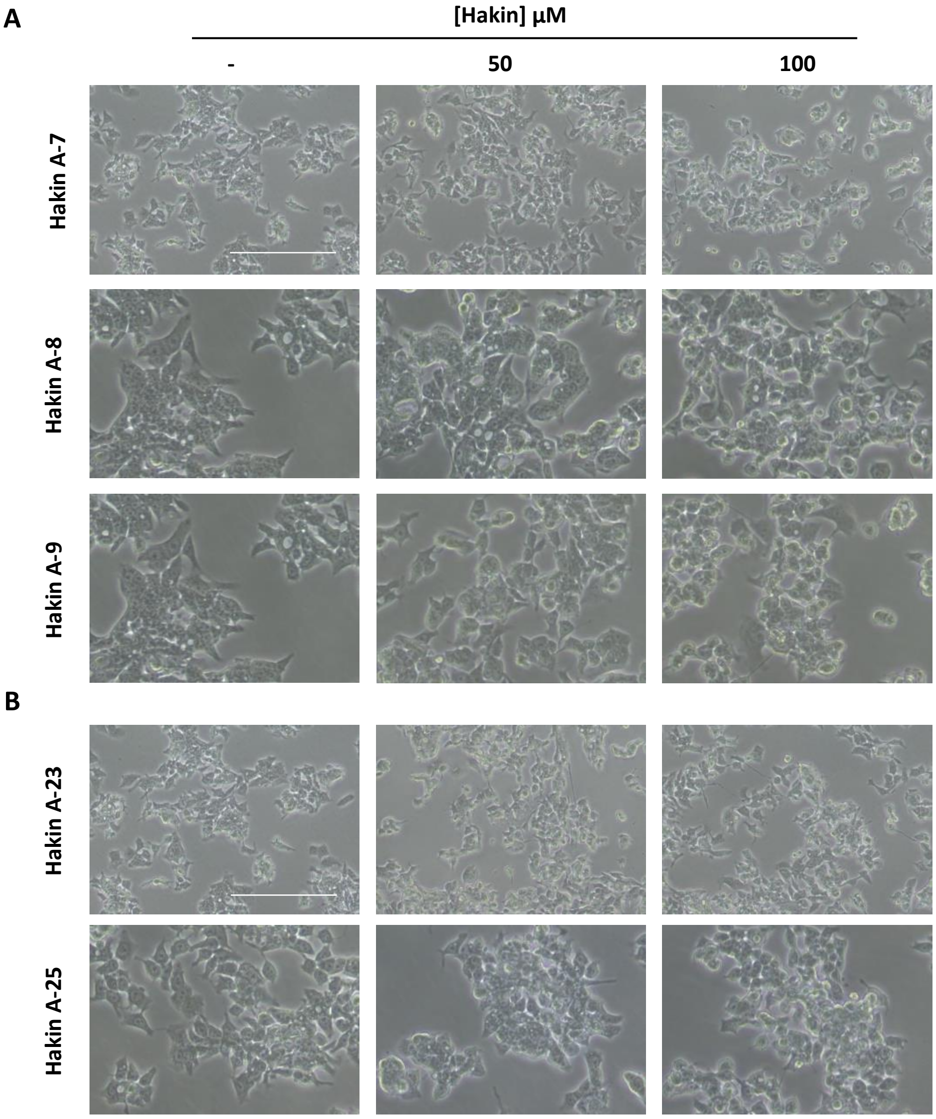

Figure 37. Effect of Hakin-1 analogues on epithelial phenotype. (**A**) Phase contrast images of LoVo cells, treated for 48 hours with increasing concentrations of Family A (Hakin A-7, Hakin A-8 and Hakin A-9) inhibitor compounds (50 µM and 100 µM) or DMSO as a control. Images were obtained using an Eclipse-Ti microscope (Nikon) and a 20x objective. Scale bar, 200 µM. (**B**) Phase contrast images of LoVo cells, treated for 48 hours with increasing concentrations of Family B (Hakin A-23 and Hakin A-25) inhibitor compounds, obtained as previously described.

5.4. Effect of Hakin-1 analogues on E-cadherin subcellular localization

E-cadherin subcellular localization under treatment with Hakin-1 analogues was studied to test if they were able to regulate E-cadherin expression at cell-cell contacts. To do so, HT29 cells were treated for 48 hours with two different concentrations of inhibitor compounds (50 µM and 100 µM) and after that immunofluorescence assay was carried out. Results show that only Hakin A-7 was able to significantly increase E-cadherin expression at cell-cell contacts in HT29 cells (**Figure 38**). In Hakin A-8 and A-9, a slight recovery of E-cadherin at cell contacts was observed, although it did not prove to be statistically significant (**Figure 38**). Finally, treatment with compounds of Family B (Hakin A-23 and Hakin A-25) did not affect E-cadherin expression at cell-cell contacts (**Figure 39**).

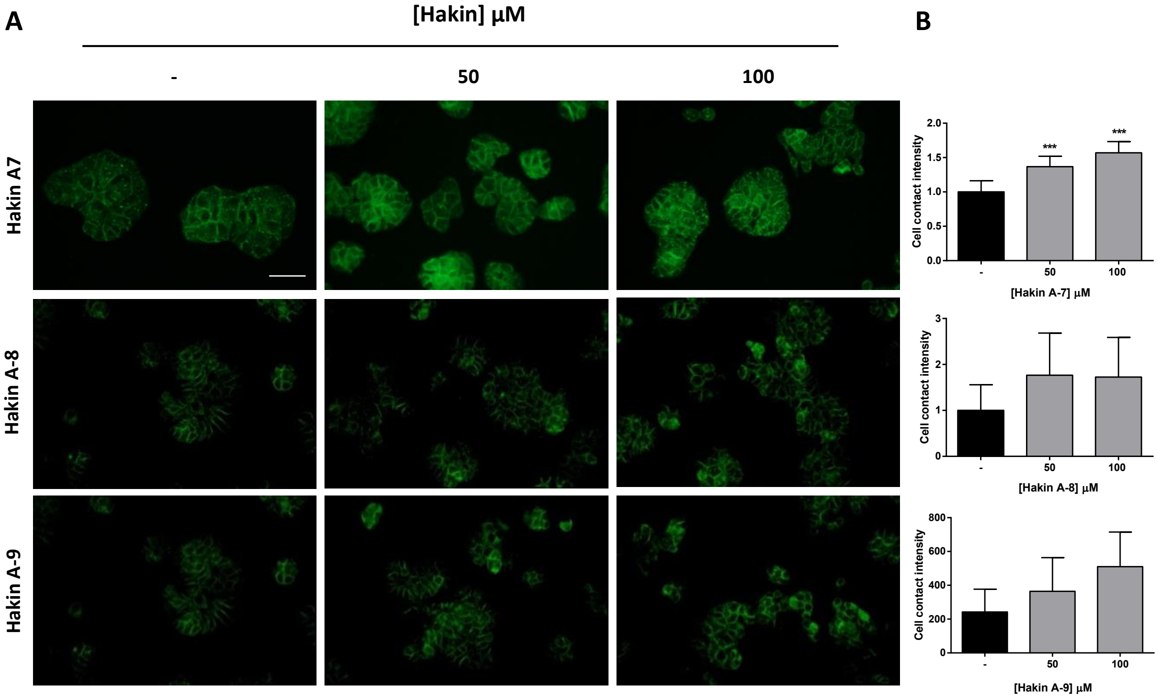
A
[Hakin] µM
-
50
100
Hakin A7
Hakin A-8
Hakin A-9
B
Cell contact intensity
***
***
[Hakin A-7] µM
[Hakin A-8] µM
[Hakin A-9] µM
-
50
100

Figure 38. Effect of analogue compounds of Family A on E-cadherin expression at cell-cell contacts. (**A**) Immunofluorescence analysis of E-cadherin expression in HT29, after treatment with Hakin A-7, A-8 and A-9 for 48 hours. DMSO was used as a vehicle control. Images were obtained with an Olympus BX61 microscope, using a 20x objective. Scale bar, 50 µm. (**B**) Quantification of E-cadherin staining at cell-cell contacts with ImageJ Software. Statistical significance was determined with one-way ANOVA statistical test (*p < 0.05; **p < 0.01; ***p < 0.001), using GraphPad Prism software.

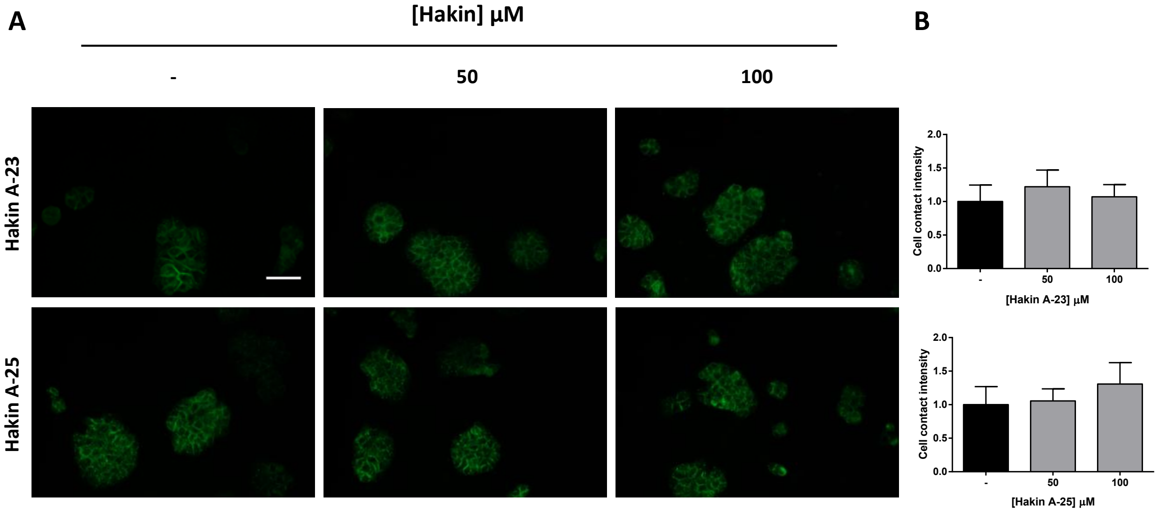
A
[Hakin] µM
-
50
100
Hakin A-23
Hakin A-25
B
Cell contact intensity
[Hakin A-23] µM
[Hakin A-25] µM
-
50
100

Figure 39. Effect of analogue compounds of Family B on E-cadherin expression at cell-cell contacts. (**A**) Immunofluorescence analysis of E-cadherin expression in HT29, after treatment with Hakin A-23 and A-25 for 48 hours. DMSO was used as a vehicle control. Images were obtained with an Olympus BX61 microscope, using a 20x objective. Scale bar, 50 µm. (**B**) Quantification of E-cadherin staining at cell-cell contacts with ImageJ Software. Statistical significance was determined with one-way ANOVA statistical test (*p < 0.05; **p < 0.01; ***p < 0.001), using GraphPad Prism software.

Taking these results into account, as well as those obtained in above-mentioned *in vitro* assays, it can be concluded that compounds of Family A (Hakin A-7, Hakin A-8 and Hakin A-9) were the most effective among the analogues tested. Hakin A-7 proved to be the most effective inhibitor compound, as observed in ubiquitination and immunofluorescence assays as well as in phenotypic change analysis. However, none of the analogues tested showed a greater antitumour effect than Hakin-1. Therefore, more studies are needed to identify new analogues as well as to improve their antitumor activity.

6. Effect of Hakin-1 on tumour progression and carcinogenesis *in vivo*

EMT process has been widely associated with numerous characteristics of carcinogenesis, such as tumour initiation, malignant transformation, cell migration, intravasation to the blood and more recently with stemness and drug resistance [50,94,103,110]. Therefore, targeting EMT-related events might be a powerful therapeutic approach for cancer treatment [210–213]. Based on previously shown *in vitro* results, where Hakin-1 was able to inhibit Hakai-E-cadherin interaction, induce epithelial differentiation and decrease cell proliferation, oncogenic potential, invasion and motility of cancer cells, a xenograft mouse model was performed to test the possible antitumor effect of Hakin-1 *in vivo*. Cell line-derived xenograft (CDX) models are frequently used for the development of cancer therapies and involve the implantation of tumour cell lines into immunodeficient mice to assess the effectiveness of such therapies *in vivo* [214].

To do so, MDCK and Hakai-MDCK cells were subcutaneously injected into the flank of athymic immunodeficient mice (BALB/c, nu/nu). BALB/c mice represent an excellent model system to study cancer *in vivo*, due to their immunodeficient nature. They possess a vestigial thymus which is unable to produce mature T-cells, thus allowing the engraftment of tumour cell lines as there is no rejection response [215]. The thymus dysgenesis and subsequent lack of T-cells are caused by a mutation in the FOX1 gene (originally described as Whn), which is responsible for the regulation of epithelial cell differentiation in the thymus and skin. Although the initial intention of FOX1 gene mutation was to generate immunodeficient mice, it also results in the lack of fur, which allows the easy assessment of subcutaneous tumour growth and therefore contributes to make BALB/c mice a good study model for cancer research [216,217]. Once tumours were palpable (around 20 days after cell injection), treatment with 5 mg/kg of Hakin-1 (or the appropriate amount of DMSO as a control) was initiated.

6.1. Hakin-1 decreases tumour size and induces cell differentiation *in vivo*

As mentioned above, tumour size began to be monitored 20 days after the injection of the cells, when the tumours started to be palpable. At that point, the treatment either with DMSO or Hakin-

1 (5mg/kg) was initiated. Mice were treated for 20 days 3 times a week. As previously reported, Hakai-MDCK cells were able to form tumours while non transformed MDCK cells were not [158]. Tumour size in mice injected with Hakai-MDCK cells (both control and treated with Hakin-1) was measured twice a week. Tumour length (L) and width (W) were measured to further determine tumour volume, calculated as (πLW^2)/6 and expressed in cubic centimetres (cm^3). Measurements were taken until day 40 after inoculation, at which time mice were sacrificed by cervical dislocation (**Figure 40A**). Immediately after animal sacrifice, tumours, lungs, kidneys and livers were collected and fixed in 4% PFA and embedded in paraffin blocks for subsequent histology and/or immunohistochemistry analyses. Histological examination of tumour samples was carried out under the supervision of Dr. Ángel Concha (Head of the Pathological Anatomy Service, Complexo Hospitalario Universitario de A Coruña, CHUAC).

Results show that Hakin-1 was able to reduce xenograft tumour growth, exhibiting statistically significant differences from day 18 (**Figure 40B**). Moreover, histological analysis of control tumour samples, showed that cells exhibited undifferentiated and spindle-shape phenotype, large nucleus and small cytoplasm size (**Figure 40C**, left panel). These structural alterations are characteristic of cancer cells, and they have been extensively used as a fundamental diagnostic standard [218]. The altered morphology was strongly modified after Hakin-1 treatment, as tumour samples displayed more differentiated cells and an increased cytoplasm size (**Figure 40C**, right panel). This suggests that Hakin-1 decreases tumour growth and induces tumour differentiation *in vivo*.

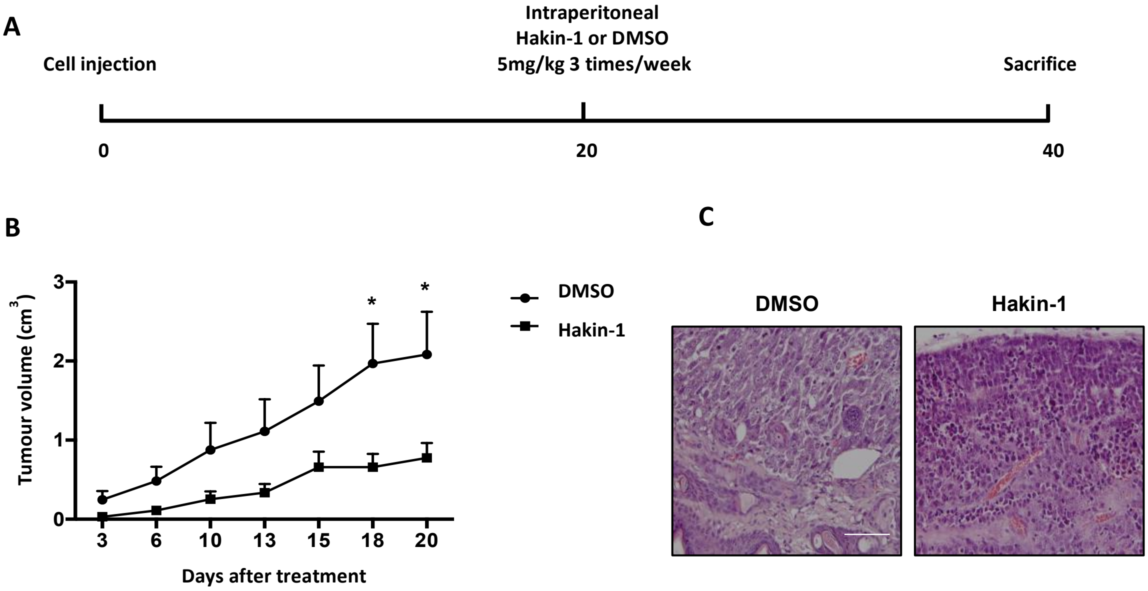

Figure 40. Hakin-1 effect on tumour growth and phenotype in immunodeficient mice (BALB/c, nu/nu). (**A**) Schematic workflow of the *in vivo* mouse model. (**B**) Tumour growth curve in mice inoculated with MDCK-cells (n=8 tumours) upon DMSO or Hakin-1 treatment. Values are represented as mean ± SEM (*$p < 0.05$), and statistical significance was determined with Mann-Whitney test, using the GraphPad Prism software. (**C**) H&E staining of Hakai-MDCK tumours at the end point, treated with DMSO (left panel) or

Hakin-1 (right panel). Images were obtained with an Olympus BX61 microscope, using a 20x objective. Scale bar, 50 µm.

6.2. Hakin-1 reduces on cell proliferation and angiogenesis, while no effect was detected on apoptosis

Hakin-1 effect on cell proliferation *in vivo* was determined by analysing Ki67 expression and the mitotic index in Hakai-MCDK xenografted tumours, treated both with DMSO or Hakin-1. To do so, immunohistochemistry assay for Ki67 marker was performed, and H&E staining was used to assess the number of mitosis. Results show that Hakin-1 significantly reduced the number of proliferative cells, which was seen as a reduction in the number of positive nuclei for Ki67 (**Figure 41A**). On the other hand, Hakin-1 also reduced the mitotic index, as a significant reduction of mitosis per high magnification field was observed after treatment with Hakin-1 (**Figure 41B**, arrows). This result might outline the potential ability of Hakin-1 to reduce cell proliferation *in vivo*.

Deregulated proliferation and inhibition of apoptosis are the basis of any tumour development, thus representing two important targets for therapeutic approaches [9,219–221]. For this reason, Hakin-1 potential ability to sensitize cells to apoptosis was also studied, by means of TUNEL assay. However, previously reported studies demonstrated that Hakai overexpression did not resulted in a reduced cell death [153]. Therefore, as expected, no effect on cell apoptosis was detected upon Hakin-1 treatment (**Figure 42**), further supporting the potential specific effect of Hakin-1 on cell proliferation.

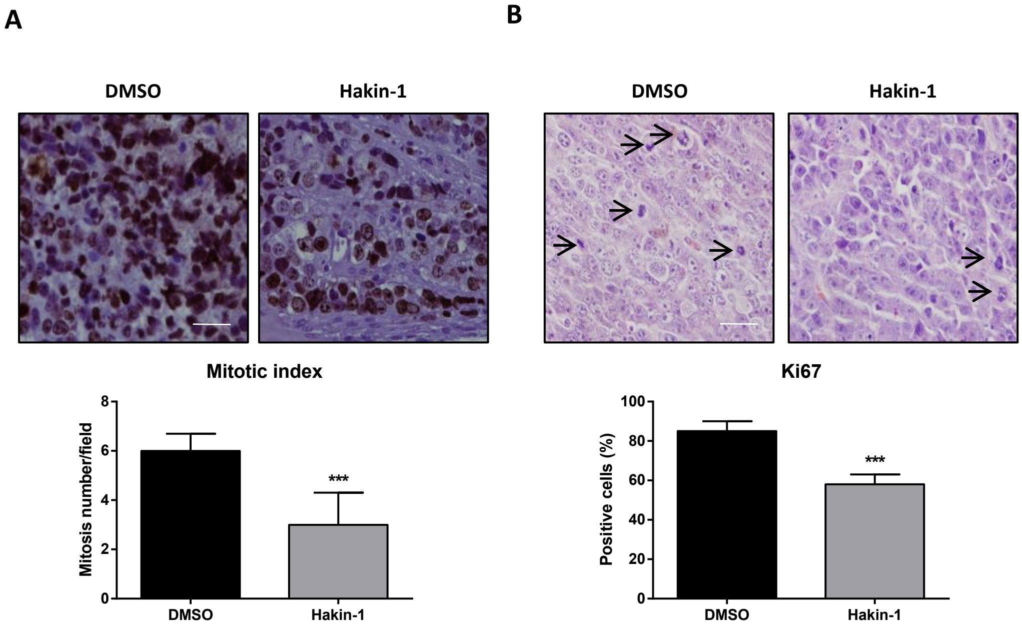

Figure 41. Hakin-1 effect on cell proliferation *in vivo*. (**A**) Immunohistochemistry of Ki67 marker in Hakai-MDCK xenografted tumours treated with DMSO (left panel) or Hakin-1 (right panel). Images were

obtained with an Olympus BX61 microscope, using a 40x objective. Scale bar, 20 µm. Quantification of the percentage of positive cells (bottom panel) was carried out with ImageJ software, and statistical significance was determined using GraphPad Prism software (***$p < 0.001$) (**B**) H&E staining of Hakai-MDCK tumours with mitotic cells marked with arrows. Quantification of mitotic index (bottom panel) was carried out by determining the number of mitosis in high magnification field (40x objective). Scale bar, 20 µm

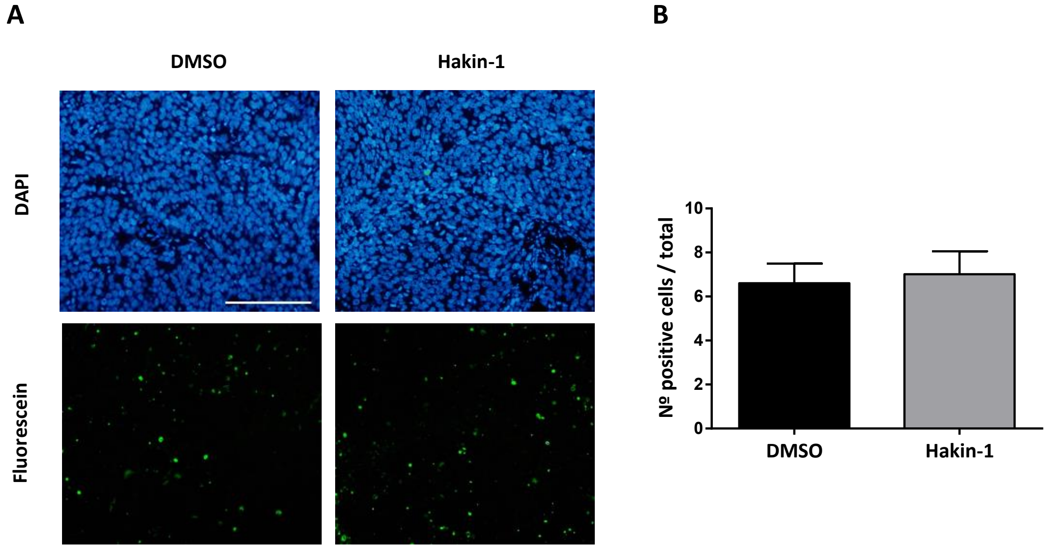

Figure 42. Hakin-1 does not affect cell apoptosis in tumour xenograft mouse model. TUNEL assay was carried out as previously described in Materials and Methods, using the *Cell Death Detection Kit, Fluorescein* (Roche) and FFPE tumour sections. Nuclei were counterstained with Hoechst 33342. Representative images (**A**) and quantification of the number of positive cells (**B**) are shown. Results are represented as mean ± SEM. Images were obtained with an Olympus BX61 epifluorescence microscope, using a with 20x objective. Scale bar, 125 µm.

Another event that takes place during tumour progression is angiogenesis. This process takes place once the tumour lesion exceeds certain size that causes hypoxia and nutrient starvation, thus inducing an angiogenic response (also known as 'angiogenic switch') [9,222]. For this reason, anti-angiogenic agents could be used for cancer treatment and metastasis prevention [223,224]. To study Hakin-1 potential ability to affect angiogenesis process during carcinoma progression, an immunohistochemistry assay for CD31 endothelial marker was carried out, using FFPE tumour xenografts from inoculated mice treated both with DMSO or Hakin-1. Results showed a strong reduction in the number of blood vessels in tumour xenografts upon Hakin-1 treatment, which was observed as a reduction in CD31 endothelial marker staining (**Figure 43**). This suggests that Hakin-1 might be able to reduce angiogenesis *in vivo*.

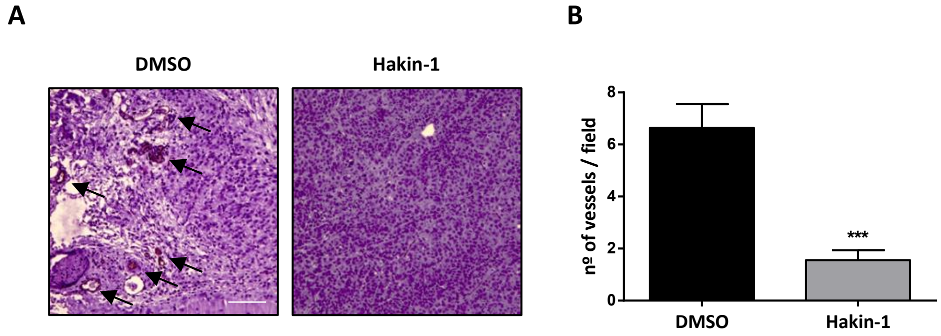

Figure 43. Effect of Hakin-1 on angiogenesis. (**A**) Immunohistochemistry of CD31 marker in Hakai-MDCK tumours of immunodeficient mice treated with DMSO (left panel, arrows) or Hakin-1 (right panel). Images were obtained with an Olympus BX61, using a 20x objective. Scale bar, 100 µm. (**B**) Quantification of the number of vessels per field, expressed as mean ± SEM. Quantification was carried out with ImageJ software, and statistical significance was determined using GraphPad Prism software (***$p < 0.001$)

6.3. Hakin-1 regulates the expression of EMT-related markers

Given the previously observed effect of Hakin-1 on the regulation of EMT markers *in vitro*, it was decided to analyse the potential ability of Hakin-1 to revert EMT process *in vivo*. To do so, the expression levels of the E-cadherin epithelial marker and N-cadherin mesenchymal marker were analysed. Cortactin expression levels were also studied, based on the results previously obtained *in vitro* and the fact that it has been reported as a new substrate of Hakai [143]. Hakai expression levels were also studied in order to determine whether Hakin-1 could affect its expression levels *in vivo*. To do so, immunohistochemistry assays were carried out, using FFPE tumour samples from the xenograft mouse model.

On the other hand, as previously observed in Hakai-MDCK cells injected *in vivo*, E-cadherin was not expressed at the protein level [153]. Therefore, E-cadherin expression was neither detected in tumour xenografts both in the presence or absence of Hakin-1 (**Figure 44A**). Since Hakin-1 acts at a posttranslational level, it was not able to increase E-cadherin levels in Hakai-MDCK tumours due to their complete absence of E-cadherin protein. Interestingly, a significant reduction of N-cadherin mesenchymal marker was observed upon Hakin-1 treatment (**Figure 44B**). This result further supports those previously obtained *in vitro*, in colorectal cancer cell lines, where Hakin-1 seemed to be able to reverse the mesenchymal phenotype. As mentioned above, Cortactin is another described substrate of E3 ubiquitin-ligase Hakai, which is also phosphorylated by Src kinase and thereafter recognized by Hakai [141,143]. Consistent with previously observed *in vitro*, Cortactin expression increased in Hakai-MDCK tumour xenografts upon Hakin-1 treatment (**Figure 44C**). This result further suggests the capacity of Hakin-1 to regulate Cortactin expression *in vivo*, probably through the inhibition of Hakai E3 ubiquitin-ligase activity, and in consequence Cortactin ubiquitination and subsequent degradation. As previously observed *in vitro*, Hakai expression levels in tumour xenografts did not significantly change upon Hakin-1 treatment (**Figure 45**).

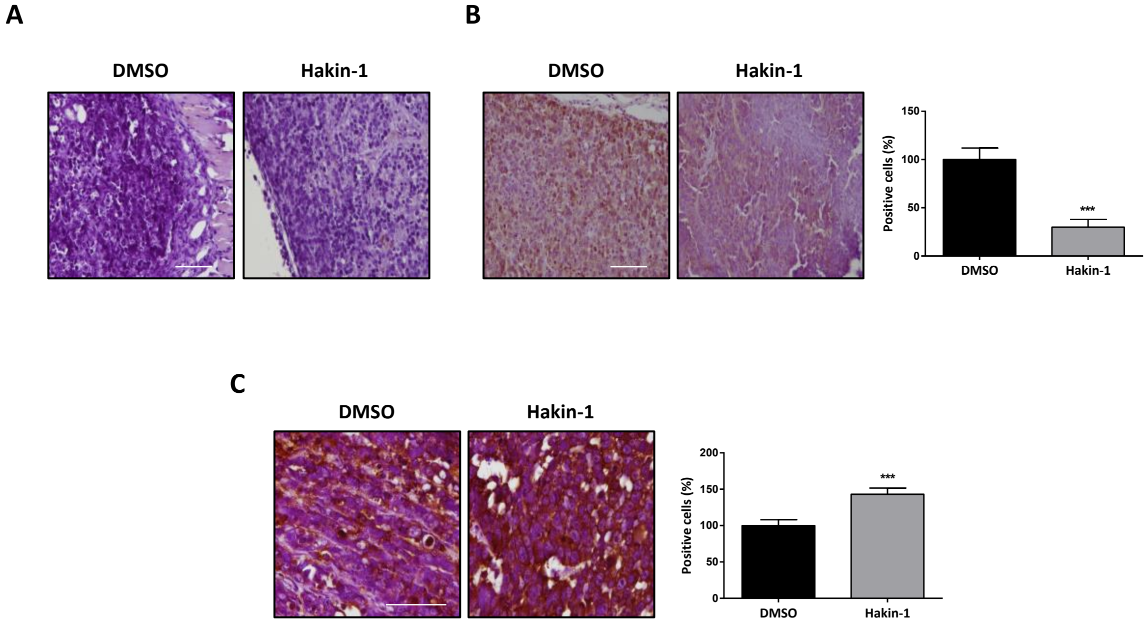
A
DMSO
Hakin-1
B
DMSO
Hakin-1
Positive cells (%)
150
100
50
0
***
DMSO
Hakin-1
C
DMSO
Hakin-1
Positive cells (%)
200
150
100
50
0
***
DMSO
Hakin-1

Figure 44. Effect of Hakin-1 on expression levels of EMT markers and Hakai substrate Cortactin *in vivo*. Immunohistochemistry assays of E-cadherin (**A**), N-cadherin (**B**) and Cortactin (**C**) proteins in Hakai-MDCK tumours of immunodeficient mice treated with DMSO (left panel) or Hakin-1 (right panel). Images were obtained with an Olympus BX61, using a 20x objective for E-cadherin and N-cadherin, and a 40x objective for Cortactin. Scale bar, 50 µm. Results are expressed as mean ± SEM (***$p < 0.001$).

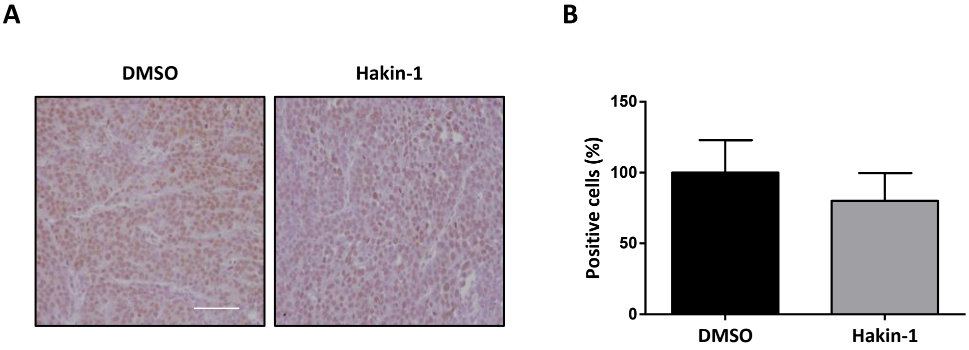
A
DMSO
Hakin-1
B
Positive cells (%)
150
100
50
0
DMSO
Hakin-1

Figure 45. Effect of Hakin-1 on Hakai expression levels in xenografted tumours *in vivo*. (**A**) Immunohistochemistry of Hakai protein in Hakai-MDCK tumours of immunodeficient mice treated with DMSO (left panel) or Hakin-1 (right panel). Images were obtained with an Olympus BX61, using a 20x objective. Scale bar, 50 µm. (**B**) Quantification of the positive nuclei for Hakai staining. Results are expressed as mean ± SEM. Quantification was carried out with ImageJ software, and statistical significance was determined using GraphPad Prism software.

6.4. Hakin-1 inhibits lung micrometastases *in vivo*.

As mentioned above, epithelial-mesenchymal transition has been associated with many features of carcinogenesis process, including metastasis development [45,50,198]. For this reason, Hakin-1 effect on the metastasis formation was also studied, by performing an H&E staining of FFPE lung sections from the mice inoculated with Hakai-MDCK cells, treated both with DMSO or Hakin-1. After an exhaustive analysis carried out by the expert pathologist Dr. Angel Concha, no distant metastatic lesions were observed in the lungs of either control or Hakin-1-treated mice (**Figure 46A**). This might be caused by the *in vivo* model used, were metastases are not yet developed to be detected at this short time. Therefore, 40 days after inoculation might not be enough to allow Hakai-MDCK cells to settle down and form metastases.

On the basis of this observation, it was decided to carry out a more sensitive detection method to assess the presence of micrometastases in the lung. For this purpose, a qPCR analysis was carried out, using DNA previously extracted from FFPE lung samples. Two specific primers were used for amplification: a first primer designed for hemagglutinin (HA) and a second primer designed for Hakai. HA is used as an epitope tag in Hakai overexpression plasmid, which allows to distinguish between endogenous and overexpressed Hakai protein. Therefore, HA primers will only hybridize with overexpressed Hakai as it is bonded to HA, despite endogenous Hakai. This allows an indirect detection of Hakai-MDCK cells, and therefore micrometastasis detection. Lungs of mice inoculated with non-transformed MDCK cells were used as a negative control. Results show that 40 days after the inoculation of Hakai-MDCK cells, micrometastases were detected in the lung of immunodeficient mice (**Figure 46B**), as previously described [158]. Moreover, micrometastasis formation was significantly reduced upon Hakin-1 treatment (**Figure 46B**), suggesting that Hakin-1 is able to inhibit lung metastasis formation *in vivo*.

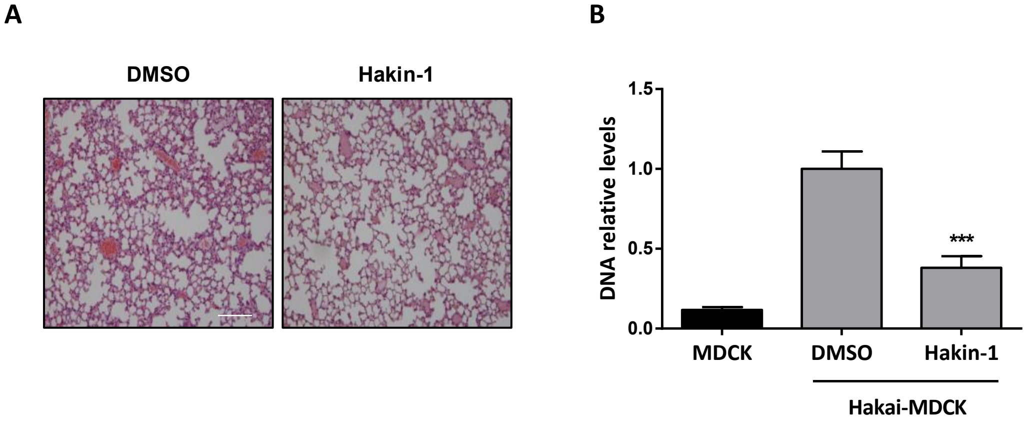

Figure 46. Effect of Hakin-1 on macro- and micrometastasis formation. (**A**) H&E of FFPE lung section of immunodeficient mice inoculated with Hakai-MDCK cells, treated both with DMSO (left panel) or Hakin-1 (right panel). Images were obtained with a 10x objective. Scale bar, 100 µm. (**B**) Real-time quantitative PCR using primers for HA epitope and Hakai to detect the presence of DNA of Hakai-MDCK cells into the mice lungs. Results are expressed as mean ± SEM (***$p < 0.001$).

6.5. Hakin-1 treatment does not cause cytotoxicity in liver and kidney

The major disadvantage of anticancer drugs is their nonselective killing, which causes the weakening of normal cells and toxic side-effects in different organs, including the kidney and liver, which usually limits the dose and the duration of the treatment [225–228]. To further determine whether Hakin-1 may cause toxicity in other organs, liver and kidney were examined. To do so, an H&E analysis was carried out, using FFPE liver and kidney samples from xenograft mice treated with Hakin-1 or DMSO as a control. Interestingly, no damage was observed in liver and kidney tissues upon Hakin-1 treatment (**Figure 47**), which showed a normal morphological structure, confirmed by the expert pathologist Dr. Angel Concha. Therefore, taken together, all these data suggest that Hakin-1 treatment inhibits tumour growth and carcinoma progression *in vivo*, with no apparent systemic toxicity.

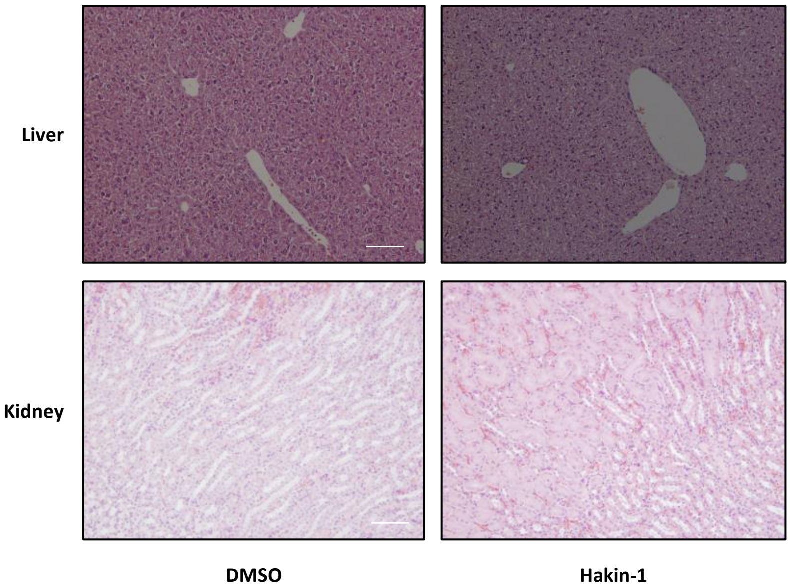

Figure 47. Intact cell morphology and tissue structure of liver and kidney in xenograft mouse model upon treatment with Hakin-1. H&E staining of liver (upper panel) and kidney (bottom panel) of immunodeficient mice treated with 5mg/kg of DMSO or Hakin-1. Images were taken with a 10x objective. Scale bar, 100 µm.

Altogether, these *in vivo* results further support previous *in vitro* findings, showing that Hakin-1 is able to inhibit tumour growth by specifically inhibiting cell proliferation, as no effect was detected on apoptosis. Moreover, Hakin-1 also modulates EMT *in vivo* as observed in immunohistochemistry analysis of Hakai-MDCK tumours, although no effect was observed on E-cadherin protein probably to its complete absence in xenografted tumours. Moreover, Hakin-1 increased Cortactin levels also *in vivo*, which correlates with results previously obtained *in vitro* in HT29 and LoVo cells. As previously observed *in vitro*, Hakin-1 did not affect Hakai expression levels neither *in vivo*. Finally, Hakin-1 inhibited angiogenesis and lung micrometastasis formation *in vivo*. Therefore, the *in vivo* findings further support the antitumour effect of Hakin-1 previously observed *in vitro*. Importantly, Hakin-1 treatment does not cause apparent systemic toxicity in mice, as observed in the histological examination of liver and kidney samples.

B. RESULTS RELATED TO OBJECTIVE 2

1. Study of Hakai role in tumour progression in a co-culture model of colon cancer tumour spheroids and cancer-associated fibroblasts (CAFs)

Nowadays, the importance of tumour stroma in tumour progression, drug resistance, and cancer relapse is widely accepted. Tumour stroma is mainly composed by an extracellular matrix (ECM) and non-malignant cells of the tumour such as CAFs, pericytes, endothelial cells, and inflammatory cells. For this reason, the development of co-cultures of multicellular tumour spheroids (three-dimensional spherical aggregates of cancers cells with an intermediate complexity between traditional monolayer cultures and *in vivo* solid tumours) and CAFs in a collagen matrix represents a very comprehensive *in vitro* model to study tumour progression. This model, also known as '*in vitro* carcinoma assay', was stablished by Dolznig *et al.* in 2011, and it closely mirrors the tumour heterogeneity that is observed *in vivo*. On the one hand, collagen embedding allows to obtain ECM properties *in vitro* and at the same time it provides a physical scaffold for cells. On the other hand, co-culture with CAFs also contributes to replicate tumour stroma, since they are important regulators of cancer progression and metastasis, through the production of proteases, growth factors and cytokines [19].

Therefore, this model represents a better approach to understand tumour behaviour than traditional 2D cultures, and thus to bring new insights into the role of Hakai during tumour progression and disease.

1.1. Establishment of co-culture model of multicellular tumour spheroids and CAFs

The first step in the establishment of co-cultures of spheroid and cancer-associated fibroblasts was spheroid culture, using DLD1, LS174T, SW620 and HCT116 cells. Cells were seeded as previously described and incubated at 37°C and 5% CO_2. 2-3 days after seeding, well-formed spheroids were obtained in all the cell lines used (**Figure 48**). However, cell lines did not behave exactly the same in 3D culture, as DLD1 and HCT116 formed slightly more compact and rounded spheroids than SW620 and LS174T.

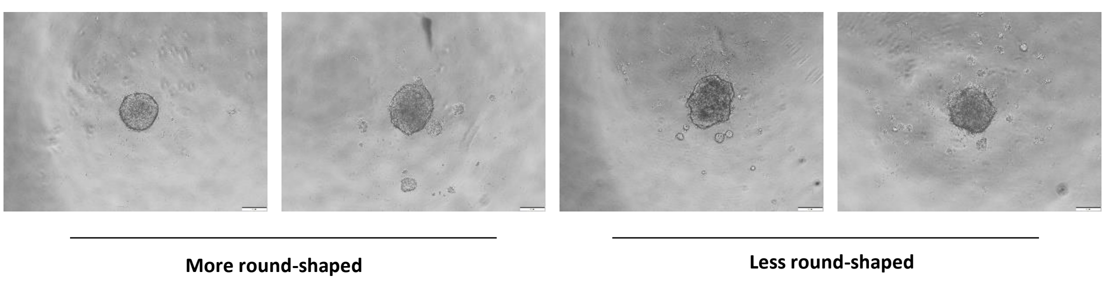

Figure 48. Establishment of colorectal cancer spheroids. Spheroids of DLD1, HCT116 (more rounded), LS174T and SW620 (less rounded) tumour cell lines. Pictures were taken 3 days after seeding with an Olympus inverted microscope, using a 4x objective. Scale bar, 200 μM.

Once spheroid structure was analysed under contrast microscopy, co-culture with CAFs was carried out by embedding both spheroids and CAFs in collagen gels. Co-cultures were incubated again at 37°C and 5% CO_2, and after 3 days spheroid phenotype was studied. It has been described that fibroblasts induce an invasive phenotype in colorectal cancer spheroids when co-cultured into collagen gels [192], so invasive spreading of spheroids was evaluated. Once again, the spheroids from different cell lines displayed different properties. HCT116 and DLD1 spheroids showed invasive structures, which are characterized by multicellular astral outgrowth into the collagen gels (**Figure 49A, 49B**). HCT116 cells developed very important invasive structures (**Figure 49B**, left panel), while DLD1 cells displayed a moderate invasive phenotype (**Figure 49B**, right panel). Conversely, LS174T and SW620 remained as compact spheres and did not show any signs of invasion (**Figure 49A**). This correlates with results previously obtained in Dr. Dolznig's laboratory, where HCT116 proved to be the most invasive cell line, while DLD1, LS174T and SW620 cells required more time to develop invasive structures.

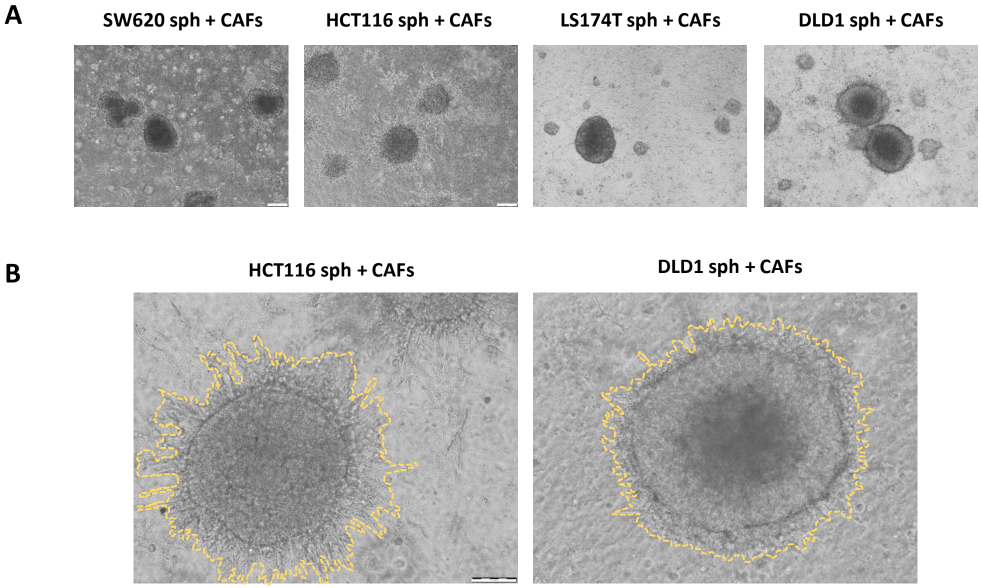

Figure 49. Co-culture of colorectal cancer spheroids and cancer-associated fibroblasts (CAFs). (**A**) Spheroids of DLD1, HCT116, and LS174T, SW620 tumour cell lines co-cultured with CAFs in a collagen matrix. Pictures were taken 3 days after co-culture with an Olympus inverted microscope, using a 4x objective. Scale bar, 200 µM. (**B**) More detailed pictures of HCT116 (left panel) and LST174T (right panel) invasive structures. Invasive area is surrounded by a dotted line. Pictures were taken with an Olympus microscope using a 10x objective. Scale bar, 100 µM.

1.2. Analysis of Hakai and E-cadherin subcellular localization in co-cultures of multicellular tumour spheroids and CAFs

EMT process contributes to the acquisition of invasive properties, which are essential for metastasis development. It promotes cell invasion through the loss of apicobasal polarity and cellular cohesion, and the acquisition of migratory properties and the ability to reorganize the extracellular matrix [229]. Therefore, based on previously shown results were HCT116 and DLD1 developed invasive structures, it was decided to analyse whether Hakai was predominantly expressed in them. To do so, an immunofluorescence assay was carried out to study Hakai and E-cadherin subcellular localization in the co-cultures of the different cell lines. Immunofluorescence assay showed that DLD1 cells developed slight invasive structures, in which both Hakai and E-cadherin were expressed (**Figure 50A**). On the other hand, invasive structures in HCT116 spheroids were perfectly visible (**Figure 50B**), and what is more important, in this invasive structures Hakai expression was clearly predominant (**Figure 50B**, right panel, arrows). This result further supports the potential role of Hakai in the acquisition of invasive capabilities. Remarkably, both in HCT116 and DLD1 co-cultures, Hakai was highly expressed in cancer-associated fibroblasts (**Figure 50**, arrowheads). This result could be the first insight of Hakai increased expression in CAFs.

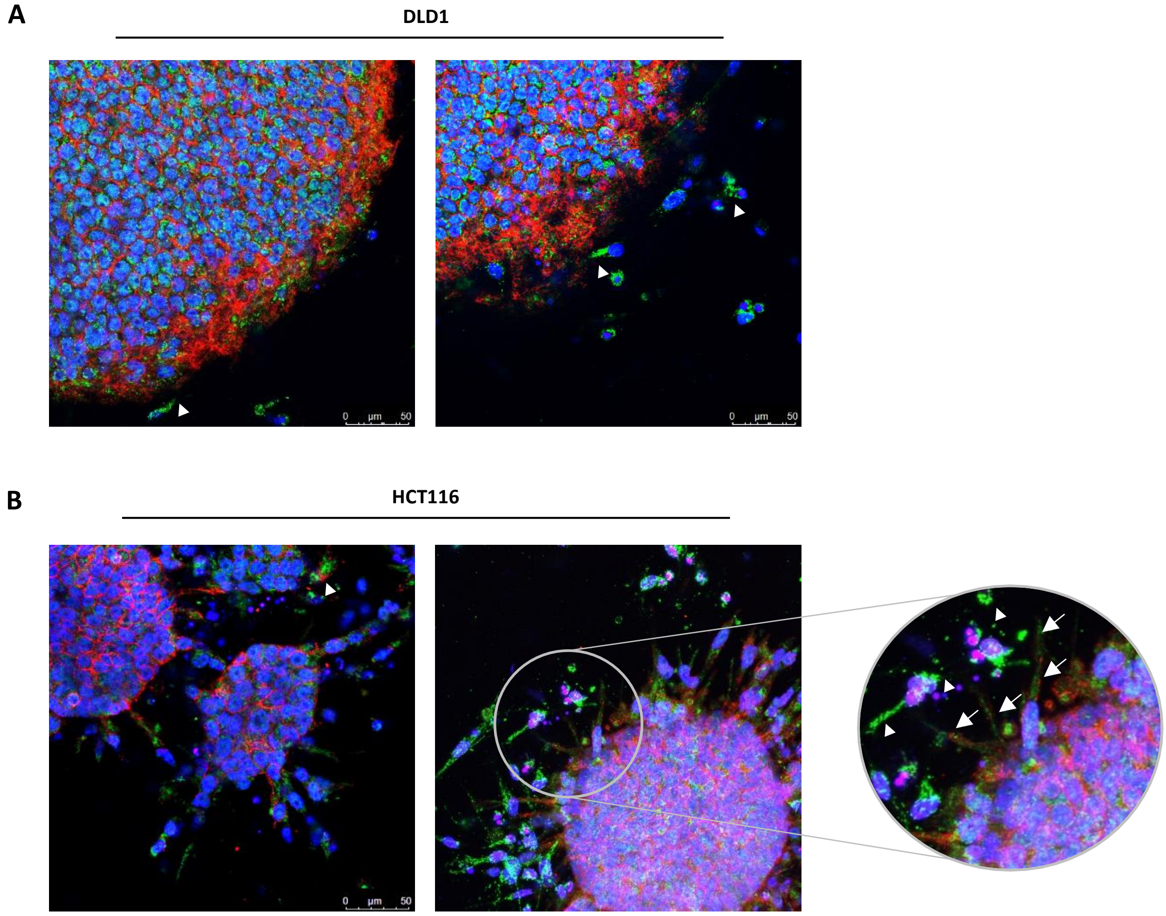

Figure 50. Hakai and E-cadherin subcellular localization in co-cultures of colorectal cancer spheroids and cancer-associated fibroblasts (CAFs). E-cadherin (red) and Hakai (green) staining in spheroids of DLD1 (**A**) and HCT116 (**B**) tumour cell lines co-cultured with CAFs in a collagen matrix. Immunofluorescence of collagen-embedded cells was carried out as described in Materials and Methods, using the indicated antibodies. A detailed image of Hakai predominant expression in invasive structures is shown in (B) (right

panel, arrows). Hakai increased expression in CAFs is indicated by arrowheads. Pictures were taken using a Zeiss LSM5-Exciter confocal microscope. Scale bar, 50 μM.

Hakai and E-cadherin subcellular localization was also studied in LS174T and SW620 co-cultures with CAFs. As these cell lines did not develop invasive structures, E-cadherin and Hakai were located only at cell-cell contacts and in the nucleus, respectively (**Figure 51**). However, as previously described [192], co-culture of LS174T spheroids with CAFs in collagen gels induced morphologic changes in the tumour cell aggregates, where hollow structures were clearly visible (**Figure 51A**). These glandular structures were not present when LS174T spheroids were cultured alone. Although LS174T and SW620 spheroids did not form invasive structures when co-cultured with CAFs, it is important to note that Hakai was highly expressed in CAFs, as previously observed in HCT116 and DLD1 co-cultures (**Figure 51**, arrowheads). This suggests once again the potential involvement of Hakai in CAFs biology.

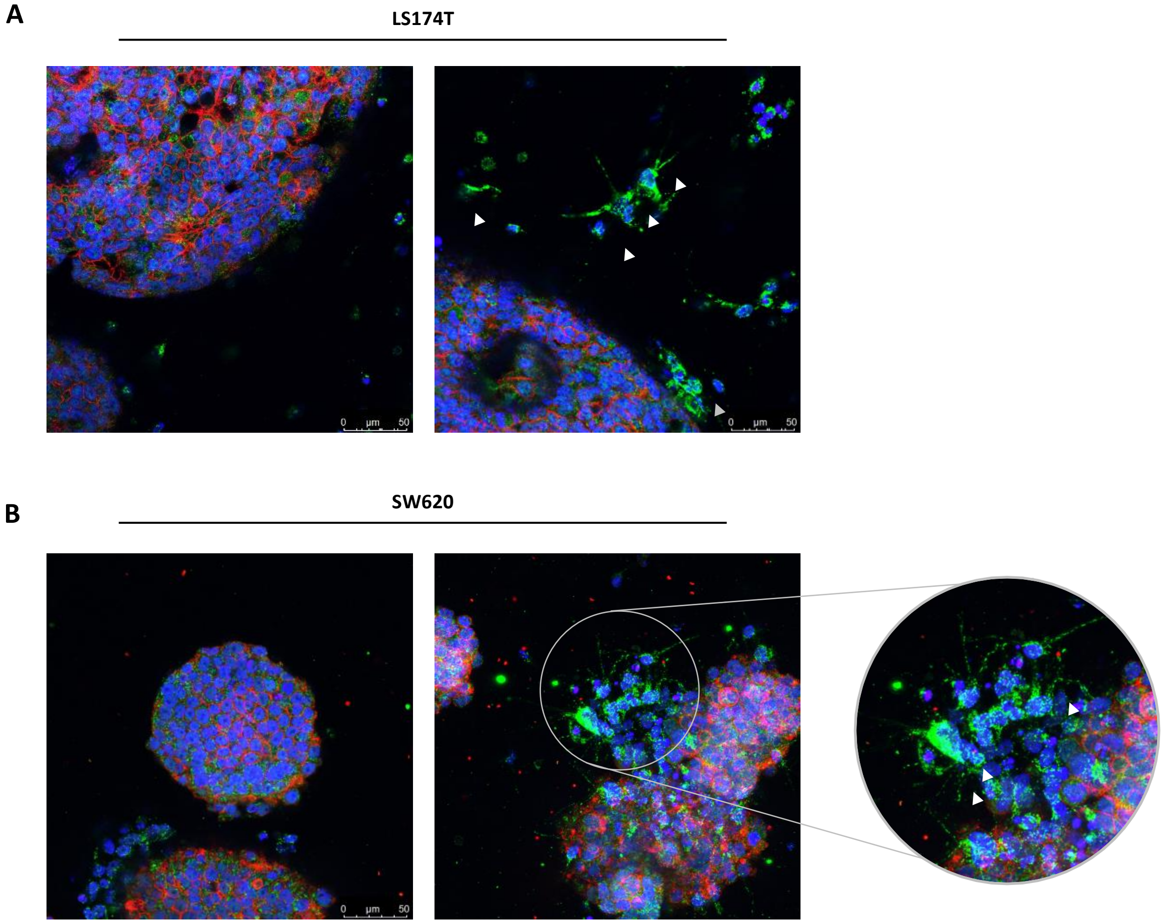

Figure 51. Hakai and E-cadherin subcellular localization in co-cultures of colorectal cancer spheroids and cancer-associated fibroblasts (CAFs). E-cadherin (red) and Hakai (green) staining in spheroids of LS174T (**A**) and SW620 (**B**) tumour cell lines co-cultured with CAFs in a collagen matrix. Immunofluorescence of collagen-embedded cells was carried out as described in Materials and Methods, using the indicated antibodies. A detailed image of Hakai predominant expression in CAFs is shown in (B) (right panel). Hakai

increased expression in CAFs is indicated by arrowheads. Pictures were taken using a Zeiss LSM5-Exciter confocal microscope. Scale bar, 50 μM.

1.3. Effect of Hakai silencing on the development of invasive structures in colorectal cancer spheroids embedded into a collagen matrix

Based on above-mentioned results, in which HCT116 proved to be the most invasive cells and considering the predominant expression of Hakai in the invasive structures formed in them, they were selected for the study of Hakai potential role in the acquisition of invasive properties. To perform such analysis, HCT116 cells were transiently transfected with 50 nM Hakai siRNA, using the same amount of a non-targeting negative control (NTC) for the control condition. The day after transfection, spheroids were grown as previously described, and embedded into a collagen gel 3 days after. The examination of the invasive structures under a phase-contrast microscope was carried out 3 days after embedding.

In this case, spheroids were embedded into the collagen gels alone, and CAF conditioned medium was used instead, to induce invasive structure formation. This allows a better visualization of the invasive structures, since the co-culture with fibroblasts makes them less detectable under phase contrast microscopy. CAF conditioned medium was used diluted 1:1 in DMEM 10%, as in conditioned media vital components, such as glucose, glutamine and serum, have been consumed. Therefore, the dilution with complete fresh medium solves this problem. The same experiment was carried out by using DMEM 10% alone, without diluting it with CAF conditioned medium. The invasive area was obtained by subtracting the spheroid area from the outgrowth area, and the percentage of the spheroid that represents the invasion area was calculated for each condition.

Results show that CAF conditioned medium significantly increased the formation of invasive structures in HCT116 cells, as previously observed in co-culture experiments. Remarkably, Hakai transient knockdown significantly reduced invasive structure formation both in culture with CAF conditioned medium and in culture with DMEM alone (**Figure 52A**, **52B**). This result further supports the potential role of Hakai in the acquisition of invasive properties. Hakai knockdown in HCT116 spheroids was validated by Western Blot assay (**Figure 52C**).

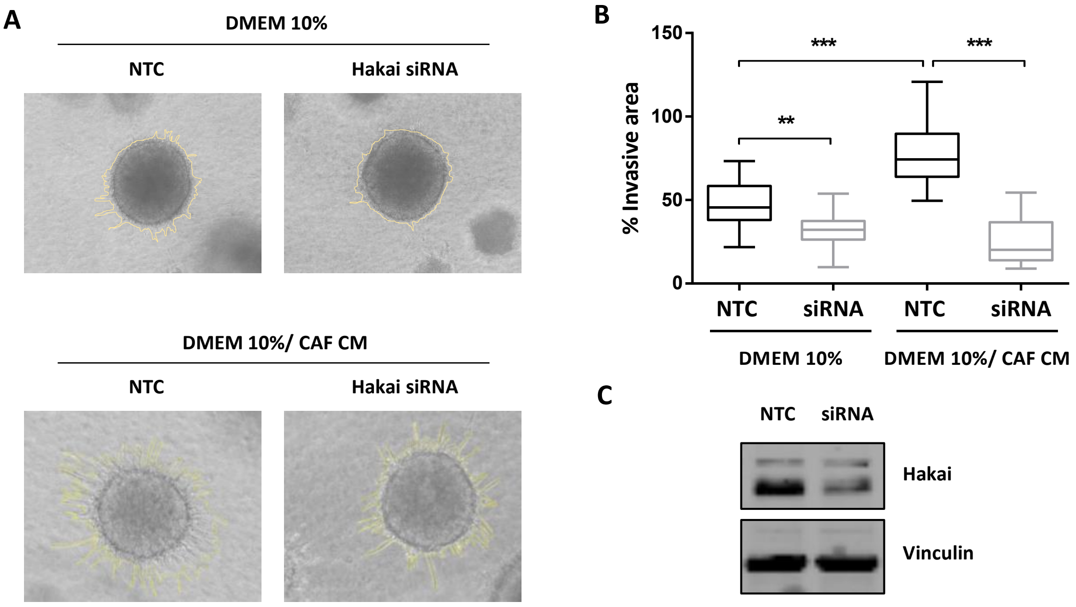

Figure 52. Effect of Hakai transient knockdown in the development of invasive structures. HCT116 were transiently transfected with 50 nM siRNA or NTC as appropriate, and 24 hours after transfection spheroids were grown. After 3 days, transfected spheroids were embedded into collagen gels and cultured in DMEM alone or in DMEM diluted 1:1 with CAF conditioned medium. Finally, development of invasive structures was evaluated 3 days after spheroid embedding. (**A**) Representative images of control and Hakai-silencing spheroids, 3 days after embedding. The invasive area is outlined in yellow. Pictures were taken with an Olympus microscope using a 10x objective. (**B**) Quantification of the invasive area in HCT116 spheroids. Results are represented as mean ± SD (**$p < 0.01$; ***$p < 0.001$). (**C**) Validation of Hakai silencing in spheroids, by means of Western Blot assay.

1.4. Effect of Hakai transient knockdown in contractility of cancer-associated fibroblasts

Fibroblasts are usually quiescent and become activated during wound healing response. Activated fibroblasts are characterized by the expression of α-smooth muscle actin (αSMA) and vimentin. αSMA is a cytoskeletal protein that is associated with smooth muscle cells, that allows activated fibroblasts to develop contractile properties. In this activated state, they are also known as myofibroblasts [230]. Cancer-associated fibroblasts represent a heterogeneous population within the tumour that becomes activated through interaction with cancer cells, with an increased expression α-SMA, activation protein (FAP), and an increased secretion of ECM proteins [231].

To determine whether Hakai knockdown in CAFs affected contractility, a collagen-gel contraction assay was performed. To do so, CAFs were transiently transfected with 50 nM Hakai siRNA and the same amount NTC in the control condition. The day after seeding, CAFs were embedded into collagen gels and gel contraction was analysed at 0, 6, 24 and 72 hours. Results showed that Hakai knockdown did not affect CAFs contractile capacity (**Figure 53A, 53B**), since no significant differences in gel contraction were observed. To discard that no effect was observed due to a failure in the silencing process, knockdown of Hakai in CAFs was validated by immunofluorescence (**Figure 53C**), as it was not clearly visible by Western Blot.

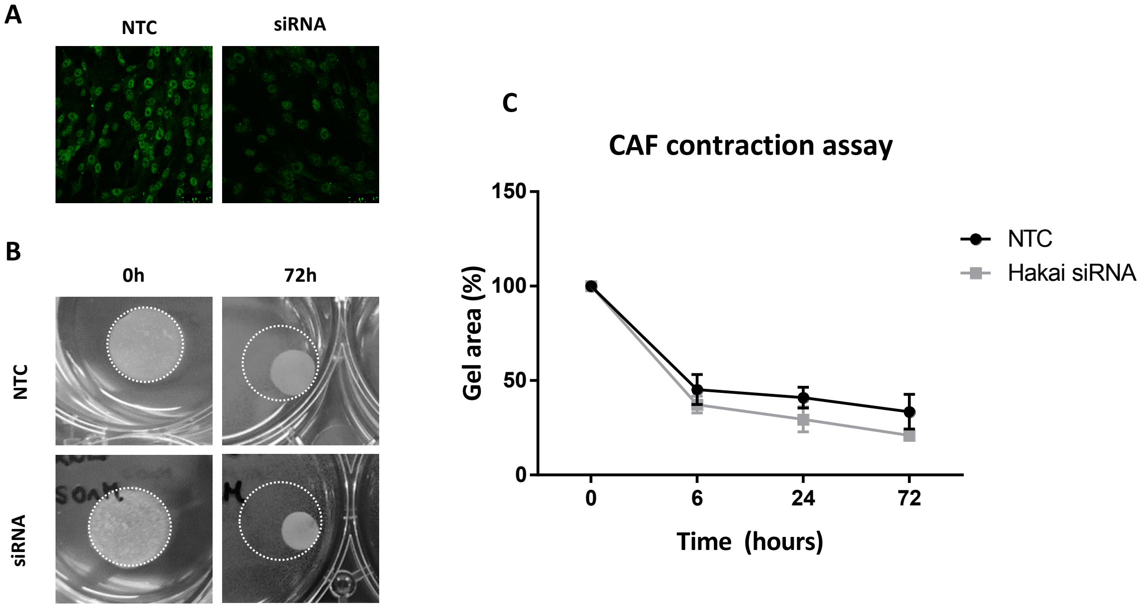

Figure 53. Effect of Hakai transient knockdown in contraction capacity of cancer-associated fibroblasts. (**A**) Validation of Hakai knockdown by immunofluorescence. Pictures were taken using a Zeiss LSM5-Exciter confocal microscope. Scale bar, 50 µm. (**B**) Representative images of gels with NTC or siRNA CAFs at 0 and 72 hours. Pictures were taken with a digital camera and the diameter of each gel was scaled with ImageJ software, using the straight-line tool. (**C**) Contraction assay. CAFs were transiently transfected with 50 nM Hakai siRNA or NTC as a control and embedded into collagen gels the day after. Gel contraction was monitored at 0, 6, 24 and 72 hours.

1.5. Study of Hakai involvement in the interaction between CAFs and carcinoma cells during tumour progression

During malignant transformation, CAFs release growth factors and cytokines, that are directly involved in the positive regulation of proliferation, cell survival, stemness and therapy resistance. Interestingly, there is also an increased evidence that suggests that cancer-associated fibroblasts play an important role in regulating epithelial-mesenchymal transition in cancer cells. However, the underlying mechanisms are not completely understood [91].

Based on above results, in which Hakai was clearly overexpressed in fibroblasts in co-culture experiments, it was decided to briefly study its possible involvement in the interaction between CAFs and tumour cells. In this case, 2D cultures were used, in which DLD1, LS174T, HCT116 and SW620 tumour cells were seeded and starved overnight the day after. Then, cells were treated with CAF conditioned medium for 24 or 48 hours, using fresh CAF culture medium (EGM) for the control condition. Finally, Hakai expression levels were studied by Western Blot.

Results show that treatment with CAF conditioned medium did not affect Hakai expression levels in any of the tested cell lines (**Figure 54**).

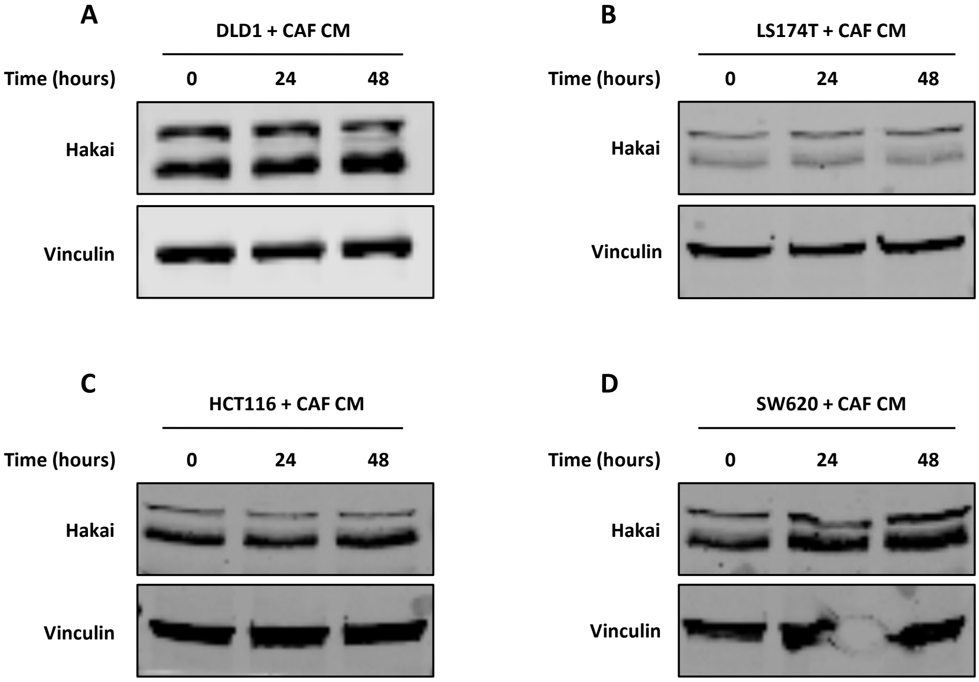
A
DLD1 + CAF CM
Time (hours)
0
24
48
Hakai
Vinculin
B
LS174T + CAF CM
Time (hours)
0
24
48
Hakai
Vinculin
C
HCT116 + CAF CM
Time (hours)
0
24
48
Hakai
Vinculin
D
SW620 + CAF CM
Time (hours)
0
24
48
Hakai
Vinculin

Figure 54. Hakai expression levels in colorectal cancer cell lines under treatment with CAF conditioned medium. Hakai expression levels in DLD1 (**A**), LS174T (**B**), HCT116 (**C**) and SW620 (**D**) after treatment with CAF conditioned medium for 24 and 48 hours. EGM was used for the control condition. Hakai expression levels were analysed by Western Blot assay, using the indicated antibodies. Vinculin was used as a loading control.

Taken together, these results further support the previously observed role of Hakai in the acquisition of invasive properties during malignant transformation. Moreover, Hakai was found to be highly expressed in CAFs, which might be the first insight into the role of Hakai in CAFs biology, as Hakai overexpression in CAFs has not been reported so far. Nevertheless, Hakai silencing in CAFs did not affect their contractile properties, so further investigations are needed to elucidate the possible involvement of Hakai in cancer-associated fibroblast biology.

2. Analysis of the potential role of Hakai in the acquisition of stem properties

2.1. Establishment of patient-derived colorectal organoid culture

Cancer cell lines have been widely used over the years as an *in vitro* model to study cancer biology, as they are easy to establish and maintain in culture and can be genetically modified using different approaches. They allow the study of specific signalling pathways that are involved in different aspects of carcinogenesis, such as metastasis, drug response and drug resistance.

Moreover, they can be readily used in high-throughput screening for drug discovery [232]. However, cell-line based drug discovery programmes usually have a high failure rate, which is in part due to the poor representation of the heterogeneity of original tumours by cancer cell lines [233,234].

Therefore, organoid technology has emerged as a powerful alternative method to model tumour initiation, metastatic progression and therapy response. Patient-derived organoid cultures represent a great advantage over traditional *in vitro* culture models as they preserve genetic, phenotypic and behavioural characteristics of *in vivo* tumours [233]. Unlike cell lines, which usually represent a homogeneous population of cells, organoids recapitulate different microenvironments that allow the differentiation and maintenance of epithelial subtypes. Moreover, organoids grow in a three-dimension manner, providing a structural approach that is much closer to *in vivo* tumours and allowing to better model the *in vivo* behaviour of cancer cells [234].

Organoid cultures might also represent a better approach than *in vivo* models, as *in vitro* study of colorectal cancer allows to make genetic alterations more easily and less expensively than in animal models. Moreover, in terms of drug development, organoid models also represent a better approach than *in vivo* studies, as they enable the testing of a range of therapeutic compounds in a model in which patient genetic and physiological characteristics remain stable. This could allow the further development of patient-specific personalised therapies [235].

Based on the above-mentioned background, patient-derived colorectal organoid cultures were established to bring new insights into the role of Hakai during tumour progression, metastasis, stemness or drug resistance, as well as to further study Hakin-1 anti-tumoral activity. In this case, organoids were generated from adult stem cell-containing tumour samples of colorectal cancer patients. Tumour samples from four different patients were collected, as well as their clinical variables, and further processed as previously described. Cells were seeded in low attachment plates containing Human Intestinal Stem Cell Medium (HISC), and each sample was identified with a code (ORG1, ORG2, ORG3 and ORG4) to monitor it in culture as well as maintain traceability. 5 days after sample processing and cell seeding, well-formed organoids were analysed under phase-contrast microscopy. Samples from patient ORG2 and ORG4 resulted in well-formed organoids within 5 days of culture (**Figure 55**), while samples from patient ORG1 and ORG3 resulted in uncompacted cellular aggregates that did not grow for more than 2-3 days. Despite these are very preliminary results, and it would be necessary to continue with the development of the protocol in order to be able to further maintain and amplify the organoids in culture, they open the possibility of establishing an organoid biobank in the future.

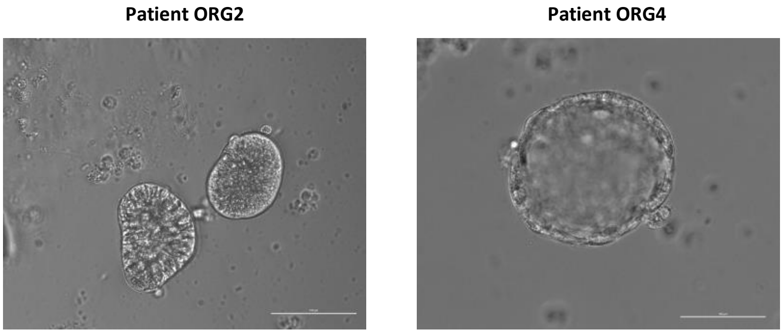

Figure 55. Establishment of patient-derived colorectal organoid culture. Patient-derived organoid culture of patients ORG2 and ORG4. Pictures were taken 5 days after sample processing and cell seeding (described in Materials and Methods), using an Eclipse-Ti microscope (Nikon) and a 20x objective. Scale bar, 100 μM.

2.2 Hakai expression is remarkably increased in tumorsphere cultures

The success of targeted therapies for cancer treatment is usually limited by the development of drug resistance, which arises as a consequence of minority populations of cells that are capable of originating new tumours, known as cancer stem cells (CSCs). Moreover, there is a strong evidence that supports the link between EMT and the entrance in the CSC state, so that the CSC-mediated tumour relapse is related to the activation of the EMT programme [94,103]. Three-dimensional (3D) *in vitro* models have been also used to study cancer stem cell expansion, as they can be developed with the aim of enrichment of cancer stem cells (CSCs) or cells with stem cell-related characteristics [236]. In this case, referred as tumorspheres, the culture method is different from the multicellular tumour spheroid model, as it is established in low attachment plates using a serum-free medium supplemented with growth factors [195].

Therefore, taking into consideration the strong evidence that supports the link between the epithelial-mesenchymal transition and the development of CSCs, it was decided to analyse Hakai involvement in the acquisition of stem properties. To do so, tumorsphere cultures (in this case, colonospheres) were carried out as described in Materials and Methods. Briefly, HCT116 cells were seeded in ultra-low attachment plates and cultured in stem cell medium for 7 days. In parallel, 2D cultures were carried out in adherent plates as a monolayer control **(Figure 56A).** Then, after RNA extraction and cDNA amplification, the expression levels of stem markers (LGR5, NANOG, SOX2, KLF4), differentiation markers (ANPEP, CDX2, CDH1) and Hakai were measured by real-time quantitative PCR.

Results show that KLF4, SOX2 and NANOG expression levels increased in tumorspheres compared to monolayer cultures, thus confirming the enrichment in CSCs of 3D tumorsphere cultures (**Figure 56B**). Moreover, the expression levels of ANPEP, CDX2 and CDH1 differentiation markers were reduced in tumorspheres in comparison to monolayer cultures, further validating the stem phenotype of the colonospheres (**Figure 56C**). Once the expression levels of pluripotency and differentiation genes were analysed, and once the enrichment in CSCs of tumorsphere cultures was confirmed, it was decided to analyse the expression levels of Hakai. Interestingly, Hakai expression levels remarkably increased in tumorsphere cultures (**Figure 56D**). Therefore, this result could be the first insight into the involvement of Hakai in the development of cancer stem cells.

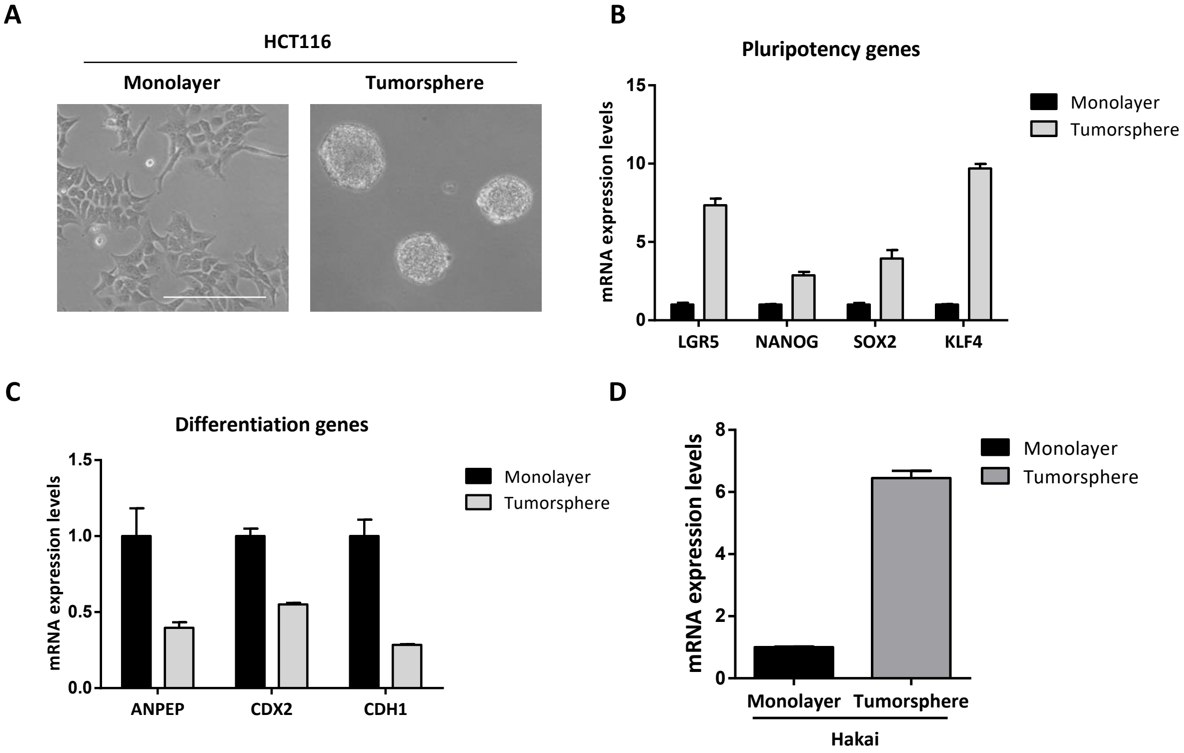

Figure 56. Analysis of the potential role of Hakai in the acquisition of stem properties. (**A**) Phase-contrast images of HCT116 monolayer and tumorsphere cultures. Pictures were taken with an Eclipse-Ti microscope (Nikon) and a 10x objective. Scale bar, 200 µm. (**B, C, D**) RT-qPCR analysis of stem markers (B), differentiation markers (C) and Hakai (D) expression levels in monolayer vs colonosphere cultures. HCT116 cells were seeded ultra-low attachment plates for 7 days and in adherent plates as a monolayer control. RT-qPCR was carried out as described in Materials and Methods, using the indicated primers. HPRT and RPLP0 were used as reference genes for normalization.

2.3. Hakin-1 reduces the expression of stem markers and increases the expression of differentiation markers *in vitro*

Taking into account the above-mentioned association between EMT and CSC state [237], as well as the increased expression of Hakai tumorsphere cultures, it was decided to explore the potential ability of Hakin-1 to modulate the stem phenotype *in vitro*. To do so, HCT116 tumorsphere cultures were carried out as previously described and cells were treated the same day with increasing concentrations of Hakin-1 (20 µM and 50 µM) using DMSO as a vehicle control. Four days after seeding, tumorsphere formation was analysed under phase-contrast microscopy.

Interestingly, Hakin-1 treatment seemed to affect the formation of tumorspheres, since they were observed as more differentiated cellular aggregates, showing a less rounded and less compact phenotype, even at the lowest dose of 20 μM (**Figure 57A**).

Therefore, given the phenotypic alteration observed after treatment with Hakin-1, it was decided to analyse its effect on the expression levels of stem and differentiation markers. To do so, RNA extraction and cDNA amplification were carried out as described in Materials and Methods, and the expression levels of stem markers (SOX2, LGR5, NANOG,) differentiation markers (CDX2, ANPEP, CDH1) and Hakai were measured by real-time quantitative PCR. Results show that Hakin-1 was able to reduce the expression levels of SOX2, LGR5 and NANOG pluripotency genes (**Figure 57B**), while it modestly increased the expression CDX2, ANPEP and CDH1 differentiation genes (**Figure 57C**). Moreover, the treatment of the tumorspheres with Hakin-1 did not affect Hakai expression levels (**Figure 57D**), which is consistent with the results previously observed in monolayer cultures (**Figure 26**). This result supports the possible involvement of Hakai in the acquisition of stem properties. Moreover, it suggests that Hakin-1 may have the ability to affect the development of a stem phenotype.

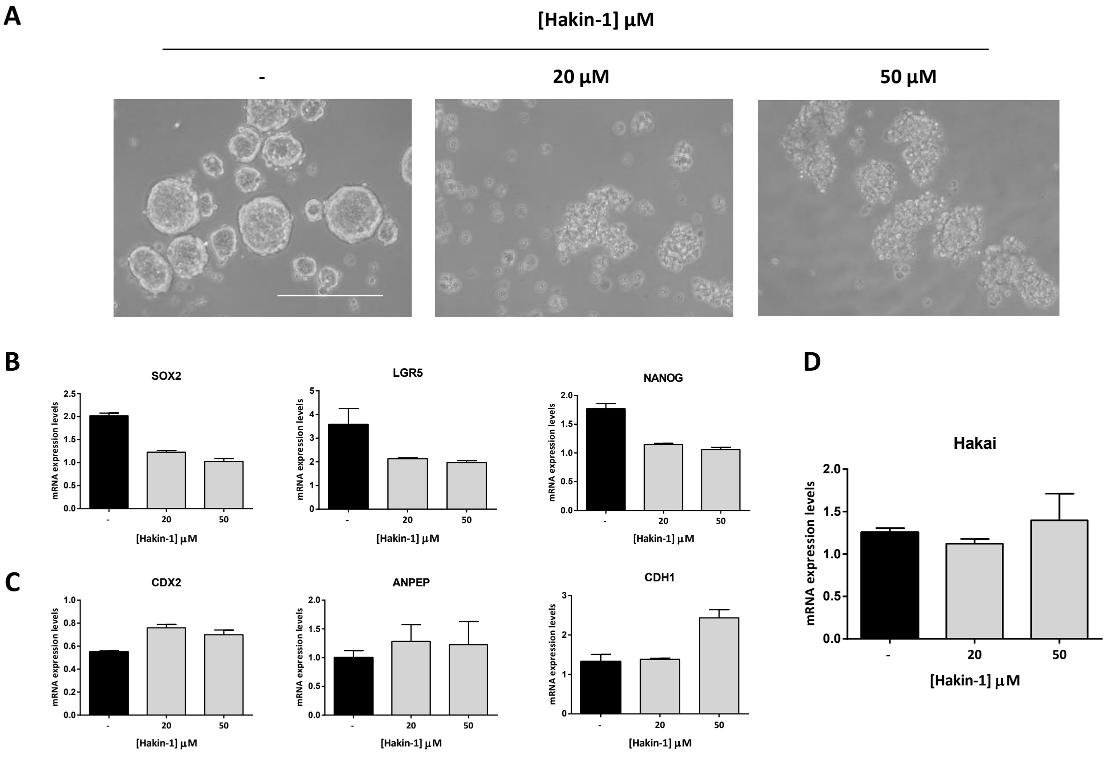

Figure 57. Effect of Hakin-1 on the acquisition of stem properties *in vitro*. (**A**) Phase contrast images of HCT116 spheroids, treated with increasing concentrations of Hakin-1 (20 μM and 50 μM) or DMSO as a control. Pictures were taken with an Eclipse-Ti microscope (Nikon) and a 10x objective. Scale bar, 200 μm. (**B**, **C**, **D**) RT-qPCR analysis of the expression of stem markers (B), differentiation genes (C) and Hakai (D), carried out as previously described, using RPLP0 and HPRT as reference genes for normalization. Primers used for amplification of target genes are described in Materials and Methods. Results are expressed as mean ± SD.

2.4. Hakin-1 reduces the expression of NANOG, SOX2 and c-MYC stem markers *in vivo*

Taking into account the increased expression of Hakai tumorsphere cultures, and the ability of Hakin-1 to modulate the expression of stem and differentiation markers, it was decided to further explore the potential ability of Hakin-1 to modulate the expression of stem cell markers in the previous *in vivo* model system. To do so, a RT-qPCR analysis of FFPE tumour samples from the xenograft mice injected with Hakai-MDCK cells (treated both with Hakin-1 or DMSO) was carried out, using primers designed for NANOG, SOX2 and c-MYC. RNA from FFPE samples was isolated as previously described in Materials and Methods. RNA expression levels were normalized to RPS5 housekeeping gene. Results show that NANOG, c-MYC and SOX2 expression levels were reduced in Hakai-MDCK tumours upon Hakin-1 treatment (**Figure 58**), suggesting that Hakin-1 might be able to inhibit the development of stem cell properties *in vivo*. Furthermore, this result indirectly suggests the possible involvement of Hakai in the development of stem properties, as Hakin-1 is acting through the inhibition of this protein.

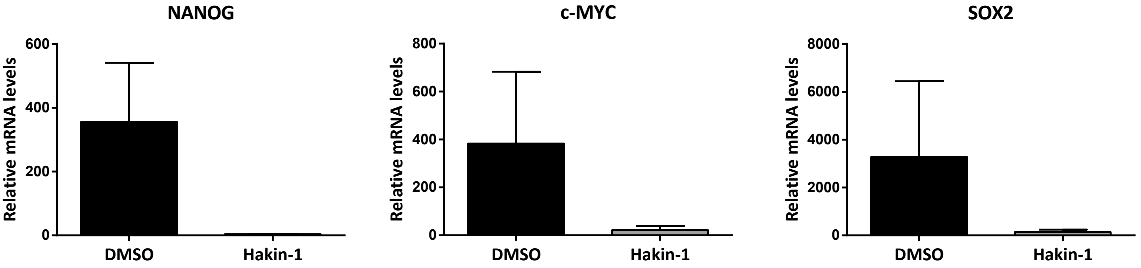

Figure 58. Effect of Hakin-1 on the expression levels of stem markers *in vivo*. RT-qPCR analysis of NANOG, c-MYC and SOX2 expression in Hakai-MDCK tumours of immunodeficient mice, treated both with Hakin-1 or DMSO as a control. RT-qPCR was carried out as previously described, using RPS5 as a reference gene for normalization. Primers used for amplification of target genes are described in Materials and Methods. Results are expressed as mean ± SEM.

V. DISCUSSION

I. Hakin-1, a small-molecule inhibitor for E3 ubiquitin-ligase Hakai, shows antitumour activity both *in vitro* and *in vivo*

Epithelial-mesenchymal transition (EMT) has extensively been documented as a crucial event during carcinoma progression and metastasis, thus having considerable clinical implications [28,48]. Due to this major role of EMT in conferring malignant capabilities on tumour cells, such as migratory and invasive properties, it has gained interest as a target for anticancer drug discovery. For this reason, significant efforts have been made to develop EMT inhibitors that target different EMT signalling pathways or EMT-inducing stimuli [238,239]. As previously mentioned, a major hallmark of EMT process is the downregulation of E-cadherin tumour suppressor at cell-cell contacts, through epigenetic, transcriptional and posttranscriptional mechanisms [240]. Therefore, with the aim of designing small-molecule inhibitors that directly target the EMT process, we focused our attention on the mechanisms responsible for E-cadherin downregulation, particularly in the E3 ubiquitin-ligase Hakai, as it is the first described posttranslational regulator of E-cadherin stability at cell-cell contacts [88]. Interestingly, it has been demonstrated that E-cadherin loss through posttranscriptional regulation is an early event during EMT process, which occurs prior to E-cadherin downregulation through transcriptional repression [169]. Therefore, the inhibition of E-cadherin posttranslational downregulation would allow to prevent the onset of EMT and the subsequent tumour progression.

Given that ubiquitination process is often dysregulated in cancer, E1, E2 and E3 enzymes as well as the DUBs and the proteasome, have traditionally been considered as potential targets for cancer treatment. However, to date, only few proteasome inhibitors (bortezomib, carfilzomib and ixazomib) have been approved by the FDA [129–132]. Despite these drugs have demonstrated high effectiveness in haematological malignancies, the results obtained in the treatment of solid tumours have been discouraging so far [133,134]. Moreover, epithelial cells undergoing EMT have been reported to show a decreased proteasome activity, therefore, proteasome inhibition-based therapies in epithelial cells might be risky as they could trigger the EMT programme and the acquisition of a CSC phenotype [141,241]. There are only two E1 activating enzymes identified in humans (UBA1 and UBA6), and they are responsible for the ubiquitination of all downstream targets. For this reason, although many E1 inhibitors have been developed, most of them display specificity problems and only one (MLN4924) has entered clinical trials. On the other hand, despite E2 enzymes may represent more specific targets than E1s, as there are more in number (around 38 in humans), results obtained in the development of specific inhibitors (i.e. CC0651) have also been disappointing [135]. The human genome encodes more than six hundred E3 ligases, and each one is specific for a small number of substrates. Therefore, the inhibition of proteasome-related DUBs or E3 ubiquitin-ligases may represent a better therapeutic strategy for cancer treatment, as it would cause fewer side effects than the inhibition of other elements of the ubiquitin pathway, such as E1 and E2 enzymes or the proteasome itself [113,135,170]. For example, the Snail1 deubiquitinase Dub3 has recently been proposed as a potential therapeutic target, given that its specific inhibition by WP113 has been reported to supress breast cancer invasion and metastasis [242]. The E3 ubiquitin-ligase FBXL14 has recently been proposed as a promising therapeutic target for cancer treatment, since it regulates the stability of EMT-TFs Snail, Slug and Twist [126]. FBXW7, an E3 ubiquitin-ligase that targets Snail, has been proposed as a therapeutic target for NSCLC [243]. RBBP6, a RING-type E3 ubiquitin-ligase that induces EMT and metastasis, has recently been proposed as a biomarker and therapeutic target for colorectal cancer treatment [244]. All these data open up a new field of research in the development of inhibitors that function at the post-translational level to regulate EMT. In the present study, a virtual screening assay was performed in order to identify small-molecule inhibitors which were potentially able to bind Hakai HYB domain, a novel E3 ubiquitin-ligase pTyr-binding domain that specifically targets tyrosine-phosphorylated E-cadherin [143,144]. Virtual screening was carried out considering the structural information available and the characteristics of Hakai pTyr-binding pocket. After the visual inspection of the first 20 top-ranking compounds, several hit candidates were selected for an initial experimental validation. Finally, Hakin-1 (Hakai inhibitor 1) was selected as the best hit candidate for further experimental validation. Considering the aforementioned background, targeting EMT process through the Hakin-1-mediated inhibition of E3 ubiquitin-ligase Hakai might be a better therapeutic approach than proteasome inhibition for treatment of epithelial tumours.

Hakin-1 regulates EMT through the inhibition of Hakai-mediated downregulation of E-cadherin

Hakai was described to interact with Src-phosphorylated E-cadherin, inducing its ubiquitination, endocytosis and further degradation into the lysosome [146]. The present study describes Hakin-1 as the first reported Hakai inhibitor that reduces Hakai-mediated ubiquitination of E-cadherin and Hakai-mediated overall ubiquitination in a dose-dependent manner, as observed in immunoprecipitation and Western Blot assays (Figures 16-18). Moreover, Hakai overexpression in colorectal cancer HCT116 cells reduced E-cadherin protein levels, which were restored after Hakin-1 treatment (Figure 19). As expected, Hakin-1 treatment did not affect Hakai expression levels, neither *in vitro* nor *in vivo*, thus supporting that it exerts its effect by inhibiting Hakai activity rather than inducing Hakai downregulation (Figures 25, 46). Studies carried out with *Drosophila melanogaster* demonstrated that Hakai complete loss impairs cell survival [147]. Moreover, significant efforts were made to establish stable Hakai knockdown human epithelial cell lines, however, this was not achieved as the cells did not survived in the complete absence of Hakai [158]. Therefore, the inhibition of Hakai activity rather than the inhibition of its expression represents a better therapeutic strategy, due to its reported role on cell survival.

EMT process leads to the disruption of cell-cell junctions and the loss of apicobasal polarization, as well as the reorganization of actin cytoskeleton and the acquisition of motile and invasive capabilities [23]. In addition to the loss of E-cadherin at cell-cell contacts, EMT process is also characterised by the downregulation of other epithelial markers such as ZO-1, desmoplakin, citokeratins and laminin, and the upregulation of mesenchymal markers such as N-cadherin or Vimentin [58]. It was previously demonstrated that Hakai overexpression in epithelial MDCK cells induced the acquisition of a mesenchymal phenotype, accompanied by the downregulation of E-cadherin epithelial marker and the upregulation of Vimentin and N-cadherin mesenchymal markers [141]. As expected, Hakin-1 increases epithelial cell differentiation in a dose-dependent manner in Hakai-MDCK cells, which showed a more compact phenotype and a reduction of cytoplasmic protrusions after Hakin-1 treatment, resembling non-transformed MDCK cells (Figure 24). Hakin-1 increased epithelial differentiation also in colorectal cancer cell lines, which is accompanied by an upregulation of E-cadherin epithelial marker and a downregulation of Vimentin mesenchymal marker (Figure 25). Remarkably, Hakin-1 effect was observed at the protein level, as the treatment of LoVo and HT29 cells with Hakin-1 did not significantly modulate E-cadherin and Hakai mRNA levels, further supporting that Hakin-1 may act through a posttranslational mechanism, as expected (Figure 27). Moreover, Hakin-1 is also able to increase E-cadherin levels at cell-cell contacts. Hakin-1 was able to modulate EMT also in an *in vivo* xenograft mouse model, as immunohistochemistry analysis of xenografted tumours of immunodeficient mice inoculated with Hakai-MDCK cells revealed that N-cadherin was significantly downregulated in mice treated with Hakin-1. However, E-cadherin expression was not detected neither in control nor in treated mice. This result is in line with those previously obtained, where it was observed that E-cadherin protein expression was completely loss in Hakai-MDCK cells injected *in vivo* [158]. Therefore, given that E-cadherin protein is not detected in Hakai-MDCK cells, it seems plausible that it was not recovered in xenografted tumours of Hakin-1 treated mice, as Hakin-1 acts at a posttranslational level by inhibiting Hakai action on E-cadherin protein. These results, together with the biochemical assays previously discussed, suggest that Hakin-1 may be able to regulate EMT process, by inhibiting Hakai-mediated ubiquitination of E-cadherin, and therefore its subsequent internalization and further degradation.

During early-stage drug discovery, once a hit compound is evaluated and considered as therapeutically promising due to its biological or pharmacological activity, analogue compounds are selected with the aim of finding a lead compound with greater effectiveness [245]. Hakin-1 analogues were selected in collaboration with a medical chemistry expert, and were further validated in cytotoxicity, ubiquitination, and epithelial cell differentiation assays. However, although Hakin A-7 was able to reduce Hakai-mediated overall ubiquitination and restore E-cadherin levels at cell-cell contacts, none of the analogues tested proved to be more effective than Hakin-1 initial compound.

Although Hakai has been described as the first posttranslational regulator of E-cadherin stability at cell-cell contacts, MDM2 has also been reported to induce E-cadherin ubiquitination and subsequent degradation [246]. MDM2 is a RING-type E3 ubiquitin-ligase who is considered one of the major negative regulators of tumour suppressor p53, that has been proposed as a promising therapeutic target for cancer treatment [247]. Moreover, it has been shown to be a negative prognostic biomarker for breast carcinoma [248]. For this reason, considerable efforts have been made to target MDM2 and numerous compounds have been developed to inhibit p53-MDM2 interaction and some of them are currently being tested in phase I clinical trials. The first described inhibitors of MDM2 were Nutlins (Nutlin-1, Nutlin-2, Nutlin-3), which have been demonstrated to impair p53-MDM2 interaction [249,250]. Nutlin-3 has been demonstrated to abolish E-cadherin downregulation caused by TGF-β-1 induced EMT, through the inhibition of Smad2 and Smad3 phosphorylation, which causes the transcriptional repression of E-cadherin repressors Snail and Slug [251]. Conversely to the indirect effect of Nutlin-3 on EMT, Hakin-1 directly targets EMT by inhibiting Hakai-mediated E-cadherin ubiquitination and subsequent degradation. The effective inhibition of p53-MDM2 interaction by Nutlin-3 requires wild-type p53 expression in cancer cells, thus showing low or no efficacy against breast cancers that exhibit mutant p53. Therefore, SP-141 was developed as a novel MDM2 inhibitor that induces MDM2 degradation and proteasomal degradation in a p53 status-independent manner. SP-141 also affects EMT, as it induces dose-dependent downregulation of EMT-related molecular markers β-catenin, vimentin, Twist and Snai1[252]. As no effect on E-cadherin has been reported so far, Hakin-1 is the first reported inhibitor for an E-cadherin post-translational regulator, that directly regulates EMT process through the inhibition of E-cadherin ubiquitination and further degradation.

Hakin-1 reduces cell invasion and migration, as well as oncogenic potential

E-cadherin loss during EMT has also been related to the acquisition of migratory and invasive capabilities, and thus with an increased metastatic potential [20,198]. The first insight into the role of Hakai overexpression in the acquisition of invasive properties was provided by Rodríguez-Rigueiro and collaborators in 2011, who demonstrated *in vitro* that Hakai-overexpressing MDCK cells displayed an enhanced invasiveness compared to non-transformed ones [157]. Later on, it was demonstrated that Hakai overexpression induced invasive capabilities also *in vivo*, which was observed as an increased invasion of adjacent muscle and an enhanced infiltration of blood vessels in mice inoculated with Hakai-overexpressing MDCK cells [158]. Hakai has also been reported to induce cell invasion in NSCLC cells, as its knockdown inhibited cell invasion through the upregulation of E-cadherin and the downregulation of matrix metalloproteinases MMP2 and

MMP9 [160]. On the other hand, miR-212-3p was reported to inhibit cell proliferation, migration, and invasion in NSCLC cells by targeting Hakai [162]. Here, we confirmed previously obtained *in vitro* results, as Hakai-MDCK cells were able to invade the extracellular matrix, while parental MDCK cells did not show an invasive ability. The acquired invasive ability of MDCK cells as a result of Hakai overexpression was strongly reduced after Hakin-1 treatment, which was also seen in LoVo cells. Moreover, Hakin-1 also reduced cell migration in HT29 cells, which were not able to invade under the experimental conditions used for LoVo and Hakai-MDCK cells.

Another feature of malignant transformation is the acquisition of oncogenic potential, which is characterized by anchorage-independent cell growth and it has also been linked to EMT [253]. Hakai overexpression was also reported to increase oncogenic potential, as Hakai-overexpressing MDCK cells grow colonies in soft agar while parental MDCK cells are not able to do so [158]. Hakai was also observed to induce anchorage-independent growth in HCC cells, by regulating Ajuba stability through neddylation [165]. Consistent with these observations, Hakin-1 significantly reduced colony formation in Hakai-MDCK cells. In addition, Hakin-1 strongly reduced oncogenic potential in HT29 cells. Altogether, these results suggest that Hakin-1 is able to reduce important features of EMT *in vitro*, such as invasion, migration and anchorage-independent cell growth.

Hakin-1 reduces cell proliferation, tumour growth and lung micrometastasis formation, without affecting cell apoptosis

Hakai has been described to play a key role in the regulation of cell proliferation as its overexpression in MDCK-cells induced the transition from G0/G1 to S phase. Hakai was reported to regulate cell proliferation in an E-cadherin-independent manner, probably by interacting with PSF and regulating its ability to bind cancer-related mRNAs [153,155]. The involvement of Hakai in G1/S cell cycle transition was further confirmed in NSCLC [160]. Moreover, it was observed that mir-203 negatively regulates cell proliferation by downregulating Hakai expression [154]. According to these observations, Hakin-1 showed an antiproliferative effect in Hakai-overexpressing MDCK epithelial cells and colorectal cancer cell lines. Interestingly, Hakin-1 reduced cell proliferation in other types of carcinomas, suggesting that it might be effective in different cancer types besides colon cancer. This correlates with previous studies where Hakai was proposed as a novel biomarker and promising therapeutic target not only for CRC treatment [158], but also in NSCLC [160,161] and HCC [165]. Conversely to this results, Hakai was reported to prevent ERα-mediated cell proliferation in breast cancer cells, suggesting that it may function as a positive or negative regulator of cell proliferation depending on the cellular context [156].

In line with results previously obtained *in vitro*, Hakin-1 decreased cell proliferation also *in vivo*, as observed in histological analyses of Ki67 expression and the mitotic index of Hakai-MDCK xenografted tumours treated either with Hakin-1 or DMSO (Figure 42). Moreover, Hakin-1 reduced tumour growth, as tumour size in treated mice was significantly reduced compared to control mice. Since cell proliferation is one the major mechanisms responsible for tumour growth, and considering the involvement of Hakai in cell proliferation as well as the observed antiproliferative effect of Hakin-1, it seems reasonable that it also affected tumour growth. This result correlates with the previously observed role of Hakai in inducing tumour growth *in vivo*, as Hakai-overexpressing MDCK cells give rise to primary tumours when injected in mice, unlike parental MDCK cells [158]. Hakai was also demonstrated to induce tumour growth in HCC, as mice inoculated with Hakai-overexpressing HCC cells showed an increased tumour growth compared to control ones, while tumours derived from Hakai-depleted HCC cells were smaller than those derived from control HCC cells [165]. Moreover, Slit-Robo signalling was reported to induce tumour growth through Hakai-mediated E-cadherin degradation in CRC [159]. A good therapeutic strategy to prevent tumour growth consists of the stimulation of proapoptotic molecules and the inhibition of the antiapoptotic ones. Targeting apoptosis works against all different cancer types, as apoptosis evasion is one of the hallmarks of cancer [9,254]. Interestingly, no effect upon Hakin-1 treatment was observed when analysing cell apoptosis in tumour samples, thus supporting that the observed reduction in tumour size is due to its antiproliferative effect and not to an enhanced apoptosis. This result is in line with previous studies in which it was observed that Hakai overexpression in MDCK cells did not result in a decreased cell death [153].

As previously described, EMT has been associated with many aspects of tumour progression, including metastasis development [21,48,50]. Remarkably, although no macrometastasis were detected in the histological analysis of mouse lungs, qPCR analysis of Hakai-MDCK DNA revealed a significant reduction in micrometastasis formation in mice treated with Hakin-1. This result suggests that Hakin-1 is able to reduce lung micrometastasis development *in vivo*, which correlates with previous studies where Hakai was reported to increase metastasis development [158,159]. However, future investigations are needed to determine how Hakin-1 may impact on metastasis formation.

The metastatic cascade that takes place during carcinoma progression consists of a sequence of events that include EMT and the reverse process, known as mesenchymal-epithelial transition (MET). The later one is necessary for metastatic colonization once than tumour cells have reached secondary organs [33]. The translation of this cellular plasticity into clinical practice still remains as a major challenge and a debatable issue. The screening for EMT inhibitors can be conducted by using different strategies: i) screening of compounds that prevent EMT induction,

ii) screening of compound that induce MET, or iii) screening of compounds that target mesenchymal tumour cells. The development of compounds that induce MET may increase cell proliferation at the metastatic sites. Therefore, a good therapeutic approach would consist in either to inhibit EMT at early stages, in order to prevent metastasis development, or to deplete mesenchymal tumour cells without inducing MET [239]. As discussed above, E-cadherin posttranscriptional downregulation is an early event during EMT process, as it takes place before its posttranscriptional repression [169]. Therefore, Hakin-1 might be considered a compound that acts at the onset of EMT rather than one that acts on mesenchymal cells [239], as it is not able to increase the expression of E-cadherin protein when it is absent. However, Hakin-1 reduces N-cadherin mesenchymal marker, which suggests that it is able to revert mesenchymal phenotype even when E-cadherin is not present. Interestingly, Hakin-1 not only inhibited tumour growth and proliferation of mesenchymal Hakai-MDCK tumours, but also reduced the development of lung micrometastasis. However, as discussed above, future investigations are needed to elucidate the underlying mechanism by which Hakin-1 may inhibit micrometastasis development.

A good therapeutic strategy for EMT inhibition-based therapies is their clinical use in combination with alternative classes of antitumour drugs, as combined regimens of compounds with overlapping cytotoxic or antiproliferative effects may cause adverse side effects [239]. Moreover, extensive evidence supports the link between EMT and the acquired resistance to classical chemotherapeutic drugs [56,255–257]. Therefore, the combination of EMT inhibitors with classical chemotherapy would allow to reduce the acquisition of therapeutic resistance. Interestingly, Hakai downregulation was reported to sensitize NSCLC cells to cisplatin [161,163]. Besides, Hakai was also reported to be involved in EMT-mediated gefitinib resistance in NSCLC cells [164]. 5-fluorouracil (5-FU) is a chemotherapeutic agent that has been used for colorectal cancer treatment over the last decades. It is commonly used in combination with folinic acid (leucovorin) together with oxaliplatin (FOLFOX) and irinotecan (FOLFIRI), as 5-FU-based combination therapies have been shown to improve overall survival of colorectal cancer patients compared to 5-FU treatment alone. However, despite the promising advances that have been made in CRC therapy so far, the response rates to therapy are still poor and de disease-free survival has not effectively been increased due to the development of chemoresistance [258]. Interestingly, Hakin-1 treatment in combination with 5-FU did not show a synergistic effect neither in cell viability nor in cell proliferation in colorectal cancer cells. Contrary to what might be expected, when analysing cell migration, combination therapy with 5-FU and Hakin-1 did not improve the effect of 5-FU treatment alone. In any case, further investigations are needed to address the effect of Hakin-1 in combination with classical chemotherapy in other aspects of tumour progression, such as invasiveness, oncogenic and metastatic potential, or drug resistance.

Hakin-1 may regulate tumour progression by acting on additional specific Hakai substrates

Besides E-cadherin, another proposed substrate for Hakai is Cortactin, which has been demonstrated to interact with Hakai HYB domain only when phosphorylated by Src [143]. Despite the physiological relevance of this interaction remains to be elucidated, Cortactin has been shown to be downregulated in Hakai-overexpressing MDCK cells, in the same way as E-cadherin [141]. Interestingly, Hakin-1 was able to increase Cortactin protein expression levels both *in vitro* and *in vivo*, further supporting that Hakin-1 targets the HYB interaction domain of Hakai. Therefore, future investigations are needed, since it is important to consider that Hakin-1 may also exert its action on additional specific Hakai substrates that remain to be described. Indeed, as previously discussed, Hakai has been demonstrated to regulate cell proliferation in an E-cadherin- independent manner, probably through the regulation of PSF and/or Cyclin D1 [153]. Moreover, Hakai has been recently proposed to interact with Ajuba through its HYB domain, inducing Ajuba neddylation and regulating its stability in HCC [165]. An additional example of Hakai-mediated regulation independent of its E3 ubiquitin-ligase activity is δ-catenin stabilization. Hakai induces Src stabilization, which in turn increases δ-catenin Tyr-phosphorylation and inhibits its ubiquitination by glycogen synthase kinase-3β (GSK-3β) [259].

Another important hallmark of tumour development is the induction of angiogenesis, which has also been considered a promising therapeutic target for cancer treatment. The first angiogenesis inhibitor approved by FDA was bevacizumab, a humanized monoclonal antibody that targets vascular endothelial growth factor (VEGF), which was used for colorectal cancer treatment in combination with 5-FU. However, although anti-angiogenic therapies have opened up new opportunities for cancer treatment, a major limitation is their toxicity. Moreover, the survival rate of patients with VEGF-targeted therapies is still poor, so new angiogenesis inhibitors need to be developed [224,260]. EMT process and angiogenesis have been reported to be closely related, as VEGF induces the expression of matrix metalloproteinases thus increasing the migratory and invasive capability of cancer cells. Moreover, VEGF has been reported as a downstream effector of hypoxia inducible factor-1α (HIF-1α), which induces EMT in a wide number of cancer tissues. HIF-1α/VEGF signalling pathway has been proposed as a promising target for cancer treatment [261,262]. Interestingly, a recent publication has demonstrated that PSF inhibits HIF-1α through the recruitment of Hakai, thus downregulating VEGF under hypoxia conditions [263]. Hakin-1 significantly reduced the number of blood vessels in Hakai-MDCK tumours, as observed in the immunohistochemistry assay of CD31 endothelial marker. Even though the mechanism by which Hakin-1 regulates the number of blood vessels remains to be elucidated, a recent publication has demonstrated that soluble E-cadherin, that is, the extracellular domain of E-cadherin cleaved by proteases and released in a soluble form, induces tumour angiogenesis in ovarian cancer [264]. Therefore Hakin-1 could inhibit angiogenesis by regulating

E-cadherin proteolysis and the subsequent release of its extracellular domain. This hypothesis may give rise to a new line of investigation.

Hence, taking into account the above-discussed results, Hakin-1 is proposed as the first small-molecule antiproliferative compound that directly targets EMT through its action on Hakai-mediated ubiquitination and degradation of E-cadherin. Interestingly, the *in vivo* antitumour effect of Hakin-1 was observed at dose of 5 mg/kg, used only every three days, which is lower in comparison with the doses used for the *in vitro* studies. This suggests that Hakin-1 metabolites could have an increased antitumour activity, although further investigations are needed. A major disadvantage of classical chemotherapy is its toxicity to normal cells, which causes side effects in different organs such as kidney and liver. This usually limits the treatment dose as well as the duration of the treatment [265,266]. On the other hand, in terms of targeted therapy, targeting E3 ubiquitin-ligases has attracted significant attention as their inhibition is expected to cause less side effects than the inhibition of other members of the ubiquitin pathway, such as the proteasome or E1 and E2 enzymes. Indeed, despite its relative success in the treatment of haematological malignancies, the therapeutic window of proteasome inhibitor bortezomib is quite limited, as toxic side effects such as peripheral neuropathy or cardiotoxicity have been observed due to the accumulation of misfolded proteins [267,268]. Conversely, the MLN4924-mediated inhibition of Cullin-RING E3 ubiquitin-ligases, has shown a great antitumour activity while being well-tolerated in mice [269]. Moreover, MLN4924 has demonstrated good systemic tolerance in phase I clinical trials of solid tumours and haematological malignancies [270,271]. Importantly, Hakin-1 showed a significant antitumour effect *in vivo* without causing apparent systemic toxicity, as observed in histological analysis of liver and kidney samples of treated mice.

Nevertheless, although Hakin-1 effect is due, at least in part, to its action on Hakai, possible off-target effects of this inhibitor compound should be considered. On the one hand, despite the HYB domain has so far been described only in Hakai and in testis-specific E3 ubiquitin-ligase ZNF645 [143,145], Hakin-1 could also bind to other E3 ubiquitin-ligases that share the HYB domain and that have not been described yet. On the other hand, as previously discussed, Hakin-1 may regulate additional specific substrates of Hakai that remain to be elucidated, such as those involved on cell proliferation. Therefore, although future research is needed to determine how Hakin-1 is regulating different aspects of tumour progression besides EMT, such as cell proliferation or angiogenesis, so far it has proven to be a promising therapeutic agent for EMT inhibition, and all these results represent a preclinical proof-of-concept for the use of Hakai inhibitors as antitumour agents [272].

II. Hakai involvement in tumour microenvironment and the acquisition of stem properties

As previously described, EMT can also be regulated by tumour microenvironment, which comprises stromal cells, stromal cell-secreted factors (cytokines, chemokines and growth factors) and the extracellular matrix (ECM) [56]. It has been shown that cytokines released by cancer-associated fibroblasts (CAFs) induce the expression of CD44v6, a colorectal CSC marker that is required for metastatic potential of colorectal CSCs [273]. On the other hand, extensive evidence supports the role of cancer-associated fibroblasts in the EMT process [92,274,275]. In 2011, Dolznig *et al*. established an *in vitro* model to study the importance of tumour stroma during carcinoma progression, known as '*in vitro* carcinoma assay', by co-culturing tumour multicellular spheroids with CAFs in a collagen matrix [192]. With the aim to bring new insights into the role of Hakai during tumour progression, a '*in vitro* carcinoma assay' was developed by using different colorectal cancer cell lines. It has been reported that CAFs induce an invasive phenotype in colorectal cancer spheroids when co-cultured into a collagen matrix [192]. Among the cell lines tested, HCT116 proved to be the most invasive one. The analysis of E-cadherin and Hakai subcellular localization in the co-cultures showed Hakai was predominantly expressed in the invasive protrusions developed by HCT116 spheroids, supporting the previously reported role of Hakai in the acquisition of invasive properties [157,158,160]. Hakai role on cell invasion was further confirmed by analysing the effect of Hakai silencing in HCT116 invasive cells, which significantly reduced the formation of invasive protrusions.

As mentioned above, there is an increasing evidence that suggests that CAFs play an important role during EMT process, although the underlying mechanisms are not yet fully understood [91]. On the other hand, ubiquitin signalling has been reported to regulate de transformation of normal fibroblasts into CAFs. For example, RING-type E3 ligase TRAF4 has been shown to induce the secretion of soluble lCAM1 in normal lung fibroblasts, thus promoting tumour progression [276]. As an additional approach to understand the role of cancer-associated fibroblasts in EMT, we analysed whether CAFs-released factors affected Hakai expression levels in monolayer cultures of colorectal cancer cell lines, cultured in CAFs conditioned medium. Although no significant effect was observed on Hakai expression in none of the cell lines tested after treatment with CAFs conditioned medium, future research is needed. It is important to note that Hakai was found to be highly expressed in CAFs, which might the first insight into the role of Hakai in CAFs biology, as Hakai overexpression in CAFs has not been reported so far. Nevertheless, Hakai silencing in CAFs did not affect their contractile properties, so further investigations are needed to elucidate the possible involvement of Hakai in cancer-associated fibroblast biology.

EMT process has traditionally been related with the acquisition of motile and invasive properties during the malignant transformation of epithelial cells. However, increasing evidence over the past decade has revealed that EMT also induces the acquisition of CSC properties [56,277]. Recent studies have demonstrated that the downregulation of FBXW7 E3 ligase increases EMT and metastasis, and induces the acquisition of CSC properties in colorectal cancer cells [278]. On the other hand, pharmacological inactivation of Skp2, an E3 ubiquitin-ligase of the SCF complex, has been reported to reduce CSC populations and self-renewal capability [279]. Moreover, it has been recently reported NEDD4 E3 ligase is involved in the maintenance of breast CSC populations [280]. Considering the aforementioned involvement of Hakai in EMT, through the downregulation of E-cadherin at cell-cell contacts, the possible role of Hakai in the acquisition of stem properties was studied, by using tumorsphere cultures of HCT116 colorectal cancer cells. Tumorsphere cultures are extensively used as a reliable tool either to analyse the self-renewal capacity of CSCs or to enrich them from other tumour cells. They also represent a useful tool for the development of anti-CSC drugs [281]. As expected, tumorsphere cultures displayed an enrichment in CSCs, since they showed increased mRNA levels of pluripotency genes and decreased mRNA levels of differentiation genes, when compared to monolayer cultures of HCT116. Interestingly, Hakai mRNA levels were remarkably increased in tumorsphere cultures compared with control HCT116 cells growing in a monolayer, supporting the involvement of Hakai in the acquisition of stem properties. This result correlates with previous observations where Hakai knockdown in gefitinib-resistant HCC827/IR cells reduced tumorsphere development [164]. Moreover, Hakai inhibition with Hakin-1 treatment significantly affected tumorsphere formation, since treated tumorspheres remained as differentiated cellular aggregates, while control tumorspheres displayed a more compact and rounded phenotype, which is characteristic of cells with stem-like features. The inhibition of tumorsphere development was also observed at the molecular level, since Hakin-1 decreased mRNA levels of stem markers while increased mRNA levels of differentiation markers. Once again, Hakin-1 treatment did not affect Hakai mRNA levels, further supporting its action on Hakai activity. Therefore, this might be a step forward in the understanding of Hakai role during tumour progression, although future research is needed to underlie the mechanisms responsible for Hakai induction of the stem phenotype. Conventional anticancer therapies are usually limited by the development of acquired resistance, as they are designed to target the bulk population of non-CSCs within a tumour. Therefore, the surviving CSCs give rise to a new tumour, causing a clinical relapse [103,110,282]. Remarkably, the analysis of tumour samples from the previously described xenograft mouse model showed that Hakin-1 also downregulated the expression levels of stem markers *in vivo*.

Altogether, these results suggest that Hakin-1 could inhibit the Hakai-mediated acquisition of stem properties, although further research is needed to understand the mechanisms by which Hakai drives stemness. This represents an innovative filed, as Hakin-1 might be able to inhibit not only EMT and metastasis but also prevent tumour relapse, unlike most current targeted therapies that are not able to eliminate CSCs. Moreover, considering the extensive evidence that supports the link between CSCs and the development of resistance to chemotherapy and immunotherapy [56,103], Hakin-1 treatment could prevent the acquisition of therapeutic resistance. Indeed, Hakai has demonstrated to be involved in the development of drug resistance in NSCLC [161,163,164]. Nevertheless, these are very preliminary results and further investigations are needed to elucidate how Hakin-1 impairs the acquisition of stem properties.

VI. CONCLUSIONS

Conclusions regarding objective 1

1. Hakin-1 reduces Hakai-mediated ubiquitination of E-cadherin as well as Hakai-mediated overall ubiquitination in a dose-dependent manner.

2. Hakin-1 significantly inhibits epithelial cancer cell viability and proliferation *in vitro*, showing an increased cytotoxic and antiproliferative effect when Hakai is overexpressed.

3. Hakin-1 regulates EMT process and induces epithelial cell differentiation both *in vitro* and *in vivo*, by increasing E-cadherin levels at cell-cell contacts and downregulating N-cadherin and Vimentin mesenchymal markers.

4. Hakin-1 reduces cell migration, invasiveness an oncogenic potential *in vitro*.

5. Hakin-1 does not show a synergistic effect in combination with 5-fluorouracil when analysing cell viability, proliferation, or migration.

6. None of the tested Hakin-1 analogous compounds shows a greater antitumour effect *in vitro* when compared to Hakin-1.

7. Hakin-1 reduces tumour growth *in vivo*, by reducing cell proliferation rather than inducing cell death.

8. Hakin-1 inhibits angiogenesis and lung micrometastasis *in vivo*, without apparent systemic toxicity.

Conclusions regarding objective 2

1. The *'in vitro* carcinoma assay' showed that Hakai is involved in the acquisition of invasive properties, exhibiting a predominant expression in invasive protrusions, whose formation is diminished when Hakai is downregulated.

2. Hakai downregulation in cancer-associated fibroblasts (CAFs) does not affect their contractile properties. CAF-secreted factors do not induce the expression of Hakai in colorectal cancer cell lines.

3. Hakai may play a role in the development of cancer stem cells (CSCs), as its expression is increased in tumorspheres compared to monolayer cultures.

4. Hakin-1 may inhibit the development of CSCs, as it increases the differentiation of tumorspheres, by downregulating pluripotency genes and upregulating differentiation ones, and reduces the expression of stem markers *in vivo*.

VII. REFERENCES

1. Cancer Today -IARC. GLOBOCAN 2020 [Internet]. [cited 2020 Dec 19]. Available from: https://gco.iarc.fr/today/home
2. Tsaousis GN, Papadopoulou E, Apessos A, Agiannitopoulos K, Pepe G, Kampouri S, et al. Analysis of hereditary cancer syndromes by using a panel of genes: Novel and multiple pathogenic mutations. BMC Cancer. 2019;19(1):535.
3. Anand P, Kunnumakara AB, Sundaram C, Harikumar KB, Tharakan ST, Lai OS, et al. Cancer is a preventable disease that requires major lifestyle changes. Pharm Res. 2008;25(9):2097–116.
4. Warren GW, Cummings KM. Tobacco and Lung Cancer: Risks, Trends, and Outcomes in Patients with Cancer. Am Soc Clin Oncol Educ B. 2013;(33):359–64.
5. Pischon T, Nimptsch K. Obesity and risk of cancer: An introductory overview. Recent Results Cancer Res. 2016;208:1–15.
6. Grosso G, Bella F, Godos J, Sciacca S, Del Rio D, Ray S, et al. Possible role of diet in cancer: Systematic review and multiple meta-analyses of dietary patterns, lifestyle factors, and cancer risk. Nutr Rev. 2017;75(6):405–19.
7. World Health Organization. Cancer Fact Sheet [Internet]. [cited 2020 Dec 5]. Available from: https://www.who.int/en/news-room/fact-sheets/detail/cancer
8. Hanahan D, Weinberg RA. The Hallmarks of Cancer. Cell. 2000;100(1):57–70.
9. Hanahan D, Weinberg RA. Hallmarks of cancer: The next generation. Cell. 2011;144(5):646–74.
10. Feitelson MA, Arzumanyan A, Kulathinal RJ, Blain SW, Holcombe RF, Mahajna J, et al. Sustained proliferation in cancer: Mechanisms and novel therapeutic targets. Semin Cancer Biol. 2015 Dec 1;35:S25–54.
11. Dick FA, Goodrich DW, Sage J, Dyson NJ. Non-canonical functions of the RB protein in cancer. Nat Rev Cancer. 2018 Jul 1;18(7):442–51.
12. Sung Y-J, Kao T-Y, Kuo C-L, Fan C-C, Cheng AN, Fang W-C, et al. Mitochondrial Lon sequesters and stabilizes p53 in the matrix to restrain apoptosis under oxidative stress via its chaperone activity. Cell Death Dis. 2018 Jun 13;9(6):697.
13. Benedict B, van Harn T, Dekker M, Hermsen S, Kucukosmanoglu A, Pieters W, et al. Loss of p53 suppresses replication-stress-induced DNA breakage in G1/S checkpoint deficient cells. Elife. 2018 Oct 1;7:e37868.
14. Chen HC, Kanai M, Inoue-Yamauchi A, Tu HC, Huang Y, Ren D, et al. An interconnected hierarchical model of cell death regulation by the BCL-2 family. Nat Cell Biol. 2015 Oct 3;17(10):1270–81.
15. Carneiro BA, El-Deiry WS. Targeting apoptosis in cancer therapy. Nat Rev Clin Oncol. 2020 Jul 1;17(7):395–417.
16. Song Y, Gao J, Guan L, Chen X, Gao J, Wang K. Inhibition of ANO1/TMEM16A induces apoptosis in human prostate carcinoma cells by activating TNF-α signaling. Cell Death Dis. 2018 Jun 13;9(6):703.
17. Childs BG, Baker DJ, Kirkland JL, Campisi J, Deursen JM. Senescence and apoptosis: dueling or complementary cell fates? EMBO Rep. 2014 Nov;15(11):1139–53.
18. Roger L, Jones RE, Heppel NH, Williams GT, Sampson JR, Baird DM. Extensive telomere erosion in the initiation of colorectal adenomas and its association with chromosomal instability. J Natl Cancer Inst. 2013 Aug 21;105(16):1202–11.

19. Unterleuthner D, Neuhold P, Schwarz K, Janker L, Neuditschko B, Nivarthi H, et al. Cancer-associated fibroblast-derived WNT2 increases tumor angiogenesis in colon cancer. Angiogenesis. 2020 May 30;23(2):159–77.

20. Lambert AW, Pattabiraman DR, Weinberg RA. Emerging Biological Principles of Metastasis. Cell. 2017 Feb 9;168(4):670–91.

21. Brabletz T, Kalluri R, Nieto MA, Weinberg RA. EMT in cancer. Nat Rev Cancer. 2018 Jan 25;18(2):128–34.

22. Perez-Moreno M, Jamora C, Fuchs E. Sticky business: Orchestrating cellular signals at adherens junctions. Cell. 2003 Feb 21;112(4):535–48.

23. Thiery JP, Sleeman JP. Complex networks orchestrate epithelial-mesenchymal transitions. Nat Rev Mol Cell Biol. 2006 Feb;7(2):131–42.

24. Garcia MA, Nelson WJ, Chavez N. Cell–Cell Junctions Organize Structural and Signaling Networks. Cold Spring Harb Perspect Biol. 2018 Apr 1;10(4):a029181.

25. Goodenough DA, Paul DL. Gap junctions. Cold Spring Harb Perspect Biol. 2009;1(1):a002576.

26. Campbell HK, Maiers JL, DeMali KA. Interplay between tight junctions & adherens junctions. Exp Cell Res. 2017 Sep 1;358(1):39–44.

27. Wang W, Zuidema A, Molder L te, Nahidiazar L, Hoekman L, Schmidt T, et al. Hemidesmosomes modulate force generation via focal adhesions. J Cell Biol. 2020 Feb 3;219(2):e201904137.

28. Aparicio LA, Blanco M, Castosa R, Concha Á, Valladares M, Calvo L, et al. Clinical implications of epithelial cell plasticity in cancer progression. Cancer Lett. 2015 Sep 28;366(1):1–10.

29. Cathcart JM, Banach A, Liu A, Chen J, Goligorsky M, Cao J. Interleukin-6 increases matrix metalloproteinase-14 (MMP-14) levels via down-regulation of p53 to drive cancer progression. Oncotarget. 2016;7(38):61107–20.

30. Winkler J, Abisoye-Ogunniyan A, Metcalf KJ, Werb Z. Concepts of extracellular matrix remodelling in tumour progression and metastasis. Nat Commun. 2020 Dec 1;11(1).

31. Sirniö P, Tuomisto A, Tervahartiala T, Sorsa T, Klintrup K, Karhu T, et al. High-serum MMP-8 levels are associated with decreased survival and systemic inflammation in colorectal cancer. Br J Cancer. 2018 Jul 17;119(2):213–9.

32. Gonzalez-Avila G, Sommer B, Mendoza-Posada DA, Ramos C, Garcia-Hernandez AA, Falfan-Valencia R. Matrix metalloproteinases participation in the metastatic process and their diagnostic and therapeutic applications in cancer. Crit Rev Oncol Hematol. 2019 May 1;137:57–83.

33. Thiery JP. Epithelial–mesenchymal transitions in tumour progression. Nat Rev Cancer. 2002;2(6):442–54.

34. Xu H, Liu L, Li W, Zou D, Yu J, Wang L, et al. Transcription factors in colorectal cancer: molecular mechanism and therapeutic implications. Oncogene. 2020 Dec 15;

35. Xie YH, Chen YX, Fang JY. Comprehensive review of targeted therapy for colorectal cancer. Signal Transduct Target Ther. 2020 Dec 1;5(1).

36. Dienstmann R, Vermeulen L, Guinney J, Kopetz S, Tejpar S, Tabernero J. Consensus molecular subtypes and the evolution of precision medicine in colorectal cancer. Nat Rev Cancer. 2017 Jan 27;17(2):79–92.

37. Van Cutsem E, Köhne CH, Láng I, Folprecht G, Nowacki MP, Cascinu S, et al. Cetuximab plus irinotecan, fluorouracil, and leucovorin as first-line treatment for metastatic colorectal cancer: Updated analysis of overall survival according to tumor KRAS and BRAF mutation status. J Clin Oncol. 2011 May 20;29(15):2011–9.

38. Amado RG, Wolf M, Peeters M, Van Cutsem E, Siena S, Freeman DJ, et al. Wild-type KRAS is required for panitumumab efficacy in patients with metastatic colorectal cancer. J Clin Oncol. 2008;26(10):1626–34.

39. Vogelstein B, Papadopoulos N, Velculescu VE, Zhou S, Diaz LA, Kinzler KW. Cancer genome landscapes. Science (80-). 2013 Mar 29;340(6127):1546–58.

40. Vogelstein B, Fearon ER, Hamilton SR, Kern SE, Preisinger AC, Leppert M, et al. Genetic Alterations during Colorectal-Tumor Development. N Engl J Med. 1988 Sep;319(9):525–32.

41. Popat S, Hubner R, Houlston RS. Systematic review of microsatellite instability and colorectal cancer prognosis. J Clin Oncol. 2005;23(3):609–18.

42. Guinney J, Dienstmann R, Wang X, De Reyniès A, Schlicker A, Soneson C, et al. The consensus molecular subtypes of colorectal cancer. Nat Med. 2015 Nov 1;21(11):1350–6.

43. Sveen A, Bruun J, Eide PW, Eilertsen IA, Ramirez L, Murumagi A, et al. Colorectal cancer consensus molecular subtypes translated to preclinical models uncover potentially targetable cancer cell dependencies. Clin Cancer Res. 2018 Feb 15;24(4):794–806.

44. Greenburg G, Hay ED. Epithelia suspended in collagen gels can lose polarity and express characteristics of migrating mesenchymal cells. J Cell Biol. 1982 Oct 1;95(1):333–9.

45. Thiery JP, Acloque H, Huang RYJ, Nieto MA. Epithelial-Mesenchymal Transitions in Development and Disease. Cell. 2009 Nov 25;139(5):871–90.

46. Santamaria PG, Moreno-Bueno G, Portillo F, Cano A. EMT: Present and future in clinical oncology. Mol Oncol. 2017 Jul 1;11(7):718–38.

47. Yang J, Weinberg RA. Epithelial-Mesenchymal Transition: At the Crossroads of Development and Tumor Metastasis. Dev Cell. 2008 Jun 10;14(6):818–29.

48. Nieto MA, Huang RYYJ, Jackson RAA, Thiery JPP. EMT: 2016. Cell. 2016 Jun 30;166(1):21–45.

49. Pastushenko I, Brisebarre A, Sifrim A, Fioramonti M, Revenco T, Boumahdi S, et al. Identification of the tumour transition states occurring during EMT. Nature. 2018 Apr 18;556(7702):463–8.

50. Yang J, Antin P, Berx G, Blanpain C, Brabletz T, Bronner M, et al. Guidelines and definitions for research on epithelial–mesenchymal transition. Nat Rev Mol Cell Biol. 2020 Apr 16;21(6):341–352.

51. Kim D, Xing T, Yang Z, Dudek R, Lu Q, Chen Y-H. Epithelial Mesenchymal Transition in Embryonic Development, Tissue Repair and Cancer: A Comprehensive Overview. J Clin Med. 2017 Dec 22;7(1):1.

52. Huang RYJ, Guilford P, Thiery JP. Early events in cell adhesion and polarity during epithelial-mesenchymal transition. J Cell Sci. 2012 Oct 1;125(19):4417–22.

53. Hay ED. The mesenchymal cell, its role in the embryo, and the remarkable signaling mechanisms that create it. Dev Dyn. 2005 Jul 1;233(3):706–20.

54. Sánchez-Tilló E, De Barrios O, Siles L, Cuatrecasas M, Castells A, Postigo A. β-catenin/TCF4 complex induces the epithelial-to-mesenchymal transition (EMT)-activator

ZEB1 to regulate tumor invasiveness. Proc Natl Acad Sci U S A. 2011 Nov 29;108(48):19204–9.

55. Peinado H, Olmeda D, Cano A. Snail, ZEB and bHLH factors in tumour progression: An alliance against the epithelial phenotype? Nat Rev Cancer. 2007 Jun;7(6):415–28.

56. Dongre A, Weinberg RA. New insights into the mechanisms of epithelial–mesenchymal transition and implications for cancer. Nat Rev Mol Cell Biol. 2019 Feb 1;20(2):69–84.

57. Derynck R, Muthusamy BP, Saeteurn KY. Signaling pathway cooperation in TGF-β-induced epithelial-mesenchymal transition. Curr Opin Cell Biol. 2014 Dec 1;31:56–66.

58. Lamouille S, Xu J, Derynck R. Molecular mechanisms of epithelial-mesenchymal transition. Nat Rev Mol Cell Biol. 2014 Mar;15(3):178–96.

59. Antolín S, Calvo L, Blanco-Calvo M, Santiago MP, Lorenzo-Patiño MJ, Haz-Conde M, et al. Circulating miR-200c and miR-141 and outcomes in patients with breast cancer. BMC Cancer. 2015 Apr 2;15(1):297.

60. Blanco-Calvo M, Calvo L, Figueroa A, Haz-Conde M, Antón-Aparicio L, Valladares-Ayerbes M. Circulating MicroRNAs: Molecular microsensors in gastrointestinal cancer. Sensors (Switzerland). 2012 Jul;12(7):9349–62.

61. Díaz-López A, Moreno-Bueno G, Cano A. Role of microRNA in epithelial to mesenchymal transition and metastasis and clinical perspectives. Cancer Manag Res. 2014 Apr 25;6(1):205–16.

62. Blanco-Calvo M, Tarrío N, Reboredo M, Haz-Conde M, García J, Quindós M, et al. Circulating levels of GDF15, MMP7 and miR-200c as a poor prognostic signature in gastric cancer. Futur Oncol. 2014;10(7):1187–202.

63. Valladares-Ayerbes M, Reboredo M, Medina-Villaamil V, Iglesias-Díaz P, Lorenzo-Patiño MJ, Haz M, et al. Circulating miR-200c as a diagnostic and prognostic biomarker for gastric cancer. J Transl Med. 2012 Sep 6;10(1):186.

64. Aparicio LA, Abella V, Valladares M, Figueroa A. Posttranscriptional regulation by RNA-binding proteins during epithelial-to-mesenchymal transition. Cell Mol Life Sci. 2013 Dec;70(23):4463–77.

65. Dupre-Crochet S, Figueroa A, Hogan C, Ferber EC, Bialucha CU, Adams J, et al. Casein Kinase 1 Is a Novel Negative Regulator of E-Cadherin-Based Cell-Cell Contacts. Mol Cell Biol. 2007 May 15;27(10):3804–16.

66. Chandhoke AS, Karve K, Dadakhujaev S, Netherton S, Deng L, Bonni S. The ubiquitin ligase Smurf2 suppresses TGFβ-induced epithelial-mesenchymal transition in a sumoylation-regulated manner. Cell Death Differ. 2016 May 1;23(5):876–88.

67. Duhamel S, Goyette MA, Thibault MP, Filion D, Gaboury L, Côté JF. The E3 Ubiquitin Ligase HectD1 Suppresses EMT and Metastasis by Targeting the +TIP ACF7 for Degradation. Cell Rep. 2018 Jan 23;22(4):1016–30.

68. Wang L, Niu Z, Wang X, Li Z, Liu Y, Luo F, et al. PHD2 exerts anti-cancer and anti-inflammatory effects in colon cancer xenografts mice via attenuating NF-κB activity. Life Sci. 2020 Feb 1;242:117167.

69. Serrano-Gomez SJ, Maziveyi M, Alahari SK. Regulation of epithelial-mesenchymal transition through epigenetic and post-translational modifications. Mol Cancer. 2016 Feb 24;15(18).

70. Van Roy F, Berx G. The cell-cell adhesion molecule E-cadherin. Cell Mol Life Sci. 2008 Nov;65(23):3756–88.

71. Saito M, Tucker DK, Kohlhorst D, Niessen CM, Kowalczyk AP. Classical and desmosomal cadherins at a glance. J Cell Sci. 2012 Jun 1;125(11):2547–52.

72. Takeichi M. Functional correlation between cell adhesive properties and some cell surface proteins. J Cell Biol. 1977 Nov 1;75(2):464–74.

73. Van Roy F. Beyond E-cadherin: Roles of other cadherin superfamily members in cancer. Nat Rev Cancer. 2014 Feb 20;14(2):121–34.

74. Christofori G, Semb H. The role of the cell-adhesion molecule E-cadherin as a tumour-suppressor gene. Trends Biochem Sci. 1999 Feb 1;24(2):73–6.

75. Berx G, van Roy F. Involvement of members of the cadherin superfamily in cancer. Cold Spring Harb Perspect Biol. 2009;1(6):a003129.

76. Berx G, Becker KF, Höfler H, Van Roy F. Mutations of the human E-cadherin (CDH1) gene. Vol. 12, Human Mutation. Hum Mutat; 1998. p. 226–37.

77. Melo S, Figueiredo J, Fernandes MS, Gonçalves M, Morais-De-Sá E, Sanches JM, et al. Predicting the functional impact of CDH1 missense mutations in hereditary diffuse gastric cancer. Int J Mol Sci. 2017 Dec 12;18(12):2687.

78. Graff JR, Herman JG, Lapidus RG, Chopra H, Xu R, Jarrard DF, et al. E-Cadherin Expression Is Silenced by DNA Hypermethylation in Human Breast and Prostate Carcinomas. Cancer Res. 1995;55(22):5195–9.

79. Wang G, Hu X, Lu C, Su C, Luo S, Luo ZW. Promoter-hypermethylation associated defective expression of E-cadherin in primary non-small cell lung cancer. Lung Cancer. 2008 Nov;62(2):162–72.

80. Wu X, Yao X, Cao Q, Wu Z, Wang Z, Liu F, et al. Clinicopathological and prognostic significance of CDH1 hypermethylation in hepatocellular carcinoma: A meta-analysis. Cancer Manag Res. 2019;11:857–64.

81. Li Z, Guo Z. Comparison of CDH1 Gene Hypermethylation Status in Blood and Serum among Gastric Cancer Patients. Pathol Oncol Res. 2020 Apr 1;26(2):1057–62.

82. Cano A, Pérez-Moreno MA, Rodrigo I, Locascio A, Blanco MJ, Del Barrio MG, et al. The transcription factor Snail controls epithelial-mesenchymal transitions by repressing E-cadherin expression. Nat Cell Biol. 2000 Jan 13;2(2):76–83.

83. Batlle E, Sancho E, Francí C, Domínguez D, Monfar M, Baulida J, et al. The transcription factor Snail is a repressor of E-cadherin gene expression in epithelial tumour cells. Nat Cell Biol. 2000;2(2):84–9.

84. Vesuna F, van Diest P, Chen JH, Raman V. Twist is a transcriptional repressor of E-cadherin gene expression in breast cancer. Biochem Biophys Res Commun. 2008 Mar 7;367(2):235–41.

85. Sánchez-Tilló E, Lázaro A, Torrent R, Cuatrecasas M, Vaquero EC, Castells A, et al. ZEB1 represses E-cadherin and induces an EMT by recruiting the SWI/SNF chromatin-remodeling protein BRG1. Oncogene. 2010 Jun 17;29(24):3490–500.

86. Heerboth S, Housman G, Leary M, Longacre M, Byler S, Lapinska K, et al. EMT and tumor metastasis. Clin Transl Med. 2015 Dec;4(6).

87. David JM, Rajasekaran AK. Dishonorable Discharge: The Oncogenic Roles of Cleaved E-Cadherin Fragments. Cancer Res. 2012;72(12):2917–2923.

88. Fujita Y, Krause G, Scheffner M, Zechner D, Leddy HEM, Behrens J, et al. Hakai, a c-Cbl-like protein, ubiquitinates and induces endocytosis of the E-cadherin complex. Nat

Cell Biol. 2002 Mar;4(3):222–31.

89. Maman S, Witz IP. A history of exploring cancer in context. Nat Rev Cancer. 2018 Jun 1;18(6):359–76.

90. Olumi A, Grossfeld G, Hayward S, Carroll P, Cunha G, Hein P, et al. Carcinoma-associated fibroblasts stimulate tumor progression of initiated human epithelium. Breast Cancer Res. 1999 Oct;59(19):5002–5011.

91. Fiori ME, Di Franco S, Villanova L, Bianca P, Stassi G, De Maria R. Cancer-associated fibroblasts as abettors of tumor progression at the crossroads of EMT and therapy resistance. Mol Cancer. 2019 Mar 30;18(70).

92. Yu Y, Xiao CH, Tan LD, Wang QS, Li XQ, Feng YM. Cancer-associated fibroblasts induce epithelial-mesenchymal transition of breast cancer cells through paracrine TGF-β signalling. Br J Cancer. 2014 Feb 4;110(3):724–32.

93. Shintani Y, Fujiwara A, Kimura T, Kawamura T, Funaki S, Minami M, et al. IL-6 secreted from Cancer-Associated fibroblasts mediates chemoresistance in NSCLC by increasing epithelial-mesenchymal transition signaling. J Thorac Oncol. 2016 Sep 1;11(9):1482–92.

94. Mani S a, Guo W, Liao M, Eaton EN, Zhou AY, Brooks M, et al. Epithelial-Mesenchymal Transition Generates Cells Which Have Stem Cell Properties. Cell. 2008;133(4):704–15.

95. Morel AP, Lièvre M, Thomas C, Hinkal G, Ansieau S, Puisieux A. Generation of breast cancer stem cells through epithelial-mesenchymal transition. PLoS One. 2008 Aug 6;3(8):e2888.

96. Lambert AW, Weinberg RA. Linking EMT programmes to normal and neoplastic epithelial stem cells. Nat Rev Cancer. 2021 Feb 5;1–14.

97. Lytle NK, Barber AG, Reya T. Stem cell fate in cancer growth, progression and therapy resistance. Nat Rev Cancer. 2018 Nov 1;18(11):669–80.

98. Gross KM, Zhou W, Breindel JL, Ouyang J, Jin DX, Sokol ES, et al. Loss of Slug Compromises DNA Damage Repair and Accelerates Stem Cell Aging in Mammary Epithelium. Cell Rep. 2019 Jul 9;28(2):394-407.e6.

99. Ota I, Masui T, Kurihara M, Yook JI, Mikami S, Kimura T, et al. Snail-induced EMT promotes cancer stem cell-like properties in head and neck cancer cells. Oncol Rep. 2016 Jan 1;35(1):261–6.

100. Krebs AM, Mitschke J, Losada ML, Schmalhofer O, Boerries M, Busch H, et al. The EMT-activator Zeb1 is a key factor for cell plasticity and promotes metastasis in pancreatic cancer. Nat Cell Biol. 2017 May 1;19(5):518–29.

101. Wang X, Xu H, Cheng C, Ji Z, Zhao H, Sheng Y, et al. Identification of a Zeb1 expressing basal stem cell subpopulation in the prostate. Nat Commun. 2020 Dec 1;11(1).

102. Morel AP, Ginestier C, Pommier RM, Cabaud O, Ruiz E, Wicinski J, et al. A stemness-related ZEB1-MSRB3 axis governs cellular pliancy and breast cancer genome stability. Nat Med. 2017 May 1;23(5):568–78.

103. Shibue T, Weinberg RA. EMT, CSCs, and drug resistance: The mechanistic link and clinical implications. Nat Rev Clin Oncol. 2017 Oct 1;14(10):611–29.

104. Qin S, Jiang J, Lu Y, Nice EC, Huang C, Zhang J, et al. Emerging role of tumor cell plasticity in modifying therapeutic response. Signal Transduct Target Ther. 2020 Dec 1;5(228).

105. Assaraf YG, Brozovic A, Gonçalves AC, Jurkovicova D, Linē A, Machuqueiro M, et al.

The multi-factorial nature of clinical multidrug resistance in cancer. Drug Resist Updat. 2019 Sep 1;46:100645.

106. Saxena M, Stephens MA, Pathak H, Rangarajan A. Transcription factors that mediate epithelial-mesenchymal transition lead to multidrug resistance by upregulating ABC transporters. Cell Death Dis. 2011 Jul;2(7):e179.

107. Dwivedi SKD, Mustafi SB, Mangala LS, Jiang D, Pradeep S, Rodriguez-Aguayo C, et al. Therapeutic evaluation of microRNA-15a and microRNA-16 in ovarian cancer. Oncotarget. 2016 Mar 22;7(12):15093–104.

108. Chang TH, Tsai MF, Su KY, Wu SG, Huang CP, Yu SL, et al. Slug confers resistance to the epidermal growth factor receptor tyrosine kinase inhibitor. Am J Respir Crit Care Med. 2011 Apr 15;183(8):1071–9.

109. Kurrey NK, Jalgaonkar SP, Joglekar A V., Ghanate AD, Chaskar PD, Doiphode RY, et al. Snail and slug mediate radioresistance and chemoresistance by antagonizing p53-mediated apoptosis and acquiring a stem-like phenotype in ovarian cancer cells. Stem Cells. 2009 Sep;27(9):2059–68.

110. Fabregat I, Malfettone A, Soukupova J. New Insights into the Crossroads between EMT and Stemness in the Context of Cancer. J Clin Med. 2016 Mar 12;5(3):37.

111. Du B, Shim JS. Targeting epithelial-mesenchymal transition (EMT) to overcome drug resistance in cancer. Molecules. 2016;21(7):965.

112. Yang L, Shi P, Zhao G, Xu J, Peng W, Zhang J, et al. Targeting cancer stem cell pathways for cancer therapy. Signal Transduct Target Ther. 2020 Dec 1;5(1):8.

113. Deng L, Meng T, Chen L, Wei W, Wang P. The role of ubiquitination in tumorigenesis and targeted drug discovery. Signal Transduct Target Ther. 2020 Dec 1;5(11).

114. Rape M. Ubiquitylation at the crossroads of development and disease. Nat Rev Mol Cell Biol. 2018 Jan 1;19(1):59–70.

115. Goldstein G, Scheid M, Hammerling U, Schlesinger DH, Niall HD, Boyse EA. Isolation of a polypeptide that has lymphocyte differentiating properties and is probably represented universally in living cells. Proc Natl Acad Sci U S A. 1975;72(1):11–5.

116. Hershko A, Heller H, Elias S, Ciechanover A. Components of ubiquitin-protein ligase system. Resolution, affinity purification, and role in protein breakdown. J Biol Chem. 1983;258(13):8206–14.

117. Hershko A, Ciechanover A. The ubiquitin system for protein degradation. Annu Rev Biochem. 1992;61:761–807.

118. Hershko A, Heller H, Eytan E, Reiss Y. The protein substrate binding site of the ubiquitin-protein ligase system. J Biol Chem. 1986;261(26):11992–9.

119. Buetow L, Huang DT. Structural insights into the catalysis and regulation of E3 ubiquitin ligases. Nat Rev Mol Cell Biol. 2016 Oct 1;17(10):626–42.

120. Metzger MB, Hristova VA, Weissman AM. HECT and RING finger families of E3 ubiquitin ligases at a glance. J Cell Sci. 2012 Feb 1;125(3):531–7.

121. Cooper JA, Kaneko T, Li SSC. Cell Regulation by Phosphotyrosine-Targeted Ubiquitin Ligases. Mol Cell Biol. 2015 Jun 1;35(11):1886–97.

122. Berndsen CE, Wolberger C. New insights into ubiquitin E3 ligase mechanism. Nat Struct Mol Biol. 2014;21(4):301–7.

123. Scheffner M, Kumar S. Mammalian HECT ubiquitin-protein ligases: Biological and pathophysiological aspects. Biochim Biophys Acta - Mol Cell Res. 2014 Jan 1;1843(1):61–74.

124. Rodríguez-Alonso A, Casas-Pais A, Roca-Lema D, Graña B, Romay G, Figueroa A. Regulation of epithelial-mesenchymal plasticity by the E3 ubiquitin-ligases in cancer. Cancers (Basel). 2020;12(11):3093.

125. Wang X, De Geyter C, Jia Z, Peng Y, Zhang H. HECTD1 regulates the expression of SNAIL: Implications for epithelial–mesenchymal transition. Int J Oncol. 2020;56(5):1186–98.

126. Díaz VM, de Herreros AG. F-box proteins: Keeping the epithelial-to-mesenchymal transition (EMT) in check. Semin Cancer Biol. 2016 Feb 1;36:71–9.

127. Xu L, Zhang Y, Qu X, Che X, Guo T, Cai Y, et al. E3 Ubiquitin Ligase Cbl-b Prevents Tumor Metastasis by Maintaining the Epithelial Phenotype in Multiple Drug-Resistant Gastric and Breast Cancer Cells. Neoplasia (United States). 2017 Apr 1;19(4):374–82.

128. Senft D, Qi J, Ronai ZA. Ubiquitin ligases in oncogenic transformation and cancer therapy. Nat Rev Cancer. 2018 Jan 25;18(2):69–88.

129. Richardson PG, Barlogie B, Berenson J, Singhal S, Jagannath S, Irwin D, et al. A Phase 2 Study of Bortezomib in Relapsed, Refractory Myeloma. N Engl J Med. 2003 Jun 26;348(26):2609–17.

130. Gandolfi S, Laubach JP, Hideshima T, Chauhan D, Anderson KC, Richardson PG. The proteasome and proteasome inhibitors in multiple myeloma. Cancer Metastasis Rev. 2017 Dec 1;36(4):561–84.

131. Khan ML, Stewart AK. Carfilzomib: A novel second-generation proteasome inhibitor. Futur Oncol. 2011 May;7(5):607–12.

132. Kumar SK, Bensinger WI, Zimmerman TM, Reeder CB, Berenson JR, Berg D, et al. Phase 1 study of weekly dosing with the investigational oral proteasome inhibitor ixazomib in relapsed/refractory multiple myeloma. Blood. 2014 Aug 14;124(7):1047–55.

133. Aghajanian C, Blessing JA, Darcy KM, Reid G, DeGeest K, Rubin SC, et al. A phase II evaluation of bortezomib in the treatment of recurrent platinum-sensitive ovarian or primary peritoneal cancer: A Gynecologic Oncology Group study. Gynecol Oncol. 2009 Nov;115(2):215–20.

134. Rosenberg JE, Halabi S, Sanford BL, Himelstein AL, Atkins JN, Hohl RJ, et al. Phase II study of bortezomib in patients with previously treated advanced urothelial tract transitional cell carcinoma: CALGB 90207. Ann Oncol. 2008 May;19(5):946–50.

135. Huang X, Dixit VM. Drugging the undruggables: Exploring the ubiquitin system for drug development. Cell Res. 2016 Apr 1;26(4):484–98.

136. Zhang X, Linder S, Bazzaro M. Drug development targeting the ubiquitin-proteasome system (UPS) for the treatment of human cancers. Cancers (Basel). 2020 Apr 1;12(4):902.

137. Behrens J, Vakaet L, Friis R, Winterhager E, Van Roy F, Mareel MM, et al. Loss of epithelial differentiation and gain of invasiveness correlates with tyrosine phosphorylation of the E-cadherin/β-catenin complex in cells transformed with a temperature-sensitive v-SRC gene. J Cell Biol. 1993;120(3):757–66.

138. Pece S, Gutkind JS. E-cadherin and Hakai: Signalling, remodeling or destruction? Nat Cell Biol. 2002;4(4):72–4.

139. Palacios F, Tushir JS, Fujita Y, D'Souza-Schorey C. Lysosomal Targeting of E-Cadherin:

a Unique Mechanism for the Down-Regulation of Cell-Cell Adhesion during Epithelial to Mesenchymal Transitions. Mol Cell Biol. 2005 Jan 1;25(1):389–402.

140. Mosesson Y, Mills GB, Yarden Y. Derailed endocytosis: An emerging feature of cancer. Nat Rev Cancer. 2008 Nov;8(11):835–50.

141. Díaz-Díaz A, Casas-Pais A, Calamia V, Castosa R, Martinez-Iglesias O, Roca-Lema D, et al. Proteomic Analysis of the E3 Ubiquitin-Ligase Hakai Highlights a Role in Plasticity of the Cytoskeleton Dynamics and in the Proteasome System. J Proteome Res. 2017;16(8):2773–88.

142. Díaz-Díaz A, Roca-Lema D, Casas-Pais A, Romay G, Colombo G, Concha Á, et al. Heat shock protein 90 chaperone regulates the E3 ubiquitin-ligase hakai protein stability. Cancers (Basel). 2020;12(1):215.

143. Mukherjee M, Chow SY, Yusoff P, Seetharaman J, Ng C, Sinniah S, et al. Structure of a novel phosphotyrosine-binding domain in Hakai that targets E-cadherin. EMBO J. 2012 Mar 7;31(5):1308–19.

144. Mukherjee M, Jing-Song F, Ramachandran S, Guy GR, Sivaraman J. Dimeric switch of Hakai-truncated monomers during substrate recognition: Insights from solution studies and NMR structure. J Biol Chem. 2014 Sep 12;289(37):25611–23.

145. Liu YQ, Bai G, Zhang H, Su D, Tao DC, Yang Y, et al. Human RING finger protein ZNF645 is a novel testis-specific E3 ubiquitin ligase. Asian J Androl. 2010 Sep;12(5):658–66.

146. Aparicio LA, Valladares M, Blanco M, Alonso G, Figueroa A. Biological influence of Hakai in cancer: A 10-year review. Cancer Metastasis Rev. 2012 Jun;31(1–2):375–86.

147. Kaido M, Wada H, Shindo M, Hayashi S. Essential requirement for RING finger E3 ubiquitin ligase Hakai in early embryonic development of Drosophila. Genes to Cells. 2009;14(9):1067–77.

148. Przybyla L, Lakins JN, Weaver VM. Tissue Mechanics Orchestrate Wnt-Dependent Human Embryonic Stem Cell Differentiation. Cell Stem Cell. 2016 Oct 6;19(4):462–75.

149. Horiuchi K, Kawamura T, Iwanari H, Ohashi R, Naito M, Kodama T, et al. Identification of Wilms' tumor 1-associating protein complex and its role in alternative splicing and the cell cycle. J Biol Chem. 2013 Nov 15;288(46):33292–302.

150. Růžička K, Zhang M, Campilho A, Bodi Z, Kashif M, Saleh M, et al. Identification of factors required for m6A mRNA methylation in Arabidopsis reveals a role for the conserved E3 ubiquitin ligase HAKAI. New Phytol. 2017 Jul 1;215(1):157–72.

151. Liu J, Yue Y, Liu J, Cui X, Cao J, Luo G, et al. VIRMA mediates preferential m6A mRNA methylation in 3′UTR and near stop codon and associates with alternative polyadenylation. Cell Discov. 2018 Dec 1;4(10).

152. Wen J, Lv R, Ma H, Shen H, He C, Wang J, et al. Zc3h13 Regulates Nuclear RNA m6A Methylation and Mouse Embryonic Stem Cell Self-Renewal. Mol Cell. 2018 Mar 15;69(6):1028-1038.e6.

153. Figueroa A, Kotani H, Toda Y, Mazan-Mamczarz K, Mueller E-C, Otto A, et al. Novel roles of hakai in cell proliferation and oncogenesis. Mol Biol Cell. 2009 Aug;20(15):3533–42.

154. Abella V, Valladares M, Rodriguez T, Haz M, Blanco M, Tarrío N, et al. miR-203 Regulates Cell Proliferation through Its Influence on Hakai Expression. PLoS One. 2012 Dec 20;7(12):e52568.

155. Figueroa A, Fujita Y, Gorospe M. Hacking RNA: Hakai promotes tumorigenesis by enhancing the RNA-binding function of PSF. Cell Cycle. 2009 Nov 15;8(22):3648–51.

156. Gong EY, Park E, Lee K. Hakai acts as a coregulator of estrogen receptor alpha in breast cancer cells. Cancer Sci. 2010 Sep;101(9):2019–25.

157. Rodríguez-Rigueiro T, Valladares-Ayerbes M, Haz-Conde M, Aparicio LA, Figueroa A. Hakai reduces cell-substratum adhesion and increases epithelial cell invasion. BMC Cancer. 2011 Nov 3;11:474.

158. Castosa R, Martinez-Iglesias O, Roca-Lema D, Casas-Pais A, Díaz-Díaz A, Iglesias P, et al. Hakai overexpression effectively induces tumour progression and metastasis in vivo. Sci Rep. 2018;8(1):3466.

159. Zhou WJ, Geng ZH, Chi S, Zhang W, Niu XF, Lan SJ, et al. Slit-Robo signaling induces malignant transformation through Hakai-mediated E-cadherin degradation during colorectal epithelial cell carcinogenesis. Cell Res. 2011;21(4):609–26.

160. Hui L, Zhang S, Wudu M, Ren H, Xu Y, Zhang Q, et al. CBLL1 is highly expressed in non-small cell lung cancer and promotes cell proliferation and invasion. Thorac Cancer. 2019 Jun 1;10(6):1479–88.

161. Liu Z, Wu Y, Tao Z, Ma L. E3 ubiquitin ligase Hakai regulates cell growth and invasion, and increases the chemosensitivity to cisplatin in non-small-cell lung cancer cells. Int J Mol Med. 2018 Aug 1;42(2):1145–51.

162. Qiu HB, Yang K, Yu HY, Liu M. Downregulation of long non-coding RNA XIST inhibits cell proliferation, migration, invasion and EMT by regulating MIR-212-3p/ CBLL1 axis in non-small cell lung cancer cells. Eur Rev Med Pharmacol Sci. 2019;23(19):8391–402.

163. Li H, Liu F, Qin W. Circ_0072083 interference enhances growth-inhibiting effects of cisplatin in non-small-cell lung cancer cells via miR-545-3p/CBLL1 axis. Cancer Cell Int. 2020 Mar 12;20:78.

164. Weng CH, Chen LY, Lin YC, Shih JY, Lin YC, Tseng RY, et al. Epithelial-mesenchymal transition (EMT) beyond EGFR mutations per se is a common mechanism for acquired resistance to EGFR TKI. Oncogene. 2019 Jan 24;38(4):455–68.

165. Liu M, Jiang K, Lin G, Liu P, Yan Y, Ye T, et al. Ajuba inhibits hepatocellular carcinoma cell growth via targeting of β-catenin and YAP signaling and is regulated by E3 ligase Hakai through neddylation. J Exp Clin Cancer Res. 2018 Jul 24;37(1):165.

166. Lu M, Wu J, Hao ZW, Shang YK, Xu J, Nan G, et al. Basolateral CD147 induces hepatocyte polarity loss by E-cadherin ubiquitination and degradation in hepatocellular carcinoma progress. Hepatology. 2018 Jul 1;68(1):317–32.

167. Shen Y, Hirsch DS, Sasiela CA, Wen JW. Cdc42 regulates E-cadherin ubiquitination and degradation through an epidermal growth factor receptor to Src-mediated pathway. J Biol Chem. 2008 Feb 22;283(8):5127–37.

168. Swaminathan G, Cartwright CA. Rack1 promotes epithelial cell-cell adhesion by regulating E-cadherin endocytosis. Oncogene. 2012 Jan 19;31(3):376–89.

169. Janda E, Nevolo M, Lehmann K, Downward J, Beug H, Grieco M. Raf plus TGFB-dependent EMT is initiated by endocytosis and lysosomal degradation of E-cadherin. Oncogene. 2006 Nov 16;25(54):7117–30.

170. Harrigan JA, Jacq X, Martin NM, Jackson SP. Deubiquitylating enzymes and drug discovery: Emerging opportunities. Vol. 17, Nature Reviews Drug Discovery. Nature Publishing Group; 2018. p. 57–77.

171. Bedard PL, Hyman DM, Davids MS, Siu LL. Small molecules, big impact: 20 years of targeted therapy in oncology. Lancet. 2020 Mar 28;395(10229):1078–88.

172. Nero TL, Morton CJ, Holien JK, Wielens J, Parker MW. Oncogenic protein interfaces: Small molecules, big challenges. Nat Rev Cancer. 2014;14(4):248–62.

173. Jubb H, Higueruelo AP, Winter A, Blundell TL. Structural biology and drug discovery for protein-protein interactions. Trends Pharmacol Sci. 2012 May;33(5):241–8.

174. Lu H, Zhou Q, He J, Jiang Z, Peng C, Tong R, et al. Recent advances in the development of protein–protein interactions modulators: mechanisms and clinical trials. Signal Transduct Target Ther. 2020 Dec 1;5(1):213.

175. Scott DE, Bayly AR, Abell C, Skidmore J. Small molecules, big targets: Drug discovery faces the protein-protein interaction challenge. Nat Rev Drug Discov. 2016 Jul 29;15(8):533–50.

176. Wells JA, McClendon CL. Reaching for high-hanging fruit in drug discovery at protein-protein interfaces. Nature. 2007 Dec 13;450(7172):1001–9.

177. Wu KJ, Lei PM, Liu H, Wu C, Leung CH, Ma DL. Mimicking strategy for protein-protein interaction inhibitor discovery by virtual screening. Molecules. 2019 Dec 4;24(24):4428.

178. Timucin AC, Basaga H, Kutuk O. Selective targeting of antiapoptotic BCL-2 proteins in cancer. Med Res Rev. 2019 Jan 1;39(1):146–75.

179. Zhao Y, Aguilar A, Bernard D, Wang S. Small-molecule inhibitors of the MDM2-p53 protein-protein interaction (MDM2 inhibitors) in clinical trials for cancer treatment. J Med Chem. 2015 Feb 12;58(3):1038–52.

180. Mayor-Ruiz C, Winter GE. Identification and characterization of cancer vulnerabilities via targeted protein degradation. Drug Discov Today Technol. 2019 Apr 1;31:81–90.

181. Mayor-Ruiz C, Bauer S, Brand M, Kozicka Z, Siklos M, Imrichova H, et al. Rational discovery of molecular glue degraders via scalable chemical profiling. Nat Chem Biol. 2020 Nov 3;16(11):1199–207.

182. Hines J, Lartigue S, Dong H, Qian Y, Crews CM. MDM2-recruiting PROTAC offers superior, synergistic antiproliferative activity via simultaneous degradation of BRD4 and stabilization of p53. Cancer Res. 2019 Jan 1;79(1):251–62.

183. Pereira DA, Williams JA. Origin and evolution of high throughput screening. Br J Pharmacol. 2007 Sep;152(1):53–61.

184. Subramaniam S, Mehrotra M, Gupta D. Virtual high throughput screening (vHTS) – A perspective. Bioinformation. 2008 Sep 2;3(1):14–7.

185. Kontoyianni M. Docking and virtual screening in drug discovery. Methods Mol Biol. 2017;1647:255–66.

186. Maia EHB, Assis LC, de Oliveira TA, da Silva AM, Taranto AG. Structure-Based Virtual Screening: From Classical to Artificial Intelligence. Front Chem. 2020 Apr 28;8:343.

187. Cabrera ÁC, Gil-Redondo R, Perona A, Gago F, Morreale A. VSDMIP 1.5: An automated structure- and ligand-based virtual screening platform with a PyMOL graphical user interface. J Comput Aided Mol Des. 2011 Sep;25(9):813–24.

188. Gil-Redondo R, Estrada J, Morreale A, Herranz F, Sancho J, Ortiz ÁR. VSDMIP: Virtual screening data management on an integrated platform. J Comput Aided Mol Des. 2009 Mar;23(3):171–84.

189. Klett J, Cortés-Cabrera Á, Gil-Redondo R, Gago F, Morreale A. ALFA: Automatic ligand flexibility assignment. J Chem Inf Model. 2014 Jan 27;54(1):314–23.

190. Cabrera ÁC, Klett J, G. Dos Santos H, Perona A, Gil-Redondo R, Francis SM, et al. CRDOCK: An ultrafast multipurpose protein-ligand docking tool. J Chem Inf Model. 2012 Aug 27;52(8):2300–9.

191. Schneider N, Lange G, Hindle S, Klein R, Rarey M. A consistent description of HYdrogen bond and DEhydration energies in protein-ligand complexes: Methods behind the HYDE scoring function. J Comput Aided Mol Des. 2013 Jan;27(1):15–29.

192. Dolznig H, Rupp C, Puri C, Haslinger C, Schweifer N, Wieser E, et al. Modeling colon adenocarcinomas in vitro: A 3D co-culture system induces cancer-relevant pathways upon tumor cell and stromal fibroblast interaction. Am J Pathol. 2011 Jul;179(1):487–501.

193. Miyoshi H, Stappenbeck TS. In vitro expansion and genetic modification of gastrointestinal stem cells in spheroid culture. Nat Protoc. 2013 Nov 14;8(12):2471–82.

194. Johnson S, Chen H, Lo P-K. In vitro Tumorsphere Formation Assays. BIO-PROTOCOL. 2013;3(3):e325.

195. Weiswald LB, Bellet D, Dangles-Marie V. Spherical Cancer Models in Tumor Biology. Neoplasia (United States). 2015 Jan 1;17(1):1–15.

196. Lavecchia A, Giovanni C. Virtual Screening Strategies in Drug Discovery: A Critical Review. Curr Med Chem. 2013 Jun 26;20(23):2839–60.

197. Nieto MA. Epithelial plasticity: A common theme in embryonic and cancer cells. Science (80-). 2013 Nov 8;342(6159):1234850.

198. Chaffer CL, San Juan BP, Lim E, Weinberg RA. EMT, cell plasticity and metastasis. Cancer Metastasis Rev. 2016 Dec 1;35(4):645–54.

199. Sabbah M, Emami S, Redeuilh G, Julien S, Prévost G, Zimber A, et al. Molecular signature and therapeutic perspective of the epithelial-to-mesenchymal transitions in epithelial cancers. Drug Resist Updat. 2008 Aug;11(4–5):123–51.

200. Alvarez A, Barisone GA, Diaz E. Focus formation: A cell-based assay to determine the oncogenic potential of a gene. J Vis Exp. 2014 Dec 31;(94):51742.

201. Mori S, Chang JT, Andrechek ER, Matsumura N, Baba T, Yao G, et al. Anchorage-independent cell growth signature identifies tumors with metastatic potential. Oncogene. 2009 Aug 6;28(31):2796–805.

202. Buchheit CL, Weigel KJ, Schafer ZT. Cancer cell survival during detachment from the ECM: Multiple barriers to tumour progression. Vol. 14, Nature Reviews Cancer. Nature Publishing Group; 2014. p. 632–41.

203. Borowicz S, Van Scoyk M, Avasarala S, Karuppusamy Rathinam MK, Tauler J, Bikkavilli RK, et al. The soft agar colony formation assay. J Vis Exp. 2014 Oct 27;(92):e51998.

204. Christensen S, Van der Roest B, Besselink N, Janssen R, Boymans S, Martens JWM, et al. 5-Fluorouracil treatment induces characteristic T>G mutations in human cancer. Nat Commun. 2019 Dec 1;10(1):4571.

205. Longley DB, Harkin DP, Johnston PG. 5-Fluorouracil: Mechanisms of action and clinical strategies. Nat Rev Cancer. 2003 May;3(5):330–8.

206. Sorokin M, Kholodenko R, Suntsova M, Malakhova G, Garazha A, Kholodenko I, et al. Oncobox bioinformatical platform for selecting potentially effective combinations of target cancer drugs using high-throughput gene expression data. Cancers (Basel). 2018

Oct 1;10(10):365.

207. Boige V, Mendiboure J, Pignon JP, Loriot MA, Castaing M, Barrois M, et al. Pharmacogenetic assessment of toxicity and outcome in patients with metastatic colorectal cancer treated with LV5FU2, FOLFOX, and FOLFIRI: FFCD 2000-05. J Clin Oncol. 2010 May 20;28(15):2556–64.

208. Douillard JY, Cunningham D, Roth AD, Navarro M, James RD, Karasek P, et al. Irinotecan combined with fluorouracil compared with fluorouracil alone. as first-line treatment for metastatic colorectal cancer: a multicentre randomised trial. Lancet. 2000 Mar 25;355(9209):1041–7.

209. Cho Y-H, Ro EJ, Yoon J-S, Mizutani T, Kang D-W, Park J-C, et al. 5-FU promotes stemness of colorectal cancer via p53-mediated WNT/β-catenin pathway activation. Nat Commun. 2020 Dec 21;11(1):5321.

210. Varga J, Greten FR. Cell plasticity in epithelial homeostasis and tumorigenesis. Nat Cell Biol. 2017 Sep 29;19(10):1133–41.

211. Pastushenko I, Blanpain C. EMT Transition States during Tumor Progression and Metastasis. Trends Cell Biol. 2019 Mar 1;29(3):212–26.

212. Malek R, Wang H, Taparra K, Tran PT. Therapeutic Targeting of Epithelial Plasticity Programs: Focus on the Epithelial-Mesenchymal Transition. Cells Tissues Organs. 2017 Feb 1;203(2):114–27.

213. Gupta PB, Onder TT, Jiang G, Tao K, Kuperwasser C, Weinberg RA, et al. Identification of Selective Inhibitors of Cancer Stem Cells by High-Throughput Screening. Cell. 2009 Aug 21;138(4):645–59.

214. Day CP, Merlino G, Van Dyke T. Preclinical Mouse Cancer Models: A Maze of Opportunities and Challenges. Cell. 2015 Sep 24;163(1):39–53.

215. Pelleitier M, Montplaisir S. The nude mouse: a model of deficient T-cell function. Methods Achiev Exp Pathol. 1975;7:149–66.

216. Nehls M, Pfeifer D, Schorpp M, Hedrich H, Boehm T. New member of the winged-helix protein family disrupted in mouse and rat nude mutations. Nature. 1994;372(6501):103–7.

217. Bukowska J, Kopcewicz M, Walendzik K, Gawronska-Kozak B. Foxn1 in skin development, homeostasis and wound healing. Int J Mol Sci. 2018 Jul 4;19(7):1956.

218. Zink D, Fischer AH, Nickerson JA. Nuclear structure in cancer cells. Nat Rev Cancer. 2004 Sep;4(9):677–87.

219. Evan GI, Vousden KH. Proliferation, cell cycle and apoptosis in cancer. Nature. 2001 May 17;411(6835):342–8.

220. Singh R, Letai A, Sarosiek K. Regulation of apoptosis in health and disease: the balancing act of BCL-2 family proteins. Nat Rev Mol Cell Biol. 2019 Mar 1;20(3):175–93.

221. Enane FO, Saunthararajah Y, Korc M. Differentiation therapy and the mechanisms that terminate cancer cell proliferation without harming normal cells. Cell Death Dis. 2018 Sep 1;9(9):912.

222. Bergers G, Benjamin LE. Tumorigenesis and the angiogenic switch. Nat Rev Cancer. 2003 Jun;3(6):401–10.

223. Weis SM, Cheresh DA. Tumor angiogenesis: Molecular pathways and therapeutic targets. Nat Med. 2011 Nov 7;17(11):1359–70.

224. Lei X, Zhong Y, Huang L, Li S, Fu J, Zhang L, et al. Identification of a novel tumor angiogenesis inhibitor targeting Shh/Gli1 signaling pathway in Non-small cell lung cancer. Cell Death Dis. 2020 Apr 1;11(4):232.

225. Porta C, Cosmai L, Gallieni M, Pedrazzoli P, Malberti F. Renal effects of targeted anticancer therapies. Nat Rev Nephrol. 2015 Jun 28;11(6):354–70.

226. Helleday T. Chemotherapy-induced toxicity-A secondary effect caused by released DNA? Ann Oncol. 2017 Sep 1;28(9):2054–5.

227. Vauthey JN, Pawlik TM, Ribero D, Wu TT, Zorzi D, Hoff PM, et al. Chemotherapy regimen predicts steatohepatitis and an increase in 90-day mortality after surgery for hepatic colorectal metastases. J Clin Oncol. 2006 May 1;24(13):2065–72.

228. Fotiou D, Roussou M, Gakiopoulou C, Psimenou E, Gavriatopoulou M, Migkou M, et al. Carfilzomib-associated renal toxicity is common and unpredictable: a comprehensive analysis of 114 multiple myeloma patients. Blood Cancer J. 2020 Nov 1;10(11):109.

229. Pearson GW. Control of Invasion by Epithelial-to-Mesenchymal Transition Programs during Metastasis. J Clin Med. 2019 May 10;8(5):646.

230. Kalluri R. The biology and function of fibroblasts in cancer. Nat Rev Cancer. 2016 Sep 1;16(9):582–98.

231. Erdogan B, Webb DJ. Cancer-associated fibroblasts modulate growth factor signaling and extracellular matrix remodeling to regulate tumor metastasis. Biochem Soc Trans. 2017 Feb 8;45(1):229–36.

232. Fan H, Demirci U, Chen P. Emerging organoid models: Leaping forward in cancer research. J Hematol Oncol. 2019 Dec 29;12(1):142.

233. Lau HCH, Kranenburg O, Xiao H, Yu J. Organoid models of gastrointestinal cancers in basic and translational research. Nat Rev Gastroenterol Hepatol. 2020 Apr 1;17(4):203–22.

234. Hill DR, Spence JR. Gastrointestinal Organoids: Understanding the Molecular Basis of the Host–Microbe Interface. CMGH. 2017 Mar 1;3(2):138–49.

235. Young M, Reed KR. Organoids as a Model for Colorectal Cancer. Curr Colorectal Cancer Rep. 2016 Oct 1;12(5):281–7.

236. Ishiguro T, Ohata H, Sato A, Yamawaki K, Enomoto T, Okamoto K. Tumor-derived spheroids: Relevance to cancer stem cells and clinical applications. Cancer Sci. 2017 Mar 1;108(3):283–9.

237. Smigiel JM, Parameswaran N, Jackson MW. Potent EMT and CSC phenotypes are induced by oncostatin-M in pancreatic cancer. Mol Cancer Res. 2017 Apr 1;15(4):478–88.

238. Huang RYJ, Huang TYY. A new dimension in drug discovery: Reversing epithelial–mesenchymal transition (EMT). Cell Death Dis. 2016 Oct 13;7(10):e2417.

239. Marcucci F, Stassi G, De Maria R. Epithelial-mesenchymal transition: A new target in anticancer drug discovery. Nat Rev Drug Discov. 2016 May 1;15(5):311–25.

240. Yilmaz M, Christofori G. EMT, the cytoskeleton, and cancer cell invasion. Cancer Metastasis Rev. 2009;28(1–2):15–33.

241. Banno A, Garcia DA, Van Baarsel ED, Metz PJ, Fisch K, Widjaja CE, et al. Downregulation of 26S proteasome catalytic activity promotes epithelial-mesenchymal transition. Oncotarget. 2016 Apr 19;7(16):21527–41.

242. Wu Y, Wang Y, Lin Y, Liu Y, Wang Y, Jia J, et al. Dub3 inhibition suppresses breast cancer invasion and metastasis by promoting Snail1 degradation. Nat Commun. 2017 Feb 15;8:14228.

243. Xiao G, Li Y, Wang M, Li X, Qin S, Sun X, et al. FBXW7 suppresses epithelial-mesenchymal transition and chemo-resistance of non-small-cell lung cancer cells by targeting snai1 for ubiquitin-dependent degradation. Cell Prolif. 2018 Oct 1;51(5):e12473.

244. Xiao C, Wu G, Zhou Z, Zhang X, Wang YP, Song G, et al. RBBP6, a RING finger-domain E3 ubiquitin ligase, induces epithelial–mesenchymal transition and promotes metastasis of colorectal cancer. Cell Death Dis. 2019 Nov 1;10(11):833.

245. Hughes JP, Rees SS, Kalindjian SB, Philpott KL. Principles of early drug discovery. Br J Pharmacol. 2011 Mar;162(6):1239–49.

246. Yang J-Y, Zong CS, Xia W, Wei Y, Ali-Seyed M, Li Z, et al. MDM2 Promotes Cell Motility and Invasiveness by Regulating E-Cadherin Degradation. Mol Cell Biol. 2006 Oct 1;26(19):7269–82.

247. Chène P. Inhibiting the p53-MDM2 interaction: An important target for cancer therapy. Nat Rev Cancer. 2003 Feb;3(2):102–9.

248. Turbin DA, Cheang MCU, Bajdik CD, Gelmon KA, Yorida E, De Luca A, et al. MDM2 protein expression is a negative prognostic marker in breast carcinoma. Mod Pathol. 2006 Jan;19(1):69–74.

249. Vassilev LT, Vu BT, Graves B, Carvajal D, Podlaski F, Filipovic Z, et al. In Vivo Activation of the p53 Pathway by Small-Molecule Antagonists of MDM2. Science (80-). 2004 Feb 6;303(5659):844–8.

250. Landré V, Rotblat B, Melino S, Bernassola F, Melino G. Screening for E3-Ubiquitin ligase inhibitors: Challenges and opportunities. Oncotarget. 2014;5(18):7988–8013.

251. Wu Y, Fu Y, Zheng L, Lin G, Ma J, Lou J, et al. Nutlin-3 inhibits epithelial-mesenchymal transition by interfering with canonical transforming growth factor-β1-Smad-Snail/Slug axis. Cancer Lett. 2014 Jan 1;342(1):82–91.

252. Wang W, Qin JJ, Voruganti S, Srivenugopal KS, Nag S, Patil S, et al. The pyrido[b]indole MDM2 inhibitor SP-141 exerts potent therapeutic effects in breast cancer models. Nat Commun. 2014;5:5086.

253. Frisch SM, Schaller M, Cieply B. Mechanisms that link the oncogenic epithelial-mesenchymal transition to suppression of anoikis. J Cell Sci. 2013 Jan 1;126(1):21–9.

254. Pfeffer CM, Singh ATK. Apoptosis: A target for anticancer therapy. Int J Mol Sci. 2018 Feb 2;19(2):448.

255. Chebouti I, Kasimir-Bauer S, Buderath P, Wimberger P, Hauch S, Kimmig R, et al. EMT-like circulating tumor cells in ovarian cancer patients are enriched by platinum-based chemotherapy. Oncotarget. 2017;8(30):48820–31.

256. Fischer KR, Durrans A, Lee S, Sheng J, Li F, Wong STC, et al. Epithelial-to-mesenchymal transition is not required for lung metastasis but contributes to chemoresistance. Nature. 2015 Nov 26;527(7579):472–6.

257. Ashrafizadeh M, Zarrabi A, Hushmandi K, Kalantari M, Mohammadinejad R, Javaheri T, et al. Association of the epithelial–mesenchymal transition (EMT) with cisplatin resistance. Int J Mol Sci. 2020 Jun 1;21(11):4002.

258. Vodenkova S, Buchler T, Cervena K, Veskrnova V, Vodicka P, Vymetalkova V. 5-fluorouracil and other fluoropyrimidines in colorectal cancer: Past, present and future.

Pharmacol Ther. 2020 Feb 1;206:107447.

259. Shrestha H, Ryu T, Seo YW, Park SY, He Y, Dai W, et al. Hakai, an E3-ligase for E-cadherin, stabilizes δ-catenin through Src kinase. Cell Signal. 2017 Feb 1;31:135–45.

260. Mukherjee A, Madamsetty VS, Paul MK, Mukherjee S. Recent advancements of nanomedicine towards antiangiogenic therapy in cancer. Int J Mol Sci. 2020 Jan 1;21(2):455.

261. Balamurugan K. HIF-1 at the crossroads of hypoxia, inflammation, and cancer. Int J Cancer. 2016 Mar 1;138(5):1058–66.

262. Li C, Wang Q, Shen S, Wei X, Li G. HIF-1α/VEGF signaling-mediated epithelial–mesenchymal transition and angiogenesis is critically involved in anti-metastasis effect of luteolin in melanoma cells. Phyther Res. 2019 Mar 1;33(3):798–807.

263. Dong L, Li W, Lin T, Liu B, Hong Y, Zhang X, et al. PSF functions as a repressor of hypoxia-induced angiogenesis by promoting mitochondrial function. Cell Commun Signal. 2021 Dec 11;19(1):14.

264. Tang MKS, Yue PYK, Ip PP, Huang RL, Lai HC, Cheung ANY, et al. Soluble E-cadherin promotes tumor angiogenesis and localizes to exosome surface. Nat Commun. 2018 Dec 1;9(1):2270.

265. Sahni V, Choudhury D, Ahmed Z. Chemotherapy-associated renal dysfunction. Nat Rev Nephrol. 2009;5(8):450–62.

266. Alessandrino F, Qin L, Cruz G, Sahu S, Rosenthal MH, Meyerhardt JA, et al. 5-Fluorouracil induced liver toxicity in patients with colorectal cancer: role of computed tomography texture analysis as a potential biomarker. Abdom Radiol. 2019 Sep 15;44(9):3099–106.

267. Nowis D, Mączewski M, Mackiewicz U, Kujawa M, Ratajska A, Wieckowski MR, et al. Cardiotoxicity of the anticancer therapeutic agent bortezomib. Am J Pathol. 2010;176(6):2658–68.

268. Pancheri E, Guglielmi V, Wilczynski GM, Malatesta M, Tonin P, Tomelleri G, et al. Non-hematologic toxicity of bortezomib in multiple myeloma: The neuromuscular and cardiovascular adverse effects. Cancers (Basel). 2020 Sep 1;12(9):2540.

269. Soucy TA, Smith PG, Milhollen MA, Berger AJ, Gavin JM, Adhikari S, et al. An inhibitor of NEDD8-activating enzyme as a new approach to treat cancer. Nature. 2009 Apr 9;458(7239):732–6.

270. Shah JJ, Jakubowiak AJ, O'Connor OA, Orlowski RZ, Harvey RD, Smith MR, et al. Phase I study of the novel investigational NEDD8-activating enzyme inhibitor pevonedistat (MLN4924) in patients with relapsed/refractory multiple myeloma or lymphoma. Clin Cancer Res. 2016 Jan 1;22(1):34–43.

271. Sarantopoulos J, Shapiro GI, Cohen RB, Clark JW, Kauh JS, Weiss GJ, et al. Phase I study of the investigational nedd8-activating enzyme inhibitor pevonedistat (TAK-924/MLN4924) in patients with advanced solid tumors. Clin Cancer Res. 2016 Feb 15;22(4):847–57.

272. Martinez-Iglesias O, Casas-Pais A, Castosa R, Díaz-Díaz A, Roca-Lema D, Concha Á, et al. Hakin-1, a new specific small-molecule inhibitor for the E3 ubiquitin-ligase Hakai, inhibits carcinoma growth and progression. Cancers (Basel). 2020 May 1;12(5):1340.

273. Todaro M, Gaggianesi M, Catalano V, Benfante A, Iovino F, Biffoni M, et al. CD44v6 is a marker of constitutive and reprogrammed cancer stem cells driving colon cancer

metastasis. Cell Stem Cell. 2014 Mar 6;14(3):342–56.

274. Wang X, Zhang W, Sun X, Lin Y, Chen W. Cancer-associated fibroblasts induce epithelial-mesenchymal transition through secreted cytokines in endometrial cancer cells. Oncol Lett. 2018 Apr 1;15(4):5694–702.

275. Wang L, Zhang F, Cui JY, Chen L, Chen YT, Liu BW. CAFs enhance paclitaxel resistance by inducing EMT through the IL-6/JAK2/STAT3 pathway. Oncol Rep. 2018 May 1;39(5):2081–90.

276. Kim E, Kim W, Lee S, Chun J, Kang J, Park G, et al. TRAF4 promotes lung cancer aggressiveness by modulating tumor microenvironment in normal fibroblasts. Sci Rep. 2017 Dec 1;7(1):8923.

277. Wilson MM, Weinberg RA, Lees JA, Guen VJ. Emerging Mechanisms by which EMT Programs Control Stemness. Trends in Cancer. 2020 Sep 1;6(9):775–80.

278. Li N, Babaei-Jadidi R, Lorenzi F, Spencer-Dene B, Clarke P, Domingo E, et al. An FBXW7-ZEB2 axis links EMT and tumour microenvironment to promote colorectal cancer stem cells and chemoresistance. Oncogenesis. 2019 Mar 1;8(3):13.

279. Chan CH, Morrow JK, Li CF, Gao Y, Jin G, Moten A, et al. Pharmacological inactivation of Skp2 SCF ubiquitin ligase restricts cancer stem cell traits and cancer progression. Cell. 2013 Aug 1;154(3):556–68.

280. Jeon SA, Kim DW, Lee D Bin, Cho JY. NEDD4 Plays Roles in the Maintenance of Breast Cancer Stem Cell Characteristics. Front Oncol. 2020 Sep 2;10:1680.

281. Lee CH, Yu CC, Wang BY, Chang WW. Tumorsphere as an effective in vitro platform for screening anticancer stem cell drugs. Oncotarget. 2016 Oct 31;7(2):1215–26.

282. Koren E, Fuchs Y. The bad seed: Cancer stem cells in tumor development and resistance. Drug Resist Updat. 2016 Sep 1;28:1–12.

VIII. APPENDIXES

APPENDIX A

Summary of the thesis in Spanish

Introducción

El cáncer representa un conjunto de enfermedades de elevada prevalencia, y la segunda causa de muerte a nivel mundial, después de las enfermedades cardiovasculares. Teniendo en cuenta los datos más recientes publicados por la Organización Mundial de la Salud, en el año 2020 se han diagnosticado 19.3 millones de nuevos casos y se han registrado 10 millones de muertes debidas al cáncer. El cáncer es una enfermedad heterogénea que tiene su origen en la transformación de células normales en células tumorales, que se produce como resultado de la interacción entre factores genéticos y la exposición a agentes externos. Mientras que únicamente el 5-10% de los cánceres pueden atribuirse a causas genéticas, la mayoría de los casos (90-95%) se deben a factores ambientales.

La progresión tumoral es un proceso complejo que engloba varias etapas, e implica alteraciones genéticas que causan cambios tanto a nivel molecular como celular, provocando la transformación progresiva de las células normales hasta dar lugar a células cancerosas. Se han descrito ocho características biológicas que las células adquieren durante el desarrollo tumoral: 1) capacidad de crecimiento sin necesidad de señales externas, 2) insensibilidad a señales antimitogénicas, 3) capacidad de evadir la muerte celular (apoptosis), 4) adquisición de un potencial replicativo ilimitado, 5) capacidad de inducir angiogénesis, 6) capacidad de invadir nuevos tejidos y metastatizar, 7) reprogramación del metabolismo energético, y 8) evasión del sistema inmune. Aproximadamente el 90% de todos los cánceres humanos son carcinomas, y se caracterizan porque tienen su origen en la transformación de las células epiteliales. Las células epiteliales se caracterizan por presentar una polaridad apicobasal, estar conectadas entre sí mediante uniones célula-célula (uniones estrechas, uniones adherentes, uniones gap y desmosomas), y estar conectadas a una matriz extracelular mediante uniones célula-matriz. En condiciones normales, las células epiteliales presentan cierta movilidad y pueden separarse de las células vecinas más cercanas, aunque permanecen siempre dentro de la barrera epitelial y no se desprenden de ella. Los carcinomas se desarrollan normalmente en la capa basal del epitelio, donde se origina una primera lesión premaligna conocida como adenoma. Posteriormente, la acumulación de alteraciones genéticas y epigenéticas conducen a la transformación maligna y al desarrollo de un carcinoma *in situ*, todavía limitado a la membrana basal. La ganancia de nuevas alteraciones puede desencadenar la adquisición de un fenotipo móvil e invasivo, como consecuencia de un proceso conocido como transición epitelio-mesénquima (TEM). Finalmente, las células pueden intravasarse en vasos sanguíneos o linfáticos y extravasarse en órganos secundarios, dando lugar a la formación de metástasis.

La transición epitelio-mesénquima (TEM) tiene lugar durante las etapas tempranas del desarrollo de carcinomas. Es un proceso celular altamente conservado, descrito por primera vez durante el desarrollo embrionario, e implicado en numerosos procesos tanto fisiológicos como patológicos. Durante la TEM, las células epiteliales pierden la polaridad apicobasal, los contactos célula-célula, y sufren la reorganización del citoesqueleto de actina, dando lugar a células mesenquimales con características móviles e invasivas. La TEM no es un proceso estático, sino que las células pueden sufrir el proceso inverso conocido como transición mesénquima-epitelio (TME). Además, las células pueden perder el fenotipo epitelial únicamente de forma parcial, mediante la pérdida de parte de sus características epiteliales o mostrando una combinación de características epiteliales y mesenquimales. De esta manera, aunque la TEM se ha considerado tradicionalmente como un proceso binario, hoy en día se entiende como un proceso que engloba numerosos estados intermedios. Esta capacidad de las células de alternar entre un fenotipo epitelial y mesenquimal, así como la adquisición de fenotipos intermedios, recibe el nombre de plasticidad epitelial. Uno de los eventos clave que tienen lugar durante la transición epitelio-mesénquima es la pérdida de la E-cadherina en los contactos celulares, concretamente en las uniones adherentes. La E-cadherina representa el miembro prototipo y mejor caracterizado de la familia de las cadherinas, una familia de proteínas transmembrana que regulan las uniones adherentes en una manera dependiente de Ca^{+2}. Su estructura se basa en un dominio extracelular formado por cinco subdominios repetitivos y un dominio citoplasmático que favorece el anclaje al citoesqueleto de actina. La E-cadherina es considerada un supresor tumoral y su pérdida durante la progresión tumoral supone un marcador de mal pronóstico. Dada la importancia de la E-cadherina durante la progresión tumoral, numerosos estudios se han centrado en los mecanismos responsables de su regulación. Entre estos mecanismos se incluyen mutaciones, silenciamiento epigenético, silenciamiento transcripcional, endocitosis o procesamiento proteolítico. El primer regulador postraduccional de la estabilidad de la E-cadherina que ha sido descrito es Hakai, una E3 ubiquitina-ligasa identificada por Fujita y colaboradores en el año 2002. Hakai se une a la E-cadherina fosforilada, mediando su internalización y su posterior degradación dependiente de ubiquitina, alterando por lo tanto los contactos célula-célula.

La progresión tumoral también está regulada por el microambiente tumoral, que se compone de células estromales, factores secretados por estas (citocinas, quimiocinas y factores de crecimiento), y elementos no celulares que conforman la matriz extracelular. Estos factores secretados por las células estromales pueden inducir la TEM de forma paracrina, promoviendo por tanto el desarrollo tumoral y la metástasis. Por otro lado, a pesar de que la TEM se ha considerado el mecanismo principal en la adquisición de características migratorias e invasivas y la formación de metástasis, en los últimos años se ha visto que la TEM se relaciona también con el desarrollo de células madre tumorales (*cancer stem cells*, CSCs). Las CSCs son poblaciones minoritarias de células dentro del tumor que son capaces de originar nuevos tumores. Estas células se caracterizan porque presentan un potencial de auto-renovación indefinido y son capaces de diferenciarse en distintos linajes. Hoy en día, la mayor parte de las terapias antitumorales no son capaces de eliminar las CSCs, lo que se traduce la adquisición de resistencia y en un desarrollo fatal de la enfermedad como consecuencia de la selección y posterior expansión de las CSCs. De esta manera, dado que la TEM aumenta no solo la motilidad y la capacidad invasiva, sino también la adquisición de propiedades de células madre tumorales, la TEM podría cooperar con las CSCs durante la adquisición de resistencia a fármacos. Así, el desarrollo de inhibidores de la TEM que complementen a fármacos quimioterápicos o a terapias dirigidas representa una buena estrategia terapéutica que podría mejorar significativamente la evolución de los pacientes con cáncer.

El proceso de ubiquitinización consiste en la conjugación covalente de ubiquitina a un sustrato proteico, en un proceso dependiente de ATP. El sistema de degradación de proteínas dependiente de ubiquitina fue descrito por Aaron Ciechanover, Avram Hershko e Irwin Rose entre los años 1970 y 1990, logro por el que fueron galardonados con el Premio Nobel de Química en el año 2004. El proceso de ubiquitinización se caracteriza por la acción secuencial de tres enzimas distintas: enzima activadora de ubiquitina (E1), enzima conjugadora de ubiquitina (E2) y enzima ubiquitina-ligasa (E3). La enzima E3 ubiquitina-ligasa es la responsable del reconocimiento y la unión a las proteínas sustrato, por lo que en ella recae la especificidad del sistema. Las E3 ubiquitina ligasas representan un grupo numeroso y heterogéneo de enzimas, y se clasifican en tres grupos distintos (RING, HECT y RBR) en base a sus dominios específicos y al mecanismo que utilizan para transferir la ubiquitina a la proteína sustrato. Dado que el proceso de ubiquitinización se encuentra muy frecuentemente desregulado en cáncer, se han diseñado numerosos compuestos inhibidores dirigidos a las enzimas E1, E2 y E3, así como a las deubiquitinasas (DUBs) y el proteasoma. Sin embargo, hasta la fecha, únicamente tres inhibidores del proteasoma (bortezomib, carfilzomib y ixazomib) han sido aprobados por la Administración de Medicamentos y Alimentos (*Food and Drug Administration*, FDA). En los últimos años, el interés por las E3 ubiquitina-ligasas como dianas terapéuticas ha ido creciendo, ya que debido a su especificidad de sustrato se espera que su inhibición cause menos efectos secundarios que la inhibición del proteasoma o las enzimas E1 y E2.

Como se ha mencionado previamente, la E3 ubiquitina-ligasa Hakai fue identificada en el año 2002 por Fujita y colaboradores como el primer regulador postraduccional de la E-cadherina. Aunque otros sustratos fosforilados han sido descritos para Hakai, hasta el momento, la E-cadherina es el único que directamente se relaciona con el proceso de TEM. Hakai fue considerada inicialmente como una E3 ubiquitina-ligasa de tipo RING, sin embargo, a diferencia de otras E3 ubiquitina-ligasas, Hakai forma un dominio de unión a fosfotirosina atípico, conocido como HYB (*Hakai-pY-binding*). A diferencia de otros dominios de unión a fosfotirosina, el dominio HYB presenta una estructura dimérica, que es clave para la interacción con los sustratos fosforilados en tirosina. Además de en Hakai, este dominio se ha encontrado únicamente en otra

E3 ubiquitina-ligasa específica de testículo, RNF645, aunque muestra distinta especificidad de sustrato. Por lo tanto, teniendo en cuenta estas características estructurales únicas, el dominio HYB ha sido propuesto como una buena diana terapéutica para el tratamiento del cáncer. Dado que Fujita y colaboradores observaron que la expresión de Hakai inducía la endocitosis de la E-cadherina en los contactos celulares, estos autores sugirieron su posible implicación en el proceso de TEM, tanto en el desarrollo embrionario como durante la progresión tumoral. Desde ese momento, numerosos estudios han respaldado el papel de Hakai en ambos procesos. En lo que se refiere al desarrollo de carcinomas, Hakai se ha propuesto como un marcador de progresión tumoral en cáncer colorrectal (CRC) y cáncer de pulmón de células no pequeñas (NSCLC). Por otro lado, se ha visto que Hakai no sólo está implicada en la pérdida de los contactos célula-célula, sino que también promueve la proliferación celular en un modo independiente de la E-cadherina. En estos estudios, se han sugerido dos proteínas a través de las cuales Hakai podría regular la proliferación celular: PSF (factor de splicing asociado a PTB) y la Ciclina D1. Además, se ha observado que la sobreexpresión de Hakai no solo provoca la pérdida contactos celulares y la adquisición de un fenotipo mesenquimal, sino que también incrementa el potencial oncogénico e induce la adquisición de características migratorias e invasivas. Por lo tanto, considerando la implicación de Hakai en distintos aspectos de la progresión tumoral, su expresión aumentada en muestras de cáncer colorrectal y cáncer de pulmón, y su dominio único de unión a sustratos fosforilados (HYB), se considera una diana terapéutica muy prometedora para el tratamiento del cáncer.

Las estrategias terapéuticas actuales para el tratamiento del cáncer están dirigidas a dianas moleculares, lo que generalmente causa menos efectos secundarios que la quimioterapia convencional. Las terapias dirigidas para el tratamiento del cáncer se basan en el uso tanto de agentes biológicos (anticuerpos) como de moléculas pequeñas. A diferencia de los anticuerpos, las moléculas pequeñas presentan cierta variabilidad en cuanto a selectividad, aunque pueden reconocer un mayor número de dianas moleculares, tanto intracelulares como extracelulares. En los últimos años, la identificación de moléculas pequeñas capaces de modular la actividad de una proteína diana se han llevado a cabo mediante técnicas de cribado de alto rendimiento (*high throughput screening,* HTS). Aunque el HTS representa una buena estrategia para la identificación de moléculas candidatas, presenta ciertas limitaciones a la hora de identificar compuestos para bloquear interacciones proteína-proteína, y puede llegar a ser muy caro y requerir mucho tiempo. Esto ha llevado al desarrollo de una alternativa más barata, conocida como cribado virtual (*virtual screening*, VS), basada en la identificación de moléculas candidatas mediante un proceso informático. El VS permite el análisis de un elevado número de compuestos, lo que reduce el número de moléculas que deben ser ensayadas para identificar fármacos potenciales. De esta manera, el VS se ha convertido en los últimos años en una herramienta esencial en el desarrollo de fármacos.

Hipótesis y objetivos

Teniendo en cuenta todos estos antecedentes, la hipótesis general de este proyecto fue la siguiente:

- *La inhibición específica de la E3 ubiquitina-ligasa Hakai mediante moléculas de pequeño tamaño supone una buena estrategia terapéutica para el tratamiento del cáncer. Además, Hakai podría estar implicado en otros aspectos de la progresión tumoral además de la TEM, como la adquisición de propiedades de CSC.*

OBJETIVO 1

1. Desarrollar un inhibidor de molécula pequeña dirigido específicamente al dominio HYB de Hakai, y analizar su efecto antitumoral tanto *in vitro* como *in vivo*.

1.1. Búsqueda, mediante un cribado virtual, de pequeñas moléculas que potencialmente puedan inhibir la E3 ubiquitina-ligasa Hakai y selección moléculas candidatas.
1.2. Estudiar el efecto del inhibidor de molécula pequeña más prometedor sobre la ubiquitinación de E-cadherina mediada por Hakai y la interacción Hakai-E-cadherina, mediante ensayos bioquímicos.
1.3. Analizar el efecto antitumoral del compuesto seleccionado *in vitro*, mediante el uso de líneas celulares de cáncer colorrectal y un modelo de sobreexpresión de Hakai.
1.4. Analizar el efecto antitumoral del compuesto seleccionado *in vivo*, empleando un modelo de xenoinjerto en ratones inmunodeficientes BALB/c.

OBJETIVO 2

2. Estudiar la implicación de la E3 ubiquitina-ligasa Hakai en otros aspectos de la carcinogénesis, centrándose fundamentalmente en la adquisición de propiedades de CSC.

2.1. Profundizar en el estudio del papel del Hakai en la progresión tumoral, utilizando co-cultivos de líneas celulares de cáncer colorrectal y fibroblastos asociados al cáncer (CAFs) en una matriz de colágeno, o ‘ensayo de carcinoma *in vitro*’.
2.2. Establecer cultivos de organoides, utilizando muestras de pacientes de cáncer colorrectal, que permitan analizar en el futuro la implicación de Hakai en el desarrollo de CSCs así como en otros aspectos de la carcinogénesis.
2.3. Analizar el papel de Hakai en la adquisición de propiedades de célula madre tumoral, así como la capacidad del compuesto inhibidor de Hakai de regular el desarrollo de CSCs *in vitro*, mediante el uso de cultivos de tumorosferas de células de cáncer colorrectal.

Resultados del objetivo 1

Tal y como se recoge en los objetivos, el desarrollo de la presente tesis doctoral se inició partiendo de un cribado virtual, realizado en colaboración con el Dr. Federico Gago (Universidad de Alcalá) y el Dr. Álvaro Cortés (GSK Medicines Research Centre). En dicho cribado, utilizando la información estructural disponible y la naturaleza del dominio HYB, se seleccionaron una serie de moléculas de entre las 20 con mayor afinidad de unión al dímero de Hakai. Tras una validación experimental inicial, se seleccionó la molécula con mejores características, denominada Hakin-1 (*Hakai inhibitor 1*), para continuar con los ensayos *in vitro*.

Para determinar la capacidad de Hakin-1 de inhibir la interacción de Hakai y E-cadherina, se realizó un ensayo de co-inmunoprecipitación utilizando células HEK293 en las que se sobreexpresó Hakai, E-cadherina y Src de forma transitoria. La sobreexpresión de Hakai y E-cadherina se realizó con el objetivo de detectar la interacción entre ambas proteínas, ya que esta no se observa al tratar de co-inmunoprecipitar las proteínas endógenas. En las mismas condiciones de transfección, la co-inmunoprecipitación desapareció cuando las células se trataron con Hakin-1. Por otro lado, el tratamiento con Hakin-1 no afectó a los niveles de proteína Hakai, por lo que Hakin-1 es capaz de bloquear la interacción entre Hakai y E-cadherina, sin afectar a los niveles de expresión de Hakai. A continuación, se analizó el efecto de Hakin-1 sobre la ubiquitinización inducida por Hakai, utilizando células HEK293T en las que se sobreexpresó Hakai, E-cadherina, ubiquitina y Src de forma transitoria, analizando posteriormente el *smear* de ubiquitinización mediante Western Blot. El tratamiento con Hakin-1 redujo significativamente la ubiquitinización mediada por Hakai, de nuevo sin afectar a los niveles de proteína. Además, Hakin-1 no afectó al *smear* de ubiquitinización cuando Hakai no estaba sobreexpresado, sugiriendo que Hakin-1 es capaz de reducir la ubiquitinización global mediada por Hakai. Posteriormente, se analizó la capacidad de Hakin-1 para inhibir la ubiquitinización de E-cadherina mediada por Hakai, mediante un ensayo de inmunoprecipitación en células HEK293 transfectadas con Src, Hakai, E-cadherina y ubiquitina. Hakin-1 redujo el *smear* de ubiquitinización de E-cadherina, de forma dosis-dependiente, y de nuevo sin afectar los niveles de expresión de Hakai. Este resultado sugiere que Hakin-1 es capaz de inhibir específicamente la ubiquitinación de E-cadherina mediada por Hakai, actuando a través de la actividad de Hakai y no reduciendo sus niveles de expresión. Dado que Hakin-1 mostró un efecto importante en la ubiquitinización de E-cadherina mediada por Hakai, se decidió analizar mediante Western Blot su efecto en la degradación de E-cadherina, usando las células de cáncer colorrectal HCT116. Como se esperaba, la sobreexpresión de Hakai en las células HCT116 redujo los niveles de expresión de E-cadherina, que se recuperaron tras el tratamiento con Hakin-1. Esto indica que el tratamiento con Hakin-1 inhibe la degradación de E-cadherina inducida por Hakai.

A continuación, se analizó el efecto de Hakin-1 en la viabilidad celular, empleando líneas de cáncer colorrectal (LoVo, HCT116 y HT29) y un modelo de sobreexpresión de Hakai (células epiteliales MDCK sin transformar y células epiteliales MDCK que sobreexpresan Hakai de forma estable, o Hakai-MDCK). El tratamiento con Hakin-1 tuvo un mayor efecto sobre las células Hakai-MDCK, ya que mostraron valores de IC_{50} más bajos que las células MDCK no transformadas. Esto sugiere que Hakin-1 podría ser más efectivo cuando los niveles de Hakai son elevados. Hakin-1 también redujo la viabilidad en las células de cáncer colorrectal, siendo las HCT116 las más sensibles al tratamiento. Utilizando las mismas células empleadas en los ensayos de viabilidad, se determinó el efecto de Hakin-1 en la proliferación celular. Hakin-1 redujo significativamente la proliferación en las células Hakai-MDCK mientras que no mostró efecto antiproliferativo en las células MDCK no transformadas, sugiriendo de nuevo que podría ser más efectivo cuando Hakai está sobreexpresado. Hakin-1 redujo la proliferación celular también en las líneas de cáncer colorrectal, siendo de nuevo las HCT116 las más sensibles al tratamiento. Para hacer una primera aproximación del efecto de Hakin-1 se estudió su efecto antiproliferativo en otro tipo de carcinomas, usando líneas celulares de mama, próstata, ovario, hígado, vejiga y riñón. Hakin-1 redujo la proliferación en todas estas líneas salvo las de ovario, lo que indica que podría ser efectivo en otros tipos de carcinomas además del de colon.

Posteriormente, se analizó el efecto de Hakin-1 en la diferenciación epitelial, analizando el cambio fenotípico de las células MDCK, Hakai-MDCK, LoVo, HT29 y HCT116 tras el tratamiento con Hakin-1. De nuevo, Hakin-1 resultó ser muy efectivo en las células Hakai-MDCK, en las que se observó la adquisición de un fenotipo más epitelial tras el tratamiento. En las células de cáncer colorrectal, Hakin-1 produjo un cambio fenotípico menos evidente, siendo en este caso las HT29 las células que respondieron mejor al tratamiento. Para continuar determinando el efecto de Hakin-1 en la diferenciación epitelial, se analizaron los niveles de expresión de marcadores de TEM mediante Western Blot en las células HT29 y HCT116. Hakin-1 incrementó los niveles de E-cadherina en ambas líneas, y redujo los niveles del marcador mesenquimal Vimentina en las células HT29. El efecto de Hakin-1 sobre los marcadores de TEM se observó únicamente a nivel de proteína, ya que los niveles de expresión del ARNm de Hakai y E-cadherina no se vieron afectados por el tratamiento. Este resultado sugiere que Hakin-1 actúa a nivel postraduccional. Por último, se analizó el efecto de Hakin-1 en la localización subcelular de la E-cadherina, mediante ensayos de inmunofluorescencia, en las líneas celulares de cáncer colorrectal. Hakin-1 aumentó los niveles de expresión de E-cadherina en los contactos célula-célula en todas las líneas analizadas, observándose un efecto más significativo en las HCT116. Todos estos resultados sugieren que Hakin-1 es capaz de incrementar la diferenciación epitelial *in vitro*, mediante la regulación de la TEM.

Dado que la TEM se relaciona con la adquisición de propiedades migratorias e invasivas, se decidió estudiar el efecto de Hakin-1 en la invasión y migración celular. El análisis de la invasión celular se llevó a cabo en las líneas MDCK, Hakai-MDCK y LoVo. Las células MDCK no fueron capaces de invadir, como ya se había observado previamente. En las células Hakai-MDCK y LoVo, el tratamiento con Hakin-1 redujo drásticamente el número de células invasivas. Por otro lado, el efecto de Hakin-1 sobre la migración celular se analizó en las células HT29, que no habían sido capaces de invadir en las condiciones experimentales utilizadas en el ensayo de invasión. El tratamiento con Hakin-1 redujo significativamente el número de células capaces de migrar. Estos resultados sugieren que Hakin-1 es capaz de reducir la migración y la invasión celular *in vitro*. A continuación, se analizó el efecto de Hakin-1 sobre el potencial oncogénico, en las células Hakai-MDCK y HT29. Hakin-1 redujo significativamente la formación de colonias tanto en las células Hakai-MDCK como en las HT29, lo que sugiere que Hakin-1 podría ser capaz de reducir la transformación maligna de las células epiteliales.

Posteriormente, se decidió analizar el efecto de Hakin-1 en combinación con 5-fluorouracilo (5-FU). El 5-FU, así como otras fluoropirimidinas, se utilizan ampliamente en el tratamiento de cánceres sólidos, especialmente el cáncer colorrectal. Se ha observado que el 5-FU mejora la tasa de respuesta objetiva cuando se administra en terapias combinadas con leucovorina junto con oxaliplatino (FOLFOX) o irinotecán (FOLFIRI). Sin embargo, los regímenes combinados no han conseguido aumentar la supervivencia libre de enfermedad en los pacientes con cáncer colorrectal, por lo que se necesitan opciones terapéuticas alternativas. De esta manera, se analizó el efecto del tratamiento combinado de Hakin-1 y 5-FU sobre la viabilidad, la proliferación y la migración celular en la línea celular LoVo. Los resultados obtenidos indican que Hakin-1 no presenta un efecto sinérgico en combinación con 5-FU en la viabilidad, la proliferación o la migración celular, ya que el efecto global observado con el tratamiento combinado de Hakin-1 y 5-FU no es mayor que la suma de los efectos individuales de cada compuesto.

Dado el notable efecto de Hakin-1 sobre la TEM y la progresión tumoral observado *in vitro*, se decidió analizar el efecto antitumoral de análogos de Hakin-1 con el objetivo de encontrar un compuesto con mayor eficacia. Durante la fase inicial del descubrimiento de fármacos, una vez que se evalúa una molécula candidata y esta se considera terapéuticamente prometedora por su actividad biológica o farmacológica, se seleccionan compuestos análogos con el objetivo de encontrar un compuesto con mayor eficacia. Los análogos de Hakin-1 se seleccionaron en colaboración con un experto en química médica, siguiendo la estructura de Markush, y se validaron posteriormente en ensayos de citotoxicidad, ubiquitinización y diferenciación epitelial. Sin embargo, aunque el compuesto análogo Hakin A-7 fue capaz de reducir la ubiquitinación global mediada por Hakai y restaurar los niveles de E-cadherina en los contactos célula-célula, ninguno de los análogos probados resultó ser más eficaz que el compuesto inicial Hakin-1.

De esta manera, se decidió continuar los experimentos con Hakin-1, analizando su efecto antitumoral también *in vivo*, mediante un modelo de xenoinjerto en ratones inmunodeficientes BALB/c. Para ello, se inyectaron células MDCK y Hakai-MDCK por vía subcutánea en el flanco de ratones inmunodeficientes, y una vez que los tumores fueron palpables, se inició el tratamiento con Hakin-1 de forma intraperitoneal. Como se había observado anteriormente, las células Hakai-MDCK fueron capaces de formar tumores, al contrario que las células MDCK no transformadas. El tratamiento con Hakin-1 redujo significativamente el crecimiento tumoral. Además, las células Hakai-MDCK de los tumores tratados con Hakin-1 mostraron un fenotipo más diferenciado y un aumento del tamaño del citoplasma en comparación con los tumores de los ratones control. Este resultado sugiere que Hakin-1 induce la diferenciación tumoral *in vivo*. A continuación, se analizó el efecto de Hakin-1 sobre la proliferación celular, mediante el análisis inmunohistoquímico del marcador Ki67 y el estudio del índice mitótico mediante una tinción de hematoxilina-eosina en los tumores de los ratones inyectados con las células Hakai-MDCK. Los resultados mostraron que el tratamiento con Hakin-1 reduce significativamente el número de células proliferativas, lo que sugiere que Hakin-1 es capaz de reducir la proliferación celular *in vivo*. Por otro lado, se analizó el efecto de Hakin-1 sobre la apoptosis, y se observó que el tratamiento con Hakin-1 no induce la muerte celular. Este resultado indica que Hakin-1 reduce el crecimiento tumoral mediante la inhibición de la proliferación, y no a través de su acción sobre la apoptosis.

A continuación, se decidió analizar la capacidad de Hakin-1 para inhibir la angiogénesis, ya que representa otro de los eventos clave que tienen lugar durante la progresión tumoral. El análisis inmunohistoquímico del marcador endotelial CD31 en los tumores de los ratones inoculados con las células Hakai-MDCK, mostró una fuerte reducción del número de vasos sanguíneos en los xenoinjertos tumorales tras el tratamiento con Hakin-1. Esto sugiere que Hakin-1 podría ser capaz de reducir la angiogénesis *in vivo*.

Dado el efecto de Hakin-1 en la regulación de los marcadores de TEM observado previamente *in vitro*, se decidió analizar la capacidad de Hakin-1 de revertir el proceso de TEM *in vivo*. El análisis inmunohistoquímico de los tumores de los ratones mostró una reducción significativa del marcador mesenquimal N-cadherina tras el tratamiento con Hakin-1. Sin embargo, no se detectó expresión de E-cadherina en los xenoinjertos tumorales tanto en presencia como en ausencia de Hakin-1. Dado que Hakai actúa a nivel postraduccional, y las células no expresan proteína E-cadherina, Hakin-1 no es capaz de incrementar los niveles proteicos de E-cadherina cuando esta está completamente ausente. Además, como se había observado previamente *in vitro*, el tratamiento con Hakin-1 no afectó a los niveles de expresión de Hakai tampoco *in vivo*. Como se ha descrito anteriormente, la TEM se ha asociado a muchos aspectos de la progresión tumoral, incluido el desarrollo de metástasis. Es importante destacar que, aunque no se detectaron metástasis en el análisis histológico de los pulmones de los ratones, el análisis por qPCR del ADN de las células Hakai-MDCK reveló una reducción significativa de la formación de micrometástasis en los ratones tratados con Hakin-1. Este resultado sugiere que Hakin-1 es capaz de reducir el desarrollo de micrometástasis pulmonares *in vivo*.

Finalmente, se decidió analizar si el tratamiento con Hakin-1 causaba toxicidad en otros órganos, por lo que examinaron el hígado y el riñón de los ratones xenoinjertados tras una tinción de hematoxilina-eosina. El análisis de los tejidos hepáticos y renales tras el tratamiento con Hakin-1 mostró que estos presentaban una estructura morfológica normal, confirmada por el experto patólogo Dr. Ángel Concha. Todos estos resultados indican que Hakin-1 inhibe el crecimiento y la progresión tumoral *in vivo*, sin causar toxicidad sistémica aparente.

Resultados del objetivo 2

El segundo objetivo de la presente tesis doctoral consistió en estudiar la implicación de la E3 ubiquitina-ligasa Hakai en otros aspectos de la carcinogénesis, centrándose fundamentalmente en la adquisición de propiedades de CSC. En primer lugar, mediante la realización de una estancia predoctoctoral en el grupo de investigación del Dr. Helmut Dolznig (Universidad Médica de Viena), se realizaron co-cultivos esferoides de células de cáncer colorrectal y fibroblastos asociados al cáncer (CAFs) en una matriz de colágeno. Este modelo, conocido como ‘ensayo de carcinoma *in vitro*’ representa una mejor alternativa que los tradicionales cultivos en monocapa para el estudio de la progresión tumoral. Mediante el análisis de estos cultivos por inmunofluorescencia, se observó la expresión predominante de Hakai en las estructuras invasivas generadas en los esferoides de las células HCT116 como consecuencia del co-cultivo con los CAFs. Este resultado respalda el papel de Hakai en la adquisición de capacidades invasivas. Además, se observó una gran expresión de Hakai en los fibroblastos, lo que constituye la primera observación de la implicación de Hakai en la biología de los CAFs.

Dada la expresión predominante de Hakai en las estructuras invasivas de los esferoides de HCT116, se decidió analizar el efecto de su silenciamiento, mediante la transfección transitoria de las células HCT116 con el ARN de silenciamiento de Hakai. El silenciamiento de Hakai redujo significativamente la formación de estructuras invasivas, lo que apoya todavía más el papel potencial de Hakai en la adquisición de propiedades invasivas. Por otro lado, y dada la expresión predominante de Hakai en los CAFs, se decidió analizar la posible implicación de Hakai en la biología de los mismos. Para ello, se analizó el efecto del silenciamiento de Hakai en la capacidad contráctil de los fibroblastos. Los resultados obtenidos mostraron que el silenciamiento de Hakai no afectó a la capacidad contráctil de los CAFs. Finalmente, se decidió analizar mediante Western Blot si los factores liberados por los CAFs incrementaban los niveles de Hakai en las células de cáncer colorrectal. Los resultados obtenidos no mostraron cambios en los niveles de expresión Hakai en las líneas celulares de cáncer colorrectal tras el cultivo de estas en medio condicionado de los CAFs. De esta manera, se necesitan más investigaciones para dilucidar la posible implicación de Hakai en la biología de los fibroblastos asociados al cáncer.

Como se ha mencionado previamente, el éxito de las terapias dirigidas para el tratamiento del cáncer suele estar limitado por el desarrollo de resistencia a los fármacos, que surge como consecuencia de las poblaciones minoritarias de células capaces de originar nuevos tumores, conocidas como células madre tumorales (*cancer stem cells,* CSCs). Dadas las fuertes evidencias que apoyan el vínculo entre la TEM y la adquisición de propiedades de CSC, se decidió analizar la implicación de Hakai en la adquisición de dichas propiedades. Para ello, se realizaron cultivos de tumorosferas (enriquecidos en CSCs) utilizando la línea celular HCT116. Los resultados mostraron un aumento de los niveles de expresión de ARNm de los marcadores de pluripotencia y una reducción de la expresión de los marcadores de diferenciación en las tumorosferas, en comparación a los cultivos en monocapa. Además, los niveles de expresión de Hakai aumentaron notablemente en los cultivos de tumorosferas en comparación con los cultivos en monocapa. Por lo tanto, este resultado podría sugerir la implicación de Hakai en el desarrollo de las células madre tumorales. Dado el aumento observado de la expresión de Hakai en los cultivos de tumorosferas, se decidió analizar la capacidad de Hakin-1 de modular la adquisición de propiedades de CSC *in vitro*. El análisis mediante contraste de fases reveló que las tumorosferas mostraron un fenotipo más diferenciado tras el tratamiento con Hakin-1. La diferenciación de las tumorosferas se corroboró con el análisis mediante qPCR de los niveles de expresión de los genes de pluripotencia y de diferenciación. El tratamiento con Hakin-1 redujo los niveles de expresión de los genes de pluripotencia y aumentó ligeramente la expresión de los genes de diferenciación en las tumorosferas. Sin embargo, los niveles de expresión de Hakai no se vieron modificados tras el tratamiento con Hakin-1, lo que concuerda con los resultados obtenidos previamente en los cultivos en monocapa. Este resultado apoya la posible implicación de Hakai en la adquisición de propiedades *stem* al tiempo que sugiere que Hakin-1 podría tener la capacidad de afectar al desarrollo de CSCs.

Por último, se decidió seguir explorando la capacidad de Hakin-1 para modular la expresión de los marcadores de células madre tumorales, utilizando las muestras de tumores de ratones inoculados con células Hakai-MDCK del modelo *in vivo* anterior. El análisis mediante qPCR mostró que el tratamiento con Hakin-1 redujo los niveles de expresión de los marcadores de pluripotencia, lo que sugiere que Hakin-1 podría ser capaz de inhibir la adquisición de propiedades de CSC *in vivo*. Además, este resultado sugiere indirectamente la posible implicación de Hakai en el desarrollo de las propiedades *stem*, ya que Hakin-1 actúa a través de la inhibición de esta proteína.

Conclusiones

Los resultados obtenidos en el presente trabajo nos han permitido extraer las siguientes conclusiones:

Conclusiones relativas al objetivo 1:

1. Hakin-1 reduce la ubiquitinación de E-cadherina mediada por Hakai, así como la ubiquitinación general mediada por Hakai, de forma dependiente de la dosis.
2. Hakin-1 inhibe significativamente la viabilidad y la proliferación de las células epiteliales cancerosas *in vitro*, mostrando un mayor efecto citotóxico y antiproliferativo cuando Hakai está sobreexpresado.
3. Hakin-1 regula el proceso de TEM e induce la diferenciación epitelial tanto *in vitro* como *in vivo*, aumentando los niveles de E-cadherina en los contactos célula-célula y disminuyendo los marcadores mesenquimales N-cadherina y Vimentina.
4. Hakin-1 reduce la migración celular, la capacidad invasiva y el potencial oncogénico *in vitro*.
5. Hakin-1 no muestra un efecto sinérgico en combinación con el 5-fluorouracilo al analizar la viabilidad, proliferación o migración celular.
6. Ninguno de los compuestos análogos de Hakin-1 analizados muestra un mayor efecto antitumoral *in vitro* en comparación con Hakin-1.
7. Hakin-1 reduce el crecimiento tumoral *in vivo*, mediante la reducción de la proliferación celular en lugar de la inducción de la apoptosis.
8. Hakin-1 inhibe la angiogénesis y las micrometástasis pulmonares *in vivo*, sin toxicidad sistémica aparente.

Conclusiones relativas al objetivo 2

1. El 'ensayo de carcinoma *in vitro*' muestra que Hakai está implicado en el desarrollo de propiedades invasivas, dada su expresión predominante en las estructuras invasivas, cuya formación disminuye cuando Hakai está silenciado.
2. El silenciamiento de Hakai en fibroblastos asociados al cáncer (CAFs) no afecta a las propiedades contráctiles de los mismos.
3. Los factores secretados por los CAFs no inducen la expresión de Hakai en las líneas celulares de cáncer colorrectal.

4. Hakai podría desempeñar un papel en el desarrollo de las células madre tumorales, ya que su expresión aumenta en los cultivos de tumorosferas.
5. Hakin-1 podría tener un efecto sobre el desarrollo de CSCs, ya que aumenta la diferenciación de las tumorosferas, al regular a la baja los genes de pluripotencia y al alza los de diferenciación, y reduce la expresión de los marcadores del pluripotencia *in vivo*.

APPENDIX B

Publications related to the present thesis

- Martinez-Iglesias O*, **Casas-Pais A***, Castosa R, Díaz-Díaz A, Roca-Lema D, Concha Á, et al. Hakin-1, a new specific small-molecule inhibitor for the E3 ubiquitin-ligase Hakai, inhibits carcinoma growth and progression. Cancers (Basel). 2020 May 1;12(5):1340 ***Co-first authors**

cancers

MDPI

Article

Hakin-1, a New Specific Small-Molecule Inhibitor for the E3 Ubiquitin-Ligase Hakai, Inhibits Carcinoma Growth and Progression

Olaia Martinez-Iglesias [1,†], Alba Casas-Pais [1,†], Raquel Castosa [1], Andrea Díaz-Díaz [1], Daniel Roca-Lema [1], Ángel Concha [2], Álvaro Cortés [3], Federico Gago [4] and Angélica Figueroa [1,*]

[1] Epithelial Plasticity and Metastasis Group, Instituto de Investigación Biomédica de A Coruña (INIBIC), Complexo Hospitalario Universitario de A Coruña (CHUAC), Sergas, Universidade da Coruña (UDC), 15006 A Coruña, Spain; oami@hotmail.es (O.M.-I.); alba.casas.pais@sergas.es (A.C.-P.); raquel.carballo.castosa@sergas.es (R.C.); andrea.diaz.diaz@sergas.es (A.D.-D.); daniel.roca.lema@sergas.es (D.R.-L.)

[2] Pathology Department and A Coruña Biobank from Instituto de Investigación Biomédica de A Coruña (INIBIC), Complexo Hospitalario Universitario de A Coruña (CHUAC), Sergas, Universidade da Coruña (UDC), 15006 A Coruña, Spain; angel.concha.lopez@sergas.es

[3] Computational Chemistry-UK, RD Platform Technology & Science, GSK Medicines Research Centre, Hertfordshire SG12 0DP, UK; alvarocortes@gmail.com

[4] Area of Pharmacology, Department of Biomedical Sciences and "Unidad Asociada IQM-CSIC", School of Medicine and Health Sciences, University of Alcalá de Henares, 28805 Alcalá de Henares, Spain; federico.gago@uah.es

* Correspondence: angelica.figueroa.conde-valvis@sergas.es

† These authors contributed equally to this work.

Received: 24 April 2020; Accepted: 21 May 2020; Published: 23 May 2020

Abstract: The requirement of the E3 ubiquitin-ligase Hakai for the ubiquitination and subsequent degradation of E-cadherin has been associated with enhanced epithelial-to-mesenchymal transition (EMT), tumour progression and carcinoma metastasis. To date, most of the reported EMT-related inhibitors were not developed for anti-EMT purposes, but indirectly affect EMT. On the other hand, E3 ubiquitin-ligase enzymes have recently emerged as promising therapeutic targets, as their specific inhibition would prevent wider side effects. Given this background, a virtual screening was performed to identify novel specific inhibitors of Hakai, targeted against its phosphotyrosine-binding pocket, where phosphorylated-E-cadherin specifically binds. We selected a candidate inhibitor, Hakin-1, which showed an important effect on Hakai-induced ubiquitination. Hakin-1 also inhibited carcinoma growth and tumour progression both in vitro, in colorectal cancer cell lines, and in vivo, in a tumour xenograft mouse model, without apparent systemic toxicity in mice. Our results show for the first time that a small molecule putatively targeting the E3 ubiquitin-ligase Hakai inhibits Hakai-dependent ubiquitination of E-cadherin, having an impact on the EMT process. This represents an important step forward in a future development of an effective therapeutic drug to prevent or inhibit carcinoma tumour progression.

Keywords: anticancer therapy; small-molecule inhibitor; epithelial-to-mesenchymal transition (EMT); E-cadherin; E3 ubiquitin-ligase; Hakai

1. Introduction

Carcinoma, the most common type of cancer, arises from epithelial cells. During carcinoma progression, epithelial cells acquire a high degree of plasticity and the ability to reversibly change phenotype [1,2]. Epithelial cells can undergo a program named epithelial-to-mesenchymal transition (EMT), priming their migration from the primary tumour, their dissemination and metastasis formation [3,4]. During EMT, epithelial cells acquire mesenchymal features due to the loss of cell-to-cell adhesion and apico-basal polarity, and the reorganization of actin cytoskeleton, which in turn causes the development of migratory and invasive capabilities. EMT has been associated with tumour initiation, migration, malignant progression, stemness, intravasation, metastasis, and drug resistance, with important clinical implications [5,6]. EMT is characterized by the loss of E-cadherin epithelial marker and the acquisition of mesenchymal markers, such as N-cadherin and vimentin. The loss of E-cadherin, the best characterized member of cadherins at cell–cell contacts in epithelial cells, is not only a hallmark of EMT but is also associated with the transition from adenoma to carcinoma [7,8]. The mechanisms involved in E-cadherin down-regulation and its pathological relevance have been extensively studied in cancer [9–11].

Hakai is the first posttranslational regulator of E-cadherin stability that has been described. Hakai is an E3 ubiquitin-ligase that interacts with tyrosine-phosphorylated E-cadherin, inducing its ubiquitination and degradation. This leads to disruption of cell–cell contacts in epithelial cells [12,13]. Ubiquitination is one of the most studied processes for post-translational regulation that signals for protein degradation via proteasome, lysosome or marks organelles for autophagy clearance [14–16]. There are three enzymatic reactions involved in the assembly of ubiquitin on substrate proteins. The E1 ubiquitin-activating enzyme is responsible for ubiquitin activation in an ATP-dependent manner. Then, ubiquitin is transferred to the E2 ubiquitin-conjugating enzyme and, finally, the ubiquitin moiety is transferred to the E3 ubiquitin-ligase, which attaches ubiquitin to the target protein to be degraded. Although ubiquitination is a multistep process, the E3 ubiquitin-ligase enzyme is responsible for the direct binding of ubiquitin to the target protein, thus conferring substrate specificity and selectivity [17,18]. Although targeting E1, E2 and the proteasome is possible, the development of inhibitors against specific E3 ubiquitin-ligases has attracted significant attention in recent years, since they can be designed to target specific substrates without affecting others, thus avoiding broader side effects [19,20]. A large body of evidence demonstrates deregulation of E3 ubiquitin-ligases in cancer [21–23], including their overexpression, which correlates with poor clinical prognosis and chemoresistance. Consequently, many different strategies to target ubiquitin-ligases for the treatment of cancer and other diseases have been investigated [24,25]. To date, the FDA has approved very few drugs that target members of the ubiquitin pathway [26]. The first 20S proteasome inhibitor, bortezomib, was approved in 2003, followed about a decade later by carfilzomib (2012) and ixazomib (2015) [27–30]. However, positive results with these drugs have only been observed in haematological malignancies; in contrast, the results from clinical trials on patients bearing solid tumours have been disappointing [31,32].

The E3 ubiquitin-ligase Hakai is essential for E-cadherin degradation and EMT induction. Moreover, Hakai-mediated down-regulation of E-cadherin is implicated in oncogenic and/or tumour-suppressive pathways such as RACK1 and Slit-Robo [13,33,34]. Hakai was not only described to regulate EMT through its action on E-cadherin [34] and cell proliferation in an E-cadherin independent manner, but also to be implicated in cell invasion and metastasis [34–41]. Although other Hakai substrates have been proposed, the physiological significance of these interactions is not well defined yet. For instance, Hakai interacts with cortactin, and mediates its ubiquitination and degradation after phosphorylation by non-receptor tyrosine kinase Src [35,42,43]. Furthermore, a recent study reports that Hakai regulates Ajuba stability, inducing Ajuba neddylation and degradation in hepatocarcinoma [44]. Hakai is a new class of RING-finger type E3 ubiquitin-ligase, which contains a novel domain named HYB (Hakai pTyr-binding, where pTyr stands for phosphotyrosine), that is structurally different from other pTyr-binding domains of E3 ubiquitin-ligases and represents a potentially attractive new drug target for anticancer therapy [32,45,46]. By using a three-dimensional structural model of Hakai's HYB domain, a virtual screening campaign identified several small molecules with putative affinity for this site. We demonstrate that our small-molecule compound Hakin-1 (Hakai inhibitor-1) reduces

Hakai-dependent total ubiquitination and Hakai-dependent ubiquitination of E-cadherin. Hakin-1 inhibits cell proliferation, oncogenic potential and invasion, and these effects are accompanied by induction of epithelial markers and reduction of mesenchymal markers in vitro. Moreover, we support the potential therapeutic value of Hakin-1 by demonstrating its antiproliferative effect in a tumour xenograft model. In conclusion, we describe Hakin-1 as the first Hakai-targeted small-molecule inhibitor that is endowed with significant antitumour activity.

2. Results

2.1. Identification of Putative Selective Hakai Inhibitors

With the aim of finding candidate molecules with the required potential to inhibit Hakai, we designed a virtual screening workflow based on the structural information available and the nature of the pTyr-binding pocket, which was explored with the aid of affinity probes [35]. As a first step, we considered only molecules in our chemical library that display a negatively charged carboxylate or phosphate group that would be complementary to the highly positive molecular electrostatic potential of the binding pocket. The selected molecules were docked into the Hakai dimer to evaluate all possible binding poses and then, they were ranked using the HYDE postprocessing scoring function to estimate the interaction energy of the hypothetical Hakai-inhibitor complexes. The first 20 top-ranking molecules were visually inspected and two of them were selected for subsequent experimental validation, namely Hakin-1 and Hakin-5 (Figure 1a). According to our binding mode model, the benzoate moiety present in Hakin-1 would be a surrogate of pTyr (Figure 1b, upper panel). The carboxylate group is placed in an extremely favourable region for a negatively charged probe, as befits matching to the area highlighted by our previously calculated affinity maps. This region is lined by residues Lys-126, Tyr-176, His-185 and Arg-189. The phenyl ring, in turn, would get sandwiched between the guanidinium side chains of Arg-174 and Arg-189 and be stabilized by cation–π interactions. The rest of the molecule would further adapt to the binding pocket by establishing hydrogen bonds with the side chains of Arg-174 from both monomers and the Gln-170 backbone. Hakin-5 (Figure 1b, lower panel), despite bearing a carboxylate group and presenting an equivalent number of potential groups for hydrogen bonding interactions, lacks a phenyl ring that could mimic a pTyr and is predicted to have lower affinity (Figure S1).

2.2. Effect of Hakin-1 on Hakai-Induced Ubiquitination

We first investigated the effect of Hakin-1 on the enzymatic activity of E3 ubiquitin-ligase Hakai in cultured tumour cells. HEK293T cells were transfected with Src (in order to induce tyrosine phosphorylation of the E-cadherin complex) together with Hakai and ubiquitin in the presence of Hakin-1 or DMSO as control (vehicle). Hakin-1 strongly reduced the ubiquitination mediated by Hakai in a dose-dependent manner (Figure 1c) while no effect was observed in Hakai protein levels. However, Hakin-1 did not affect ubiquitination when Hakai was not overexpressed, confirming that Hakin-1 reduced the ubiquitination in a Hakai-dependent manner (Figure 1d). Moreover, no effect was detected on Hakai-mediated ubiquitination when cells were treated in the presence of Hakin-5, (Figure 1e), further supporting the specific effect of Hakin-1 on Hakai-induced ubiquitination. Finally, we observed a reduction of Hakai-dependent ubiquitination of the E-cadherin complex when cells were treated with Hakin-1 (Figure 1f). Collectively, our data show that Hakin-1 inhibits Hakai-mediated ubiquitination without affecting Hakai protein levels.

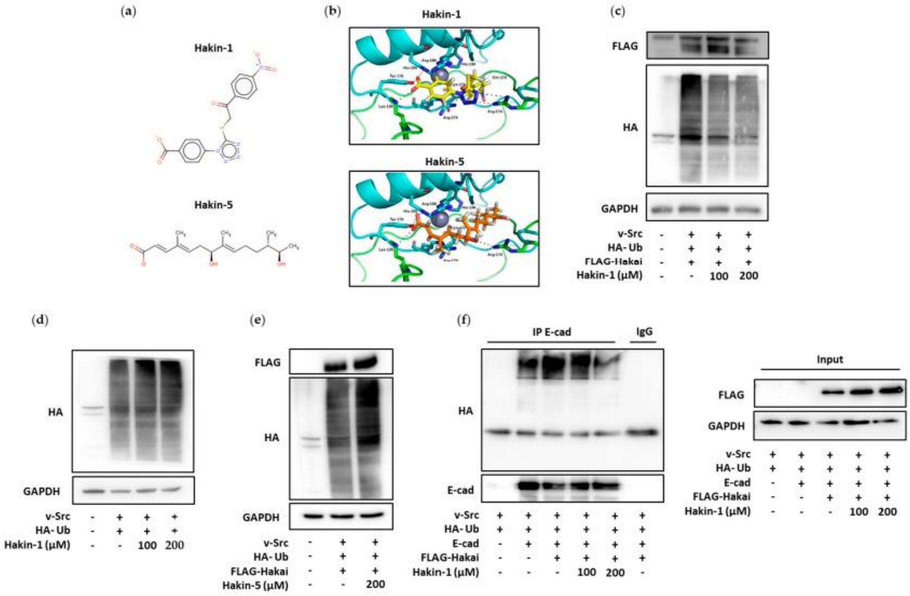

Figure 1. In silico and in vivo screening of E3 ubiquitin-ligase Hakai inhibitors (**a**) Chemical structure of Hakin-1 and Hakin-5. (**b**) Predicted binding poses for Hakin-1 (upper panel, in yellow) and Hakin-5 (bottom panel, in orange) molecules docked within Hakai dimers (represented in blue and green), as determined by the CRDOCK docking program. (**c**) Hakai-dependent ubiquitination assay in HEK293 cells transfected with Flag-Hakai, v-Src and HA-ubiquitin in the presence of either DMSO or compound Hakin-1. (**d**) Ubiquitination assay in HEK293T cells transfected with v-Src and HA-ubiquitin in presence of DMSO or compound Hakin-1. (**e**) Hakai-dependent ubiquitination assay in HEK293T cells transfected with Flag-Hakai, v-Src and HA-ubiquitin in the presence of either DMSO or compound Hakin-5. (**f**) Effects of Hakin-1 on Hakai-dependent ubiquitination of the E-cadherin complex. Flag-Hakai, myc-E-cadherin, v-Src and HA–ubiquitin were transiently transfected into HEK293 cells. Immunoprecipitation was performed with the anti-E-cadherin antibody before Western blotting using the indicated antibodies.

2.3. Hakin-1 Activates Epithelial Cell Differentiation in Tumour Cells

Next, we studied the effect of Hakin-1 on cancer cell viability. We observed a dose-dependent effect of Hakin-1 on the viability of HT-29 and LoVo colon cancer cell lines (Figure 2a). In contrast, no inhibitory effect was detected when treating the same cells with Hakin-5 (Figure S2). Furthermore, we previously showed that Hakai overexpression in immortalized epithelial MDCK cells (Hakai-MDCK) induced a fibroblastic-like phenotype accompanied by the loss of E-cadherin-based cell–cell contacts [38,40]. Hakin-1 treatment was more effective at reducing the proliferation of Hakai-MDCK clones than in control MDCK nontransformed epithelial cells without overexpression (Figure 2b). These results further suggest that Hakin-1 may be particularly more cytotoxic against cancer cells that overexpress Hakai, accompanied by a slightly increased apoptosis in vitro (Figure S3). Based on the role of Hakai inducing EMT, we analysed the effect of Hakin-1 on the epithelial phenotype. By phase contrast microscopy, we observed that Hakin-1 modestly increased the epithelial phenotype of HT-29 and LoVo cells (Figure 2c). Moreover, we observed an induction of an epithelial phenotype, increased cell–cell contacts, and reduction of cytoplasmic protrusions formation, in Hakai-MDCK but not in control cells (Figure 2d). On the contrary, no effect was observed upon Hakin-5 treatment (Figure S4). We further studied the effect of Hakin-1 on the reversion of EMT markers. Increased E-cadherin epithelial marker and reduced vimentin levels were detected in Hakin-1 treated HT-29 cells (Figure 3a). We also detected that Hakin-1 increased cortactin protein, another described substrate of Hakai ubiquitination [42].

These results were confirmed in LoVo colon cancer cells (Figure 3b). Moreover, in both HT-29 and LoVo cell lines, a slight but not statistically significant decrease in Hakai expression after Hakin-1 treatment was detected (Figure S5).

Moreover, Hakin-1 did not modulate the mRNA levels of E-cadherin or Hakai confirming that its activity is mostly to control target protein degradation (Figure 3c). Hakin-1 increased the amount of E-cadherin levels at cell–cell contacts in HT-29 and LoVo cells, as detected by immunofluorescence (Figure 3d). However, no effect was detected on protein levels or localization of E-cadherin upon Hakin-5 treatment in HT-29 cells (Figure S6). Finally, we observed that Hakin-1 did not increase E-cadherin expression in Hakai-MDCK cells which, as previously reported, had a complete lack of E-cadherin basal levels [38,41]. Taken together, these results demonstrate that Hakin-1 induces epithelial differentiation in different tumour cells that is accompanied by a reduction of mesenchymal markers.

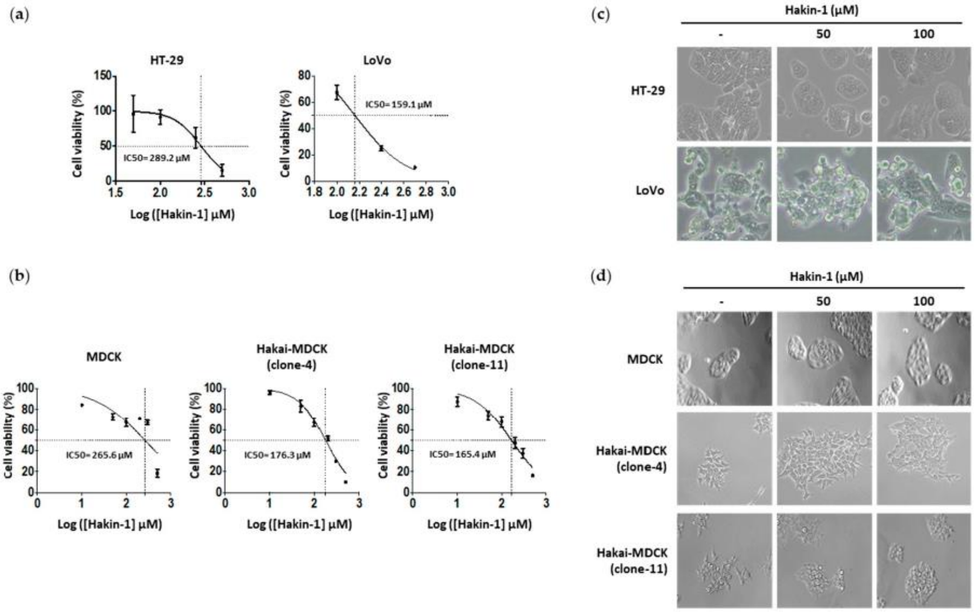

Figure 2. Hakin-1 induces cytotoxicity and an epithelial phenotype on epithelial tumour cell lines. (**a**) HT-29 and LoVo cells were treated with an increasing range of concentrations of Hakin-1 and cell viability was measured by means of the MTT assay (3-(4,5-dimethylthiazol-2-yl)-2,5-diphenyltetrazolium bromide). This assay was performed in six replicates and represented as mean ± SD of three independent experiments. (**b**) Cell viability was measured as indicated in panel (**a**), for MDCK and Hakai-MDCK cell lines (clone 4 and clone 11) using Hakin-1. (**c**,**d**) Phase-contrast images of HT-29 and LoVo cell lines (**c**) and MDCK, Hakai-MDCK cell lines, clone 4 and clone 11 (**d**) under Hakin-1 treatment. Images were obtained using a 20× objective.

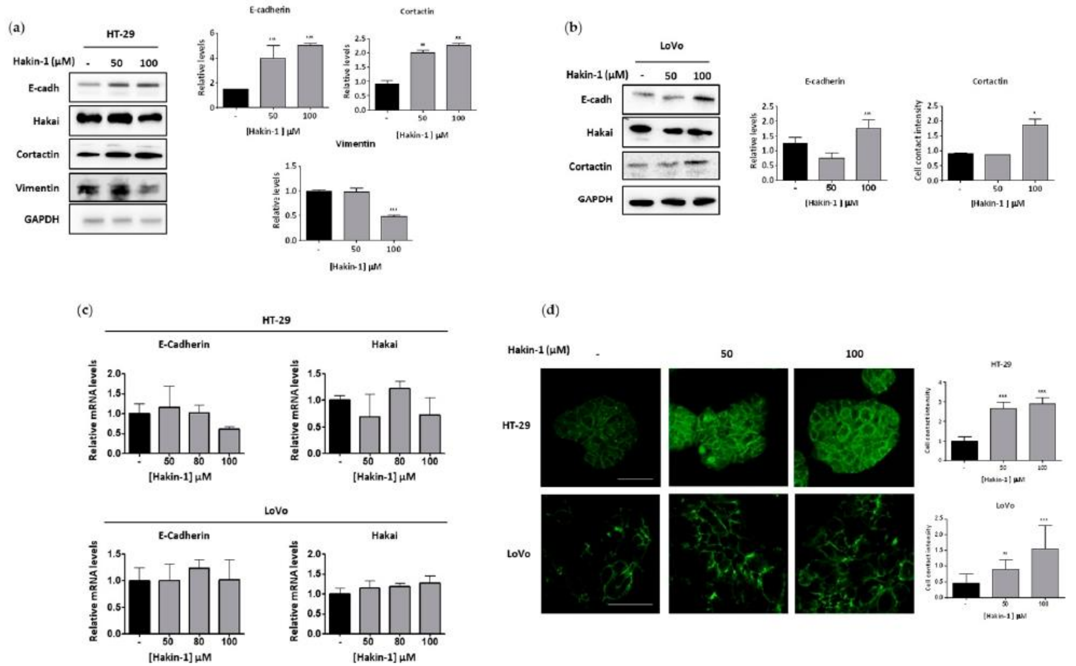

Figure 3. Hakin-1 induces mesenchymal-to-epithelial transition in epithelial tumour cell lines. (**a**) Western blotting analyses of epithelial-to-mesenchymal transition (EMT) markers upon Hakin-1 treatment in HT-29 cell line (left panel), and quantification by densitometry are shown (right panel). (**b**) Western blotting analyses of EMT markers upon Hakin-1 treatment in LoVo cells (left panel), and quantification by densitometry are shown (right panel). GAPDH was used as the loading control. Data show the average of three independent experiments and are represented as mean ± SD (* $p < 0.05$; ** $p < 0.01$; *** $p < 0.001$). (**c**) Hakai and E-cadherin mRNA expression levels normalized to control. RPL13A mRNA were measured in HT-29 and LoVo cells treated with Hakin-1 for 48 h. (**d**) Immunofluorescence of E-cadherin in HT-29 and LoVo cell lines in the presence of DMSO or Hakin-1 treatment after 48 h. Images were obtained with a 20× objective for HT-29 cells and a 40× objective for LoVo cells. Quantification was performed with ImageJ programme and results are expressed as mean ± SD of three independent different experiments (** $p < 0.01$; *** $p < 0.001$). Scale bar, 50 µm for HT-29 cells and 175 µm for LoVo cells.

2.4. Hakin-1 Inhibits Proliferation, Oncogenic Potential and Invasiveness of Epithelial Tumour Cells

Given that Hakai affects not only cell–cell contacts but also proliferation in fibroblast and epithelial cells [38], we decided to determine the possible effect of Hakin-1 on proliferation. Indeed, Hakin-1 (Figure 4a) but not Hakin-5 (Figure 4b) reduced cell proliferation in HT-29 and LoVo cells. Moreover, we confirmed that MDCK cells strongly proliferated when Hakai was overexpressed (Figure 4c). Interestingly, Hakin-1 was able to suppress proliferation of Hakai-MDCK cells whereas MDCK control cells were unaffected (Figure 4c). These results suggest that Hakin-1 may function as an antiproliferative agent when Hakai is highly expressed in epithelial cells, as observed in tumours from colorectal cancer patients [39,45,47]. Hakin-1 also inhibits cell proliferation in other epithelial cells lines such as breast cancer MCF7 cells, prostate cancer PC3 cells, bladder cancer 5637 cells, renal cancer ACHN cells and liver cancer HepG2 cells (Figure S7). We also observed a significant reduction of colony formation in soft agar upon treating HT-29 and Hakai-MDCK cells with Hakin-1 (Figure 4d). As we previously described, MDCK nontransformed cells do not form colonies, thus no effect was detected upon Hakin-1 treatment [38]. As stated above, the EMT process is characterized by the acquisition of migratory and invasive capabilities. We demonstrated that Hakin-1 strongly reduced the invasion capacity of LoVo cancer cells (Figure 5a). Moreover, we show that Hakin-1 blocked the invasion induced by Hakai overexpression in MDCK cells (Figure 5b). Finally, given that HT-29 cells were unable to invade under these experimental conditions, the effect of Hakin-1 on cell motility was tested and an important reduction of cell migration was observed (Figure 5c). All of these findings support an in vitro antitumour effect of Hakin-1 by acting on cell proliferation, oncogenic potential, cell motility and invasiveness.

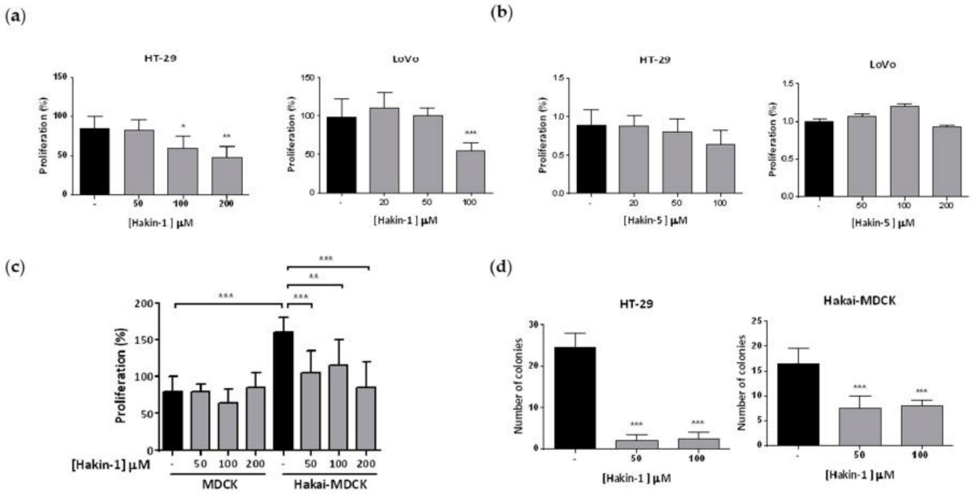

Figure 4. Antiproliferative and antioncogenic effect of Hakin-1 in tumour epithelial cells. (**a**) HT-29 and LoVo cells were treated with Hakin-1 for 48 h and proliferation was measured by performing a BrdU assay as indicated in Material and Methods. Results are expressed as mean ± SD of eight replicates and experiments were repeated three times (* $p < 0.05$; ** $p < 0.01$; *** $p < 0.001$). (**b**) HT-29 and LoVo cells were treated with Hakin-5 for 48 h and proliferation was measured as indicated in (**a**). (**c**) MDCK and Hakai-MDCK cells were treated with increasing concentrations of Hakin-1 for 48h and proliferation was measured as indicated in (**a**). (**d**) Soft agar assay in HT-29 (left panel) and Hakai-MDCK (right panel) cell lines. Colonies grew for 28 days (HT-29) or 21 days (Hakai-MDCK) and were counted as indicated in Materials and Methods. Quantification of the colonies was performed in triplicates and represented as mean ± SD of three independent experiments; (*** $p < 0.001$).

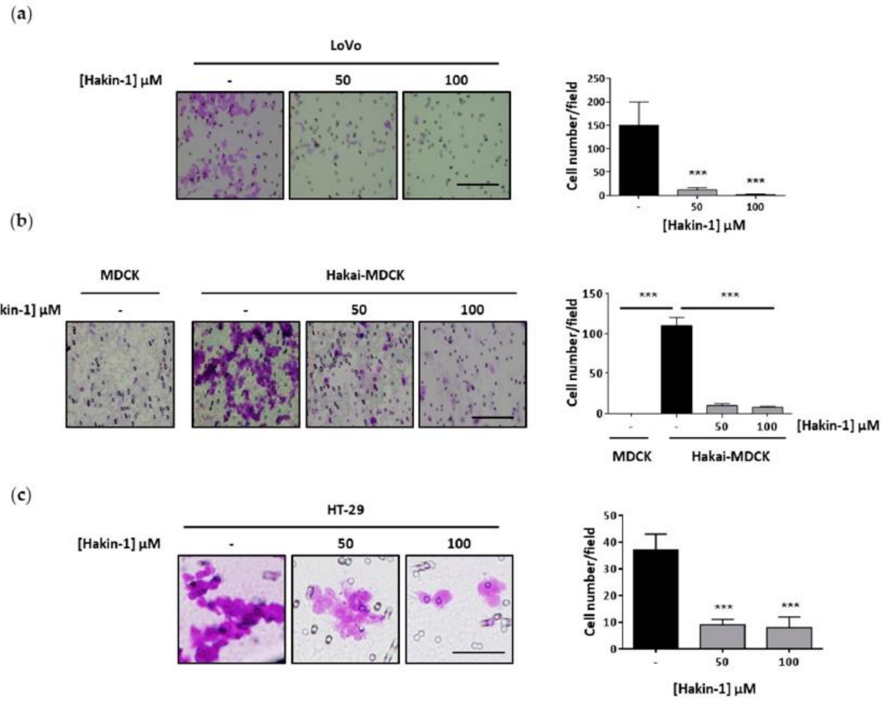

Figure 5. Hakin-1 reduces cell invasion and cell migration of epithelial tumour cells. (**a**) Invasion assay in LoVo cell line was performed as described in Materials and Methods. Cells were treated in the presence of DMSO or Hakin-1 for 48 h before being seeded into an invasion chamber. Representative images were taken using the 20× objective (right panel) and quantification of the photographed invasive cells are shown (left panel). (**b**) Invasion assay was performed as previously indicated by using MDCK and Hakai-MDCK cells. (**c**) Migration assay in HT-29 cells was analysed after treatment with DMSO or Hakin-1 during 48 h. Cells were seeded in a migration chamber as described in Materials and Methods. Representative images taken with 20× objective (right panel) and quantification of migrating cells (left panel) are shown. Results are represented as mean ± SD of triplicates of three independent experiments (*** $p < 0.001$).

2.5. *Antitumour Effect of Hakin-1 in Tumour Xenografts In Vivo*

The acquisition of migratory and invasive capabilities during EMT are crucial events in the formation of distant metastases, therefore targeting these events is an ideal approach for cancer treatment [1–4]. Based on our results with Hakin-1 blocking cell proliferation, oncogenic potential, invasiveness and motility of cancer cells in culture, we decided to study its efficacy on tumour growth in vivo. Control-MDCK and Hakai-MDCK cell were subcutaneously injected into the flank of nude mice. As previously reported, Hakai-MDCK cells formed primary tumours whereas parental MDCK cells did not [41]. Hakin-1 displayed a potent effect on inhibiting xenograft tumour growth (Figure 6a). Morphologically, xenograft tumour cells exhibited an undifferentiated and spindle-shape phenotype, a large nucleus and a small cytoplasm size. This morphology was strongly altered by Hakin-1 treatment, inducing tumour cell differentiation and an increase in cytoplasmic size (Figure 6b). Furthermore, by analysing Ki67 and the mitotic index, we show that Hakin-1 markedly reduced the number of proliferative cells (Figure 6c,d), whereas no effect was detected on apoptosis (Figure S8). These results underscore Hakin-1's effect on cell proliferation inhibition in vivo. We also detected a strong reduction in the number of blood vessels in tumour xenografts upon Hakin-1 treatment by staining for the CD31 endothelial marker (Figure 6e). Interestingly, no damage was observed in liver and kidney tissues in

Hakin-1-treated nude mice (Figure S9), which showed a normal morphological structure, supporting that Hakin-1 treatment inhibits tumour growth in nude mice apparently without systemic toxicity.

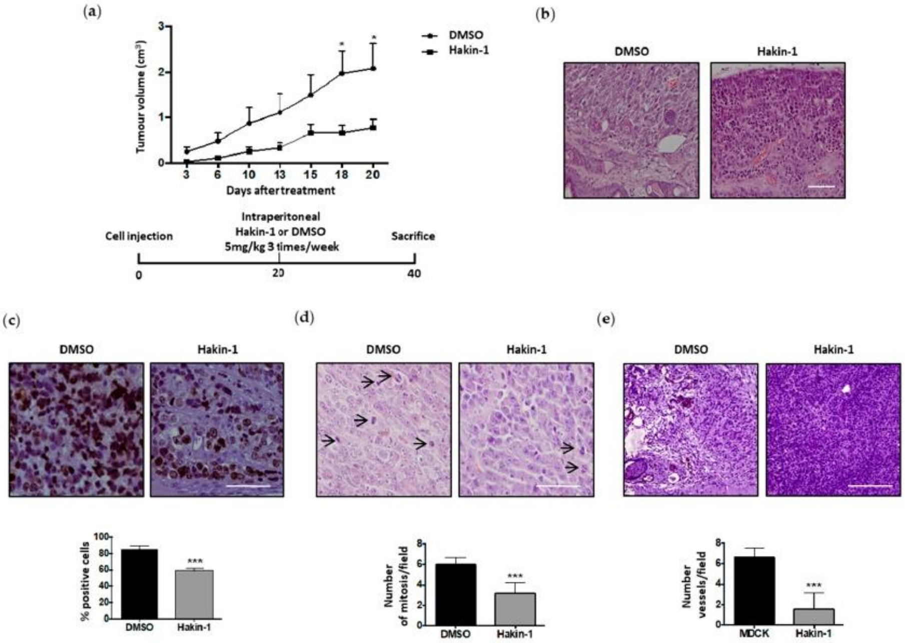

Figure 6. Hakin-1 inhibits tumour growth in xenografted mice. (**a**) Hakin-1 effect on tumour growth in nude mice inoculated into the flank with Hakai-MDCK cells (n = 8 tumours). Tumour growth curve is shown in the upper panel. Error bars represented the mean ± SEM (* $p < 0.05$). A schematic representation of the experiment design is shown in the bottom panel. (**b**) Haematoxylin and eosin (H&E) staining of Hakai-MDCK tumours at the end point, treated with DMSO (left panel) or Hakin-1 (right panel). Images were obtained with a 20× objective. Scale bar, 300 µm. (**c**) Immunohistochemistry of Ki67 marker in Hakai-MDCK tumours treated with DMSO (left panel) or Hakin-1 (right panel). Representative images were obtained with 40× objective. Scale bar, 500 µm. Quantification of the percentage of positive cells is shown in the bottom panel. (**d**) Representative image of Hakai-MDCK tumours in nude mice stained with H&E is shown. Pictures were obtained with a 40× objective (upper panel). Quantification of the number of mitosis (arrows) in high magnification field is shown (bottom panel). Scale bar, 500 µm. (**e**) Immunohistochemistry of CD31 marker in Hakai-MDCK tumours of injected nude mice treated with DMSO (left panel) or Hakin-1 (right panel). Images were obtained with a 20× objective. Scale bar, 500 µm. Quantification of the number of fields is shown in the bottom panel and is expressed as mean ± SEM (*** $p < 0.001$).

2.6. Hakin-1 Treatment Reduces N-Cadherin Mesenchymal Marker in Tumour Xenografts and Initiation of Lung Metastases

We further evaluated the in vivo effect of Hakin-1 on the reversion of EMT, as a crucial process in tumour progression and invasion. First, we confirmed that the levels of Hakai protein were not affected by Hakin-1 in tumour xenografts growing in nude mice (Figure 7a). As no E-cadherin protein was detected in Hakai-MDCK cells, we did not detect E-cadherin in tumour xenografts either in the presence or the absence of Hakin-1 (Figure 7b). However, we observed a strong reduction of N-cadherin, a mesenchymal marker of EMT, upon Hakin-1 treatment in tumour xenografts (Figure 7c). These data further support that Hakin-1 reverts the cell mesenchymal phenotype by a reduction of N-cadherin EMT mesenchymal marker. In consonance with this, we also analysed the effect of Hakin-1 on cortactin, another well-described substrate for Hakai. Hakai mediates the interaction and ubiquitination of cortactin protein inducing its degradation [42]. As shown in Figure 7d, cortactin is increased in Hakai-MDCK tumour xenografts upon Hakin-1 treatment. This result further supports the capacity of Hakin-1 to inhibit the ubiquitination and degradation of cortactin by Hakai. To determine whether Hakin-1 may affect cancer metastasis, lung tissues from nude mice were analysed by haematoxylin and eosin (H&E) staining. Nevertheless, after an exhaustive analysis, distant metastases were not detected under the experimental conditions (Figure 7e). Finally, we detected that Hakin-1 caused a significant reduction of micrometastasis formation in lungs of mice subcutaneously injected with Hakai-MDCK cells (Figure 7f). Metastases were not detected by histological H&E staining but by amplifying exogenous Hakai using PCR on lung tissue DNA, using HA-epitope as the first primer and Hakai as the second primer. These results demonstrate the capacity of Hakin-1 to inhibit lung metastasis in vivo.

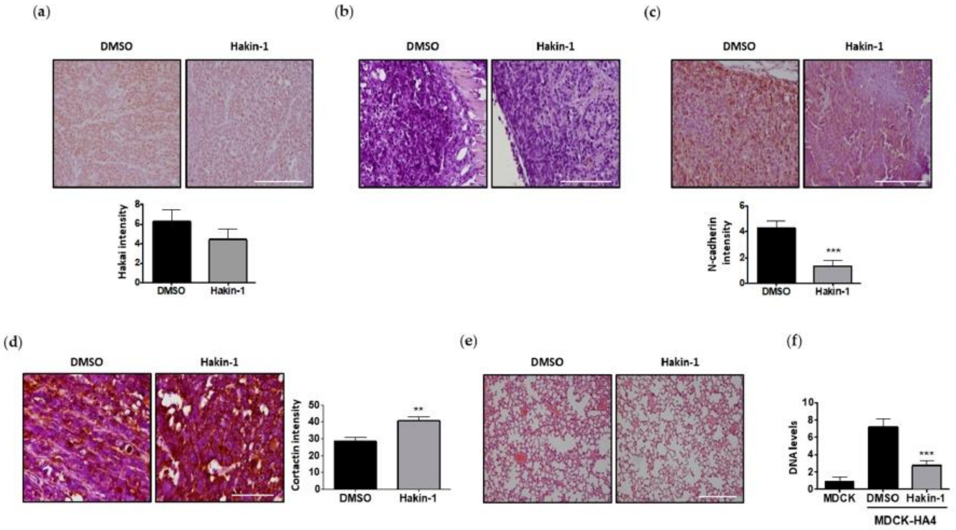

Figure 7. Hakin-1 treatment reduces mesenchymal markers of tumour xenografts and micrometastasis formation in lungs of immunosuppressed mice. (**a**–**c**) Immunohistochemical staining for Hakai (**a**), E-cadherin (**b**) and N-cadherin (**c**). Representative images were obtained with a 20× objective (upper panel). Quantification of significantly protein expression intensity is shown in bottom panel. (**d**) Immunohistochemical staining for cortactin and protein expression quantification is shown (left and right panels, respectively). Images were obtained with 40× objective. (**e**) H&E staining of mice lungs did not show a histological evidence of metastases. Representative images were obtained with a 10× objective. (**f**) Real-time quantitative PCR using primers for HA epitope and Hakai to detect the presence of DNA of Hakai-MDCK cells into the mice lungs. Results are expressed as mean ± SEM (*** $p < 0.001$). Scale bar, 500 µm.

3. Discussion

Epithelial plasticity is a well-documented and a crucial event for efficient invasion and metastasis, with relevant clinical implications [5,6]. As an important precondition of metastasis, the EMT process has become a promising target for anticancer therapy. In our search for small-molecule inhibitors directly targeted against EMT, we focused our attention on the E3 ubiquitin-ligase Hakai, a post-translational regulator that induces E-cadherin degradation, whose loss at cell–cell contacts is a major hallmark of EMT. In this study, a virtual screening campaign identified several small molecules inhibitors with potential affinity for HYB domain of Hakai, a novel pTyr-binding domain for E3 ubiquitin-ligases that targets specific substrates, such as phosphorylated E-cadherin [35,45]. We address several important points. First, we demonstrate that Hakin-1 is the first reported inhibitor that reduces Hakai-mediated total ubiquitination and Hakai-mediated ubiquitination of E-cadherin in a dose-dependent manner. Second, Hakin-1 significantly inhibits epithelial cancer cell viability and proliferation, showing much lower cytotoxic and antiproliferative effect in normal epithelial cells with lower levels of Hakai; this suggests that it may be particularly more effective when Hakai is highly expressed. Third, Hakin-1 increases epithelial differentiation, which is accompanied by an increased expression of Hakai substrate, E-cadherin at cell–cell contacts, and a reduction of vimentin mesenchymal markers. These findings support that Hakin-1 reverts the EMT process in vitro. Fourth, Hakin-1 also reduces important features of EMT in vitro, such as migration and invasiveness. Fifth, Hakin-1 decreases tumour growth in a xenograft mouse model without apparent systemic toxicity. Finally, Hakin-1 reduces N-cadherin mesenchymal markers in tumour xenografts and lung micrometastasis in vivo. Therefore, we postulate that Hakin-1 is an effective antiproliferative agent that can inhibit EMT, at least in part, through its specific action on Hakai-mediated ubiquitination and degradation of E-cadherin. To date, there is an extended interest in developing EMT inhibitors targeting different signalling pathways or stimuli related to EMT in order to block or prevent tumour progression and metastasis [47]. It is proposed that anti-EMT drugs are expected to preferentially block metastasis initiation and drug resistance rather than tumour growth. Unfortunately, the clinical activity of most EMT inhibitors has been exclusively evaluated based on their capacity to reduce tumour growth. This is mostly due to the fact that EMT-related inhibitors were not initially developed to directly block EMT [47]. In consequence, conventional clinical trial designs have underestimated the antitumour potential of anti-EMT drugs that may not significantly impact on tumour growth but rather in metastasis formation and drug resistance. Interestingly, although it is unknown how Hakin-1 may reduce the number of blood vessels in tumour xenografts, a recent publication demonstrated that soluble E-cadherin promotes tumour angiogenesis and localizes to exosome surface in ovarian cancer [48]. Given that Hakin-1 inhibits the degradation of E-cadherin and increases its localization at cell–cell contacts, we could speculate that Hakin-1 could reduce the amount of soluble E-cadherin that is internalized into exosomes. This hypothesis opens up a new line of investigation to explore the possible antiangiogenic effects of Hakin-1. In addition, given that Hakai was described not only as a key regulator of EMT, by its action on E-cadherin degradation, but also as a regulator of cell proliferation, Hakin-1 becomes the first small-molecule compound that directly affects EMT by its action on Hakai, thus being a great candidate for future clinical development.

However, although Hakin-1 regulates Hakai-mediated ubiquitination and degradation of E-cadherin, it may also exert its action on additional specific Hakai substrates that have not been discovered yet. This unexplored possibility merits further investigations. Furthermore, although Hakin-1 effect are, at least in part, mediated by its action on Hakai, possible off-target effects cannot be ruled out as Hakin-1 could also bind to and inhibit other yet unidentified E3 ubiquitin-ligases expressed in epithelial cells that share the HYB domain, such as the testis-specific E3 ubiquitin-ligase ZNF645, also known as CBLL2 [35]. In fact, our bioinformatic analysis reveals a high degree of sequence identity and structural conservation between these two targets (Figure S1). Future investigations will aim to more deeply evaluate its effect as an anti-EMT drug that inhibits metastasis. Further work is also required to determine how Hakin-1 may impact on angiogenesis, mediated by other potentially druggable targets. On the other hand, it was reported that early stages of EMT involve a post-translational downregulation of E-cadherin, whereas loss of E-cadherin via transcriptional repression is a late event in EMT [49,50]. Recently, it has been proposed that novel compounds with the ability to potentiate the activity of FBXL14, a convergent E3 ubiquitin-ligase that controls protein stability of the EMT transcription factors Snail, Slug, and Twist, could also make up another class of plausible anti-EMT therapeutic agents [51]. In this regard, inhibition of the Dub3 deubiquitinase by its specific inhibitor WP1130 has been reported to suppress breast cancer invasion and metastasis by promoting Snail1 degradation. All these data open a new field of investigation of searching for inhibitors that act post-translationally to control EMT [52].

On the other hand, although Hakai was the first reported post-translational regulator of E-cadherin stability, MDM2, a RING-finger type E3 ubiquitin-ligase, also induces E-cadherin ubiquitination and degradation [53]. Considerable efforts have been made to target MDM2, given that it also mediates the degradation of p53 tumour suppressor. Indeed, an important number of compounds, including Nutlin-3, have been identified to suppress the p53-MDM2 interaction [54,55]. Nutlin-3 and other analogues were tested in preclinical assays and/or registered for phase I trial for an array of malignancies [56]. In this regard, Nutlin-3 abolishes E-cadherin downregulation through TGF-β in p53-deficient tumour cells, by blocking Smad2 and Smad3 phosphorylation, and subsequently decreased Snail and Slug transcription [57]. In contrast, our results show a direct effect of Hakin-1 on E-cadherin ubiquitination and degradation mediated by Hakai. Later on, a novel compound was reported to directly bind to MDM2 (SP-141) and inhibits its protein levels by inducing autoubiquitination and proteasome degradation, independently of the p53 status. SP-141 also affects EMT-related proteins, such as β-catenin, vimentin, Twist and Snail and suppresses breast cancer migration in vitro and metastasis in vivo. However, no direct effect on E-cadherin expression was observed in MDA-MB-231 breast cancer cells. Therefore, to the best of our knowledge, Hakin-1 is the first reported inhibitor of an E-cadherin post-translational regulator that has been specifically selected for its affinity for the binding pocket wherein phosphorylated-E-cadherin specifically binds and influences EMT.

Important publications propose MDM2 as a promising therapeutic drug to treat human cancer, including breast cancer. Indeed, MDM2 is a negative prognostic marker and it has been shown that high MDM2 protein levels are detected in tumour biopsies from breast cancer patients with lymph node metastases [58]. Similarly, Hakai has been proposed as a novel biomarker for colon cancer progression [39,41]. Hakai protein expression gradually increases in human colon adenocarcinoma (TNM-stages I–IV) compared to adjacent healthy colon tissue, and statistically significant differences are indeed detected in colon adenoma compared to healthy tissue. Given that we show that Hakin-1 exerts an antitumour activity in LoVo and HT-29 colon cancer cells, by inhibiting proliferation, colony formation, migration and invasiveness, accompanied by an increase of E-cadherin expression at cell–cell contacts, we propose that Hakin-1 has promising therapeutic potential against colon cancer growth and progression.

The development of inhibitors against specific E3 ubiquitin-ligases has attracted significant attention, since they can be designed to target specific substrates without affecting others, thus avoiding broader side effects. Remarkably, the observed antitumour effect of Hakin-1 in tumour xenografts was noticeable even at a low dose of 5 mg/kg, only used every three days. Moreover, by histological examination of several tissues and the body weight control in the mouse, we did not detect any toxicity upon Hakin-1 administration. Therefore, it seems plausible to further optimize the doses, frequency or formulation of Hakin-1 in order to abolish tumour growth and metastasis completely.

As we previously mentioned, to date, the FDA has so far approved three drugs designed to target the ubiquitin pathway, including the proteasome inhibitors bortezomib, carfilzomib and ixazomib. Moreover, the proved efficacy of these drugs is for haematological malignancies, while clinical activity in solid tumours has been limited [27,28,59]. Since epithelial cells undergoing EMT reported to show decreased proteasome activity, a potential risk of proteasome inhibitor-based therapy in this type of malignancies has been noted [42,60]. Interestingly, we show that Hakin-1 inhibits cell proliferation in different epithelial cell lines, while no inhibition was detected in haematological tumour cells. Therefore, we propose that the use of Hakai-inhibitors targeting the ubiquitin pathway might be a better therapeutic strategy in epithelial tumours undergoing EMT.

Cancer metastasis consists of a sequential series of events including EMT and the reverse process known as mesenchymal-to-epithelial transition (MET). MET is necessary for metastatic colonization once malignant cells find their niche in distant organs. Therefore, this cellular plasticity during EMT has to be taken into consideration when analysing the contribution of EMT to cancer, as different degrees of epithelial plasticity may be present. In consequence, the translation of the EMT paradigm into the clinic represents an important challenge and remains as a controversial issue [47,61]. With the aim of identifying compounds acting on EMT, it is extremely meaningful to search for inhibitors that could block metastasis at the early stage, in order to prevent or inhibit EMT before metastases have taken place. In this regard, compounds acting on mesenchymal-type cells may accelerate tumour cell growth at distant metastasis because of MET. Interestingly, we observed that Hakin-1 treatment reduced tumour growth in Hakai-MDCK tumour xenografts, on which E-cadherin was not expressed, and this effect was accompanied by a reduced expression of N-cadherin mesenchymal marker and reduced formation of lung micrometastases. Future investigations will help to elucidate the beneficial effect of Hakin-1 in human colon cancer treatment. In conclusion, Hakin-1 emerged as an effective therapeutic agent for EMT inhibition with therapeutic potential and our results constitute the first preclinical proof-of-concept that Hakai inhibitors could be useful as anticancer agents.

4. Materials and Methods

4.1. Protein and Ligands Models

The X-ray crystal structure of the pTyr-binding domain of Hakai (PDB 3VK6) [35] was downloaded from the Protein Data Bank and the dimer modelled using the proper symmetry operations. Amino acid protonation was carried out using the pdb2pqr server [62] at a pH of 7.2. 3D models for the ligands were built using the virtual screening and data management integrated platform (VSDMIP), as described elsewhere [63,64]. Briefly, the initial 3D coordinates for each ligand were generated with CORINA. Thereafter, ALFA [65] was used to generate a large variety of conformers for each of which MOPAC-calculated atomic partial charges were assigned by employing the AM1 semiempirical model and the ESP method. All ligand models were stored in the VSDMIP database to be used in the different virtual screening campaigns.

4.2. Virtual Screening

Ligands in the eMolecules catalogue (https://www.emolecules.com/info/products-screening-compounds.html) were downloaded and processed as described in the preceding section. Only molecules presenting a carboxylic acid moiety and/or a phosphate group capable of mimicking a pTyr residue were considered. Next, CRDOCK [66] was used to lodge the selected molecules inside the binding pocket of Hakai by using the CRScore scoring function and the BFGS energy minimizer. The ligands were then ranked according to the predicted score and the top 350 molecules were re-evaluated by using an in-house implementation of the HYDE scoring function [60]. Finally, the best 20 molecules were visually inspected to select a final set of six prospective candidates.

4.3. Binding Pocket Analysis

To better analyse the results of the virtual screening campaign, we used our in-house cGRILL software [67] to produce affinity maps within the binding pocket of Hakai's pTyr-binding domain based on the van der Waals, Coulombic and hydrogen bonding interactions of hypothetical atomic probes. The negatively charged acceptor probe (=O) was used to map possible locations for the molecular recognition of the pTyr residue to help filter the docking solutions during the visual inspection of the poses.

4.4. Plasmids, Inhibitors and Antibodies

pcDNA-Flag-Hakai, pBSSR-HA–ubiquitin, pSG-v-Src and pcDNA-myc-E-Cadherin plasmids were previously described. Compounds Hakin-1 [4-(5-{[2-(4-nitrophenyl)-2-oxoethyl]thio}-1H-tetrazol-1-yl) benzoic acid] and Hakin-5 [(2E,4E,8E)-7,13-Dihydroxy-4,8,12-trimethyl-2,4,8-tetradecatrienoic acid] were obtained from ChemBridge Corporation and TimTec or Analyticon Discovery, respectively. Compounds were resuspended in DMSO (Sigma Aldrich, St Louis, MO, USA) at 100 mM for in vitro and in vivo assays. The highest concentration of DMSO was used as the vehicle control for the experiments. The antibodies used are listed in Supplementary Materials.

4.5. Cell Culture

MDCK, HEK293T, HEK293, HepG2, MCF7, and ACHN cells were cultured in Dulbecco´s modified Eagles medium (DMEM). MDCK stably expressing Hakai cells (Hakai-MDCK) were previously reported and were growth in DMEM with G418 (800 µg/mL) [38]. Different clones of Hakai-MDCK cells shown comparable phenotypes and characteristics as demonstrated previously [38]. LoVo and PC-3 cells were cultured in Ham´s F-12 Medium and HT-29 cells in McCoy's 5A medium. 5637 cells were cultured in RPMI medium. All culture media were supplemented with 1% penicillin/streptomycin and 10% of heat-inactivated foetal bovine serum (FBS) at 37 °C in a humidified incubator with 5% CO_2. Cells were monthly tested for mycoplasma contamination and used only for 1–3 months after defrosted. LoVo and HT-29 cells were authenticated with the StemElite ID system (Promega, Madison, WI, USA). For phase-contrast images, culture cells were photographed with a Nikon Eclipse-TI microscope.

4.6. Ubiquitination Assays

For ubiquitination assays, 7.5×10^5 HEK293T cells were seeded in 60 mm dishes and after 24 h were transfected with 0.25 µg Src, 0.75 µg Flag-Hakai, and 0.5 µg HA-ubiquitin with Lipofectamin 2000 (Invitrogen, Carlsbad, CA, USA). Six hours after transfection, cells were treated with indicated concentrations of Hakin 1 or Hakin-5 for 36h. Whole cell extracts were obtained in lysis buffer (20 mM Tris/HCl pH 7.5, 150 mM NaCl and 1% Triton X-100) containing 10 µg/mL leupeptin, 10 µg/mL aprotinin and 1 mM phenylmethanesulphonyl fluoride (PMSF), supplemented with 10 mM N-ethylmaleimide. Cells were harvested and subjected to Western blotting using anti-HA antibody to detect ubiquitination.

4.7. Immunoprecipitation

For immunoprecipitation experiments, 4×10^6 HEK293 cells were transfected with 3 µg Src, 4 µg Flag-Hakai, and 2 µg HA-ubiquitin and 3 µg E-cadherin with Lipofectamin 2000 (Invitrogen, Carlsbad, CA, USA). Six hours after transfection, cells were treated with indicated concentrations of Hakin-1 for 24 h. Then, cells were lysed for 20 min in 1 mL of 1% Triton X-100 lysis buffer (20 mM Tris-HCl pH 7.5, 150 mM NaCl and 1% Triton X-100) containing 10 µg/mL leupeptin, 10 µg/mL aprotinin and 1 mM phenylmethanesulphonyl fluoride (PMSF), supplemented with 10 mM N-ethylmaleimide and 2.5 mM sodium orthovanadate. After centrifugation at 18,000× g for 10 min, the supernatants were immunoprecipitated for 2 h with 2 µg of anti-E-cadherin antibody bound to 60 µL of protein G PLUS-Agarose beads (Santa Cruz Biotechnology, Dallas, TX, USA), followed by SDS-polyacrylamide gel electrophoresis (PAGE) and Western blotting with the indicated antibodies as previously reported.

4.8. Viability Assays

For cytotoxicity assays, 1×10^4 cells were seeded per well into a 96-well plate. After 24 h, cells were treated with the indicated inhibitors for 72 h and an MTT colorimetric cell viability assay was performed following manufacturer's instructions (Sigma Aldrich). Absorbance was measured at 570 and 630 nm using a Multiskan Plus Reader (Nanoquant Infinite M200 Tecan Trading AG, Switzerland). Dose-response curves were designed with GraphPad Prism Software and the half-maximal inhibitory concentration (IC_{50}) values were calculated. Represented data are the mean ± SD of at least three independent experiments with eight replicates per condition.

4.9. Western Blotting and Immunofluorescence

For Western blot analysis, cells were treated with the indicated inhibitors for 48 h and the whole cell extracts were obtained as described previously. Twenty micrograms of lysates were resolved on a 10% polyacrylamide SDS-PAGE and Western blot analysis was performed as previously described. For immunofluorescence assays, cells were grown for 24 h on glass coverslips and treated with the indicated inhibitors for 48 h. Cells were fixed with 4% PFA for 15 min, permeabilized with 0.5% Triton X-100 and incubated with E-cadherin antibody for 2 h. Coverslips were incubated with fluorescein-tagged secondary antibody (Alexa-Fluor, ThermoFisher Scientific, Waltham, MA, USA) for 1 h. Finally, coverslips were mounted with ProLong Gold antifade reagent (LifeTech, Carlsbad, CA, USA) and images were taken in an epifluorescence microscope (Olympus) using a 40× objective.

4.10. Real-Time Quantitative PCR (qRT-PCR)

HT-29 and LoVo cells were treated with increasing concentrations of Hakin-1 (50, 80 and 100 μM) for 48 h. Total RNA extraction was performed using a TRIzol™ RNA isolation protocol and cDNA synthesis was carried out by RT-PCR, under the specifications of the reverse retrotranscriptase kit (NZYTech). mRNA levels were analysed in technical triplicates by real-time PCR (qPCR) in a Light Cycler 480. Comparative CT method (ΔΔCT method) was performed to analyse qPCR data. Primers used were as follow: for E-cadherin F-AGTGTCCCCCGGTATCTTCC and R-CAGCCGCTTTCAGATTTTCAT and for Hakai F-CGCAGACGAATTCCTATAAAGC and R-CCTTCTTCATCACCAGGTGG. RPL13A was used as a housekeeping using the following primers F-CAAGCGGATGAACACCAAC and R-TGTGGGGCAGCATACCTC.

4.11. Proliferation Assays

For BrdU assays, 1×10^4 of indicated cells were plated per well into a 96-well plate. After 24 h, cells were treated with the indicated inhibitors for 48 h. Three independent experiments were plated with eight replicates per each condition. Cells were treated with 10 mM BrdU for 2 h. BrdU incorporation into newly synthesized DNA was measured using a cell proliferation colorimetric immunoassay kit according to the manufacturer's instructions (Roche, Switzerland). Results are expressed as mean ± SD. Results are represented as percentage of positive cells (mean ± SD) of three independent experiments.

4.12. Soft Agar-Colony Formation Assay

Soft agar-colony formation assay was performed on 12-well plates in triplicates at a density of 5×10^3 MDCK and Hakai-MDCK cells/well, or 12×10^3 HT-29 cells/well. Cells were seeded in medium with 0.5% low-melting agarose over a layer with 0.75% low-melting agarose (Lonza Rockland, ME, USA). Cells were treated with the indicated inhibitors and DMSO was used as vehicle. Treatment was refreshed every 3 days and, after 21 days for MDCK and Hakai-MDCK cells or 28 days for HT-29 cells, number of colonies were quantified. Quantification of five randomly selected fields of each condition was photographed with a Nikon Eclipse-TI microscope (objective 4×). Experiments were conducted with three triplicates and were repeated three times. Data are represented as mean ± SD.

4.13. Migration and Invasion Assay

For invasion assays, cells were treated with Hakin-1 or DMSO as vehicle for 48 h using 1% FBS during the last 24 h. Then, 3×10^5 MDCK, Hakai-MDCK or LoVo cells were seeded in a cell invasion chamber (cell invasion assay kit, Chemicon International) containing medium with 2% FBS and after 16 h, invasive cells that reached the lower chamber containing 30% FBS were fixed and stained with crystal violet (Sigma Aldrich, St Louis, MO) following the manufacturer's specifications. For migration assays, HT-29 cells were cultured with Hakin-1 or DMSO as vehicle for 48 h, using medium without serum for the last 24 h. 3×10^5 HT-29 cells were seeded in the cell migration chamber (Cell migration kit, Millipore, Bedford, MA, USA) containing medium without serum. After 16 h, migrated cells in the lower chamber containing serum with 30% FBS were stained with crystal violet and counted following the manufacturer's specifications. For both invasion and migration assays, cells were counted in five fields photographed with an Olympus microscope using a 20× objective. Experiments were performed in triplicates for each condition and the assays were repeated at least three times. Results are expressed as mean ± SD.

4.14. Tumour Xenograft Model

Xenograft experiments were performed in the Experimental Surgery Unit—Technological Training Center from INIBIC in compliance with the European Community Law (86/609/EEC) and the Spanish law (R.D. 53/2013). The experiment was approved by the Ethics Committee for Animal Experimentation of Xerencia de Xestion Integrada da Coruña (XXIAC, ethic code: 2017/R12). Mice were in a 12/12 h light/dark cycle with water and food available ad libitum. Six weeks old athymic nu/nu mice were randomly distributed in groups. One million of MDCK cells, resuspended in DMEM without serum and antibiotic, were subcutaneously inoculated in both flanks in two groups of 3 animals. The same number of Hakai-MDCK cells was injected in two groups of 4 animals. Twenty days after inoculation, tumours in Hakai-MDCK were palpable. Then, half of the animals were treated with Hakin-1 (5 mg/kg) and the other half with the same concentration of DMSO every 3 days. Tumour outgrowth was monitored twice a week taking measurements of tumour length (L) and width (W) with an electronic calypter. Tumour volume was calculated as $pLW^2/6$. Forty days after inoculation, animals were euthanised. Tumours, lungs, kidneys and livers were collected and fixed in 4% PFA and embedded in paraffin blocks for histology and/or immunohistochemistry analyses.

4.15. Histology and Immunohistochemistry

Tumours and tissues were deparaffinised, rehydrated and stained with haematoxylin and eosin (H&E) as previously described [68]. Tumour sections (4 µm) were also deparaffinised and hydrated for immunohistochemistry. Antigen retrieval was carried by heating the samples (2100 Retriever; PickCell Laboratories, Amsterdam, The Netherlands) in citrate buffer or in EDTA buffer (Agilent, Santa Clara, CA, USA). Then, endogenous peroxidase activity was blocked with peroxidase blocking (Agilent). Samples were blocked and permeabilized with 0.2% BSA and 0.1% Tx-100 for 1 h and incubated with the indicated primary antibodies overnight at 4 °C in a wet chamber. Slides were incubated for 1 h at room temperature and the secondary antibody and detection was carried out using DAB (Dako Real Envision kit, Agilent) according to manufacturer instructions. The antibodies used are listed in Supplementary Materials. Finally, nuclei were counterstained with Gill´s haematoxylin and mounted with DePeX. Pictures were taken with an Olympus microscope. Quantification of images was performed with ImageJ software by analysing 5 photographs of each animal, and the represented results are shown as mean ± SEM. The number of mitosis was counted in sections stained with H&E. In this case, ten pictures of each tumour were taken with an Olympus BX50 microscope (objective 40×) and the number of mitosis was counted manually. Results are represented as mean ± SEM and a representative photograph is shown for each condition.

4.16. Quantification of Lung Metastasis from In Vivo Mouse Model

Real-time PCR [69] was used to study the presence of metastasis in the lung mice. Primers for HA epitope and Hakai present in ectopic HA-tagged Hakai expressed in Hakai-MDCK cells (5′-TCTGGGACGTCGTATGGGTA-3′; 5′-TTCTTCATCACCTTGCGGG-3′) were used for the quantification. Primers for mouse apolipoprotein B (apob) (5′- CGTGGGCTCCAGCATTCTA-3′; 5′-TCACCAGTCATTTCTGCCTTTG-3′) were used as endogenous control. MDCK cell line was used as negative control. Lung DNA was extracted from 10–15 sections of paraffin blocks (4 µm) using the QIAamp DNA Mini Kit (Qiagen) as previously described [70]. The amplification and quantification of DNA was carried by quantitative PCR in technical triplicates by using a Light Cycler 480 real-time light cycler (Roche). Relative DNA levels were calculated by $2^{-\Delta\Delta Ct}$ method.

4.17. Statistical Analysis

Statistical analyses were carried out by using GraphPad Prism software. The Shapiro–Wilk test was used to check a normal distribution and Levene test to assess the equality of variances. Statistical significance of data was determined with ANOVA with the Bonferroni test or Kruskal–Wallis with the

Tukey correction test. Significance among the experimental groups indicated in the figures is shown as * $p < 0.05$, ** $p < 0.01$ and *** $p < 0.001$. Results obtained are expressed as mean ± SD or mean ± SEM as indicated. Results are represented as fold induction of treated cells over the values obtained in the untreated cells.

5. Conclusions

To date, the FDA has approved very few drugs targeting the ubiquitin pathway, and they were only authorised for haematological malignancies. However, the inhibitors designed against this pathway show limited clinical benefit in solid tumours. On the other hand, the epithelial-to mesenchymal transition (EMT) process is considered as a promising therapeutic target to block cancer progression before metastases have taken place. We demonstrate that Hakin-1 is an effective inhibitor against the E3-ubiquitin-ligase Hakai that targets E-cadherin for degradation, a hallmark of EMT, showing a potent antitumour effect in vitro and in vivo in epithelial tumours. Our results represent an important step forward in a future development an effective therapeutic drug to prevent or inhibit metastasis that may benefit patients with a carcinoma.

6. Patents

A patent has been solicited. A Figueroa, F Gago, O Martínez, R Carballo, A Cortés, A Casas. (PCT/EP2019/081522). Compounds that selectively and effectively inhibit Hakai-mediated ubiquitination, as anticancer drugs. Fund. Prof. Novoa Santos.

Supplementary Materials: The following are available online at http://www.mdpi.com/2072-6694/12/5/1340/s1, Table S1: List of antibodies included, Figure S1: X-ray crystal structure of the pTyr-binding domain of a Hakai dimer (PDB id. 3VK6) [35], Figure S2: Hakin-5 does not affect cell viability in epithelial tumour cell lines, Figure S3: Hakin-5 does not increase epithelial phenotype on epithelial tumour cell lines, Figure S4: Hakin-1 slightly increases apoptosis in Hakai-MDCK epithelial cells, Figure S5: Hakin-1 does not significantly affect the endogenous levels of Hakai, Figure S6: Hakin-5 does not affect the expression levels of EMT markers, Figure S7: Effect of Hakin-1 on proliferation in human cancer cells, Figure S8: Hakin-1 does not affect cell apoptosis in tumour xenograft mouse model, Figure S9: Intact cell morphology and tissue structure of liver and kidney in xenograft mice model upon treatment with Hakin-1, Figure S10: Full blots corresponding to Figure 1, Figure S11: Full blots corresponding to Figure 3, Supplementary Materials and Methods: In vitro apoptosis assay, In vivo TUNEL assay.

Author Contributions: Conceptualization, A.F. and F.G.; methodology, O.M.-I., A.C.-P., R.C. and Á.C.; Software, Á.C. and F.G.; validation, O.M.-I., A.C.-P., R.C., A.C.-L., A.D.-D., D.R.-L. and Á.C.; formal analysis, O.M.-I., A.C.-P. and R.C.; investigation, O.M.-I., A.C.-P., R.C.; writing—original draft preparation, A.F. and F.G.; writing—review and editing, O.M.-I., A.C.-P., F.G., and A.F.; visualization, O.M.-I., A.C.-P., Á.C., F.G. and A.F.; supervision, A.F. and F.G.; project administration, A.F.; funding acquisition, A.F. All authors have read and agreed to the published version of the manuscript.

Funding: This work has been supported by Plan Estatal I + D + I 2013–2016, cofunded by the Instituto de Salud Carlos III (ISCIII, Spain) under grant agreements PI13/00250 and PI18/00121 by Fondo Europeo de Desarrollo Regional (FEDER) "A way of Making Europe", as well as the Spanish MINECO/MEC project SAF20015-64629-C2 (to F.G.). The project leading to these results has received funding from "la Caixa" Foundation (ID 100010434) under the agreement (LCF/TR/CI19/52460016). The project was also funded by Fundación para la Innovación y la Prospectiva en Salud (FIPSE-3693-20), PRIS3 project from ACIS, both from Xunta de Galicia and by I.M.Q. San Rafael Foundation (A Coruña). Casas-Pais has been supported by a predoctoral contract (IN606A-2017/013) from Axencia Galega Innovación (GAIN)-Consellería de Economía, Empleo e Industria (Xunta de Galicia, Spain), Castosa by a technical-scientific contract (10CSA916023PR) from Consellería de Economía e Industria (Xunta de Galicia, Spain), Díaz-Díaz by FPU contract (FPU014/02837) from Ministerio de Educación Cultura y Deporte (Spain) and Roca-Lema by a postspecialization fellowship from Fundación Profesor Novoa Santos and a public grant from Deputación de A Coruña (Spain).

Acknowledgments: Thanks to H.G Palmer (Vall d'Hebron Institute of Oncology) for critical reading of the manuscript. C. Hogan (European Cancer Stem Cell Research Institute, Cardiff University) and M. Loza are acknowledged for technical advice. I. Santamarina (Instituto de Investigación Biomédica de A Coruña) is acknowledged technical help.

Conflicts of Interest: The authors declare no conflict of interest.

References

1. Nieto, M.A. Epithelial plasticity: A common theme in embryonic and cancer cells. *Science* **2013**, *342*, 1234850. [CrossRef]
2. Varga, J.; Greten, F.R. Cell plasticity in epithelial homeostasis and tumorigenesis. *Nat. Cell Biol.* **2017**, *19*, 1133–1141. [CrossRef]
3. Pastushenko, I.; Blanpain, C. EMT transition states during tumor progression and metastasis. *Trends Cell Biol.* **2018**. [CrossRef] [PubMed]
4. Pastushenko, I.; Brisebarre, A.; Sifrim, A.; Fioramonti, M.; Revenco, T.; Boumahdi, S.; Van Keymeulen, A.; Brown, D.; Moers, V.; Lemaire, S.; et al. Identification of the tumour transition states occurring during EMT. *Nature* **2018**, *556*, 463–468. [CrossRef] [PubMed]
5. Nieto, M.A.; Huang, R.Y.; Jackson, R.A.; Thiery, J.P. EMT: 2016. *Cell* **2016**, *166*, 21–45. [CrossRef] [PubMed]
6. Aparicio, L.A.; Blanco, M.; Castosa, R.; Concha, Á.; Valladares, M.; Calvo, L.; Figueroa, A. Clinical implications of epithelial cell plasticity in cancer progression. *Cancer Lett.* **2015**, *366*, 1–10. [CrossRef] [PubMed]
7. Perez-Moreno, M.; Jamora, C.; Fuchs, E. Sticky business: Orchestrating cellular signals at adherens junctions. *Cell* **2003**, *112*, 535–548. [CrossRef]
8. Gumbiner, B.M. Regulation of cadherin-mediated adhesion in morphogenesis. *Nat. Rev. Mol. Cell Biol.* **2005**, *6*, 622–634. [CrossRef]
9. Peinado, H.; Olmeda, D.; Cano, A. Snail, Zeb and bHLH factors in tumour progression: An alliance against the epithelial phenotype? *Nat. Rev. Cancer* **2007**, *7*, 415–428. [CrossRef]
10. Peinado, H.; Portillo, F.; Cano, A. Transcriptional regulation of cadherins during development and carcinogenesis. *Int. J. Dev. Biol.* **2004**, *48*, 365–375. [CrossRef]
11. Aparicio, L.A.; Abella, V.; Valladares, M.; Figueroa, A. Posttranscriptional regulation by RNA-binding proteins during epithelial-to-mesenchymal transition. *Cell. Mol. Life Sci.* **2013**, *70*, 4463–4477. [CrossRef] [PubMed]
12. Fujita, Y.; Krause, G.; Scheffner, M.; Zechner, D.; Leddy, H.E.; Behrens, J.; Sommer, T.; Birchmeier, W. Hakai, a c-Cbl-like protein, ubiquitinates and induces endocytosis of the E-cadherin complex. *Nat. Cell Biol.* **2002**, *4*, 222–231. [CrossRef]
13. Aparicio, L.A.; Valladares, M.; Blanco, M.; Alonso, G.; Figueroa, A. Biological influence of Hakai in cancer: A 10-year review. *Cancer Metastasis Rev.* **2012**, *31*, 375–386. [CrossRef] [PubMed]
14. Hershko, A.; Ciechanover, A.; Varshavsky, A. Basic Medical Research Award. The ubiquitin system. *Nat. Med.* **2000**, *6*, 1073–1081. [CrossRef] [PubMed]
15. Komander, D.; Rape, M. The ubiquitin code. *Annu. Rev. Biochem.* **2012**, *81*, 203–229. [CrossRef] [PubMed]
16. Clague, M.J.; Urbé, S. Ubiquitin: Same molecule, different degradation pathways. *Cell* **2010**, *143*, 682–685. [CrossRef]
17. Deshaies, R.J.; Joazeiro, C.A. RING domain E3 ubiquitin ligases. *Annu. Rev. Biochem.* **2009**, *78*, 399–434. [CrossRef]
18. Schulman, B.A.; Harper, J.W. Ubiquitin-like protein activation by E1 enzymes: The apex for downstream signalling pathways. *Nat. Rev. Mol. Cell Biol.* **2009**, *10*, 319–331. [CrossRef]
19. Buac, D.; Shen, M.; Schmitt, S.; Kona, F.R.; Deshmukh, R.; Zhang, Z.; Neslund-Dudas, C.; Mitra, B.; Dou, Q.P. From bortezomib to other inhibitors of the proteasome and beyond. *Curr. Pharm. Des.* **2013**, *19*, 4025–4038. [CrossRef]
20. Micel, L.N.; Tentler, J.J.; Smith, P.G.; Eckhardt, G.S. Role of ubiquitin ligases and the proteasome in oncogenesis: Novel targets for anticancer therapies. *J. Clin. Oncol.* **2013**, *31*, 1231–1238. [CrossRef]
21. Senft, D.; Qi, J.; Ronai, Z.A. Ubiquitin ligases in oncogenic transformation and cancer therapy. *Nat. Rev. Cancer* **2018**, *18*, 69–88. [CrossRef] [PubMed]
22. Sun, Y. E3 ubiquitin ligases as cancer targets and biomarkers. *Neoplasia* **2006**, *8*, 645–654. [CrossRef] [PubMed]
23. Qi, J.; Ronai, Z.A. Dysregulation of ubiquitin ligases in cancer. *Drug Resist. Updat.* **2015**, *23*, 1–11. [CrossRef] [PubMed]
24. Huang, X.; Dixit, V.M. Drugging the undruggables: Exploring the ubiquitin system for drug development. *Cell Res.* **2016**, *26*, 484–498. [CrossRef]
25. Mani, A.; Gelmann, E.P. The ubiquitin-proteasome pathway and its role in cancer. *J. Clin. Oncol.* **2005**, *23*, 4776–4789. [CrossRef] [PubMed]

26. Morrow, J.K.; Lin, H.K.; Sun, S.C.; Zhang, S. Targeting ubiquitination for cancer therapies. *Future Med. Chem.* **2015**, *7*, 2333–2350. [CrossRef] [PubMed]
27. Richardson, P.G.; Barlogie, B.; Berenson, J.; Singhal, S.; Jagannath, S.; Irwin, D.; Rajkumar, S.V.; Srkalovic, G.; Alsina, M.; Alexanian, R.; et al. A phase 2 study of bortezomib in relapsed, refractory myeloma. *N. Engl. J. Med.* **2003**, *348*, 2609–2617. [CrossRef]
28. Gandolfi, S.; Laubach, J.P.; Hideshima, T.; Chauhan, D.; Anderson, K.C.; Richardson, P.G. The proteasome and proteasome inhibitors in multiple myeloma. *Cancer Metastasis Rev.* **2017**, *36*, 561–584. [CrossRef]
29. Khan, M.L.; Stewart, A.K. Carfilzomib: A novel second-generation proteasome inhibitor. *Future Oncol.* **2011**, *7*, 607–612. [CrossRef]
30. Kumar, S.K.; Bensinger, W.I.; Zimmerman, T.M.; Reeder, C.B.; Berenson, J.R.; Berg, D.; Hui, A.M.; Gupta, N.; Di Bacco, A.; Yu, J.; et al. Phase 1 study of weekly dosing with the investigational oral proteasome inhibitor ixazomib in relapsed/refractory multiple myeloma. *Blood* **2014**, *124*, 1047–1055. [CrossRef]
31. Aghajanian, C.; Blessing, J.A.; Darcy, K.M.; Reid, G.; DeGeest, K.; Rubin, S.C.; Mannel, R.S.; Rotmensch, J.; Schilder, R.J.; Riordan, W.; et al. A phase II evaluation of bortezomib in the treatment of recurrent platinum-sensitive ovarian or primary peritoneal cancer: A Gynecologic Oncology Group study. *Gynecol. Oncol.* **2009**, *115*, 215–220. [CrossRef] [PubMed]
32. Rosenberg, J.E.; Halabi, S.; Sanford, B.L.; Himelstein, A.L.; Atkins, J.N.; Hohl, R.J.; Millard, F.; Bajorin, D.F.; Small, E.J.; Cancer and Leukemia Group, B. Phase II study of bortezomib in patients with previously treated advanced urothelial tract transitional cell carcinoma: CALGB 90207. *Ann. Oncol.* **2008**, *19*, 946–950. [CrossRef] [PubMed]
33. Swaminathan, G.; Cartwright, C.A. Rack1 promotes epithelial cell-cell adhesion by regulating E-cadherin endocytosis. *Oncogene* **2012**, *31*, 376–389. [CrossRef] [PubMed]
34. Zhou, W.J.; Geng, Z.H.; Chi, S.; Zhang, W.; Niu, X.F.; Lan, S.J.; Ma, L.; Yang, X.; Wang, L.J.; Ding, Y.Q.; et al. Slit-Robo signaling induces malignant transformation through Hakai-mediated E-cadherin degradation during colorectal epithelial cell carcinogenesis. *Cell Res.* **2011**, *21*, 609–626. [CrossRef]
35. Mukherjee, M.; Chow, S.Y.; Yusoff, P.; Seetharaman, J.; Ng, C.; Sinniah, S.; Koh, X.W.; Asgar, N.F.; Li, D.; Yim, D.; et al. Structure of a novel phosphotyrosine-binding domain in Hakai that targets E-cadherin. *EMBO J.* **2012**, *7*, 1308–1319. [CrossRef]
36. Weng, C.H.; Chen, L.Y.; Lin, Y.C.; Shih, J.Y.; Lin, Y.C.; Tseng, R.Y.; Chiu, A.C.; Yeh, Y.H.; Liu, C.; Lin, Y.T.; et al. Epithelial-mesenchymal transition (EMT) beyond EGFR mutations per se is a common mechanism for acquired resistance to EGFR TKI. *Oncogene* **2019**, *38*, 455–468. [CrossRef]
37. Figueroa, A.; Fujita, Y.; Gorospe, M. Hacking RNA: Hakai promotes tumorigenesis by enhancing the RNA-binding function of PSF. *Cell Cycle* **2009**, *8*, 3648–3651. [CrossRef]
38. Figueroa, A.; Kotani, H.; Toda, Y.; Mazan-Mamczarz, K.; Mueller, E.C.; Otto, A.; Disch, L.; Norman, M.; Ramdasi, R.M.; Keshtgar, M.; et al. Novel roles of hakai in cell proliferation and oncogenesis. *Mol. Biol. Cell* **2009**, *20*, 3533–3542. [CrossRef]
39. Abella, V.; Valladares, M.; Rodriguez, T.; Haz, M.; Blanco, M.; Tarrío, N.; Iglesias, P.; Aparicio, L.A.; Figueroa, A. miR-203 regulates cell proliferation through its influence on hakai expression. *PLoS ONE* **2012**, *7*, e52568. [CrossRef]
40. Rodríguez-Rigueiro, T.; Valladares-Ayerbes, M.; Haz-Conde, M.; Aparicio, L.A.; Figueroa, A. Hakai reduces cell-substratum adhesion and increases epithelial cell invasion. *BMC Cancer* **2011**, *11*, 474. [CrossRef]
41. Castosa, R.; Martinez-Iglesias, O.; Roca-Lema, D.; Casas-Pais, A.; Díaz-Díaz, A.; Iglesias, P.; Santamarina, I.; Graña, B.; Calvo, L.; Valladares-Ayerbes, M.; et al. Hakai overexpression effectively induces tumour progression and metastasis in vivo. *Sci. Rep.* **2018**, *8*, 3466. [CrossRef] [PubMed]
42. Díaz-Díaz, A.; Casas-Pais, A.; Calamia, V.; Castosa, R.; Martinez-Iglesias, O.; Roca-Lema, D.; Santamarina, I.; Valladares-Ayerbes, M.; Calvo, L.; Chantada, V.; et al. Proteomic Analysis of the E3 Ubiquitin-Ligase Hakai Highlights a Role in Plasticity of the Cytoskeleton Dynamics and in the Proteasome System. *J. Proteome Res.* **2017**, *16*, 2773–2788. [CrossRef] [PubMed]
43. Díaz-Díaz, A.; Roca-Lema, D.; Casas-Pais, A.; Romay, G.; Colombo, G.; Concha, Á.; Graña, B.; Figueroa, A. Heat Shock Protein 90 Chaperone Regulates the E3 Ubiquitin-Ligase Hakai Protein Stability. *Cancers* **2020**, *12*, 215. [CrossRef] [PubMed]

44. Liu, M.; Jiang, K.; Lin, G.; Liu, P.; Yan, Y.; Ye, T.; Yao, G.; Barr, M.P.; Liang, D.; Wang, Y.; et al. Ajuba inhibits hepatocellular carcinoma cell growth via targeting of β-catenin and YAP signaling and is regulated by E3 ligase Hakai through neddylation. *J. Exp. Clin. Cancer Res.* **2018**, *37*, 165. [CrossRef]
45. Mukherjee, M.; Jing-Song, F.; Ramachandran, S.; Guy, G.R.; Sivaraman, J. Dimeric switch of Hakai-truncated monomers during substrate recognition: Insights from solution studies and NMR structure. *J. Biol. Chem.* **2014**, *289*, 25611–25623. [CrossRef]
46. Cooper, J.A.; Kaneko, T.; Li, S.S. Cell regulation by phosphotyrosine-targeted ubiquitin ligases. *Mol. Cell Biol.* **2015**, *35*, 1886–1897. [CrossRef]
47. Marcucci, F.; Stassi, G.; De Maria, R. Epithelial-mesenchymal transition: A new target in anticancer drug discovery. *Nat. Rev. Drug Discov.* **2016**, *15*, 311–325. [CrossRef]
48. Tang, M.; Yue, P.; Ip, P.P.; Huang, R.L.; Lai, H.C.; Cheung, A.; Tse, K.Y.; Ngan, H.; Wong, A. Soluble E-cadherin promotes tumor angiogenesis and localizes to exosome surface. *Nat. Commun.* **2018**, *9*, 2270. [CrossRef]
49. Janda, E.; Nevolo, M.; Lehmann, K.; Downward, J.; Beug, H.; Grieco, M. Raf plus TGFbeta-dependent EMT is initiated by endocytosis and lysosomal degradation of E-cadherin. *Oncogene* **2006**, *25*, 7117–7130. [CrossRef]
50. Yang, J.; Antin, P.; Berx, G.; Blanpain, C.; Brabletz, T.; Bronner, M.; Campbell, K.; Cano, A.; Casanova, J.; Christofori, G.; et al. Guidelines and definitions for research on epithelial-mesenchymal transition. *Nat. Rev. Mol. Cell Biol.* **2020**. [CrossRef]
51. Díaz, V.M.; de Herreros, A.G. F-box proteins: Keeping the epithelial-to-mesenchymal transition (EMT) in check. *Semin. Cancer Biol.* **2016**, *36*, 71–79. [CrossRef] [PubMed]
52. Wu, Y.; Wang, Y.; Lin, Y.; Liu, Y.; Wang, Y.; Jia, J.; Singh, P.; Chi, Y.I.; Wang, C.; Dong, C.; et al. Dub3 inhibition suppresses breast cancer invasion and metastasis by promoting Snail1 degradation. *Nat. Commun.* **2017**, *8*, 14228. [CrossRef] [PubMed]
53. Yang, J.Y.; Zong, C.S.; Xia, W.; Wei, Y.; Ali-Seyed, M.; Li, Z.; Broglio, K.; Berry, D.A.; Hung, M.C. MDM2 promotes cell motility and invasiveness by regulating E-cadherin degradation. *Mol. Cell Biol.* **2006**, *26*, 7269–7282. [CrossRef] [PubMed]
54. Landré, V.; Rotblat, B.; Melino, S.; Bernassola, F.; Melino, G. Screening for E3-ubiquitin ligase inhibitors: Challenges and opportunities. *Oncotarget* **2014**, *5*, 7988–8013. [CrossRef] [PubMed]
55. Vassilev, L.T.; Vu, B.T.; Graves, B.; Carvajal, D.; Podlaski, F.; Filipovic, Z.; Kong, N.; Kammlott, U.; Lukacs, C.; Klein, C.; et al. In vivo activation of the p53 pathway by small-molecule antagonists of MDM2. *Science* **2004**, *303*, 844–848. [CrossRef]
56. Weathington, N.M.; Mallampalli, R.K. Emerging therapies targeting the ubiquitin proteasome system in cancer. *J. Clin. Investig.* **2014**, *124*, 6–12. [CrossRef]
57. Wu, Y.; Fu, Y.; Zheng, L.; Lin, G.; Ma, J.; Lou, J.; Zhu, H.; He, Q.; Yang, B. Nutlin-3 inhibits epithelial-mesenchymal transition by interfering with canonical transforming growth factor-β1-Smad-Snail/Slug axis. *Cancer Lett.* **2014**, *342*, 82–91. [CrossRef]
58. Turbin, D.A.; Cheang, M.C.; Bajdik, C.D.; Gelmon, K.A.; Yorida, E.; De Luca, A.; Nielsen, T.O.; Huntsman, D.G.; Gilks, C.B. MDM2 protein expression is a negative prognostic marker in breast carcinoma. *Mod. Pathol.* **2006**, *19*, 69–74. [CrossRef]
59. Mackay, H.; Hedley, D.; Major, P.; Townsley, C.; Mackenzie, M.; Vincent, M.; Degendorfer, P.; Tsao, M.S.; Nicklee, T.; Birle, D.; et al. A phase II trial with pharmacodynamic endpoints of the proteasome inhibitor bortezomib in patients with metastatic colorectal cancer. *Clin. Cancer Res.* **2005**, *11*, 5526–5533. [CrossRef]
60. Banno, A.; Garcia, D.A.; van Baarsel, E.D.; Metz, P.J.; Fisch, K.; Widjaja, C.E.; Kim, S.H.; Lopez, J.; Chang, A.N.; Geurink, P.P.; et al. Downregulation of 26S proteasome catalytic activity promotes epithelial-mesenchymal transition. *Oncotarget* **2016**, *7*, 21527–21541. [CrossRef]
61. Santamaria, P.G.; Moreno-Bueno, G.; Portillo, F.; Cano, A. EMT: Present and future in clinical oncology. *Mol. Oncol.* **2017**, *11*, 718–738. [CrossRef] [PubMed]
62. Dolinsky, T.J.; Nielsen, J.E.; McCammon, J.A.; Baker, N.A. PDB2PQR: An automated pipeline for the setup of Poisson-Boltzmann electrostatics calculations. *Nucleic Acids Res.* **2004**, *32*, W665–W667. [CrossRef] [PubMed]
63. Gil-Redondo, R.; Estrada, J.; Morreale, A.; Herranz, F.; Sancho, J.; Ortiz, A.R. VSDMIP: Virtual screening data management on an integrated platform. *J. Comput. Aided Mol. Des.* **2009**, *23*, 171–184. [CrossRef] [PubMed]
64. Cabrera, Á.; Gil-Redondo, R.; Perona, A.; Gago, F.; Morreale, A. VSDMIP 1.5: An automated structure- and ligand-based virtual screening platform with a PyMOL graphical user interface. *J. Comput. Aided Mol. Des.* **2011**, *25*, 813–824. [CrossRef]

65. Klett, J.; Cortés-Cabrera, Á.; Gil-Redondo, R.; Gago, F.; Morreale, A. ALFA: Automatic ligand flexibility assignment. *J. Chem. Inf. Model.* **2014**, *54*, 314–323. [CrossRef]
66. Cortés Cabrera, Á.; Klett, J.; Dos Santos, H.G.; Perona, A.; Gil-Redondo, R.; Francis, S.M.; Priego, E.M.; Gago, F.; Morreale, A. CRDOCK: An ultrafast multipurpose protein-ligand docking tool. *J. Chem. Inf. Model.* **2012**, *52*, 2300–2309. [CrossRef]
67. Schneider, N.; Lange, G.; Hindle, S.; Klein, R.; Rarey, M. A consistent description of HYdrogen bond and DEhydration energies in protein-ligand complexes: Methods behind the HYDE scoring function. *J. Comput. Aided Mol. Des.* **2013**, *27*, 15–29. [CrossRef]
68. Rodríguez-Rigueiro, T.; Valladares-Ayerbes, M.; Haz-Conde, M.; Blanco, M.; Aparicio, G.; Fernández-Puente, P.; Blanco, F.J.; Lorenzo, M.J.; Aparicio, L.A.; Figueroa, A. A novel procedure for protein extraction from formalin-fixed paraffin-embedded tissues. *Proteomics* **2011**, *11*, 2555–2559. [CrossRef]
69. Fujiki, Y.; Tao, K.; Bianchi, D.W.; Giel-Moloney, M.; Leiter, A.B.; Johnson, K.L. Quantification of green fluorescent protein by in vivo imaging, PCR, and flow cytometry: Comparison of transgenic strains and relevance for fetal cell microchimerism. *Cytometry* **2008**, *73*, 11–118. [CrossRef]
70. Lin, J.; Kennedy, S.H.; Svarovsky, T.; Rogers, J.; Kemnitz, J.W.; Xu, A.; Zondervan, K.T. High-quality genomic DNA extraction from formalin-fixed and paraffin-embedded samples deparaffinized using mineral oil. *Anal. Biochem.* **2009**, *395*, 265–267. [CrossRef]

© 2020 by the authors. Licensee MDPI, Basel, Switzerland. This article is an open access article distributed under the terms and conditions of the Creative Commons Attribution (CC BY) license (http://creativecommons.org/licenses/by/4.0/).

APPENDIX C

Funding sources

This work has been supported by funds from:

- Axencia Galega de Innovación (GAIN) - Consellería de Economía, Emprego e Industria (Xunta de Galicia). Axudas de apoio á etapa predoutoral (**IN606A-2017/013**).

- Instituto de Salud Carlos III (ISCIII, Spain) and Plan Estatal I+D+i. Grant agreements PI13/00250 and PI18/00121 by Fondo Europeo de Desarrollo Regional (FEDER) "A way of Making Europe".

- Obra Social "la Caixa" - La Caixa Capital Risc. CaixaImpulse program (ID 100010434) under the agreement LCF/TR/CI19/52460016.

- Agencia Gallega para la Gestión del Conocimiento en Salud (ACIS) Xunta de Galicia. Programa de Desarrollo Precomercial de los Resultados de Investigación. Grant agreement Tercer PRIS3.